KGS
OF
90-58

DEPOSITIONAL AND DIAGENETIC CONTROL OF RESERVOIR ARCHITECTURE AND QUALITY, BINDLEY FIELD (MISSISSIPPIAN), HODGEMAN COUNTY, KANSAS

by

REED A. JOHNSON

B.S., State University of New York
at Stony Brook, 1980

A thesis submitted to the
Faculty of the Graduate School of the
University of Colorado in partial fulfillment
of the requirements of the degree of
Master of Science
Department of Geological Sciences
1990

KANSAS GEOLOGICAL SURVEY
OPEN-FILE REPORTS

>>>>>>>>>>>>>>>>NOT FOR RESALE<<<<<<<<<<<<<<<<

Disclaimer

The Kansas Geological Survey does not guarantee this document to be free from errors or inaccuracies and disclaims any responsibility or liability for interpretations based on data used in the production of this document or decisions based thereon. This report is intended to make results of research available at the earliest possible date, but is not intended to constitute final or formal publication.

This thesis for the Master of Science degree by

Reed A. Johnson

has been approved for the

Department of

Geological Sciences

by

David A. Budd

Philip W. Choquette

Neil F. Hurley

Date 1/7/91

Johnson, Reed A. (M.S., Geology)
Depositional and Diagenetic Control of Reservoir Architecture and Quality, Bindley Field (Mississippian), Hodgeman County, Kansas
Thesis directed by Assistant Professor David A. Budd

Bindley Field is a multilayered reservoir which has produced 2.5 million barrels of oil from the lower Meramecian (Mississippian) "Warsaw dolomite." The trap is defined by erosional, stratigraphic, and structural elements.

An informal stratigraphic subdivision of lower Meramecian rocks is presented which identifies time-correlative parasequence sets. In ascending order, the parasequence sets are designated Meramec 1, Meramec 2, Meramec 3, and Meramec 4. Bindley Field produces primarily from Meramec 2.

Meramec 2 consists of six parasequences, designated Meramec 2A-2F in ascending order. Each parasequence aggrades upward from normal marine, skeletal sediments to restricted, subtidal sediments. The percentage of grain-supported sediments increases volumetrically in successive parasequences, reaching a maximum in Meramec 2E. Depositional fabrics grade from grain-supported along the central axis of the field to mud-supported on the flanks. Meramec 2D and 2E are the primary reservoir intervals in Bindley Field.

Reservoir quality is controlled by matrix permeability. Permeable reservoir rock is confined to a single lithotype, echinoderm/bryozoan dolopackstone/grainstone (Lithotype 4C). The origin of this permeable reservoir rock is dependent on three principal factors: 1) skeletal, grain-supported depositional fabric, 2) pervasive but incomplete dolomitization, and 3) dissolution of undolomitized calcite. The magnitude of permeability is related to dolomitized mud content and pore-throat size.

The distribution of reservoir rocks mimics the depositional architecture. Stacked, horizontal layers of permeable Lithotype 4C are each capped by thin, low-permeability dolomudstones which act as barriers to vertical fluid flow. Each permeable Lithotype 4C layer represents a separate reservoir flow unit. Bindley Field contains two permeable flow units, one each in Meramec 2D and 2E, which are distributed widely throughout the field.

Cumulative fluid production correlates linearly with matrix permeability development in perforated flow units, defining a permeability/productivity baseline. A small number of wells vary from the baseline trend in one of two ways. Anomalously high volumes of water produced from low-permeability wells are considered to be related to open, vertical fractures proximal to the wellbore. Anomalously high volumes of oil and water produced from high-permeability wells are considered to result from fracture-mediated reservoir recharge distal from the wellbore.

ACKNOWLEDGMENTS

The author gratefully acknowledges the support and assistance of those individuals and institutions which contributed to this study. Cores, financial assistance, and services were provided by the Kansas Geological Survey under the supervision of W. Lynn Watney. Cores, production and petrophysical data, and financial assistance were provided by Conoco, Inc. The Department of Geological Sciences at the University of Colorado provided financial assistance, analytical and sample preparation services, and facilities. Additional financial assistance was contributed by an AAPG Grant-in-Aid and by the Energy and Minerals Applied Research Center of the University of Colorado. Bartshe Exploration, Inc. provided data and financial support. Energy Projects, Inc. contributed financial assistance for drafting services. David A. Budd, Philip W. Choquette, and Neil F. Hurley provided advice, encouragement, and editorial review.

CONTENTS

APPENDICES

FIGURES

Figure

CHAPTER I

INTRODUCTION

Lower Meramecian (Mississippian) rocks produce oil and gas in Kansas along a regional sub-Pennsylvanian subcrop belt which surrounds the central Kansas uplift (Figure 1). In western Kansas, dolostones generally ascribed to the Warsaw and Salem formations account for the majority of production in the lower Meramecian subcrop trend. Even though the petroleum resources within this western subcrop belt are well developed (Figure 2) and have a production history dating back to the 1950s (Newell et al., 1987), the nature of the reservoir rocks, their depositional and diagenetic history, and their lateral and vertical heterogeneity are poorly understood. The Bindley Field (sections 33-34, T21S-R24W and sections 3-4, T22S-R24W, Hodgeman County, Kansas) is centrally located in the western subcrop belt (Figures 1 and 2) and is the only field in western Kansas producing from lower Meremecian rocks which has substantial core coverage. As such, it serves as an excellent natural laboratory to determine the relationships between depositional/diagenetic factors and reservoir quality and distribution in the lower

FIGURE 1- Pre-Pennsylvanian subcrop of Mississippian rocks in western Kansas. The location of the study area is indicated within the subcrop of the "Warsaw" Formation (from Ebanks et al., 1977)

FIGURE 2- Distribution of fields in Ness and Hodgeman Counties, Kansas. Fields which produce primarily from Mississippian reservoirs are indicated by open field outlines, those which produce principally from non-Mississippian reservoirs are denoted by solid black. The lower Meramecian production fairway is comprised primarily of fields producing from Meramec 2 through Meramec 4 reservoirs and generally parallels the subcrop belt of these intervals.

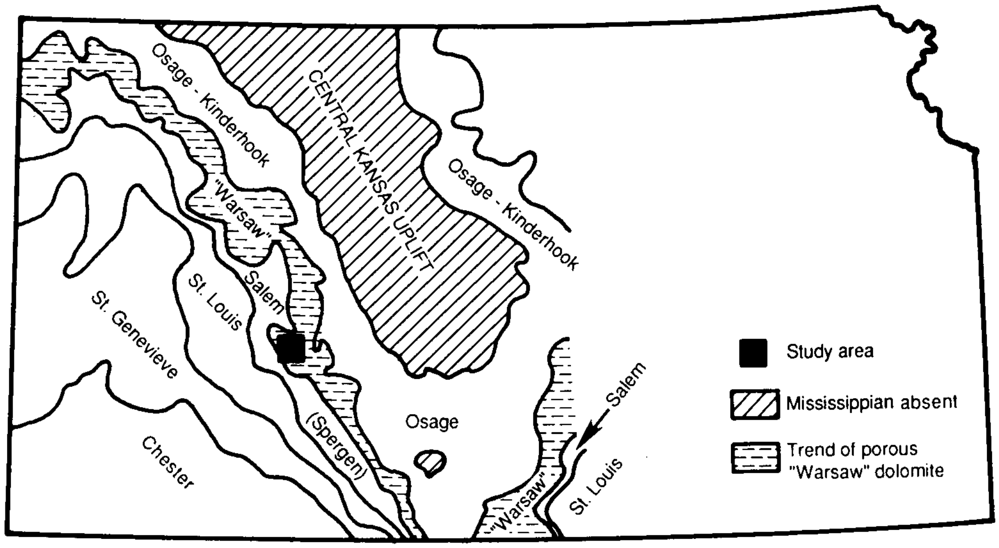

Figure 1

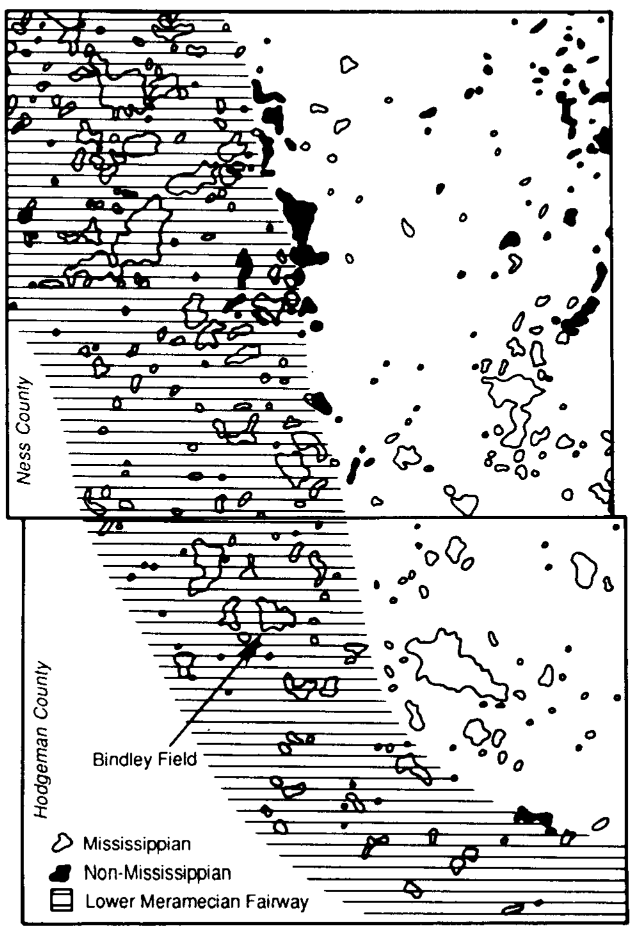

Figure 2

Meramecian trend. To the extent that Bindley Field may be a suitable analog for other lower Meramecian reservoirs, detailed understanding of the reservoir and trap in this field will likely lead to improved exploration models and more efficient recovery methods for these reservoirs.

The objective of this study is to develop a reservoir model for Bindley Field. This is accomplished by (1) defining lithotypes, mapping their distribution, and interpreting their depositional origins and sedimentary dynamics, (2) determining the diagenetic history of the reservoir interval and surrounding rocks with emphasis on those aspects which influence reservoir quality and distribution, (3) relating the petrophysical properties of the reservoir to the depositional/ diagenetic architecture, and (4) testing the geologic controls on reservoir distribution and quality by comparison with fluid production histories.

CHAPTER II

PREVIOUS STUDY

The general geologic history of Kansas is summarized by Merriam (1963) and the generalized stratigraphy is described by Zeller (1968). Lee (1940) and Goebel (1966, 1968) have described the lithostratigraphic features of the Mississippian system of western Kansas and have attempted to correlate lithostratigraphic units within a time-stratigraphic framework. Lane and De Keyser (1980) discussed the paleogeographic setting of Kansas during early Mississippian time within the broader context of the central and southwestern United States. The conodont biostratigraphy of Meremecian rocks in Kansas has been studied by Thompson and Goebel (1963, 1968).

Few detailed studies of lower Meremecian reservoir rocks in western Kansas have been published. Various reports of general field attributes have been published (e.g. Beauchamp, 1985; James, 1985; Beene, 1965; Linehan, 1965; Stewart, 1965). Wilson (1988) studied the petroleum geology of the Warsaw Formation in Kiowa and Comanche Counties, Kansas utilizing subsurface mapping and core materials from dispersed parts of his study area. Wilson (1988) concluded that the distribution of oil fields is controlled primarily by structural closure and not by lateral variation in lithofacies.

The most detailed study of a lower Meramecian reservoir is that of Ebanks, et al. (1977). The Bindley Field reservoir interval was interpreted by Ebanks et al. (1977) to have been deposited as a muddy, bryozoan mound with significant relief above the seafloor, which was diagenetically altered to reservoir-quality rock by dolomitization of mud and subsequent leaching of the undolomitized, bryozoan skeletal calcite. While Ebanks et al. (1977) provided a valuable starting point for reservoir description, their generalized facies model provides insufficient detail to aid directly in developing exploration and/or production models of the reservoir. Newly available core materials and recent advances in carbonate stratigraphy, diagenesis, and reservoir geology warrant further study of the Bindley Field.

CHAPTER III

FIELD HISTORY

Bindley Field was discovered in May, 1972. By mid-1975, 33 wells had been completed as oil producers. Two additional wells were temporarily completed as oil producers in the 1980s for a combined total of 35 producing wells. The productive interval is Mississippian "Warsaw dolomite" at depths ranging from 4,600' to 4,700'. Wells are generally spaced on 40-acre locations. The total productive area has been approximately 1,360 acres. As of the end of 1989, 5 wells have been abandoned. In 1985, the principal field operator, Conoco, Inc., began a pilot waterflood by converting a single producing well to a water injector (Oasis #3 Deutsch, NW/4 SW/4, 34-21S-24W). In September, 1988, the central portion of the field was unitized (Figure 3) and a waterflood program was implemented. Two dry holes and seven former producing wells have been converted to water injectors in a peripheral waterflood pattern. Conoco, Inc. is currently monitoring the waterflood performance and is modifying the waterflood plan to improve performance as new data becomes available.

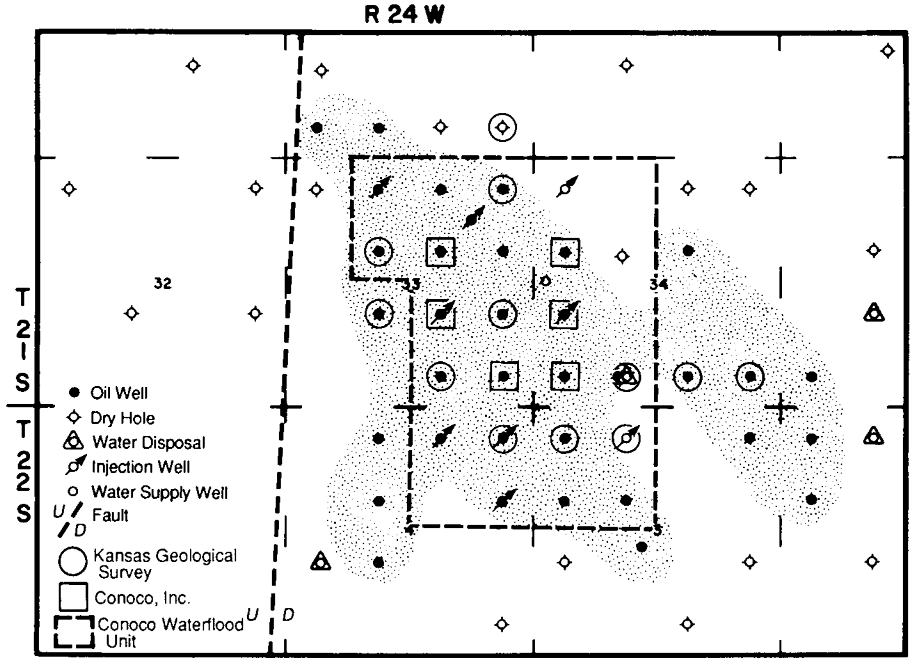

FIGURE 3- Distribution of available Mississippian cores in Bindley Field. Circles represent cores in the Kansas Geological Survey repository. Squares represent cores in the possession of Conoco, Inc. which were not available to Ebanks et al. (1977). The boundary of the Conoco waterflood unit is shown for reference, and the field area is indicated by the stipled background.

Cumulative field production, as of December, 1989 was 2,508,000 barrels of oil. Some individual wells have produced in excess of 200,000 barrels (e.g. Oasis Petroleum #1 Smith, SW/4 NW/4 34-T21S-R24W; 232,000 BO, 7/72-9/88). Cumulative oil production from the Conoco Unit through the time of unitization was 2,041,000 barrels, and an additional 61,600 barrels have been produced since unitization (through December, 1989). Cumulative water production in the Conoco Unit from September, 1973 through June, 1990 was approximately 4,700,000 barrels (water production data prior to the purchase of the Conoco Unit wells by Conoco, Inc. in September, 1973 and for wells outside the Conoco Unit are not available).

Cores of Mississippian strata were taken in 20 of the Bindley Field wells, of which 18 were available for this study. Six of those cores, which are held by Conoco, Inc. and are from wells located in the central portion of the field (Figure 3), were not available to Ebanks et al. (1977).

CHAPTER IV

GEOLOGIC SETTING

Regional Structural and Depositional Setting

Bindley Field is situated on the margin of the Hugoton Embayment of the Anadarko Basin. The Hugoton Embayment is a broad shelf extension of the northwestern portion of the Anadarko Basin, bounded on the northeast by the Central Kansas uplift, on the southwest by the Sierra Grande uplift, and on the northwest by the Transcontinental Arch (Figure 4). During early Meramecian time, the depositional setting of the Bindley Field area was likely that of a shallow, inner-shelf environment (Lane and De Keyser, 1980). It is probably reasonable to consider the inner Hugoton shelf at that time to have been a carbonate ramp with a distally steepened margin (in the sense of Read, 1985) to the south. Early and middle Mississippian rocks (Kinderhookian, Osagian, Lower Meramecian) are dominated by carbonate facies whereas later Mississippian rocks (Upper Meramecian, Chesteran) are increasingly dominated by siliciclastic sediments. Lower Meramecian rocks

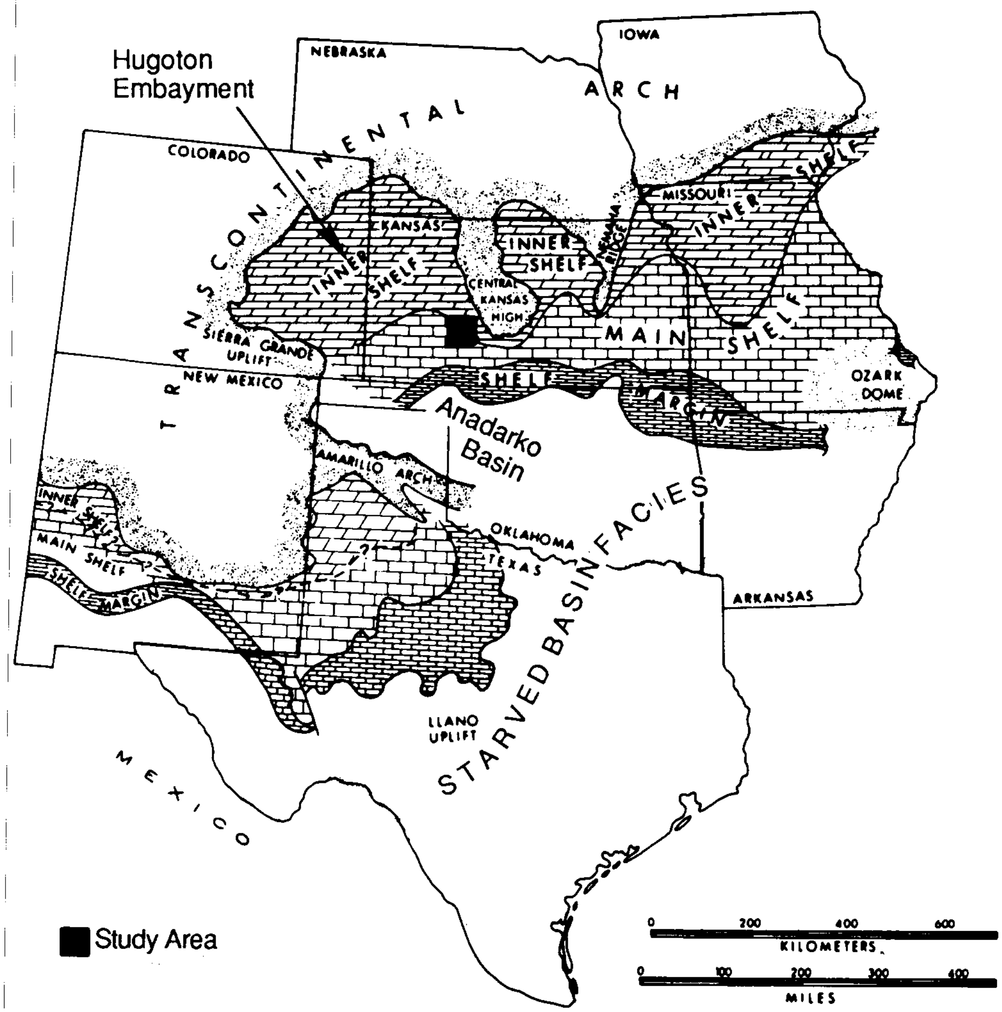

FIGURE 4- Distribution of early Mississippian depositional systems on the southeastern flank of the Transcontinental Arch. Study area is located within the inner shelf to main shelf tracts. (Modified from Lane and De Keyser, 1980)

(excluding the St. Louis Formation) are primarily dolostones with minor percentages of limestone.

Regional, pre-Pennsylvanian uplift resulted in the exposure and truncation of Mississippian through Cambro-Ordovician rocks overlying the Central Kansas uplift. This regional unconformity was subsequently transgressed by Pennsylvanian seas and overlain by Pennsylvanian sediments. The resultant pre-Pennsylvanian subcrop pattern is characterized by sinuous rock-unit belts surrounding the Central Kansas uplift with progressively older rock units subcropping toward the axis of the uplift (Figure 1). The Bindley Field is located within the subcrop of the lower Meramecian (Mississippian) Warsaw Formation.

Mississippian Stratigraphy

A generalized stratigraphic column representative of Mississippian strata in western Kansas is illustrated in Figure 5. The description of these stratigraphic units has been largely limited to lithostratigraphic criteria (Zeller, 1968; Merriam, 1963). Attempts to unify the lithostratigraphic terminology with the distribution of time-stratigraphic units (Goebel, 1966,1968) have yielded ambiguous results, especially in light of modern principles of sequence stratigraphy. Current stratigraphic usage

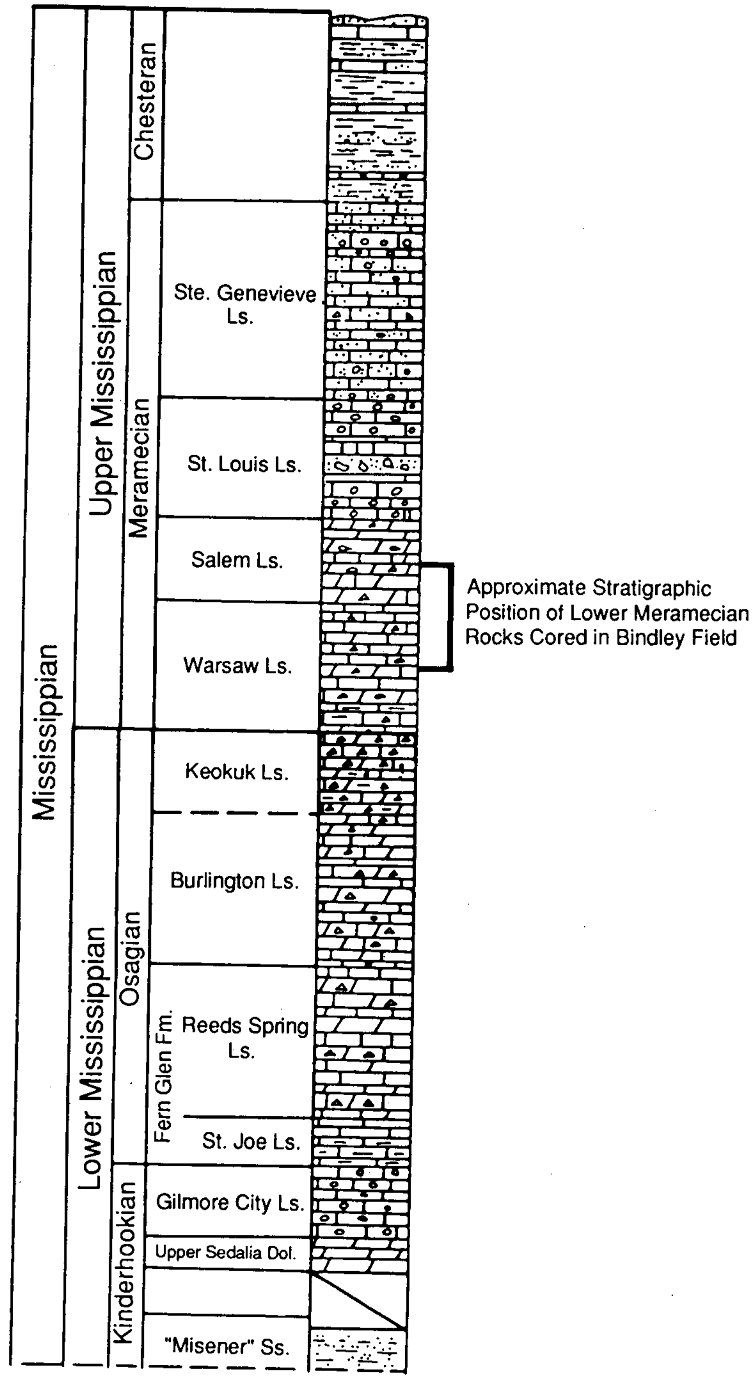

FIGURE 5- Generalized stratigraphic column of Mississippian rocks in western Kansas showing approximate stratigraphic position of Bindley Field reservoir rocks. (Modified from Goebel, 1968)

continues to rely on lithostratigraphic criteria to divide Mississippian units into generalized formations within the framework of larger-scale series (e.g. the Warsaw and Salem formations of the Meramecian series). These formation designations may not be strictly time equivalent throughout western Kansas and therefore do not provide an adequate framework within which to view smaller-scale sedimentary units and sedimentary processes.

Based on subsurface correlation of Mississippian units throughout a two-county region (Ness and Hodgeman Counties, Kansas; Figure 2) and corroboration with core materials from the Bindley Field, a new lower Meramecian stratigraphic framework is presented herein. The correlation is based on wells which penetrated the entire Mississippian section and a substantial portion of the Ordovician section. Based largely on gamma-ray log character and, secondarily on porosity/resistivity log character, discrete intervals of lower Meramecian rocks may be recognized throughout the correlation area. These intervals are generally separated by a relatively distinct increase in gamma-ray response and, as such, may represent time-stratigraphic events as opposed to simple lithologic change. The sedimentary basis for this division of intervals, as indicated by the Bindley Field core materials, and the implications for time-stratigraphic definition will be addressed in a later section.

The stratigraphic subdivision of lower Meramecian rocks proposed in this study is illustrated in Figure 6. The base of the Meramecian series is coincident with the top of the Osagian series. For the purposes of this study, the top of the "Osagian" series is selected to coincide with a gamma-ray marker which may be correlated regionally (i.e. at least within the two-county area). It is important to note that this horizon may not precisely correspond to the top Osagian as selected on the basis of lithologic criteria, biostratigraphic evidence, or oilfield usage. It is simply used as the most distinct reference horizon which is near that generally ascribed to the top of the Osagian series.

In ascending order beginning at the top of the Osagian reference, each distinct, overlying interval is designated as Meramec 1, Meramec 2, Meramec 3, etc., respectively, to the point of truncation at the basal Pennsylvanian unconformity. No attempt is made to differentiate these intervals in terms of the more commonly used formation names (e.g. Warsaw, Salem, etc.). However, Ebanks et al. (1977) stated that certain rocks in Bindley Field contain foraminiferal

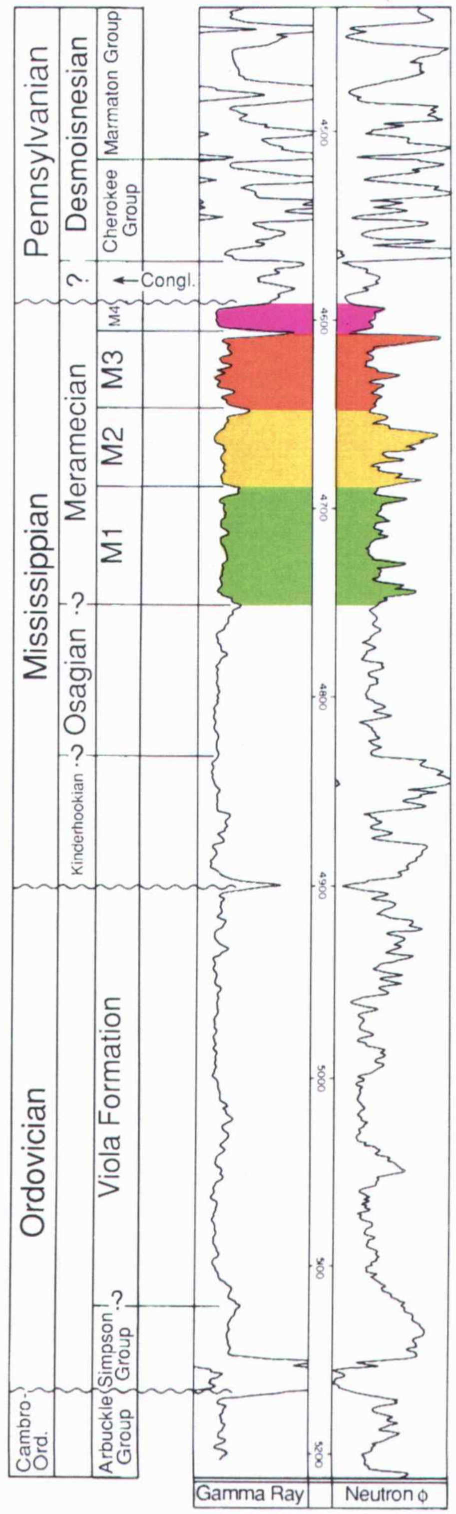

FIGURE 6- Type log for northwestern Hodgeman County, Kansas illustrating the division of lower Meramecian stratigraphic intervals utilized in this study (Kewanee Oil #2 Larkin; SE/4 NW/4 SE/4, 15-T22S-R25W; Hallet Field).

associations indicative of the Salem Formation (Figure 5), but ascribed the productive rocks in Bindley Field to the Warsaw Formation.

Regional correlation of the Meramec 1,2,3 and 4 intervals allows the construction of a detailed sub-Pennsylvanian subcrop map and the correlation of individual producing horizons. Figure 7 illustrates the sub-Pennsylvanian subcrop pattern in northwestern Hodgeman County. Coincident with the regional subcrop illustrated in Figure 1, the local subcrop pattern is consistent with uplift and truncation of progressively older intervals to the northeast. In addition, smaller-scale, pre-Pennsylvanian structural features are revealed.

The subcrop pattern is also evident in cross-section. Figures 8 (cross-sections HB-HB'; rear pocket) and 9 (cross-sections SB-SB'; rear pocket) illustrate dip and strike cross-sections, respectively, through northwestern Hodgeman County, which display the progressive truncation of lower Meramecian intervals at the basal Pennsylvanian unconformity. In each figure, two representations of the same cross-section are shown. The upper cross-section in each figure is a stratigraphic section (Figures 8A and 9A) using the base of the lowermost Cherokee limestone (Pennsylvanian; Desmoinesian series) as the datum (see Figure 6). To

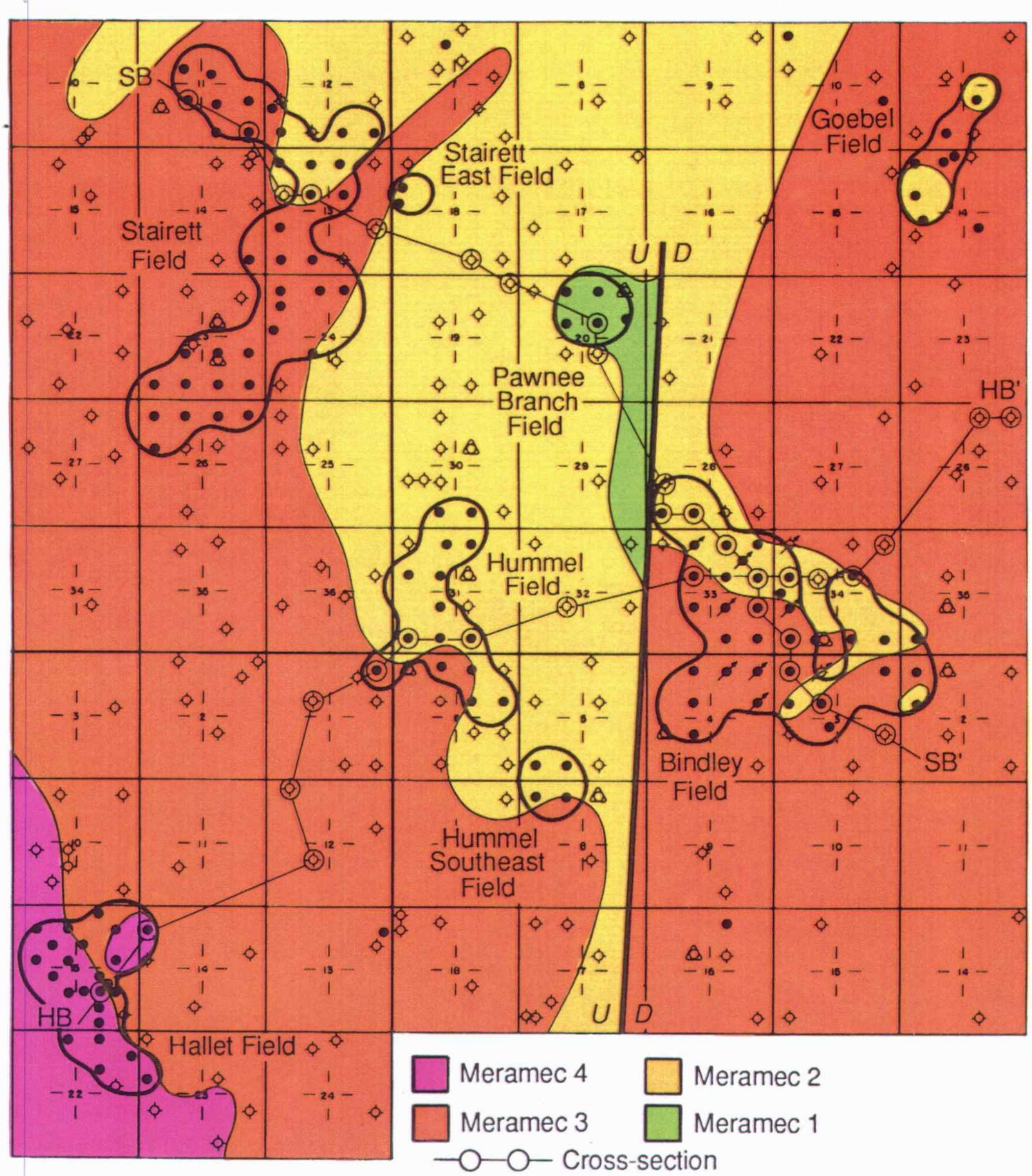

FIGURE 7- Sub-Pennsylvanian subcrop of lower Meramecian (Mississippian) stratigraphic intervals in northwestern Hodgeman County, Kansas illustrating the location of fields producing from lower Meramecian reservoirs. Hallet Field produces primarily from Meramec 4. Stairett, Hummel, Hummel Southeast, Bindley, and Goebel Fields produce principally from Meramec 2. Pawnee Branch Field produces from Meramec 1. Refer to Figures 8 and 9 for cross-sections HB-HB' and SB-SB', respectively.

the extent that the base of the lowermost Cherokee limestone was a relatively flat surface at the time of deposition, the stratigraphic section (upper cross-section) represents the approximate structural configuration of the lower Meramecian intervals at the time of Cherokee transgression (i.e. reflective of structure shortly after the close of the unconformity event). The lower cross-section in each figure is a structural section (Figures 8B and 9B) hung on a present subsea datum, reflecting the present structural attitude of the intervals.

Figure 8 (cross-section HB-HB'; rear pocket) demonstrates the relation of lower Meramecian intervals to the basal Pennsylvanian unconformity in the regional dip direction (NE-SW); from Hallet Field, to Hummel Field, and through Bindley Field. Figure 8 illustrates the progressive truncation of lower Meramecian intervals to the northeast through the Hummel Field, and a structural reversal between the Hummel and Bindley Fields (probable fault). The Meramec 2 interval is emergent at the unconformity over the crest of Bindley Field.

Figure 9 (cross-sections SB-SB'; rear pocket) illustrates the relation of lower Meramecian intervals to the basal Pennsylvanian unconformity in the regional strike direction (NW-SE); from Stairett Field, to Pawnee

Branch Field, through Bindley Field. Figure 9 demonstrates the progressive truncation of the Meramec 3 and Meramec 2 intervals approaching the Pawnee Branch Field from both the northwest (Stairett Field) and the southeast (Bindley Field). Stairett Field and Bindley Field produce primarily from the Meramec 2 interval on the flanks of the positive structural feature underlying Pawnee Branch Field, as the Meramec 2 interval approaches and emerges at the basal Pennsylvanian unconformity.

It is noteworthy that post-unconformity structural movement is generally an amplification of more subtle structure which existed at or shortly after the time of the close of the unconformity event, as demonstrated by the difference in structural attitude between the stratigraphic (Figures 8A and 9A) and structural (Figures 8B and 9B) cross-sections.

Recognition of this stratigraphic framework allows the assignment of specific productive intervals to each field. In doing so, it is evident that reservoirs develop discretely within each of these lower Meramecian intervals. For example, referring to Figures 7,8, and 9 for field locations, the Hallet Field produces primarily from the Meramec 4 interval; the Hummel, Bindley, and Stairett Fields produce primarily from the Meramec 2 interval; and the Pawnee Branch Field produces from the Meramec 1 interval. Each of these fields produce at a location where the productive interval is either exposed at the basal Pennsylvanian unconformity or is in close proximity beneath it.

CHAPTER V

GEOLOGY OF BINDLEY FIELD

Mississippian Subcrop

Bindley Field is situated where the Meramec 2 interval, the primary producing interval in the field, emerges from beneath the Meramec 3 interval at the basal Pennsylvanian unconformity (Figure 10). An erosional wedge of the Meramec 3 interval overlies much of the southwestern portion of the field. The progressive truncation of the Meramec 3 interval on the flanks of Bindley Field is evident in Figures 8 and 9. Three wells along the southwestern margin of the field were originally perforated in both the Meramec 2 and remnant Meramec 3 intervals. Four wells were originally perforated in the Meramec 3 interval only. The Meramec 3 producers were among the poorest producers in the field.

Within the Meramec 2 subcrop displayed in Figure 10, contour lines indicate the thickness of the Meramec 2 interval which has not been truncated at the basal Pennsylvanian unconformity (i.e. is preserved). The original thickness of the Meramec 2 interval, where it

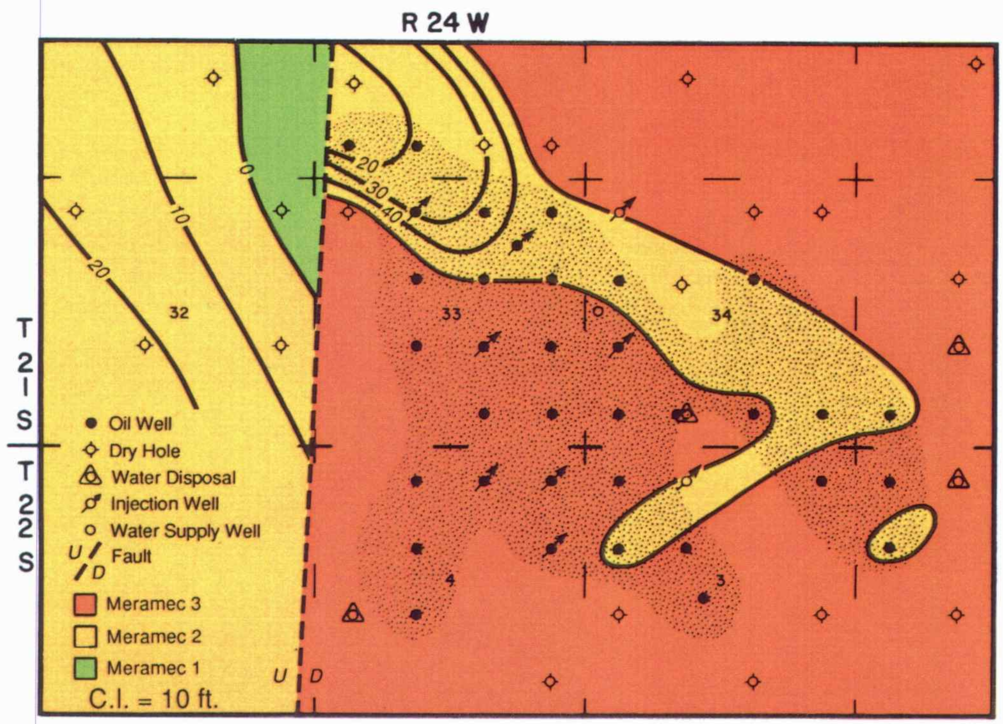

FIGURE 10- Pre-Pennsylvanian subcrop of lower Meramecian stratigraphic intervals in the Bindley Field area. Within the Meramec 2 subcrop, contour lines indicate the preserved thickness of Meramec 2 (i.e. not truncated at the basal Pennsylvanian unconformity). The average thickness of Meramec 2 where it is not truncated is 45-50 feet. Note the progressive truncation of the Meramec 2 on the northwestern end of the field approaching an inferred normal fault. The abrupt shift in subcrop pattern across the fault suggests that the fault originated prior to the end of the unconformity event.

has not been truncated, averages 45-50 feet. In the northwestern portion of the field a significant portion of the Meramec 2 interval has been truncated. This erosion is associated with a southeastward plunging antiform structure discussed below.

Mississippian Structure

Bindley Field is situated on a southeast trending antiform structure which is comprised of smaller-scale structural prominences as indicated by present structure on top of the Meramec 2 interval (Figure 11A). Present structural closure in the majority of the field ranges from 50-75 feet. The field is also situated on the downthrown side of an inferred north-south trending normal fault which borders the field on the west. The fault is indicated by the abrupt shift in the subcrop pattern (Figures 7 and 10), as well as by significant, present relief of up to 100 feet at the Mississippian level across the fault trend (Figure 11A)..

The evolution of the structure through time is evidenced by the significantly smaller closure surrounding the field at the time of the Cherokee transgression (i.e. shortly after the close of the unconformity event), as indicated by the paleostructure of the top of the Meramec 2 interval (Figure 11B). The

FIGURE 11A- Present subsea structure on top of Meramec 2. The field is situated on a southeast trending antiform structure which is comprised of smaller-scale structural prominences. True structural closure exceeds 50 feet in the majority of the field. The coincidence of the field boundary with structural closure indicates that structure is an integral component of trapping in Bindley Field. Over 100 feet of apparent offset at the Meramec 2 level is evident across the inferred fault bordering the field to the west. Contours are dashed in the northwestern portion of the field where the Meramec 2 is partially truncated by pre-Pennsylvanian subaerial exposure. The position of the "true" top of the Meramec 2 was restored by adding the estimated amount of removed section (see Figure 10). The field area is indicated by the stipled background.

FIGURE 11B- Paleostructure on top of Meramec 2. Paleostructure is represented by the isopach of the interval from the base of the lower Cherokee transgressive limestone to the top of Meramec 2 (refer to Figure 6). Assuming that the lower Cherokee limestone was deposited on a relatively flat surface, the isopach illustrates the approximate structural configuration of the top of Meramec 2 at the time of the Cherokee transgression (i.e. at the close of the unconformity event). The top of Meramec 2 in the northwestern portion of the field was restored in the same manner as described for Figure 11A. Comparison of Figure 11B to Figure 10 demonstrates that the structurally highest portion of the field (northwestern end) experienced the greatest truncation of the Meramec 2. The same antiform structure is evident as in Figure 11A but with closure of only 20-30 feet. The difference in structural development between paleostructure and present structure and the similarity in structural trend demonstrates that present structure is an amplification of pre-existing structure.

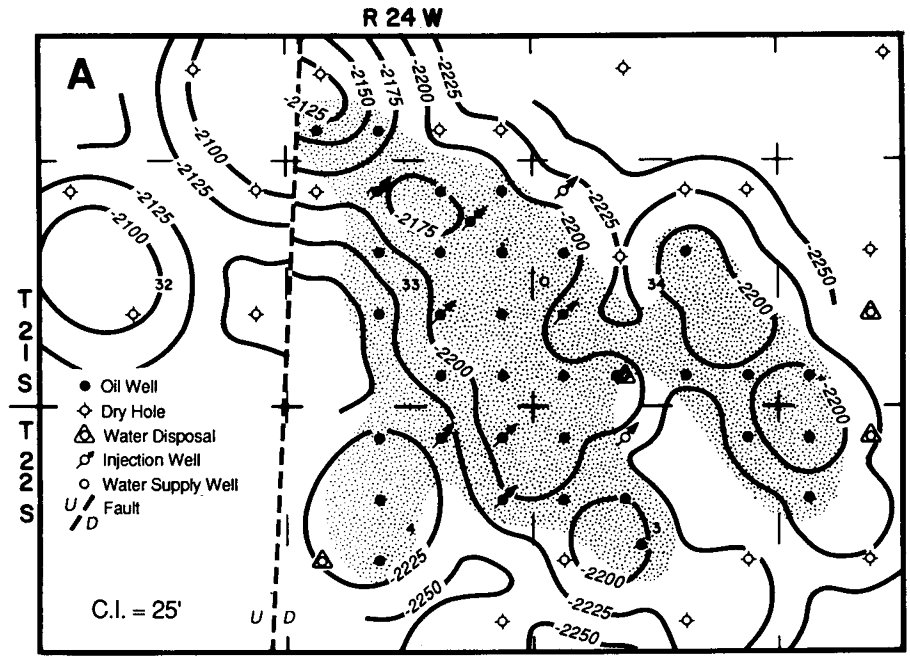
R 24 W
A
T 21 S
T 22 S
Oil Well
Dry Hole
Water Disposal
Injection Well
Water Supply Well
U D Fault
C.I. = 25'
32
33
34
4
3
-2100
-2125
-2150
-2175
-2200
-2225
-2250

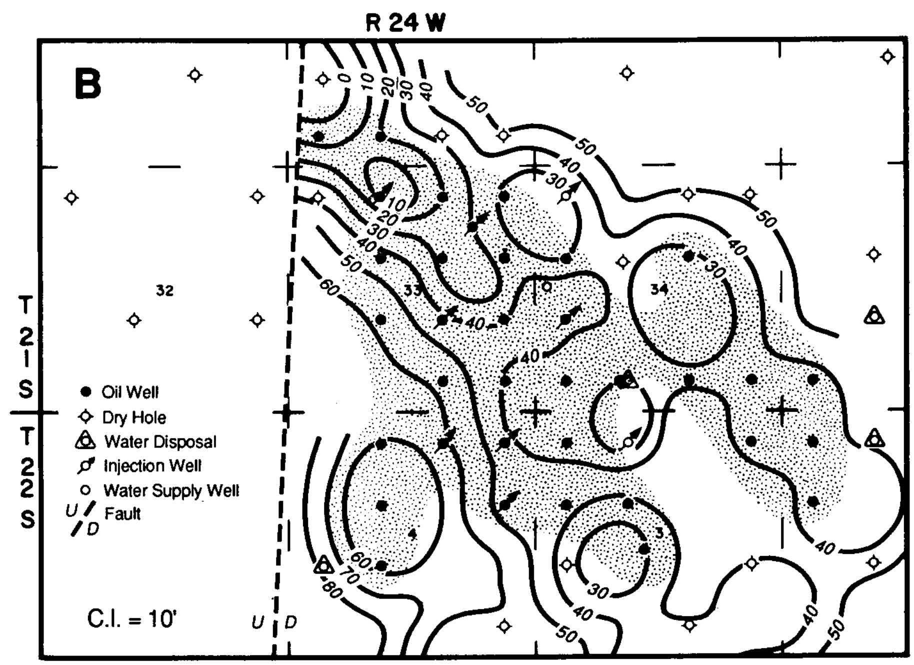
R 24 W
B
T 21 S
T 22 S
Oil Well
Dry Hole
Water Disposal
Injection Well
Water Supply Well
U D Fault
C.I. = 10'
32
33
34
4
3

paleostructural trend approximates that of Figure 11A, but structural closure in the majority of the field at this time only ranged from 20-30 feet, demonstrating that present structure is an amplification of pre-Pennsylvanian structure. The local structural prominences which comprise the overall antiform trend are also more evident on the paleostructure (Figure 11B) than on the present structure (Figure 11A).

The present configuration of the Mississippian erosional surface (Figure 12A) represents the present topographic expression of the Mississippian surface with an overprint of post-unconformity structural movement. The present highs on the erosional surface are delineated by prominent northwest-southeast trending lows, and by less prominent southwest-northeast trending lows (the contours have been drawn to accentuate these features). The trend of these lows is suggestive of preferential dissolution of exposed Mississippian rocks in quasi-orthogonal, sublinear trends which are probable fracture trends, and is consistent with observations of the configuration of the basal Pennsylvanian unconformity surface in other portions of the lower Meramecian subcrop as well as in the subcrop of the Cambro-Ordovician Arbuckle dolostones exposed over the Central Kansas uplift (Figure 1). The paleotopography of the Mississippian surface at the time of the Cherokee

FIGURE 12A- Present subsea "structure" on top of Mississippian. The top Mississippian datum represents the top of the uppermost in situ carbonate beneath the basal Pennsylvanian conglomerate (refer to Figure 6). Because this represents a disconformable erosional surface, the subsea configuration of this surface does not represent true structure, but represents the topography of the Mississippian erosional surface with the overprint of post-unconformity structural movement. Due to the effect of post-unconformity structural movement, the southeast-trending antiform feature is evident, especially over the central axis of the field. The field area is indicated by the stipled background.

FIGURE 12B- Paleotopography of the Mississippian unconformity. The paleostructure is represented by the isopach of the interval from the base of the lower Cherokee transgressive limestone to the top of the uppermost in situ carbonate beneath the basal Pennsylvanian conglomerate (refer to Figure 6). Assuming the lower Cherokee limestone was deposited on a relatively flat surface, the isopach indicates the approximate topographic expression of the Mississippian unconformity at the close of the unconformity event. Distinct NW-SE and NE-SW trending lows are evident (contours have been drawn to accentuate these linear features) which represent probable fracture trends.

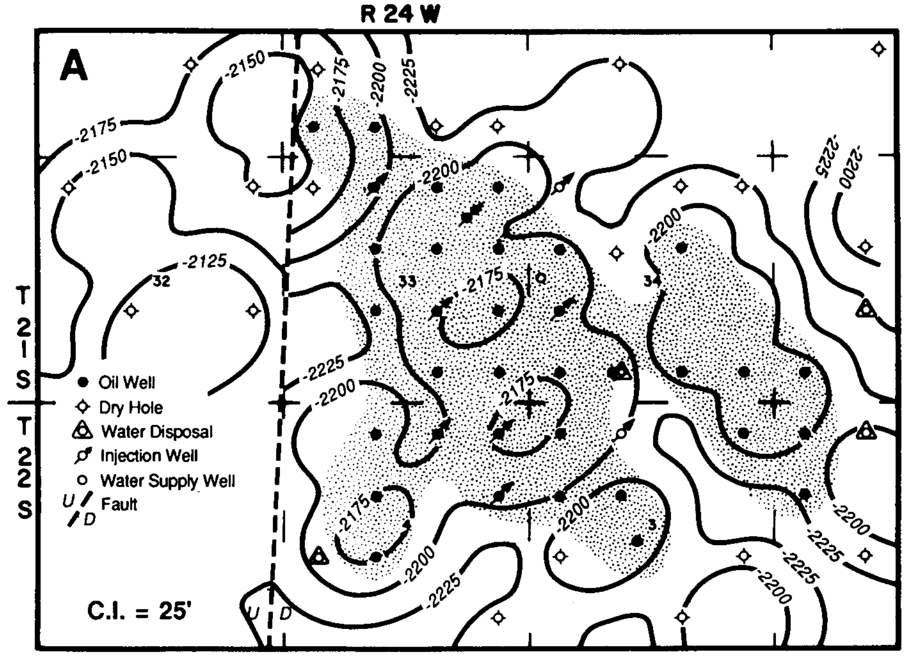
R 24 W
A
T 21 S
T 22 S
-2150
-2175
-2200
-2225
-2125
32
33
34
3
Oil Well
Dry Hole
Water Disposal
Injection Well
Water Supply Well
U D Fault
C.I. = 25'

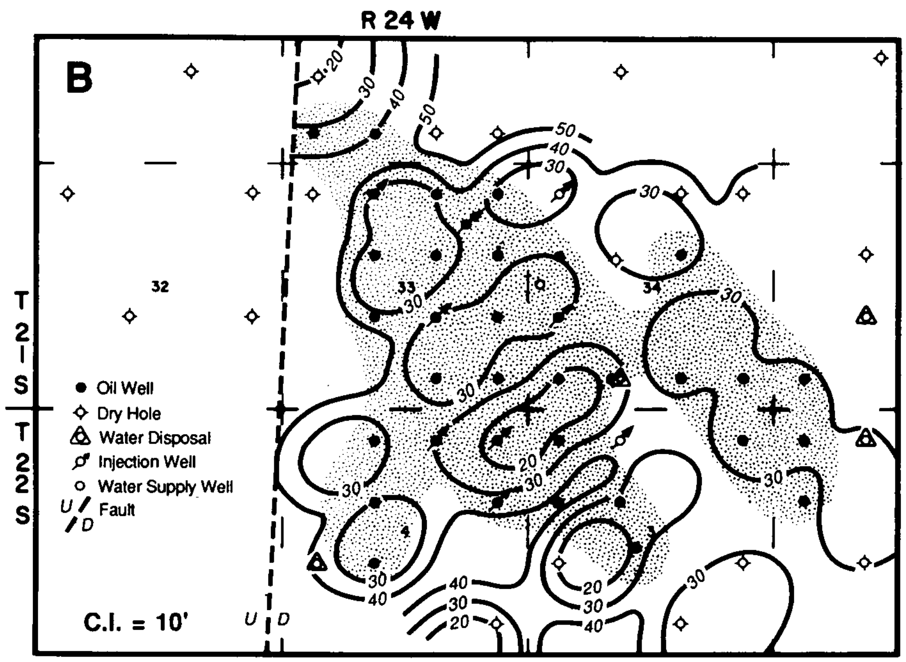
R 24 W
B
T 21 S
T 22 S
20
30
40
50
32
33
34
4
Oil Well
Dry Hole
Water Disposal
Injection Well
Water Supply Well
U D Fault
C.I. = 10'

transgression (Figure 12B), which does not include the overprint of post-unconformity structural movement, emphasizes the trends in the erosional (dissolution) lows.

Lithotypes

Bindley Field cores collectively sample the stratigraphic sequence from the lower portion of the Meramec 1 interval to the lower portion of the Meramec 3 interval. No single core encompasses this entire interval. Each core, with two exceptions, covers a significant portion of the Meramec 2 interval. The two exceptions include rocks from the lower Meramec 3 interval only.

Six distinct lithotypes are recognized and are numbered sequentially in ascending order of first occurrence. Three lithotypes (Lithotypes 1,2, and 4) contain subtypes, designated by sequential letter designations (i.e. Lithotypes 4A, 4B, 4C, 4D). Each lithotype, and most subtypes, represents a discernable rock type of probable environmental significance. The six lithotypes are listed below and, where applicable, the equivalent facies of Ebanks et al. (1977) is included in parentheses. Though Ebanks et al. (1977) recognized a similar number of lithotypes as in this study (five vs. six), they did not discern any subtypes.

Lithotype 1- Interlayered Organic Dolomudstone and Cherty Dolostone (Cherty dolomite facies)

Lithotype 2- Spiculitic Dolomudstone (Spicule dolomite facies)

Lithotype 3- Wavy Laminated, Argillaceous Dolomudstone (included in Cherty dolomite facies)

Lithotype 4- Echinoderm/Bryozoan Lithofacies (Bryozoan dolomite facies)

Lithotype 5- Argillaceous Dolomudstone/Dolomitic Shale (Conglomeratic shale facies)

Lithotype 6- Breccia (Breccia facies)

Lithotype 1- Interlayered Organic Dolomudstone and Cherty Dolostone

Description. Lithotype 1 (Figure 13) consists of interlayered medium brown, organic-rich, slightly argillaceous dolomudstone (Lithotype 1A) and tan to light brownish gray, spiculitic, cherty dolostone (Lithotype 1B). Individual layers range in thickness from one to four inches. Contacts between alternating layers range from sharp, planar (or concavo-convex) to contorted and burrowed. The most distinctive features of Lithotype 1 are alternating color banding (Lithotypes 1A vs. 1B; Figure 13A), the occurrence of white and light gray chert nodules in Lithotype 1B (Figure 13A),

FIGURE 13- Core and Thin-Section Photographs of Lithotype 1.

A) Core Photograph of Lithotype 1 illustrating the contrast between Lithotype 1A (medium brown, organic dolomudstone) and Lithotype 1B (light brown, cherty dolostone). Contact between Lithotype 1A and 1B is sharp. Lithotype 1A contains chalcedony and quartz-lined geodes (G) whereas Lithotype 1B contains abundant silicified, sponge spicule concentrations (S) and sparse, solid chalcedony/quartz nodules (C). Scale bar is 1 cm. Oasis #1 Deutsch (NE/4 SE/4, 33-21S-24W), 4,691-92'.

B) Core photograph of chalcedony and quartz-lined geodes in Lithotype 1A. Silicified spicule concentrations in Lithotype 2B can be seen at top and bottom of photo. Scale bar is 1 cm. Oasis #1 Deutsch (NE/4 SE/4, 33-21S-24W), 4,688-89'.

C) Thin-section photomicrograph of Lithotype 1A dolomudstone exhibiting bimodal fabric. Larger rhombs display euhedral cores which are darker than the surrounding rims. Disseminated dark brown material is organic matter. Scale bar is 100 microns. Oasis #1 Deutsch (NE/4 SE/4, 33-21S-24W), 4,680.5'.

D) Thin-section photomicrograph of amorphous, semi-opaque, organic material (O) in Lithotype 1A. This material is typically oriented parallel to bedding and is commonly contorted around dolomite crystals. The opacity decreases toward the margins and on top of dolomite crystals, giving the appearance of a fluid phase. The inclusions are interpreted as bitumen. Scale bar is 100 microns. Oasis #1 Deutsch (NE/4 SE/4, 33-21S-24W), 4,680.5'.

E) Thin-section photomicrograph of silica-cemented spicule concentration in Lithotype 1B. Brown chalcedony cement (C) surrounds chert-cemented molds and pseudomorphs of monaxon sponge spicules. Note the centered pseudomorph of a spicule axial canal (S). Scale bar is 100 microns. Plane light. Oasis #1 Deutsch (NE/4 SE/4, 33-21S-24W), 4,686.2'.

F) Thin-section photomicrograph of the same view as Figure 13E in reflected light. Pseudomorphs of former sponge spicules are more evident in reflected light. Scale bar is 100 microns. Oasis #1 Deutsch (NE/4 SE/4, 33-21S-24W), 4,686.2'.

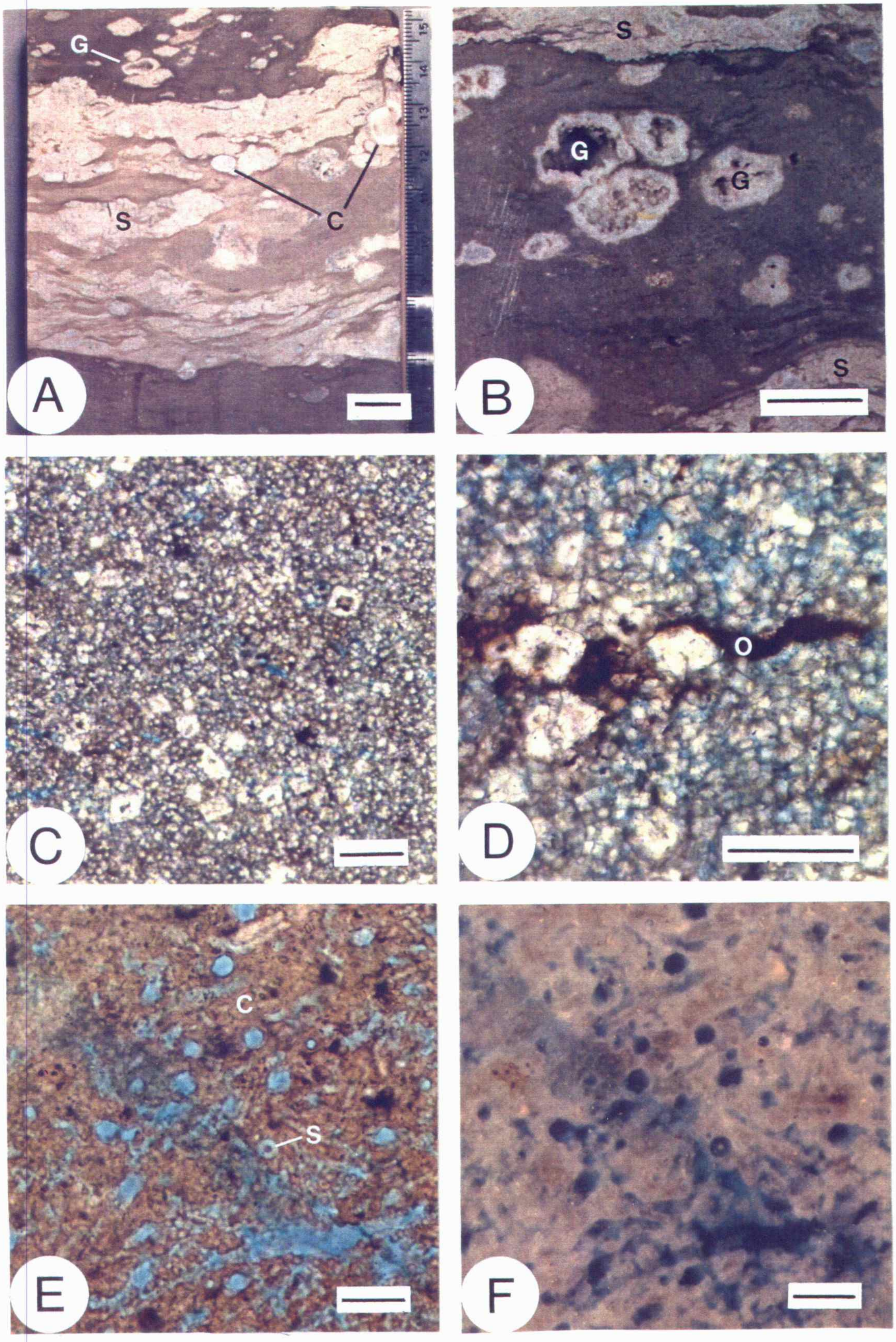
G
S
C
A
S
G
G
S
B
C
O
D
C
S
E
F

and the presence of silica-lined geode structures (Figure 13B) in Lithotype 1A. Lithotype 1 is limited to the lower portion of the Meramec 1 interval.

The dolomudstone of Lithotype 1A contains sparse monaxon sponge spicules and/or silica-cemented spicule molds and a small volume of detrital clay (generally less than 5% of matrix volume). Based on petrographic character (fibrous crystal habit, yellowish birefringence) and X-ray diffraction patterns, the clay is composed principally of illite. Disseminated, subangular quartz silt grains (20-50 micron diameter) comprise less than one percent of matrix volume. Dolomite fabric exhibits bimodal character with 30-50 micron, subhedral to euhedral dolomite rhombs dispersed in a matrix of 5-20 micron, subhedral to euhedral dolomite (Figure 13C). The larger rhombs commonly contain a rhombic core which is darker and more inclusion-rich than the outer rim. Abundant reddish brown, semi-opaque, amorphous inclusions which occur in elongate and contorted form between dolomite crystals are probable bitumen (Figure 13D). These inclusions and the presence of fine organic matter contribute to the rich brown color of the dolomudstone. Fine, disseminated pyrite is a minor constituent and is frequently observed as a replacement of the core of larger dolomite crystals. Pyrite also occurs as a replacement of the amorphous organic inclusions. Compacted horizontal burrow traces of one millimeter or less in diameter are present. Randomly dispersed geodes of less than 1 centimeter in diameter and lined by chalcedony and quartz are abundant. These geodes also occur in discrete, horizontal layers within and near the top of Lithotype 1 intervals. The chalcedony and quartz contain abundant, lath-like to irregular inclusions of anhydrite.

The cherty dolostone of Lithotype 1B contains abundant monaxon sponge spicules, spicule molds, and silica cemented spicule molds (Figure 13A). Dolomite fabric is similar to that of Lithotype 1A (i.e. bimodal, same size ranges). Large burrows one to two centimeters in diameter within Lithotype 1B commonly disrupts the contact between Lithotypes 1A and 1B. Many burrows are selectively silicified if filled with spicules. Small, horizontal burrow traces of approximately one millimeter in diameter are common. White to light gray, irregularly-shaped "chert" nodules are abundant and distinguish Lithotype 1B from Lithotype 1A. Petrographic examination reveals that these nodules are typically chalcedony and chert-cemented, grain-supported concentrations of spicules (Figures 13E, 13F). The margins of the silicified nodules typically contain bimodal dolomite. Areas surrounding the chert nodules are dolomudstone and contain fewer spicules and/or chalcedony-cemented spicule molds. Chert nodules display clusters of preferentially aligned spicules (or cemented spicule molds). Chert nodules commonly contain fractures cemented by chalcedony and/or quartz. In addition to the chert nodules, small chalcedony/quartz nodules containing abundant inclusions of anhydrite are present. They are of similar size to the chalcedony/quartz geodes of Lithotype 1A, but lack hollow centers and are much less abundant.

Interpretation. Lithotype 1A is interpreted to represent sedimentation in a quiet, evaporitic, lagoonal environment. Deposition in such an environment is indicated by the abundance of replaced evaporites (chalcedony/quartz nodules) which do not occur in the immediately overlying sediment, the highly restricted fauna, the presence of an apparent elevated concentration of organic matter, the paucity of vertical burrowing and bioturbation, and the presence of detrital clay. Chalcedony/quartz nodules and geodes are interpreted to be replaced, displacive evaporite nodules with characteristics similar to those described by Chowns and Elkins (1974). Geodes result from replacement of the periphery of the evaporite nodule followed by dissolution of the unreplaced interior evaporite, and solid nodules result from complete replacement and/or cementation of precursor geodes with quartz (for more detailed discussion of chalcedony/quartz nodules, refer to Lithotype 2 below).

The interlayers of Lithotype 1B are interpreted to represent periodically deposited storm layers from adjacent tracts of Lithotype 2A. The repeated alternation of layers of Lithotypes 1A and 1B, the sharp contacts between alternate layers (with rare evidence of scour) and the marked contrast in sediment type are consistent with episodic introduction of "foreign" sediment. The light color and preferential burrowing of Lithotype 1B reflect the oxygenated character of the storm-deposited sediments. The mud-free, grain-supported concentrations of preferentially aligned spicules within a spiculitic dolomudstone fabric probably represent storm-graded layers and/or sponge fragments deposited within a muddy host sediment.

Ebanks et al. (1977) referred to these rocks as the "cherty dolomite facies" and interpreted that they were deposited in a supratidal environment. No genetic distinction, however, was made by Ebanks et al. between chalcedony/quartz nodules and chert nodules. Both types of silica structure were interpreted by Ebanks et al. to be silica-replaced evaporites. Their supratidal interpretation was based on the interpretation of chert nodules as replaced evaporites and the structural similarity of the chert nodules to modern supratidal evaporite structures. Other sedimentary structures which they noted (e.g. curled dolomite laminae, wavy-interlaminated dolomite and shale, scoured bedding surfaces) are either non-diagnostic or bear only superficial resemblance to supratidal structures.

Lithotype 2- Spiculitic Dolomudstone

Description. In general, Lithotype 2 is a tan to light greenish gray dolomudstone with monaxon sponge spicules, spicule molds, or molds cemented by calcite or chalcedony as the dominant skeletal constituent. Spicules may be dispersed or concentrated in wispy layers which, when represented by molds, are typically oil stained. Subordinate concentrations of pelmatozoan and fenestrate bryozoan fragments occur in some layers. Skeletal concentrations range from the mudstone limit of 10% grains (Dunham, 1962) down to negligible amounts. A vaguely pelleted fabric can be seen in thin section. Dolomite fabric is bimodal, with 30-50 micron, subhedral to euhedral rhombs dispersed in a matrix of 5-20 micron, subhedral to euhedral dolomite. The larger rhombs often display euhedral cores which are darker and more inclusion rich than the enclosing rims.

The variety of Lithotype 2 rocks necessitates its subdivision into two subordinate lithofacies.

Lithotype 2A occurs in the upper portion of the Meramec 1 interval and Lithotype 2B occurs as thin, laterally continuous layers within the Meramec 2 interval. Lithotype 2A (Figure 14A) is characterized by a very light tan color, graded layers, and amorphous chert structures. Small, horizontal burrow traces are abundant (Figure 14B). Larger, vertical or sinuous burrow traces are much less abundant. Thin, planar laminations and short, vertical cracks which terminate at a common horizon are observed rarely.

Graded layers of skeletal grains (Figure 14C) are common in Lithotype 2A. These layers typically display a sharp, scoured contact with underlying mudstone, overlain by grain-supported sediment which grades vertically to spiculitic dolomudstone. Skeletal grains in the lower portions of graded layers are commonly pelmatozoan and fenestrate bryozoan fragments. Layers range from approximately 2 to 8 inches in thickness and are commonly observed in a regularly repeated vertical sequence.

Lithotype 2B (Figure 14D) is characterized by a light brownish gray to greenish gray color, admixtures of small bryozoan and echinoderm grains, indistinct burrow mottling, and may contain thin (up to a few centimeters), gradational interlayers of greenish gray, argillaceous dolomudstone (Lithotype 5). Small,

FIGURE 14- Core and Thin-Section Photographs of Lithotype 2.

A) Core photograph of Lithotype 2A. Amorphous chert zones (A) and small, horizontal burrow traces (H) are evident. Scale bar is 1 cm. Oasis #1 Deutsch (NE/4 SE/4, 33-21S-24W), 4,672-73'.

B) Core photograph of horizontal burrow traces (H) in Lithotype 2A. Scale bar is 1 cm. Oasis #1 Deutsch (NE/4 SE/4, 33-21S-24W), 4,673-74'.

C) Core photograph of successive graded layers in Lithotype 2A. Graded layers exhibit a scoured base (underscored by black lines) and upward gradational, muddier fabric. Clasts in the base of graded layers are commonly echinoderm and bryozoan bioclasts and sponge spicules. Scale bar is 1 cm. Oasis #1 Deutsch (NE/4 SE/4, 33-21S-24W), 4,670-71'.

D) Core photograph of Lithotype 2B. Vague burrow mottling, indicated by color mottling, is characteristic of Lithotype 2B. Scale bar is 1 cm. Oasis #2 Deutsch (NW/4 SE/4, 33-21S-24W), 4,620-21.

E) Amorphous chert zone (A) in Lithotype 2A which crosscuts sedimentary features. Margins of the chert zone are rounded and sharply defined. Dark blotches bordering the chert zone are concentrations of oil-stained spicule molds. Scale bar is 1 cm. Oasis #1 Deutsch (NE/4 SE/4, 33-21S-24W), 4,666-67'.

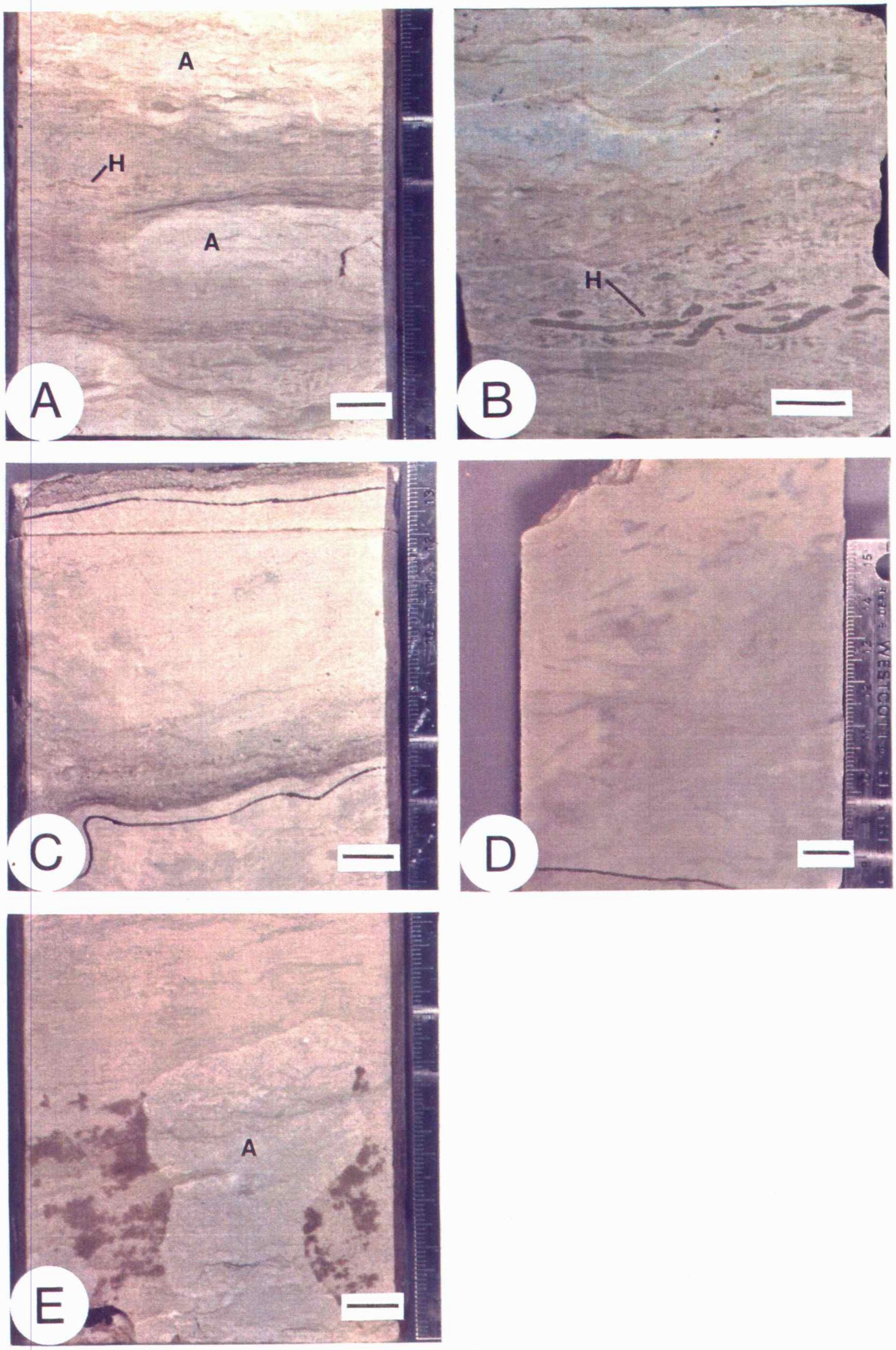
A
H
A
A
B
H
C
D
WESTCOTT
E
A

horizontal burrow traces, distinct from the vague burrow mottling, are most evident in the argillaceous material. Chalcedony/quartz nodules are most frequently observed in Lithotype 2B. Calcite-cemented vertical fractures are also common in Lithotype 2B.

Two types of silica structures are present in Lithotype 2: 1) amorphous chert zones (Lithotype 2A) and 2) well-defined, chalcedony/quartz nodules and geodes (Lithotype 2B). The zones of amorphous chert are white to medium gray in color with sharp, smoothly curved boundaries (Figure 14E). Shape ranges from horizontally digitate to amorphous. Sedimentary fabrics pass through the silicified areas without interruption indicating that the silicified areas are not burrows. Concentrations of oil-stained spicule molds commonly surround the silicified areas (Figure 14E). In some cases, it is evident that a grain-rich, skeletal layer was preferentially silicified; however, in the majority of cases no such skeletal layer is evident.

The well-defined, chalcedony/quartz nodules and geodes are distinctly different from the amorphous chert structures. Both solid and hollow (geodal) nodules occur in three morphologic forms: 1) as horizontal layers of vertically elongate nodules (Figure 15A); 2) as horizontal layers of isolated or laterally coalescing, enterolithic, subround nodules (Figure

FIGURE 15- Core and Thin-Section Photographs of Lithotype 2.

A) Core photograph of vertically elongate chalcedony/quartz nodule layer in Lithotype 2B. Layer exhibits a sharp contact above and below with enclosing sediment. Dark blotchy areas below the nodule layer are concentrations of oil-stained spicule molds (M). Black line below nodule layer is artificial. Scale bar is 1 cm. Oasis #1 Walter (NW/4 NW/4, 3-22S-24W), 4,679-80'.

B) Core photograph of chalcedony/quartz nodule layer in Lithotype 2B comprised of laterally coalescing, subround nodules. Scale bar is 1 cm. Oasis #2 Deutsch (NW/4 SE/4, 33-21S-24W), 4,649-50'.

C) Core photograph of isolated, subround chalcedony/quartz nodules in Lithotype 2B. Scale bar is 1 cm. Oasis #1 Smith (SW/4 NW/4, 34-21S-24W), 4,647-48'.

D) Thin-section photomicrograph of the interior of a chalcedony/quartz nodule (geode) which has been cemented with calcite. Euhedral quartz (Q) lines the interior of the geode. A large, inclusion-free, euhedral calcite crystal (C) has partially grown into the void leaving open pore space (P). The light areas at the edge of the calcite crystal represent removal of the crystal edge during thin section preparation. The dolomudstone encasing the nodule (M) is evident at the edge of the photo. Scale bar is 100 microns. Oasis #1 Deutsch (NE/4 SE/4, 33-21S-24W), 4,645.4'.

E) Thin-section photomicrograph of fitted fragments of dolomudstone which occur between vertically elongate chalcedony/quartz nodules. Quartz (Q) containing anhydrite inclusions occurs in the openings between fragments. Scale bar is 100 microns. Oasis #1 Everton (SW/4 SE/4, 34-21S-24W), 4,677.3'.

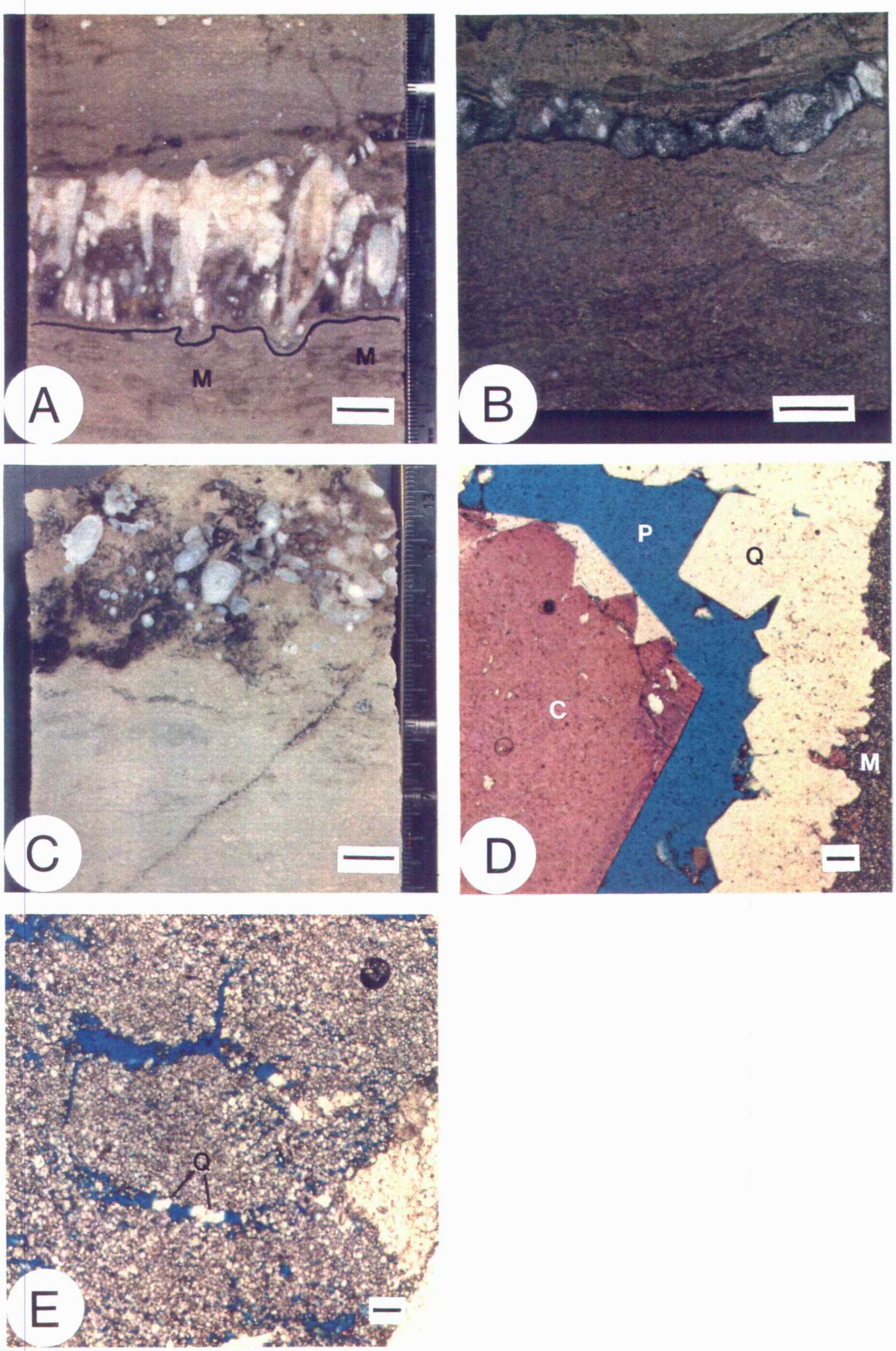
A
M
M
B
C
D
P
Q
C
M
E
Q

15B); and 3) as isolated subround nodules (Figure 15C). The isolated nodules and layers of subround nodules were previously noted in Lithotype 1A where geodal forms predominate. Vertically elongate nodules are subround in cross-section and coalesce laterally. Internodule areas in the horizontally layered forms (vertically elongate and enterolithic) commonly contain small, angular to subangular fragments of dolomudstone which may display a fitted fabric (Figure 15E). Interfragment voids commonly contain isolated patches of quartz which contain relict inclusions of anhydrite. Remaining void space between nodules and the dolomudstone fragments (if present) is typically cemented with poikilotopic or coarse, equant calcite. Dolomudstone enclosing the nodules and nodule layers is commonly spicule-moldic, and sediment is deformed around the isolated nodules.

Silica within nodules is generally characterized by alternating zones of spherules, radiating blades, or fans of chalcedony, and mosaic quartz. The term "chalcedony" as used with regard to these nodules includes fibrous forms of quartz which typically display a brown color in transmitted light, and is inclusive of quartzine and lutecine as described by Milliken (1979). Nodules are also observed which consist solely of a single silica phase.

Four observations indicate that the nodules are replaced anhydrite structures. First, chalcedony and quartz contain abundant lath-like to blocky inclusions of anhydrite with the greater concentration in quartz crystals (Figures 16A, 16B). Inclusions display rounded, diffuse edges, and adjacent inclusions commonly exhibit the same optical orientation. Secondly, quartz crystals which contain anhydrite inclusions commonly exhibit a sweeping extinction characteristic of quartz which has replaced evaporite minerals (Milliken, 1979). Third, as reported by Ebanks, et al. (1977), the chalcedony exhibits length-slow character which has been construed as evidence of chalcedony replacement of evaporite minerals (Folk and Pittman, 1971). Lastly, pseudomorphs of bundles or rosettes of laths of probable former evaporite minerals are also evident. Centers of some nodules in Lithotype 2B which were once hollow are cemented with coarsely crystalline calcite (Figure 15D), ferroan baroque dolomite, mosaic quartz, or banded chalcedony. Where carbonate minerals fill the center of nodules, the carbonate surrounds euhedral quartz terminations and is inclusion-free, indicating that the carbonate is a void-filling cement rather than a replacement of anhydrite. Mosaic quartz and banded chalcedony in the center of some nodules are inclusion-free whereas quartz and/or chalcedony comprising the

FIGURE 16- Core and Thin-Section Photographs of Lithotypes 2 and 3.

A) Thin-section photomicrograph of a euhedral quartz crystal (Q) bordering pore space (P) in the interior of a chalcedony/quartz nodule. Lithotype 2B. Plane light. Scale bar is 100 microns. Oasis #1 Everton (SW/4 SE/4, 34-21S-24W), 4,677.3'.

B) Same view as in Figure 16A in cross-polarized light. Quartz contains abundant lath-shaped inclusions of anhydrite (A). Scale bar is 100 microns. Oasis #1 Everton (SW/4 SE/4, 34-21S-24W), 4,677.3'.

C) Core photograph of Lithotype 3. Wispy shale partings (S) and irregularly shaped chalcedony/quartz nodules (N) are characteristic of Lithotype 3. Scale bar is 1 cm. Oasis #6 Deutsch (SW/4 SW/4, 34-21S-24W), 4,686-87'.

D) Core photograph of swarms of horizontal burrows (H) with oxidized halos in Lithotype 3. The localization of the burrows may represent a burrowed layer of oxygenated sediment (e.g. a storm layer of LIthotype 1B). Scale bar is 1 cm. Oasis #6 Deutsch (SW/4 SW/4, 34-21S-24W), 4,687-88'.

E) Core photograph of laterally coalescing chalcedony/quartz nodules (N) within organic-rich dolomudstone in Lithotype 3. Scale bar is 1 cm. Oasis #1 Schauvliege (SE/4 NW/4, 33-21S-24W), 4,710-11'.

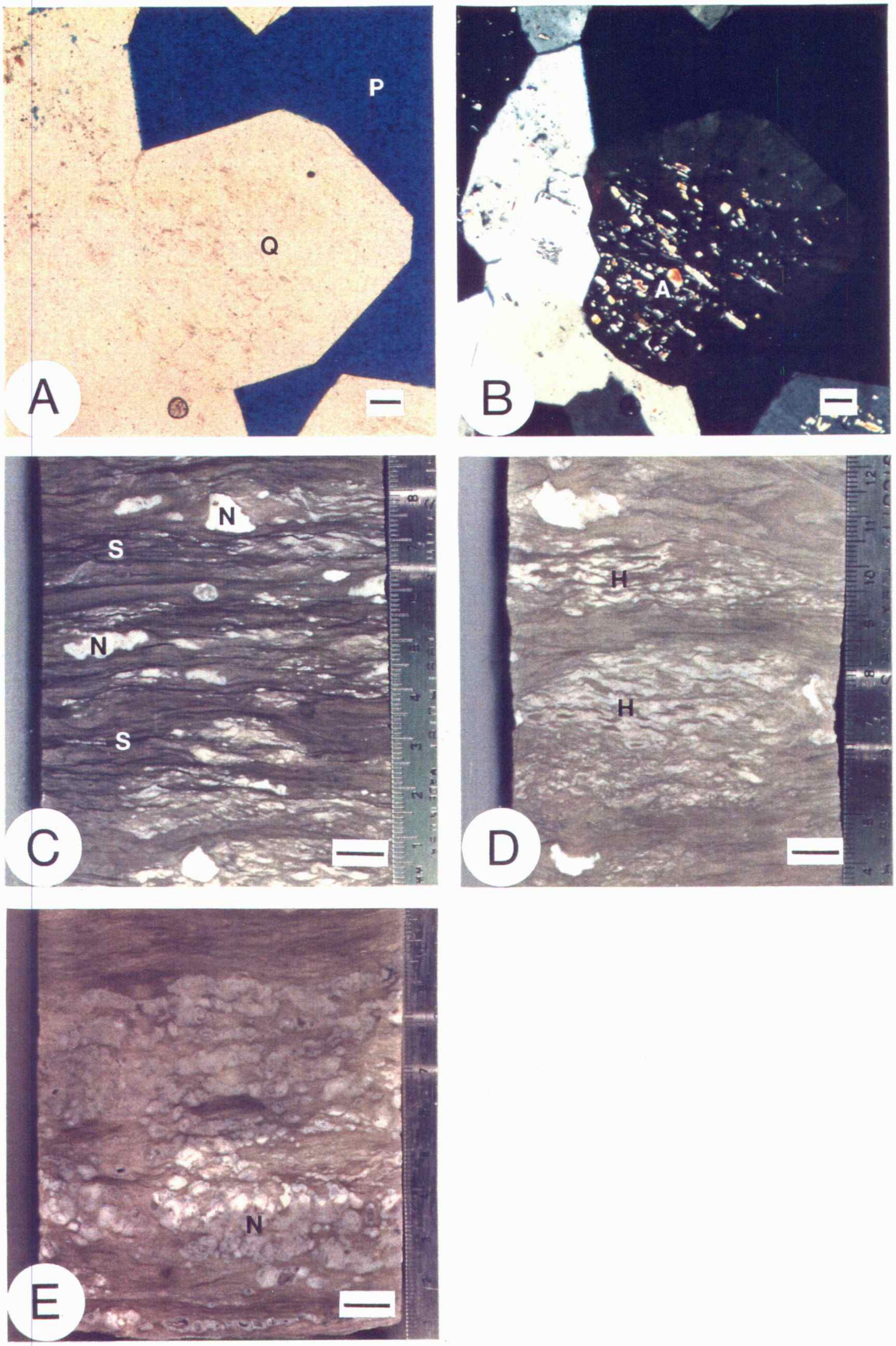
P
Q
A
A
B
N
S
N
S
C
H
H
D
N
E

perimeter of the nodule contain abundant inclusions. The inclusion-free quartz does not exhibit sweeping extinction. These characteristics indicate that the inclusion-free silica is a void-filling phase.

The chalcedony/quartz nodules are not distributed uniformly or randomly within Lithotype 2B, but typically are concentrated in discrete horizons within, or near the top of Lithotype 2B units. All three forms do not always occur in the same unit.

Interpretation. Lithotype 2A is interpreted to represent deposition in a restricted, oxygenated, lower intertidal environment with periodic episodes of storm scouring and sedimentation. The highly restricted fauna and the predominance of small, horizontal burrows argue for a stressed environment. The lack of clearly defined algal laminations, mud cracks, fenestral or birdseye structures, root zones, oxidized horizons, or flat pebbles exclude any supratidal influence; however, a peritidal influence is possible. Certain features, such as flat, millimeter-scale laminations (Hardie, 1977)and short vertical fractures which terminate at a common level (mud cracks?) may be construed as intertidal zone indicators. A very light sediment color is also generally associated with intertidal sediments (Shinn, 1983), and attests to oxidized conditions within the sediment during deposition. The amorphous chert structures are interpreted to be products of local redistribution of dissolved spicule silica which preferentially replaced concentrations of grain-supported skeletal fragments, and silicified spiculitic mudstone in association with fluid migration/diffusion zones.

Lithotype 2B is interpreted to represent deposition in a low energy, subtidal environment which ranged from restricted to evaporitic. The low diversity fauna of small forms and the presence of clay minerals attest to restricted, low energy conditions. The cause of restriction is not apparent but may relate to shelf-wide restriction caused by buildup of offshore barrier complexes or by the lowering of relative sea level across broad expanses of low-angle, shallow shelf which dampen wave and tidal mixing (Irwin, 1965).

The occurrence of chalcedony/quartz nodules, interpreted as replaced evaporites, within the upper portions of Lithotype 2B occurrences further indicates a restricted, evaporitic environment. Vertically aligned forms of evaporite minerals are currently regarded as indicative of precipitation of single crystals of gypsum in subaqueous evaporitic settings at or slightly below the sediment/water interface (Warren and Kendall, 1985). The observation that the vertically elongate chalcedony/quartz nodule layers are horizontal and have sharp contacts with underlying and overlying sediment supports this interpretation. The presence of fitted fragments of spiculitic sediment between vertically elongate nodules may indicate that the sediment was partly lithified at the time of evaporite crystallization and that the crystals grew partially within the sediment. Interfragment quartz which contains anhydrite inclusions indicates that fragmentation occurred prior to or concurrent with evaporite emplacement. Subaerial exposure, however, is doubtful because it is unlikely that the vertically aligned nodule layers would have remained upright and aligned if subjected to periodic exposure. The poikilotopic or coarse, equant calcite in internodule areas may fill void space created by dehydration of gypsum to anhydrite.

Layers of laterally coalescing subround nodules (enterolithic form) and isolated subround nodules are indicative of displacive evaporite growth within sediment (Warren, 1989). The observed sediment deformation surrounding isolated chalcedony/quartz nodules is consistent with displacive growth; however, post-depositional compaction of mud around an evaporite nodule may cause a similar effect. The lack of features indicative of periodic subaerial exposure or supratidal conditions supports a subtidal origin for these replaced evaporites. Enterolithic layers and isolated nodules are interpreted to have been emplaced below the sediment-water interface during periods of evaporitic conditions in the overlying water mass.

The general interpretation of these silica nodules and geodes as replaced evaporites is consistent with the interpretation of similar nodules from Meramecian rocks in other areas of the U.S. (Chowns and Elkins, 1974; Milliken, 1979; Maliva, 1987). However, these authors have proposed modes of formation of the evaporite nodules which are different from the subtidal interpretation of this study. Chowns and Elkins (1974) considered such nodules to have been emplaced within sediment in a supratidal environment, but acknowledged that no sedimentary features diagnostic of supratidal environments were observed other than the presence of replaced evaporite minerals. Maliva (1987) proposed a mechanism of evaporite nodule emplacement in sediments buried at shallow depths (tens of meters) in association with reflux dolomitization during a later period of evaporitic surface conditions; however, the reasons for dismissing a peritidal, supratidal, or syndepositional subtidal origin were the lack of features indicative of a supratidal setting and the interpretation that the muddy layers or lenses containing nodules were of normal marine origin. Ebanks et al. (1977) attributed the origin of the Bindley Field nodules to periodic supratidal exposure of discontinuous portions of a mound as it built to sea level.

Lithotype 3- Wavy Laminated, Argillaceous Dolomudstone

Description. Lithotype 3 (Figure 16C) is a variant of Lithotype 1A and occurs as the dominant capping Lithotype of the Meramec 1 interval. In addition to the characteristics described for Lithotype 1A, Lithotype 3 exhibits concentrations of wavy, horizontal shale partings. Subhorizontal zones of concentrated organic material are also evident. Relics of silicified, tan dolomudstone commonly are observed between shale partings. Thin concentrations (one inch or less) of swarms of horizontal burrows with oxidized rinds may represent bioturbated remnants of tan, spiculitic dolomudstone layers (Figure 16D). Isolated chalcedony/quartz nodules and contorted enterolithic chalcedony/quartz layers which represent replaced evaporites are a distinctive feature of Lithotype 3 (Figure 16E). Individual nodules display irregular, horizontally elongate shapes (as opposed to subround) and occur between shale partings.

Interpretation. Lithotype 3 is interpreted to represent deposition in an intertidal environment, probably in a higher position on the tidal flat than

Lithotype 2A. The concentration of shale partings causes the increased gamma-ray response which separates the Meramec 1 from the overlying Meramec 2 interval on radioactivity logs (Figure 6). The shape, orientation, and size of the chalcedony/quartz nodules and their proximity to shale partings superficially resemble cemented fenestral voids within algal laminated sediments deposited in high intertidal to supratidal settings. The presence of replaced evaporites which are confined to Lithotype 3 and the underlying Lithotype 1, but do not occur in the immediately overlying sediment, the abundance of horizontal burrow traces, the restricted fauna, and the presence of organic matter, all support the interpretation of deposition in a high intertidal environment. Lithotype 3 gradationally caps Lithotype 2A at the top of the Meramec 1 interval. A very thin veneer of Lithotype 2B containing vertically elongate chalcedony/quartz nodules commonly overlies Lithotype 3 at the top of the Meramec 1 interval.

Lithotype 4- Echinoderm/Bryozoan Lithofacies

Description. Lithotype 4 is subdivided into four subtypes which reflect depositional fabric and dominant mineralogy as follows:

Lithotype 4A- Dolomudstone (Figure 17A)

Lithotype 4B- Dolowackestone (Figure 17B)

Lithotype 4C- Dolopackstone/grainstone (Figure 17C)

Lithotype 4D- Lime grainstone (Figure 17D)

Dolopackstone and dolograinstone fabrics are not defined separately (Lithotype 4C) due to the difficulty in discriminating former interparticle mud in pervasively dolomitized rocks. Lithotype 4 is confined to the Meramec 2 and Meramec 3 intervals.

Lithotype 4 ranges from light grayish brown to dark brown in color, the darker brown hues being imparted by oil stain. The dominant skeletal constituents are pelmatozoan and fenestrate bryozoan fragments. In the grainier subtypes, ramose bryozoa and brachiopods are common, and pelecypods and endothyrid foraminifera are present in minor numbers. Pelmatozoan fragments are typically disarticulated but are not highly abraded or micritized. Articulated stem and calyx segments occur in the grainier subtypes. Pelmatozoan fragments range from 0.5 to 4 millimeters in dimension, with the largest bioclasts generally concentrated in the grainiest subtypes. Fenestrate bryozoa are preserved as frond fragments with larger fragments generally preserved in muddier subtypes. Brachiopod and pelecypod tests are typically

FIGURE 17- Core and Thin-Section Photographs of Lithotype 4.

A) Core photograph of Lithotype 4A (dolomudstone) illustrating burrow mottled texture and disseminated echinoderm and bryozoan bioclasts. Scale bar is 1 cm. Oasis #1 Walter (NW/4 NW/4, 3-22S-24W), 4,6644-45'.

B) Core photograph of Lithotype 4B (dolowackestone). Oil-stained molds of fenestrate bryozoa are abundant. Molds of echinoderm grains are also evident. Scale bar is 1 cm. Oasis #1 Deutsch (NE/4 SE/4, 33-21S-24W), 4,619-20'.

C) Core photograph of Lithotype 4C (dolopackstone/grainstone). Molds and dolomitized pseudomorphs of echinoderm and bryozoan bioclasts are abundant. Scale bar is 1 cm. Oasis #1 Deutsch (NE/4 SE/4, 33-21S-24W), 4,627-28'.

D) Core photograph of Lithotype 4D (lime grainstone) with prominent horizontal stylolite. Echinoderm and bryozoan bioclasts are dominant. Interparticle areas are cemented with calcite. Scattered echinoderm grains have been selectively silicified. Scale bar is 1 cm. Oasis #1 Walter (NW/4 NW/4, 3-22S-24W), 4,668-69'.

E) Core photograph of the muddy top of a graded layer and the base of the overlying graded layer. The base of the overlying layer is in sharp (scoured?) contact with the muddy top of the underlying layer. The muddy cap and the contact surface have been slightly burrowed (B). Scale bar is 1 cm. Oasis #1 Smith (SW/4 NW/4, 34-21S-24W), 4,637-38'.

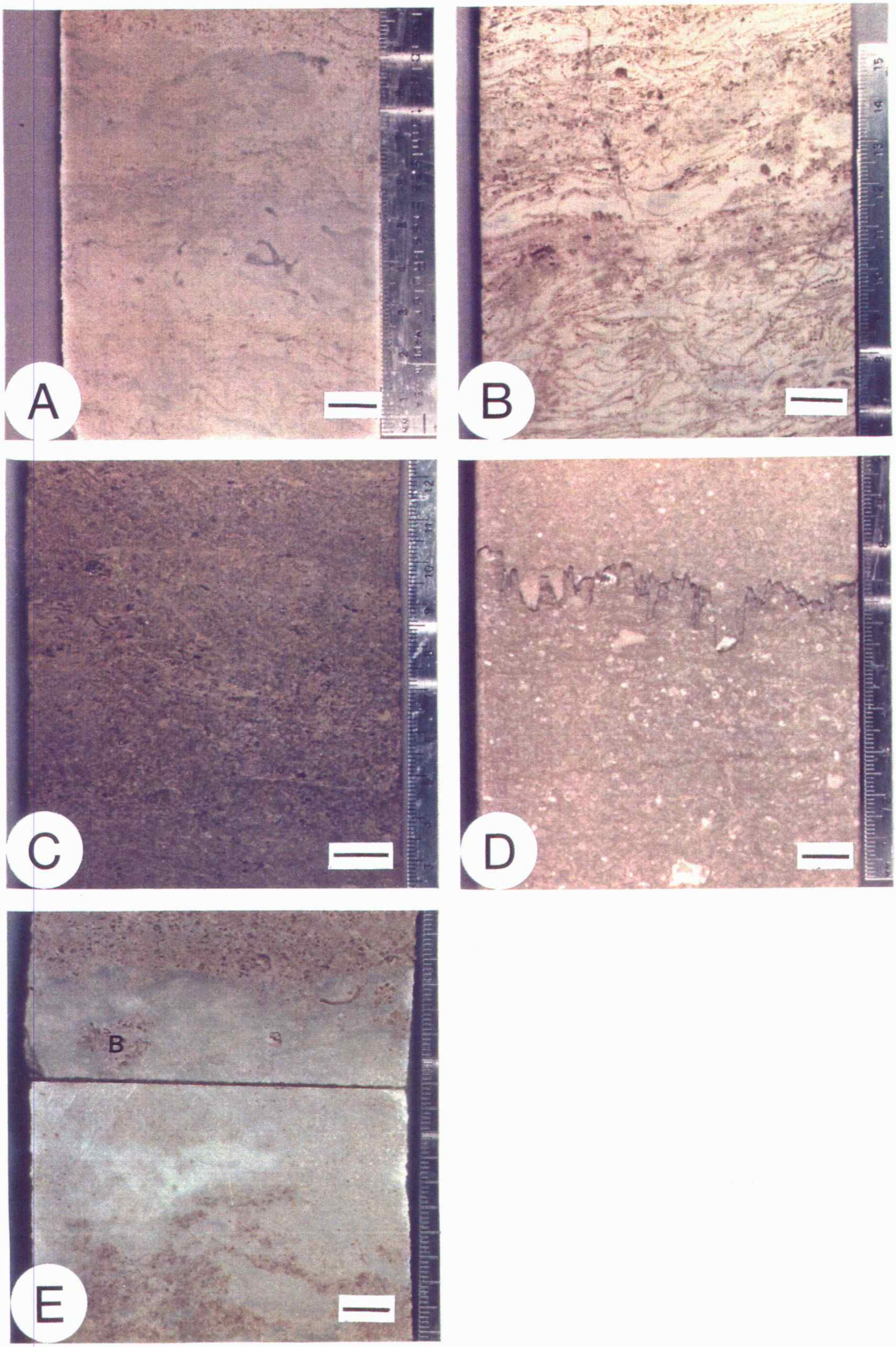
A
B
C
D
B
E

disarticulated but articulated pelecypod valves with no internal sediment were observed. Monaxon sponge spicules occur in the muddiest subtypes. Small subround intraclasts of dolomudstone (0.5-1 centimeter) are rare constituents of Lithotype 4C. Skeletal fragments may be preserved as skeletal calcite, as fully dolomitized pseudomorphs, as molds, as molds of partially dolomitized grains (dolomite remains undissolved), or as calcite-cemented molds. Detrital mud is pervasively dolomitized.

Graded layers are common in Lithotype 4 (Figure 17E). In the grainier subtypes (Lithotypes 4C and 4D), a scoured basal contact with underlying sediment is common, overlain by grain-supported sediment which grades vertically into muddier sediment, frequently capped by dolomudstone (Lithotype 4A). Graded layers typically range from 4 to 8 inches in thickness and commonly occur in repeated vertical sequence. Wavy to undulose layering and fabric transitions are common. In the muddier subtypes, basal scours are less frequent and the fabrics are more mud dominated. Successive graded layers may cannibalize all or a portion of the preceding layer, leaving little or no evidence of the precursor layer, particularly the muddy cap.

Lithotype 4 is highly bioturbated by vertical burrowers and individual burrow traces up to 1 centimeter in diameter are common. Burrows in the mud caps of graded layers are filled with grain-supported sediment from the overlying layer (Figure 18A). Mud caps of graded layers may be bioturbated to the extent that very little evidence of the mud layer remains (Figure 18B). Stylolites are very common in Lithotype 4, particularly in Lithotypes 4C and 4D. Vertical fractures occur but are not abundant. Fractures are either open and solution widened or cemented with calcite.

The fabric of dolomitized mud is characterized by 10-20 micron, anhedral to subhedral dolomite matrix with dispersed 30-60 micron, anhedral to subhedral rhombs (Figure 18C). The larger crystals are less abundant than those in Lithotypes 1-3 (i.e., Figure 18C vs. Figure 13C). The fabric of dolomitized skeletal fragments is characterized by 20-60 micron, anhedral to euhedral dolomite (Figure 18C). Dolomite crystal size and fabric is a good general guide to precursor host sediment (i.e. skeletal grains vs. mud), but it is not absolute. Dolomitized pelmatozoan fragments exhibit variable dolomite fabrics ranging from that stated above to 10-20 micron, anhedral dolomite which may resemble dolomitized mud if grain boundaries are not evident. Partially dolomitized syntaxial calcite cement exhibits

FIGURE 18- Core and Thin-Section Photographs of Lithotype 4.

A) Core photograph of grain-filled burrows (B) in the muddy cap of a graded, Lithotype 4C layer. Burrows are filled with dolomitized bioclasts from the overlying graded layer. Burrowing has partially degraded the muddy cap. Scale bar is 1 cm. Oasis #3 Deutsch (NW/4 SW/4, 34-21S-24W), 4,655-56'.

B) Core photograph of a former muddy cap of a graded layer which has been nearly completely obliterated by burrowing. Only patches of mud (M) which are confined to a thin, horizontal zone remain. Scale bar is 1 cm. Oasis #3 Deutsch (NW/4 SW/4, 34-21S-24W), 4,656-57'.

C) Thin-section photomicrograph of dolomite fabrics in dolomitized mud and skeletal grains of Lithotype 4. Dolomitized mud (M) is characterized by 10 micron, cloudy, subhedral to anhedral dolomite. Dolomite in partially dolomitized and leached skeletal grains (G) is comprised of larger (20-30 micron), clear, subhedral to euhedral crystals. Dissolution of undolomitized skeletal calcite in partially dolomitized skeletal grains has resulted in partial molds of former bioclasts. Scale bar is 100 microns. Oasis #3 Deutsch (NW/4 SW/4, 34-21S-24W), 4,631.9'.

D) Thin-section photomicrograph of calcite cemented interparticle pore in Lithotype 4D. The majority of the pore is filled by a syntaxial calcite overgrowth (O) on the adjacent echinoderm grain (E). A very thin crust of equant calcite crystals (C) border bryozoan grains (B). Oasis #7 Deutsch (SE/4SW/4, 34-21S-24W), 4,650.1'.

E) Thin-section photomicrograph illustrating the preferential dolomitization of non-echinoderm constituents in Lithotype 4D. Dolomite is distributed preferentially in mud-filled bryozoa (B), at grain contacts, and at the boundary between echinoderm grains (E) and associated syntaxial cement (S). The interior of cemented bryozoa (C) has not been dolomitized. Scale bar is 100 microns. Oasis #1 Everton (SW/4 SE/4, 34-21S-24W), 4,676.2'.

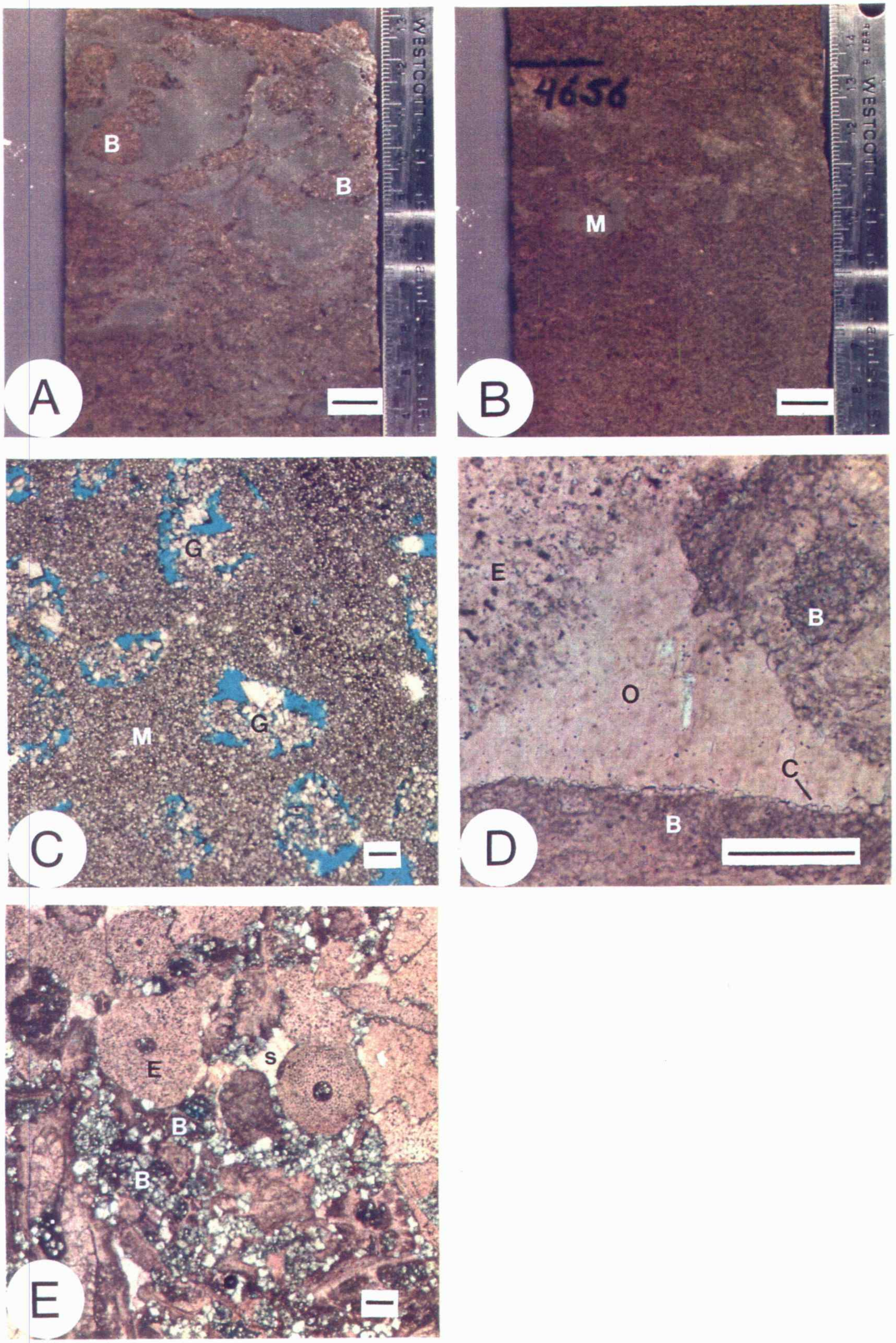
B
B
WESTCOTT
A
4656
M
WESTCOTT
B
G
G
M
C
E
B
O
C
B
D
S
E
B
B
E

larger, clear, euhedral dolomite rhombs which commonly exceed 100 microns.

Undolomitized skeletal grains are most frequently preserved in the grain-supported Lithotypes 4D and 4C. Micritic sediment fills bryozoan zooecia and the stereome pore network of some pelmatozoan grains. Some zooecia contain bladed and/or equant calcite cement, either in conjunction with micritic sediment or as a complete intraparticle pore-filling . Where micritic sediment and calcite cement occur in a single zooecium, geopetal associations are observed.

Interparticle pore space in Lithotype 4D (lime grainstone) is generally fully cemented by calcite, both as syntaxial overgrowths on pelmatozoan grains and as equant crystals bordering non-pelmatozoan grains (Figure 18D). Graded layers are present in Lithotype 4D, the upper portions of which are characterized by less muddy fabrics as compared to other Lithotype 4 subtypes. Burrowing and bioturbation are sometimes evident in the upper portions of such graded layers.

Lithotype 4D may be partially dolomitized with dolomite content ranging from zero to less than 50% of the rock matrix. Dolomitization occurs preferentially in mud and non-pelmatozoan grains (Figure 18E). Many such non-pelmatozoan grains are indentifiable as bryozoa whereas others are not clearly identifiable. The presence of dolomitized mud, mud clasts, or other dolomitized skeletal grains cannot be ruled out.

<u>Interpretation</u>. Lithotype 4 represents deposition in a normal marine, shelf environment which was periodically winnowed by storms. The stenohaline faunal assemblage (Heckel, 1972, his Figure 3; Flügel, 1982, his Table 49) and the high degree of bioturbation indicate a normal marine environment. The preservation of graded layers implies that normal wave action was at a minimum; otherwise it would be expected that the graded layers would have been reworked into a more homogeneous fabric. The lack of coated grains in grain-supported subtypes also indicates a lack of constant agitation. Such an environment could result from a position below normal wave base or from the damping of normal waves in a more offshore locality by a barrier complex or a broad expanse of a gently sloping ramp.

The presence of repeated graded layers with scoured bases and vertically gradational textures is consistent with periodic storm deposition (Aigner, 1984; Handford, 1986; Morton, 1988). The presence of mud in pelmatozoan stereome pores and bryozoan zooecia within otherwise mud-free subtypes indicates original deposition of skeletal grains in a muddier sediment and subsequent winnowing of the mud fraction. The occurrence of mud clasts in Lithotype 4C is also consistent with episodic, high-energy deposition. The non-abraded nature of skeletal grains and the presence of articulated pelmatozoan segments in Lithotypes 4C and 4D argues for local redeposition, as opposed to transport and redeposition distal from the sediment source (e.g. as a storm sheet; Kreisa, 1981). Structures considered diagnostic of storm layers such as oscillatory ripples, climbing ripple cross-stratification, and hummocky cross-stratification formed by waning oscillatory or bidirectional flows (Aigner, 1984; Handford, 1986; Morton, 1988) were not observed. However, graded layers typically display indistinct, wavy lamination and undulose fabric transitions which may represent similar processes. In addition, the absence of such features does not disqualify a storm interpretation. Such structures may not have formed, they may not have been preserved (i.e. destroyed by subsequent sedimentary processes, burrowing, or dolomitization) or, as pointed out by Morton (1981), they may not be discernable within the narrow diameter of a core.

Each subtype represents a position within an energy spectrum ranging from low energy (Lithotype 4A) to high energy (Lithotypes 4C and 4D). In the grain-supported Lithotypes 4C and 4D, graded layers most frequently display basal scours and, where no muddy caps of graded layers are evident, complete bioturbation of muddy caps or cannibalization of the muddy caps by overlying graded layers is suggested. In addition, grain size reaches a maximum in these subtypes.

In the mud-supported Lithotypes 4A and 4B, basal scours in graded layers are less frequently observed, fabrics in graded layers are muddier, and grain sizes are generally smaller than those in the grain-supported subtypes.

Lithotype 4 is gradational upward into Lithotype 2B. As such, vertical transitions from muddier Lithotype 4 fabrics (i.e. Lithotype 4A) to Lithotype 2B may represent an evolution of restriction and stress on the normal marine skeletal constituents as opposed to simply representing normal marine, lower energy conditions.

<u>Lithotype 5- Argillaceous Dolomudstone/Dolomitic Shale</u>

<u>Description</u>. Lithotype 5 occurs as the capping lithotype of the Meramec 2 interval and as very thin (up to a few centimeters), gradational intercalations within Lithotype 2B layers within the Meramec 2 interval. Lithotype 5 ranges from medium brownish gray to greenish gray in color (Figure 19A). Detrital clay is abundant and may comprise more than 50% of the matrix volume (Figure 19B). X-ray diffraction analysis indicates the

FIGURE 19- Core and Thin-Section Photographs of Lithotypes 5 and 6.

A) Core photograph of Lithotype 5 (argillaceous dolomudstone/dolomitic shale). The high clay content contributes to the horizontal fissility. Scale bar is 1 cm. Oasis #3 Deutsch (NW/4 SW/4, 34-21S-24W), 4,642-43'.

B) Thin-section photomicrograph of dolomite and clay fabric in Lithotype 5. Dolomite crystals (D) are rhombic to irregularly shaped. Clay minerals (C) are dominated by laths of illite distributed between dolomite crystals. Scale bar is 100 microns. Beardmore Oil #1 Shelton "A" (SE/4 SE/4, 28-21S-24W), 4,629.5'.

C) Thin-section photomicrograph of chert-cemented monaxon spicule mold in Lithotype 5. Scale bar is 100 microns. Beardmore Oil #1 Shelton "A" (SE/4 SE/4, 28-21S-24W), 4,619.6'.

D) Core photograph of Lithotype 6 (breccia) consisting of chaotic, well-lithified clasts of Lithotype 2B. Green silty and sandy clay (C) fills the areas between clasts and encloses chalcedony/quartz nodules (N) derived from the brecciated host rocks. Scale bar is 1 cm. Oasis #1 Deutsch (NE/4 SE/4, 33-21S-24W), 4,611-12'.

E) Core photograph of Lithotype 6 consisting of fitted clasts of Lithotype 2B. Scale bar is 1 cm. Oasis #1 Schauvliege (SE/4 NW/4, 33-21S-24W), 4,673-74'.

F) Core photograph of one side of a vertical fissure crosscutting Lithotype 4B. Green clay (C) and rubble clasts (R) filled the fissure. Scale bar is 1 cm. Oasis #4 Deutsch (SE/4 SE/4, 33-21S-24W), 4,639-40'.

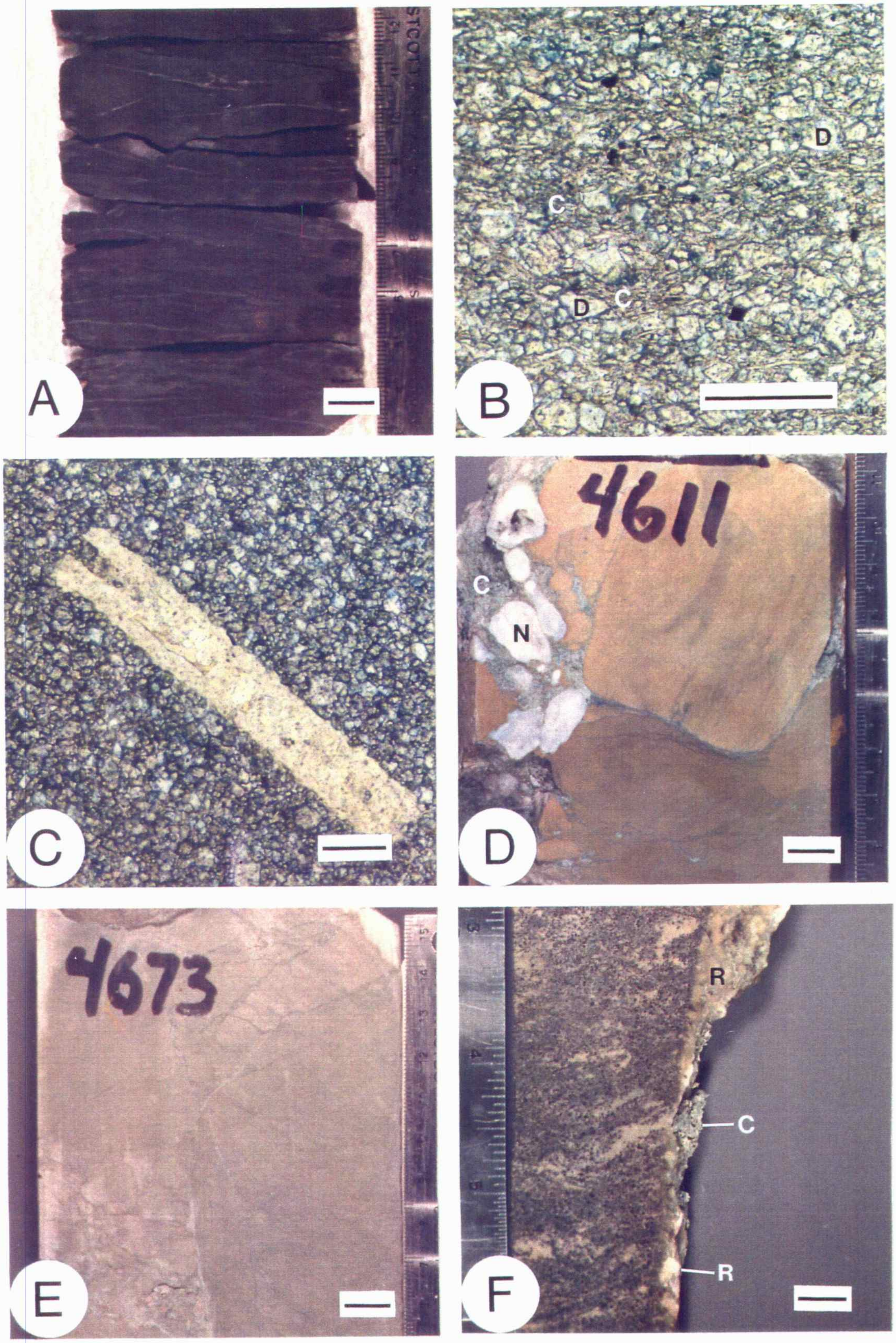
A
B
D
C
D
C
C
4611
C
N
D
4673
E
R
C
R
F

clay is dominantly illite with subordinate amounts of kaolinite. Where clay content is high, the rock exhibits darker color and horizontal fissility. Changes in clay content are gradational. Disseminated, subangular quartz silt (20-50 micron) comprises less than one percent of the rock matrix. Skeletal constituents are sparse and consist mainly of monaxon sponge spicules or chalcedony-cemented spicule molds (Figure 19C). Compacted traces of fenestrate bryozoa are present. Thin wavy laminae are characteristic with darker, argillaceous laminae commonly alternating with lighter colored, less argillaceous laminae. Reddish brown, amorphous organic inclusions, as described in Lithotype 1, are common. Small, compacted, horizontal burrow traces are present but are not abundant. Dolomite fabric is bimodal and is characterized by 5-20 micron, anhedral to subhedral matrix dolomite with disseminated rhombs of 30-50 micron subhedral to euhedral dolomite (Figure 19B). The larger rhombs commonly exhibit a euhedral, inclusion-rich core surrounded by a clear rim. Irregularly shaped and subround chalcedony/quartz nodules are present as isolated or layered forms, but in low abundance as compared to Lithotype 1. The petrographic character of the nodules is as described in Lithotype 2B, indicating the former presence of evaporite nodules. Fine, disseminated pyrite is common.

Interpretation. Lithotype 5 represents deposition in a quiet, slightly evaporitic, possibly brackish environment. The highly restricted and sparse fauna, the abundance of detrital clay, the presence of organic matter and the presence of replaced evaporites attest to these conditions. The type of clay minerals, the nature of the quartz silt constituent, the occurrence of isolated chalcedony/quartz nodules, and the dolomite fabric are very similar to Lithotype 1. Lithotype 5 lacks interlayers of cherty dolostone, contains a substantially larger fraction of clay, and contains less apparent organic material and a lower abundance of replaced evaporites, but is otherwise very similar to Lithotype 1. No features were observed which indicate a periodically exposed or supratidal environment. As such, the depositional environment is interpreted to be similar to that of Lithotype 1 with the exception that the setting was not proximal to a source of distinctly different sediment (e.g. Lithotype 2A) which was introduced by storms, or the setting was more protected from the effects of storm energy. Such an environment may represent a more widely restricted (geographically), less evaporitic setting than that of Lithotype 1. The high clay content and less abundant replaced evaporites as compared to Lithotype 1 may reflect brackish conditions related to shoreline-derived freshwater sources. Carozzi (1989, p. 108) has described very argillaceous, silty carbonate sediments from the Cretaceous of Brazil which were deposited in a restricted lagoon proximal to a fluvio-deltaic shoreline.

Lithotype 6- Breccia

Description. Lithotype 6 ranges from light brown to medium brownish green. Poorly sorted, angular to subangular breccia clasts range from sand to boulder size and consist of well-lithified fragments and residuum of surrounding lithotypes (Figure 19D). Lithotype 2B is most frequently observed as breccia clasts. Fragments of skeletal-moldic Lithotype 4C with oil stain also occur. Interclast matrix generally consists of light to medium green silty and sandy clay (Figure 19D). Breccia fabrics range from fitted mosaics to chaotic (Figures 19D, 19E). Rubble and clay-filled vertical fissures are present (Figure 19F). Breccia blocks larger than the diameter of cores are indicated by zones of tilted depositional layering defined by zones of smaller breccia fragments or green clay residue. Breccia zones are most common immediately below the basal Pennsylvanian unconformity, but solution brecciation effects are observed tens of feet below the unconformity surface, particularly on the flanks of the field.

Interpretation. Lithotype 6 represents dissolution and brecciation associated with influx of meteoric water during exposure at the basal Pennsylvanian unconformity. The concentration of breccia zones below the unconformity surface and the diminished occurrence distal from the unconformity surface support the association with the unconformity event. Presence of rubble and clay-filled vertical fissures indicates downward eluviation of residues. The nearly ubiquitous association of green clay residues with brecciated zones suggests that brecciation is of common origin. No conclusive evidence was observed which would indicate that any substantial portion of the brecciation occurred prior to the infiltration of meteoric water in association with pre-Pennsylvanian exposure, although that possibility can not be entirely ruled out.

Distribution of Lithotypes

The vertical and lateral distribution of lithotypes define the three dimensional depositional architecture of the field. Study of the depositional architecture makes it possible to reconstruct the depositional morphology, the relationship of depositional factors to reservoir distribution, and the dynamics of sedimentation.

The vertical sequence of lithotypes in the center of the field is illustrated in Figure 20. The Meramec 1 interval is comprised of Lithotype 1 (interlayered organic dolomudstone and cherty dolostone) in the lower portion which is conformably overlain by Lithotype 2A (spiculitic dolomudstone), which is capped in turn by Lithotype 3 (wavy laminated, argillaceous dolomudstone). Lithotypes 1, 2A, and 3 are confined to the Meramec 1 interval. The Meramec 2 interval generally exhibits a sharp, scoured contact with the underlying Meramec 1 rocks which is overlain by a skeletal lag.

The Meramec 2 interval is comprised of six layers, each consisting of Lithotype 4 (echinoderm/bryozoan lithotypes) at the base and capped by a thin layer of Lithotype 2B. The base of each Lithotype 4 layer commonly exhibits a sharp contact with the top of the underlying Lithotype 2B layer. Such a zonation allows the separation of the Meramec 2 interval into six subintervals designated A through F in ascending order, each ranging from 4 to 14 feet in thickness (Figure 20). The principal reservoir zones in

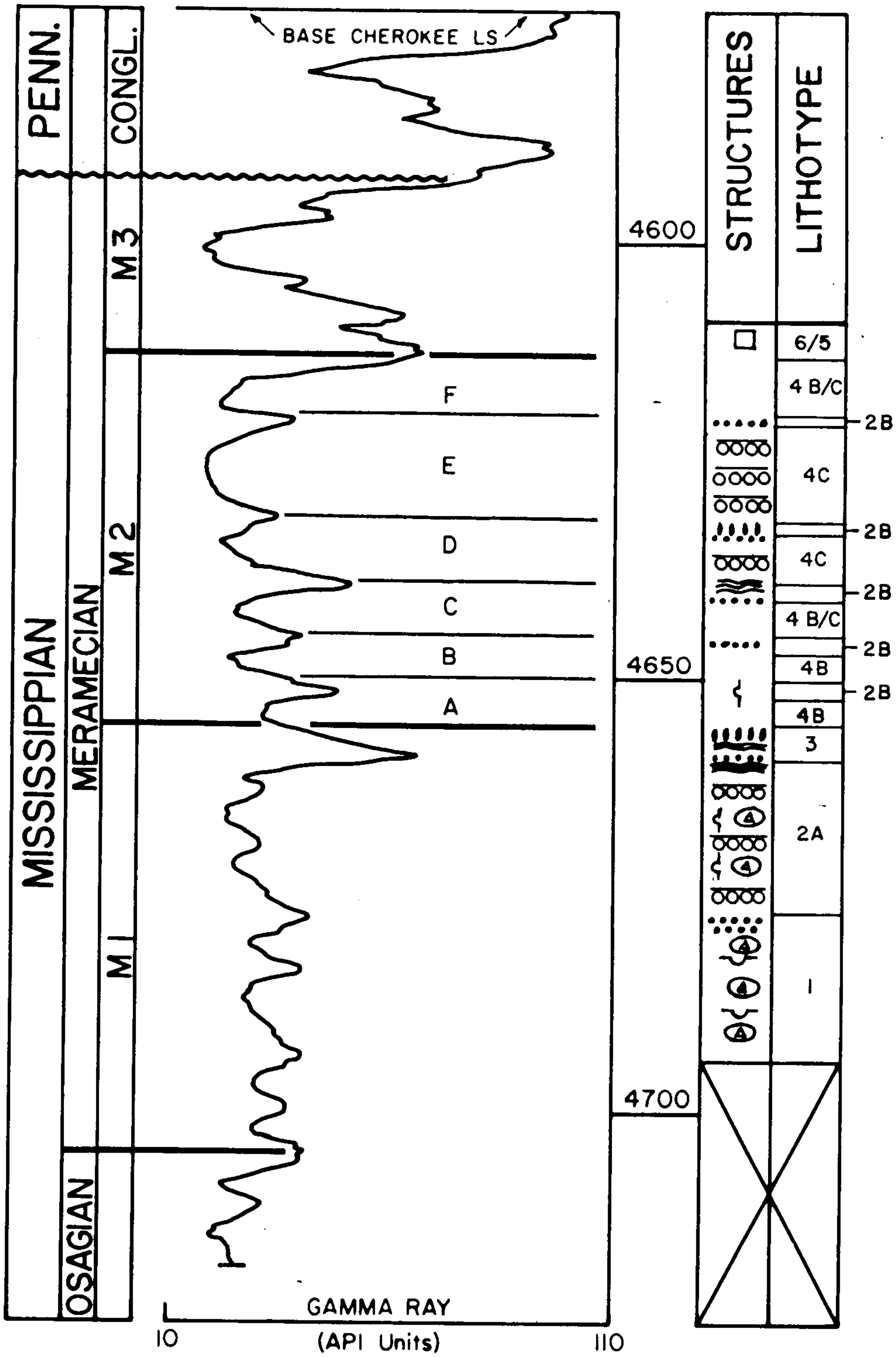

FIGURE 20- Vertical distribution of lithotypes in a representative Bindley Field well (Oasis #1 Deutsch, NE/4 SE/4 33-21S-24W). The division of the Meramec 2 into A-F subintervals is discussed in the text. The principal reservoir zones are contained within the Meramec 2D and 2E. Refer to Appendix A for key to structures.

Bindley Field are within the Meramec 2D and 2E subintervals.

The Meramec 2 interval is typically capped by Lithotype 5 (argillaceous dolomudstone/dolomitic shale) except where it has been truncated by the basal Pennsylvanian unconformity or disrupted by brecciation (brecciation has disrupted Lithotype 5 in the well illustrated in Figure 20). Lithotype 5 correlates to the gamma-ray marker which defines the top of the Meramec 2 interval.

Textural characteristics and the distribution of sedimentary structures change in consistent patterns within the Meramec 2 interval and indicate an evolution toward normal marine-dominated sedimentation and increasing energy regimes which culminate in the Meramec 2E interval. Increasing energy regimes are indicated by several lines of evidence. Lithotype 4 fabrics generally decrease in mud content with the deposition of successive subintervals, reaching minimum mud content (packstone/grainstone) in the Meramec 2E subinterval. The overlying Meramec 2F subinterval contains muddier Lithotype 4 fabrics than the Meramec 2E. Graded layers in Lithotype 4 become more evident and basal scours at the base of graded layers are most frequently observed in the Meramec 2D and 2E subintervals. The bases of the Meramec 2D and 2E subintervals exhibit a scoured contact with the underlying subinterval more commonly than do lower subintervals (except Meramec 2A). Grain size reaches a maximum in the Meramec 2E subinterval.

The degree of restriction represented by Lithotype 2B at the top of each Meramec 2 subinterval also diminishes upward. This diminishing degree of restriction upward is indicated by the distribution of chalcedony/quartz nodules. The size and frequency of nodule layers in the Lithotype 2B caps diminish in the upper Meramec 2 subintervals as compared to the lower subintervals. The largest nodules are observed at the tops of the Meramec 2B and 2C subintervals whereas nodules are generally smaller or nonexistent at the top of the Meramec 2E and 2F subintervals, probably indicating less evaporitic conditions during deposition of the top of the Meramec 2E and 2F subintervals.

Within each Meramec 2 subinterval, Lithotype 4 fabric tends to exhibit gradational, lateral changes in a transect perpendicular to the long axis of the field (Figure 21), but remains fairly consistent along the central axis of the field (Figure 22). Lithotype 4 in each subinterval contains the least mud in the central portion of the field and becomes muddier on the flanks (Figure 21). Graded layers and basal scours associated with graded layers are also more prominent in the central axis of the field than on the flanks. Lithotype

FIGURE 21- Distribution of lithotypes in the Meramec 2 interval along cross-section Fd-Fd' which is perpendicular to the long axis of the field (refer to Figure 23A for cross-section trend). The datum for the cross-section is the log marker at the base of the Meramec 1 interval. Grain-supported sediments (Lithotypes 4C and 4D) are thickest along the central axis of the field. Lithotype 4 depositional fabrics grade laterally to muddier facies. Maximum development of grain-supported sediments occurs in the Meramec 2D and 2E subintervals. Lithotype 5, which caps the Meramec 2 interval, thickens on the southwest flank of the field. Refer to Appendix A for key to structures.

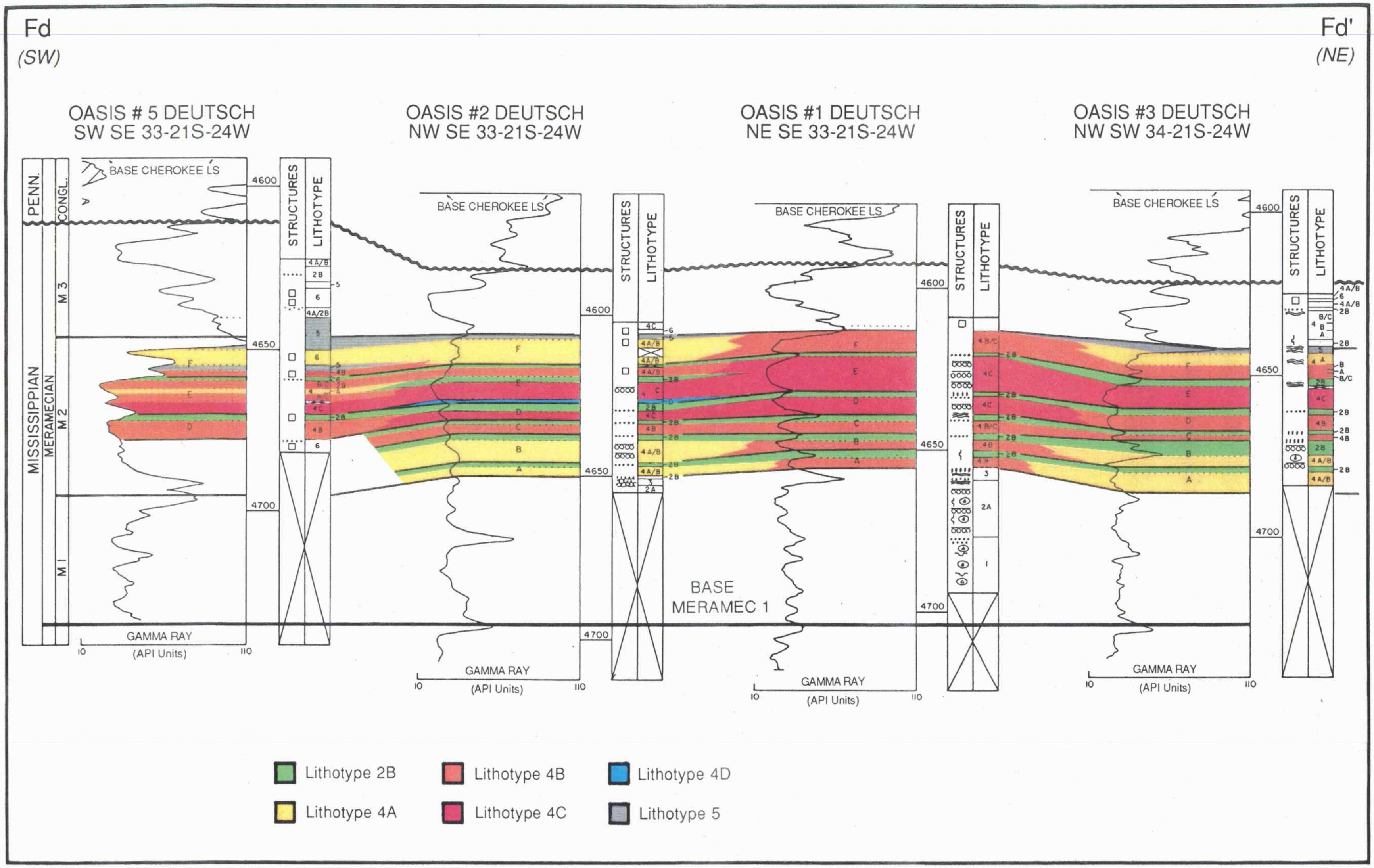

Fd
(SW)
Fd'
(NE)
OASIS # 5 DEUTSCH
SW SE 33-21S-24W
OASIS #2 DEUTSCH
NW SE 33-21S-24W
OASIS #1 DEUTSCH
NE SE 33-21S-24W
OASIS #3 DEUTSCH
NW SW 34-21S-24W
PENN.
CONGL.
MISSISSIPPIAN
MERAMECIAN
M 3
M 2
M 1
BASE CHEROKEE LS
STRUCTURES
LITHOTYPE
4600
4650
4700
BASE
MERAMEC 1
GAMMA RAY
(API Units)
10
110
Lithotype 2B
Lithotype 4A
Lithotype 4B
Lithotype 4C
Lithotype 4D
Lithotype 5

FIGURE 22- Distribution of lithotypes in the Meramec 2 interval along cross-section Fs-Fs' which parallels the central axis of the field (refer to Figure 23A for cross-section trend). The datum for the cross-section is the log marker at the base of the Meramec 1 interval. Where the marker was not drilled or logged, the location was estimated based on correlation with nearby wells. Grain-supported sediments (Lithotypes 4C and 4D) in the Meramec 2D and 2E subintervals are distributed fairly uniformly (relative to Figure 21) along the central axis of the filed. Refer to Appendix A for key to structures.

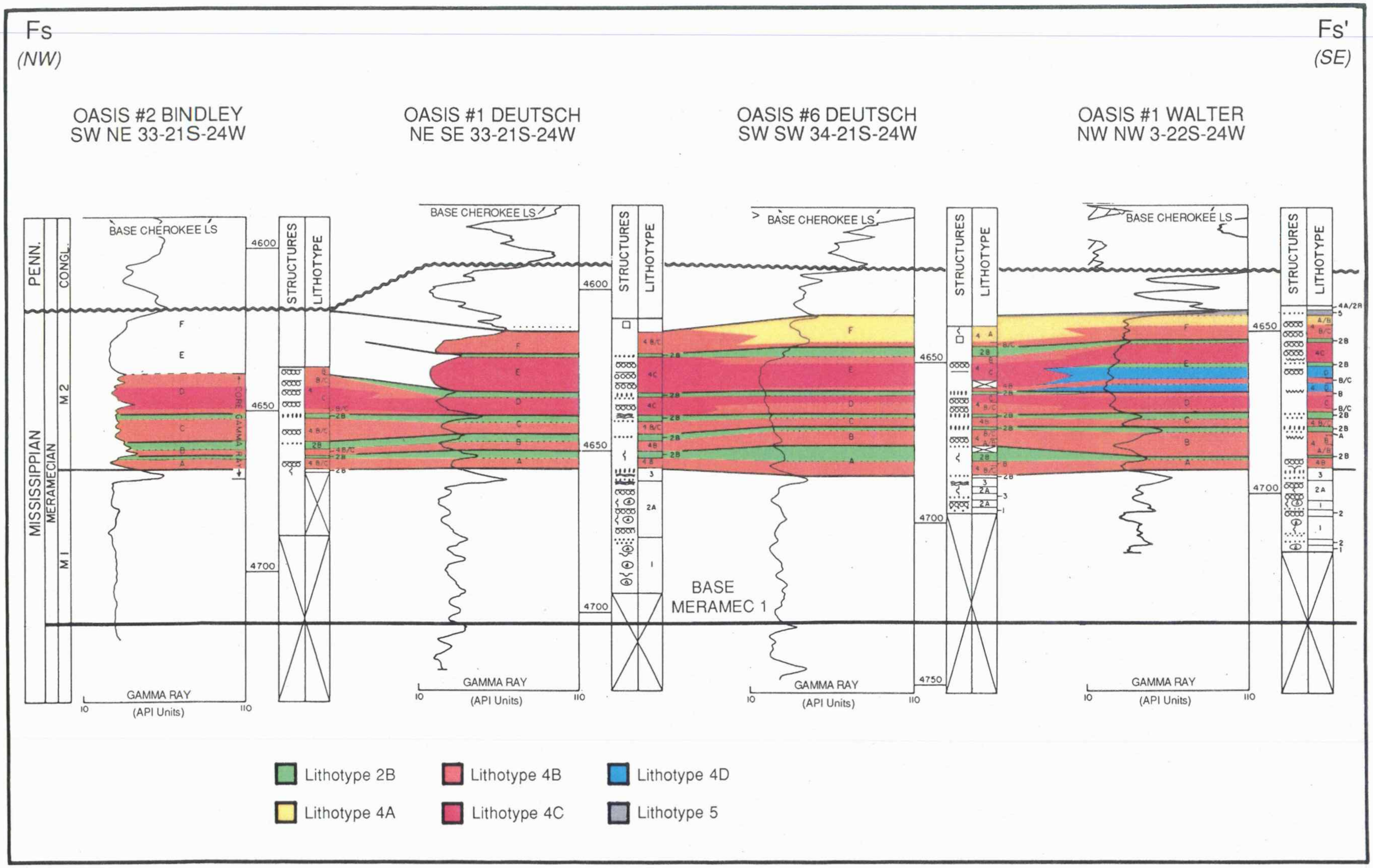
Fs
(NW)
Fs'
(SE)
OASIS #2 BINDLEY
SW NE 33-21S-24W
OASIS #1 DEUTSCH
NE SE 33-21S-24W
OASIS #6 DEUTSCH
SW SW 34-21S-24W
OASIS #1 WALTER
NW NW 3-22S-24W
PENN.
CONGL.
MISSISSIPPIAN
MERAMECIAN
M 2
M 1
BASE CHEROKEE LS
STRUCTURES
LITHOTYPE
4600
4650
4700
4750
BASE
MERAMEC 1
GAMMA RAY
(API Units)
10
110
Lithotype 2B
Lithotype 4B
Lithotype 4D
Lithotype 4A
Lithotype 4C
Lithotype 5

5 at the top of the Meramec 2 interval is thinnest over the center of the field and thickens on the flanks (Figure 21). Layers of Lithotype 2B capping each Meramec 2 subinterval are correlative throughout the field.

Depositional Morphology

The depositional morphology, or the shape of the sediment accumulation, is of importance in understanding the causes of localization of lithotypes and, to the extent that reservoir distribution may be related to lithotypes, the controls on reservoir distribution. Grain-supported lithotypes (Lithotypes 4C and 4D) in the Meramec 2 interval are concentrated along the central axis of the field (Figure 23A). Mud-supported lithotypes (Lithotypes 2B, 4A, and 4B) are distributed in a reciprocal pattern (Figure 23B) such that the areas of thickest mud-supported lithotypes coincide with the areas of thinnest grain-supported lithotypes (i.e. on the flanks of the field). Grain-supported lithotypes became thicker and more widespread as Meramec 2 deposition proceeded (Figures 24A-24D), culminating with the deposition of the Meramec 2E subinterval. The areal distribution of grain-supported lithotypes diminishes considerably in the overlying Meramec 2F subinterval.

The areas of thicker grain-supported lithotypes correlate very closely with present, positive structural

FIGURE 23A- Cumulative thickness (feet) of grain-supported lithotypes in the Meramec 2 interval. The trend of cross-sections illustrated in Figures 21 and 22 are shown. The field area is indicated by the stipled background.

Figure 23B- Cumulative thickness (feet) of mud-supported lithotypes in the Meramec 2 interval. Area of maximum thickness is indicated by diagonal pattern.

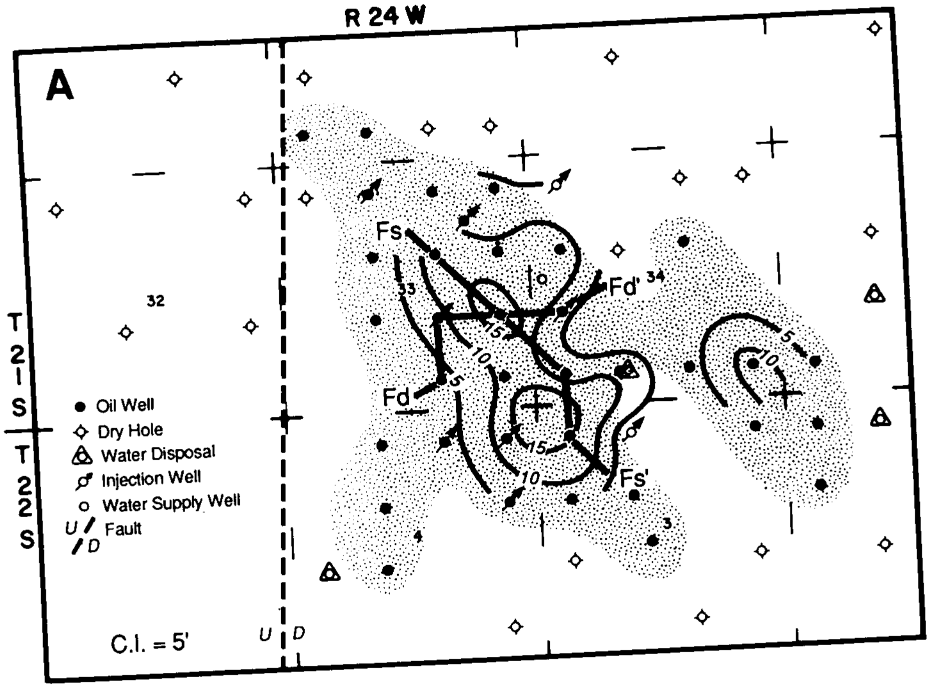
R 24 W
A
32
33
34
3
4
Fs
Fs'
Fd
Fd'
5
10
15
T 21 S
T 22 S
Oil Well
Dry Hole
Water Disposal
Injection Well
Water Supply Well
U D Fault
C.I. = 5'
U D

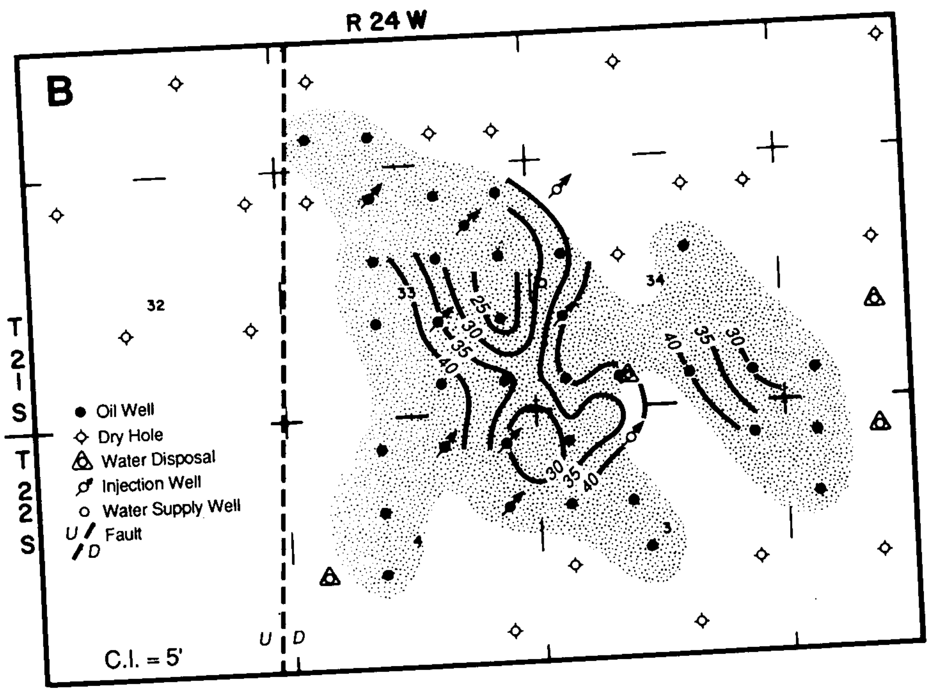
R 24 W
B
32
33
34
3
4
25
30
35
40
T 21 S
T 22 S
Oil Well
Dry Hole
Water Disposal
Injection Well
Water Supply Well
U D Fault
C.I. = 5'
U D

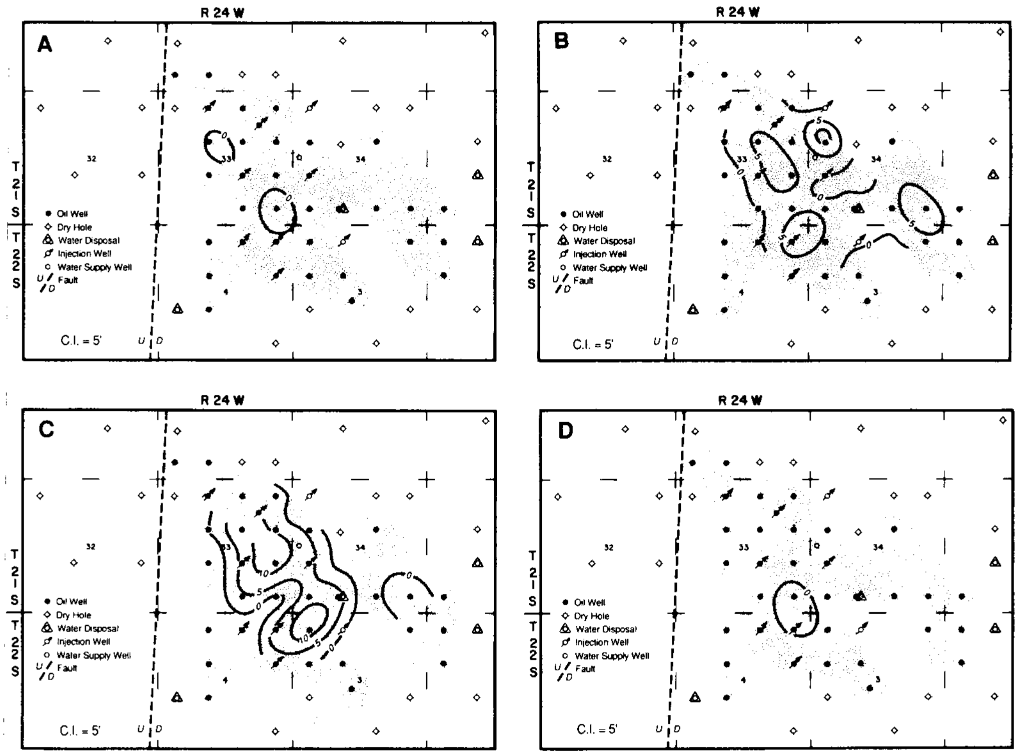

FIGURE 24- Thickness (feet) of grain-supported lithotypes in Meramec 2 subintervals. A) Meramec 2C, B) Meramec 2D, C) Meramec 2E, D) Meramec 2F. The field area is indicated by the stipled background.

features (Figure 11A). This, combined with the observations that 1) present structural relief is an apparent amplification of pre-existing structure (at least as far back as the time of the basal Pennsylvanian unconformity; Figures 11A and 11B), and that 2) sedimentary structures indicative of higher energy (e.g. graded layers and basal scours) are more prevalent in these same areas, suggests that the grainier lithotypes were concentrated in areas of slight, structurally induced bathymetric relief (i.e., shoals). The lack of significant thickening of Meramec 2 subintervals on the flanks of the field (refer to Figure 22) indicate that the amount of relief was minimal. The thickening of Lithotype 5 on the southwest flank of the field at the end of Meramec 2 deposition (Figure 21) indicates that the amount of total relief (structural and stratigraphic) at that time was in the range of 6-8 feet.

Consistent with the above, it is interpreted that Bindley Field is centered on a low-relief skeletal-sand buildup which is elongate in the northwest-southeast direction in association with very subtle structural/bathymetric relief at the time of deposition. The term "buildup" is used in the sense of Heckel (1974) which refers to a carbonate mass in which the sediment differs in nature to some degree from surrounding sediments and which probably exhibited some degree of topographic relief at some time during its deposition. The term is used in a descriptive sense with no genetic implication. Total relief across the buildup was insufficient to have caused any syndepositional, gravity-induced features on the flanks of the buildup, such as slumps or debris slides. The distribution and succession of lithotypes are indicative of a relatively shallow, periodically storm-swept, inner shelf environment which was subject to periodic changes in sedimentary base level (relative sea level) and/or changes in the degree of sea-water circulation.

Ebanks et al. (1977) interpreted the Bindley Field reservoir interval to have been deposited as a muddy bryozoan mound or bioherm, flanked by shaly sediments, which developed enough relief above the surrounding seafloor to exhibit syndepositional, gravity-induced sedimentary features on its flanks ("...debris blocks and submarine slide material incorporated....on the flanks of some bathymetric prominence in the Mississippian sea, specifically the mound..."). While thin interbeds of various lithologies were noted within the "mound" facies (bryozoan dolomite facies) and the "mound" sediments were described as bedded wackestones and packstones, no description of their distribution within the "mound" was given. A schematic representation of the facies distribution by Ebanks et al. (1977) depicts the "mound" as a relatively homogeneous sediment accumulation (Figure 25A). Thin interbeds of shale or argillaceous dolomite within the "mound" were interpreted as "extensions onto the mound of thicker, similar deposits in wells on the perimeter of the field area, the conglomeratic shale facies" which contributes to the impression of a discrete mound laterally encased in shaly sediments. It was proposed that these shaly flank facies were preferentially eroded at the time of the pre-Pennsylvanian unconformity, exhuming the more resistant "mound" facies at the unconformity surface. Ebanks et al. (1977) recognized the chalcedony/quartz nodules as replaced evaporites but interpreted their origin within the "mound" to supratidal deposition "in discontinuous areas of the mound top when it grew to sea level" and did not recognize the vertically repeated, laterally correlative position of the chalcedony/quartz nodules throughout the field.

The recognition of lower Meramecian stratigraphic intervals (i.e. the Meramec 1, 2, and 3 intervals) and the highly stratified nature of the Meramec 2 interval in this study allows correlation of thin units of laterally equivalent rocks throughout the field and results in the more detailed interpretation of

FIGURE 25A- Schematic depositional facies model of Bindley Field in a north-south cross-section by Ebanks et al. (1977). The model suggests that the reservoir facies (bryozoan mound) was deposited as a relatively homogeneous mound with flanking shaly sediments (Lithotype 5 of this study).

FIGURE 25B- Schematic depositional facies model of the Meramec 2 interval proposed herein in Bindley Field. Section is perpendicular to the long axis of the field (SW-NE). The bulk of the Meramec 2 interval is included in the "bryozoan mound" facies of Ebanks et al. (1977). The layered depositional architecture, the progressive, upward increase in grain-supported sediments, and the relation of Lithotype 5 to the flank areas are evident. Reservoir is developed in grain-supported areas. Figure is not drawn to scale.

A

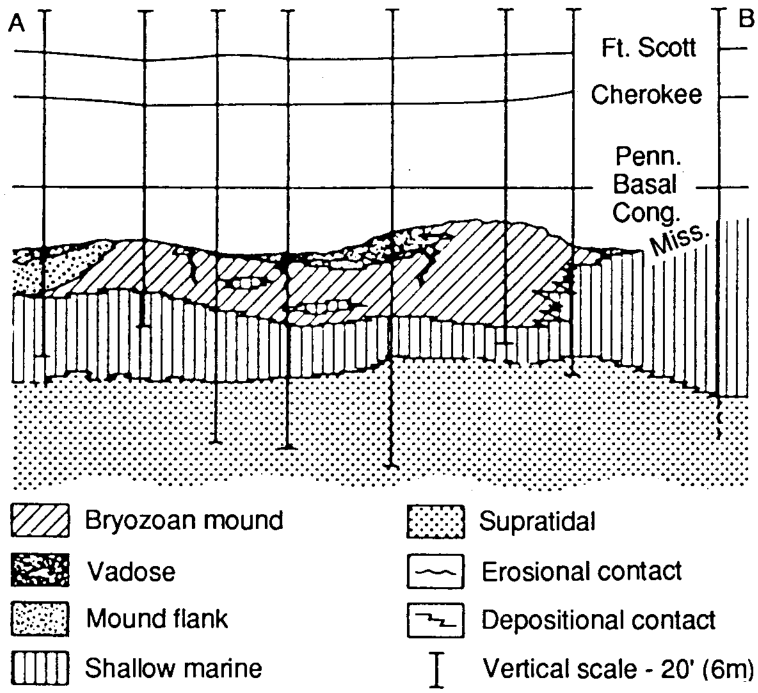
1
2
3
4
5
6
7
8
A
B
Ft. Scott
Cherokee
Penn. Basal Cong.
Miss.
Bryozoan mound
Vadose
Mound flank
Shallow marine
Supratidal
Erosional contact
Depositional contact
Vertical scale - 20' (6m)

B

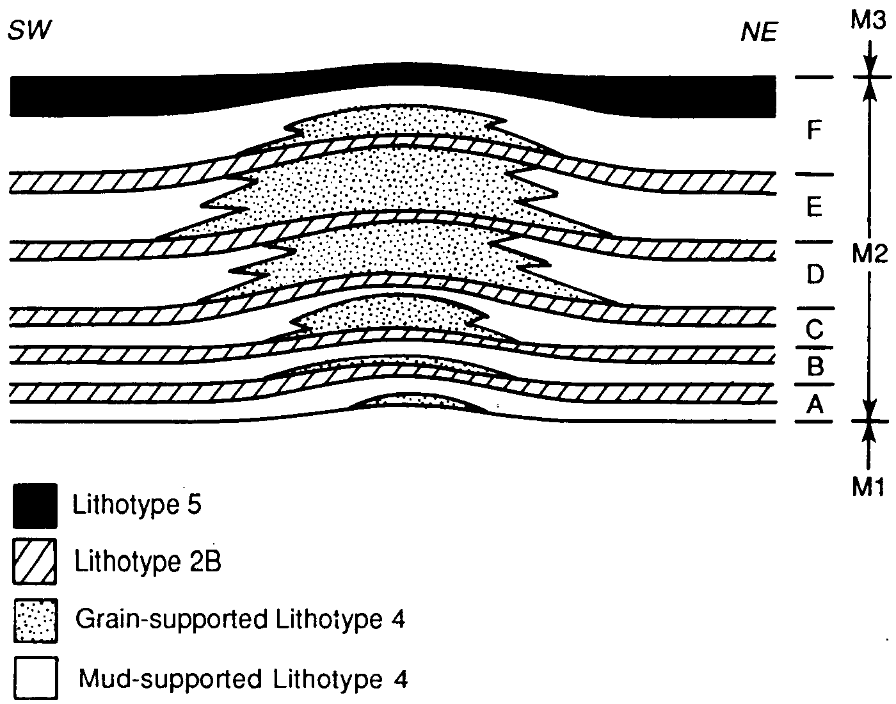
SW
NE
M3
M2
M1
F
E
D
C
B
A
Lithotype 5
Lithotype 2B
Grain-supported Lithotype 4
Mud-supported Lithotype 4

depositional morphology presented herein as compared to that given by Ebanks et al. (1977). The overall shape of the buildup, the trend in lateral facies changes, the probable degree of maximum relief, and the cause of localization are more apparent. Deposition of the Meramec 2 interval in the field area was characterized by a series of six, laterally contiguous cycles of normal marine sediments which are each capped by restricted subtidal sediments (Figure 25B). Lateral, time-correlative facies changes within the area sampled by cores are represented by changes in sedimentary fabric (i.e. grain-supported to mud-supported) rather than a complete change in lithotype. The conglomeratic shale facies of Ebanks et al. (1977), which is equivalent to Lithotype 5 of this study, was not deposited as a flanking facies to the Bindley Field reservoir interval (Meramec 2), but was deposited at the end of Meramec 2 deposition and only marginally thickened on the flanks of the field in accommodation of the low, depositional relief existing at that time (Figure 21).

<u>Depositional Dynamics</u>

Bindley Field cores provide necessary data to interpret the significance of the stratigraphic subdivision of lower Meramecian rocks utilized in this study. It is important to evaluate the nature of the gamma-ray markers which separate the lower Meramecian intervals (i.e. Meramec 1, 2, 3, and 4), determine whether they have time-stratigraphic significance, and assess what the intervening sediments represent in terms of depositional dynamics.

The Meramec 1 sequence represents a shoaling upward peritidal sequence with restricted lagoonal sediments (Lithotype 1) in the lower portion grading vertically into lower intertidal rocks (Lithotype 2A) and culminating with upper intertidal sediments (Lithotype 3). The gamma-ray marker separating the Meramec 1 from the overlying Meramec 2 interval represents the thin layer of argillaceous, organic-rich sediments (Lithotype 3) at the top of the sequence.

The Meramec 2 interval represents transgression over the Meramec 1 interval and records six punctuated, shallowing upward and/or restricting upward minor cycles. Each subinterval (Meramec 2A-2F) represents transgression over the underlying subinterval by more normal marine sediments (Lithotype 4) and subsequent aggradation to restricted, evaporitic sediments (Lithotype 2B). These subintervals are similar to the punctuated aggradational cycles of Goodwin and Anderson (1985). Each successive minor transgression generally resulted in a further shift to more normal marine sedimentation of successively longer duration (as indicated by the trends of grainier fabric and increasing thickness of accumulated sediments) culminating with the deposition of the Meramec 2E subinterval. Deposition of the Meramec 2A through Meramec 2E subintervals records net transgression. The overlying Meramec 2F subinterval records the reversal of the normal marine trend and the onset of early restriction which progresses through the deposition of restricted, argillaceous dolomudstone (Lithotype 5) at the top of the Meramec 2 interval. The concentrated clay content of Lithotype 5 is responsible for the gamma-ray marker separating the Meramec 2 from the overlying Meramec 3 interval.

Core control in the lower portion of the Meramec 3 interval is sparse and the transition zone between the Meramec 2 and Meramec 3 intervals is commonly brecciated in Bindley Field. No sharp, transgressive boundary above Lithotype 5 was observed; however, lower Meramec 3 rocks rapidly grade upward into more normal marine character (Lithotype 4), which indicates a non-erosive transgression. Zones of layered chalcedony/quartz nodules are observed in the lower portion of the Meramec 3 interval which indicate punctuated restriction as observed in the Meramec 2 interval.

In summary, each successive lower Meramecian interval (at least through Meramec 3 time) records an initial transgressive deepening event and a shift toward more normal marine conditions . The overall sequence of each lower Meramecian interval is punctuated by smaller scale transgressive/aggradational events. Gamma-ray markers between the lower Meramecian intervals represent response to lithologic constituents which denote the top of shallowing upward (or restricting upward) cycles which are overlain by rocks which record rapid facies shifts due to subsequent transgression. As such, the gamma-ray markers (or the log response to an equivalent rapid facies shift) may be viewed as time-correlative.

Using the terminology of Van Wagoner et al. (1988), the lower Meramecian intervals (i.e. Meramec 1, Meramec 2, Meramec 3) may also be viewed as parasequence sets comprised of stacked parasequences (Meramec 2A, 2B, 2C, etc.). The top of each Meramecian subinterval (e.g. Meramec 2D, 2E, etc.) is defined by a distinctive shift from a restricted lithotype to overlying normal marine lithotypes. Contacts are commonly represented by a scoured surface. As such, the top of each subinterval may be considered a marine flooding surface and each subinterval is thus viewed as a parasequence. Similarly, the Meramec 2 interval is confined above and below by marine flooding events and consists of stacked parasequences with recognizable stacking patterns, the entire interval may be viewed as a parasequence set.

Based on limited core data and the similarity of confining log markers to those of the Meramec 2 interval, the Meramec 1 and Meramec 3 intervals are likely to be parasequence sets as well.

Diagenesis Relating to Reservoir Development/Preservation

The post-depositional physical and chemical changes in the sediments represented in the Bindley Field cores include compaction, cementation by calcite, dolomite, and silica, replacement of evaporite minerals by silica, dolomitization, dissolution of residual calcite, and brecciation. The early cementation history, dolomitization, and dissolution were critical in the development and preservation of porous and permeable reservoir rock, and these critical diagenetic factors were the focus of the diagenetic portion of this study.

A reconstruction of the burial history of lower Meramecian rocks in Bindley Field (Figure 26) illustrates the major diagenetic environments to which the sediments and rocks have been exposed. The general phases of burial and the associated pore fluid systems serve as a useful framework within which to consider the observed diagenetic products. Six major burial-related phases are discerned: 1) initial burial during

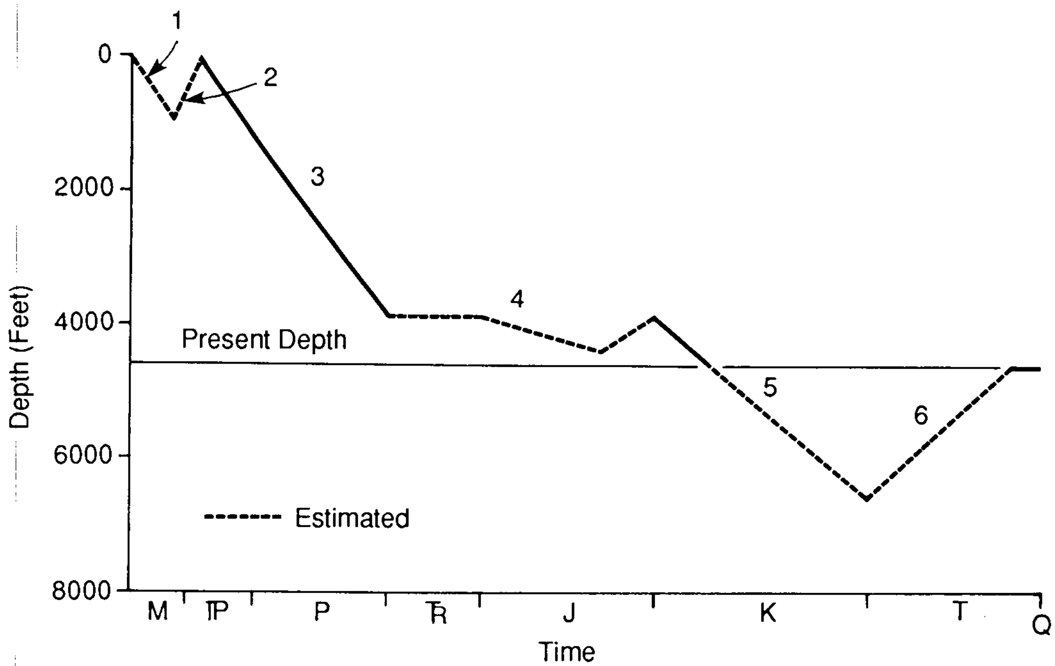

FIGURE 26- Schematic burial history of lower Meramecian rocks in Bindley Field. Six burial phases are distinguished: 1) initial post-depositional burial, 2) late Mississippian-early Pennsylvanian uplift, 3) Pennsylvanian-Permian burial, 4) Triassic-Jurassic burial (?) and late Jurassic-early Cretaceous (?) uplift, 5) Cretaceous burial, and 6) post-Cretaceous uplift. The depth of Mississippian burial was estimated from thickness data in southwestern Kansas contained in Goebel (1968) and is a probable upper limit. The depth of Pennsylvanian-Permian burial is derived from the thickness of Pennsylvanian and Permian rocks presently overlying Bindley Field. The Triassic-Jurassic burial history is uncertain due to the lack of preserved rocks of this age in the field area. Triassic rocks are present only in extreme southwestern Kansas. Jurassic rocks are present only in northwestern Kansas and reach a maximum preserved thickness of approximately 300 feet. The Jurassic-Cretaceous boundary in northwestern Kansas is considered to be unconformable (Merriam, 1963). Permian burial may be understated due to post-Permian/pre-Cretaceous erosion. The depth of Cretaceous burial is estimated from thickness data in northwestern Kansas contained in Merriam (1963).

Mississippian time to an estimated maximum depth of approximately 1,000 feet. Pore water was of probable marine origin; however, the influx of some fresh water due to possible periodic subaerial exposure of sediments as they built to sea level cannot be ruled out. 2) Uplift and erosion of overlying rocks during late Mississippian to early Pennsylvanian time, resulting in subaerial exposure of lower Meramecian strata at the basal Pennsylvanian unconformity. As a result of subaerial exposure, pore fluid in the lower Meramecian rocks ranged from fresh to a mixture of fresh and marine-derived water (brackish). 3) A second phase of burial to a depth of approximately 3,800 feet by the end of the Permian period. Pore fluid in lower Meramecian rocks was probably burial-modified brackish water. 4) A probable period of burial and subsequent uplift during the Triassic and Jurassic periods. No rocks of this age are preserved over Bindley Field. Pore fluid in lower Meramecian rocks was probably burial-modified brackish water. 5) Final burial to an estimated depth of approximately 7,600 feet during the Cretaceous period. Pore fluid in lower Meramecian rocks was likely burial-modified brackish water and/or oil(?). 6) Post-Cretaceous uplift of lower Meramecian strata to their present position. Pore fluids presently consist of oil and brackish water (approximately 20-25 parts per thousand dissolved solids).

Reservoir rocks in Bindley Field are confined to Lithotype 4 (echinoderm/bryozoan lithotypes). The highest quality reservoir rocks (refer to Chapter VI for reservoir description) are confined to Lithotype 4C (dolopackstone-grainstone), and poorer quality reservoir rocks occur in Lithotype 4B (dolowackestone). No reservoir occurs in Lithotypes 4A (dolomudstone) and 4D (lime grainstone).

The observed diagenetic changes recorded in Lithotype 4 are:

1) intraparticle cementation by isopachous calcite in bryozoan zooecia,
2) physical and chemical compaction,
3) interparticle and intraparticle cementation by equant and syntaxial calcite,
4) dolomitization, consisting of
    a. initial dolomitization (dolomite I),
    b. replacement of dolomite I by secondary dolomite (dolomite II),
    c. growth of third generation of dolomite (dolomite III) as an overgrowth on precursor dolomites I and II, as a replacement of dolomite I, and as a replacement of undissolved skeletal calcite,

5) dissolution of undolomitized calcite (skeletal and cement) in dolomitized rocks,
6) cementation of select areas by zoned ferroan and non-ferroan calcite, and
7) brecciation.

A very minor amount of chert replacement of the interior of pelmatozoan and brachiopod fragments was also observed but will not be addressed further due to its volumetric insignificance.

The order in which diagenetic changes are listed represents the interpreted general chronological sequence of diagenetic events. However, clear evidence for chronological placement of certain diagenetic phases is lacking as detailed below in the discussion of each diagenetic event.

Isopachous Intraparticle Cementation

Bryozoan zooecia in lithotype 4D are commonly lined by isopachous, non-ferroan calcite cement with indistinct boundaries between crystals and prismatic terminations (Figure 27A). This pore-lining cement exhibits an extinction pattern which sweeps radially around the circumference of the intraparticle pore, commonly in conjunction with the extinction of the zooecial wall. The pore-lining cement also occurs as a complete pore-filling phase which exhibits the same

FIGURE 27- Thin-Section Photomicrographs

A) Thin-section photomicrograph of bryozoan zooecium lined with isopachous calcite cement (I). Remainder of zooecium is cemented by a single calcite crystal (C). Lithotype 4D. Scale bar is 100 microns. Oasis #7 Deutsch (SE/4SW/4, 34-21S-24W), 4,672'.

B) Thin-section photomicrograph of the interior of bryozoan zooecia lined with isopachous calcite cement (I). The remainder of each zooecium is filled with micritic calcite (M). Lithotype 4D. Scale bar is 100 microns. Oasis #7 Deutsch (SE/4 SW/4, 34-21S-24W), 4,672'.

C) Thin-section photomicrograph of syntaxially cemented interparticle pore (P) adjacent to echinoderm bioclasts (E) with sutured contact (S). Euhedral dolomite rhombs simultaneously crosscut echinoderm grains and syntaxial cement (D). Euhedral dolomite rhombs also occur at sutured contact between grains. Lithotype 4D. Scale bar is 100 microns. Oasis #1 Everton (SW/4 SE/4, 34-21S-24W), 4,672.7'.

D) Thin-section photomicrograph of stylolite (S) crosscutting interparticle calcite cements (C). Lithotype 4D. Scale bar is 100 microns. Oasis #7 Deutsch (SE/4SW/4, 34-21S-24W), 4,672'.

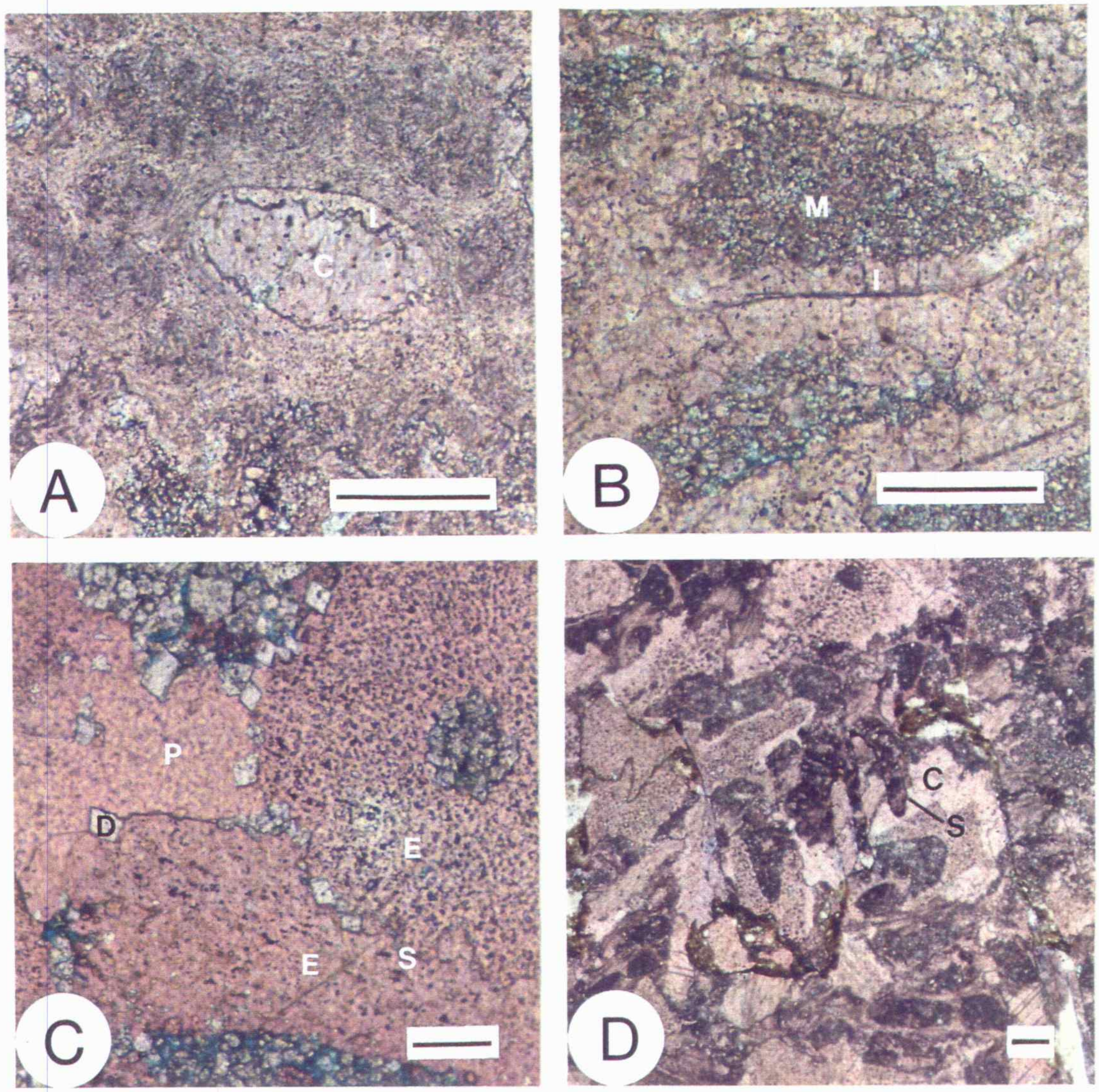
A
I
C
B
M
I
C
P
D
E
E
S
D
C
S

sweeping, radial extinction. The extinction behavior possibly represents a trait inherited from precursor fibrous cements which have been neomorphosed.

Micritic calcite sometimes coexists with isopachous, intraparticle cement in Lithotype 4D, both as geopetal sediment (Figure 27B) and as a pore filling over the pore-lining cement (Figure 27C). The majority of intraparticle micrite is interpreted as detrital mud as evidenced by the geopetal association of mud with cement. Micrite pore fillings inside the perimeter of pore-lining cement are likely to represent mud introduced after initial cementation.

The isopachous, intraparticle cement is interpreted to be of marine origin as indicated by the infilling of micritic marine sediment after initial cementation, and by the fact that it is restricted to intraparticle pores. Cement morphology is equivocal, although the isopachous nature and the apparent fibrous habit, as implied by the extinction behavior, are consistent with a marine origin (Longman, 1980; James and Choquette, 1983).

Compaction

Early burial of Lithotype 4 sediments (Figure 26, phase 1) resulted in physical and chemical compaction as expressed by sutured contacts between pelmatozoan grains (Figure 27D), bryozoan fragments which are fitted between pelmatozoan grains, and broken or contorted brachiopod fragments. Stylolites which crosscut the interparticle cements represent later burial effects (Figure 27E).

Interparticle and Intraparticle Cementation by Equant and Syntaxial Calcite

In Lithotype 4D and in mud-poor portions of Lithotype 4C, interparticle voids and intraparticle pore space not previously cemented or filled with micrite were fully cemented by calcite. Interparticle pores were cemented by syntaxial overgrowths on pelmatozoan grains, and by equant crystals rimming non-pelmatozoan grains (Figure 18D). Intraparticle pore space was cemented by coarse, equant calcite which overlies the earlier-formed isopachous cements (Figure 27A). Staining with a solution of Alizarin Red S and potassium ferricyanide imparts a mottled pink to very pale purplish pink color to the equant and syntaxial cements which indicates a slightly ferroan composition (Dickson, 1966). No distinct zonation between ferroan and non-ferroan calcite was observed. The rate of cementation by syntaxial overgrowth apparently exceeded the rate of cementation by equant calcite in interparticle pores, as evidenced by the volumetric dominance of syntaxial calcite over equant calcite in individual interparticle areas bordered by both pelmatozoan and bryozoan grains

(Figure 18D). Interparticle cementation postdated early compaction (Figure 26, probable late phase 1 or phase 2) as indicated by cements which completely fill interparticle voids bordered by pelmatozoan grains which display sutured contacts (Figure 27D).

Dolomitization

Dolomitization of Lithotype 4 resulted in the complete alteration of non-intraparticle detrital muds (dolomicrite) and variable replacement of skeletal grains, calcite cements, and intraparticle micrite. As a general rule, partially dolomitized skeletal grains exhibit larger, more euhedral dolomite crystals than dolomitized mud (Figure 18C). Non-pelmatozoan grains, particularly mud-filled bryozoa, are preferentially dolomitized in comparison to pelmatozoan grains (Figure 18E). Dolomitization of pelmatozoan grains is commonly represented by mosaics of cloudy, anhedral dolomite within grains, and by larger, clear euhedral rhombs distributed along grain contacts and grain-cement boundaries (Figure 28A). Large, euhedral dolomite rhombs are observed within syntaxial calcite cements and cross-cutting pelmatozoan grains and their associated syntaxial overgrowths (Figure 27D), demonstrating that some dolomitization postdates early compaction and interparticle cementation. Dolomitized, circular to elliptical grains which are circumscribed by larger,

FIGURE 28- Thin-Section Photomicrographs

A) Thin-section photomicrograph illustrating the modes of occurrence of dolomite in Lithotype 4D. Dolomite occurs as fine, anhedral to subhedral mosaics within echinoderm grains (A), and as larger, clear, euhedral crystals distributed along grain contacts (G) and the boundaries between echinoderm bioclasts and their associated syntaxial cement (C). Scale bar is 100 microns. Oasis #1 Everton (SW/4 SE/4, 34-21S-24W), 4,672.7'.

B) Thin-section photomicrograph of dolomite fabrics in Lithotype 4C. Large, dark, circular to elliptical areas of anhedral to subhedral dolomite (E) surrounded by larger, clear, euhedral to subhedral dolomite (C) are interpreted to represent dolomitized echinoderm bioclasts (E) and partially dolomitized interparticle cement (C), respectively. Dissolution of undolomitized calcite resulted in open skeletal molds (M) and open dolomite mosaics in interparticle areas. This rock is a former, calcite-cemented, skeletal grainstone. Scale bar is 100 microns. Oasis #4 Deutsch (SE/4 SE/4, 33-21S-24W), 4,644.5'.

C) Thin-section photomicrograph of undolomitized, bryozoan-dominated, lime grainstone (Lithotype 4D). Interparticle areas are fully cemented with calcite (c). The interior of two echinoderm bioclasts are partially silicified (S). Scale bar is 100 microns. Oasis #7 Deutsch (SE/4SW/4, 34-21S-24W), 4,672'.

D) Thin-section photomicrograph of a partially dolomitized and partially leached skeletal grainstone. Large, clear, subhedral to euhedral dolomite crystals (D) denote the location of probable, former interparticle cement and former grain contacts. Undissolved calcite consists of partially dissolved echinoderm grains (E). Scale bar is 100 microns. Oasis #1 Deutsch (NE/4 SE/4, 33-21S-24W), 4,629.9'.

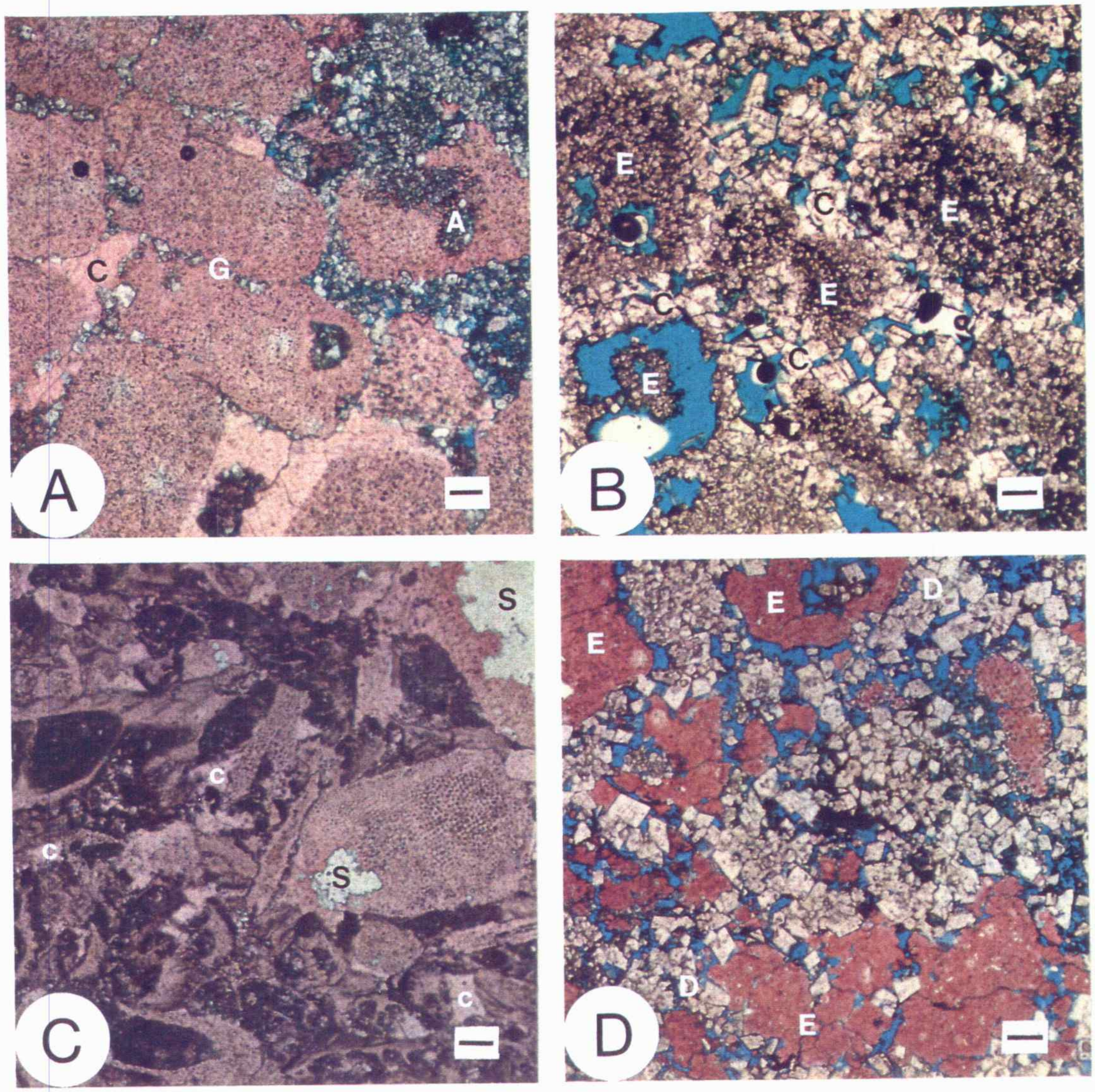
A
C
G
A
B
E
C
E
E
C
C
E
C
S
c
c
S
c
D
E
E
D
D
E

more euhedral, clear dolomite crystals are interpreted to be dolomite pseudomorphs of pelmatozoan grains and associated syntaxial cements (Figure 28B).

Lithotypes 4C (dolopackstone/grainstone) and 4D (lime grainstone) are distinguished mainly by the degree of dolomitization which has occurred in the grain-supported sediments (i.e. the arbitrary cutoff between the two is at 50% dolomite content). The minimal dolomitization of Lithotype 4D may be partially explained by limited invasion of dolomitizing fluids into the well-cemented rock.

The degree of interparticle cementation in grainstones and mud-poor packstones may be related to skeletal composition. In consideration of the apparent rapid rate of syntaxial cementation of pores bordered by pelmatozoan bioclasts, it seems unlikely that syntaxial cementation would result in varying degrees of cementation of interparticle pores bordered by pelmatozoan bioclasts. Incompletely cemented, pelmatozoan-rich lime grainstones were not observed; therefore it is probable that all pelmatozoan-dominated grainstones were fully cemented. Grain-supported rocks dominated by non-echinoderm grains (e.g. bryozoa) may have experienced less cementation due to the greater fraction of pores bordered by non-pelmatozoan grains, resulting in the retention of some interparticle pore space and permeability. However, skeletal composition of grain-supported rocks does not appear to be a universal determinant of susceptibility to dolomitization. Undolomitized, completely cemented grainstones include bryozoan-dominated assemblages (Figure 28C) as well as pelmatozoan-dominated assemblages.

Interparticle cementation does not preclude dolomitization of grainstones. Examples of partially to fully dolomitized grainstones which are interpreted to have been syntaxially cemented pelmatozoan grainstones are observed (Figures 28B, 28D). The interpretation of the cemented grainstone precursor is based on 1) examination of intermediate phases between undolomitized grainstones and pervasively dolomitized grainstones containing relict skeletal calcite and cement, and 2) differences in dolomite size, fabric, and clarity between dolomitized bioclasts and cement. The occurrence of cemented, pelmatozoan grainstones which have been pervasively dolomitized suggests that the variable degree of dolomitization of grainstone fabrics is not controlled solely by the degree of interparticle cementation. Other contributing factors are thickness of cemented grainstones accumulations, proximity to permeable and/or muddy sediments, and time. The only constant with respect to dolomitization is the ubiquitous dolomitization of non-intraparticle mud. It is probable that the areas of grainstone layers or lenses which are proximal to muddier fabrics (i.e. the outer portions) are likely to be dolomitized most readily because of the greater exposure to dolomitizing fluids there. Due to the impeded flow of dolomitizing fluids in cemented or partially cemented grainstones, interior areas of cemented grainstone accumulations should exhibit the least dolomitization. Therefore, the interior of thicker, more areally extensive cemented grainstone accumulations would be expected to remain undolomitized (Lithotype 4D) whereas thinner accumulations and the exterior of thicker accumulations would be expected to be dolomitized (Lithotype 4C). This is in contrast to the interpretation of Ebanks et al. (1977) in which the only grainstone fabrics recognized in Bindley Field were the pervasively cemented, undolomitized lime grainstones with no reservoir potential. While cemented, undolomitized lime grainstones (Lithotype 4D) do occur in Bindley Field, the conclusion that all cemented grainstones experienced the same diagenetic history is not necessarily valid. Many examples of dolomitized grainstones which were originally cemented by calcite (included in Lithotype 4C) were observed in this study.

The interpretation of this study that interparticle cementation predates dolomitization, and that dolomitization of grainstones is retarded, rather than precluded, in cemented grainstones is in contrast with the interpretation of rocks of similar composition, age, and geologic setting in Iowa and Illinois (Harris and Meyers, 1987). Harris and Meyers (1987) have proposed that interparticle cementation postdated dolomitization, and calcite cements overgrew and enclosed pre-existing dolomite rhombs. While this possibility cannot be ignored in Bindley Field rocks, it is considered unlikely for the following reasons:

1) If dolomitization preceded interparticle cementation, dolomitizing fluids presumably circulated through an open, interparticle pore system. Therefore, some evidence of dolomitization would be expected throughout a small grainstone accumulation of uniform composition. This is not the case in Bindley Field grainstones. Fully cemented, completely undolomitized grainstones occur adjacent to partially or pervasively dolomitized grainstones of similar composition. Non-uniform dolomitization seems more likely in a well cemented grainstone than in an uncemented grainstone.

2) Single, euhedral dolomite rhombs crosscut both pelmatozoan grains and their associated syntaxial cements (Figure 27D). The fact that a euhedral dolomite

rhomb grew as a replacement of a skeletal grain and extended into the interparticle area adjacent to the grain implies that a solid phase existed in the interparticle area at the time of dolomite replacement. However, if more than one episode of dolomitization occurred in the rock, this evidence only indicates that some dolomitization, but not necessarily all dolomitization, postdated cementation.

Cathodoluminescence petrography of Lithotype 4 dolomite reveals three distinct phases of dolomite (Figures 29A, 30). The petrographic associations between the three dolomite phases are schematically summarized in Figure 30. Dolomite I exhibits dull to moderately bright, orange luminescence. Dolomite II exhibits very dull, pale orange-red luminescence. Dolomite III is non-luminescent. Dolomite I is commonly observed at the margins of euhedral rhombs which are otherwise composed of Dolomite II, with an irregular contact between the two phases. Dolomite I is also observed as irregular patches within such rhombs. Dolomite I is not considered to be an overgrowth of Dolomite II due to the irregular contact between the two phases and the fact that Dolomite I also occurs as irregular blotches within areas of Dolomite II. As such, one is likely to be a replacement of the other. No conclusive evidence was observed which indicates the

FIGURE 29- Thin-Section Photomicrographs

A) Cathodoluminescence photomicrograph of Lithotype 4C dolomite illustrating three phases of dolomite. Dolomite I occurs at the outer margins of dolomite rhombs and as irregular patches within dolomite rhombs. Dolomite II occurs in the interior of dolomite rhombs and displays an irregular contact with Dolomite I in the same rhombs. Dolomite III forms euhedral overgrowths on precursor rhombs composed of Dolomites I and II. Oasis #6 Deutsch (SW/4 SW/4, 34-21S-24W), 4,655.5'.

B) Cathodoluminescence photomicrograph illustrating the preferential association of Dolomite II with areas of subhedral to euhedral dolomite fabric (dolomitized skeletal grains). Dolomite with anhedral fabrics (dolomitized muds) are comprised primarily of Dolomite I. Dolomite III occurs between precursor rhombs in subhedral to euhedral fabrics. Scale bar is 100 microns. Oasis #3 Deutsch (NW/4 SW/4, 34-21S-24W), 4,675.6'.

C) Cathodoluminescence photomicrograph of large, euhedral Dolomite III rhomb within an open skeletal mold. Scale bar is 100 microns. Oasis #4 Deutsch (SE/4 SE/4, 33-21S-24W), 4,644.5'.

D) Cathodoluminescence photomicrograph illustrating the irregular contact (C) between Dolomite III and precursor Dolomites I and II. Dolomite III occurs within precursor rhombs (i) where it is surrounded by Dolomite I. Scale bar is 100 microns. Oasis #4 Deutsch (SE/4 SE/4, 33-21S-24W), 4,644.5'.

E) Cathodoluminescence photomicrograph showing the presence of inclusions (i) of Dolomite I within Dolomite III. Scale bar is 100 microns. Oasis #4 Deutsch (SE/4 SE/4, 33-21S-24W), 4,644.5'.

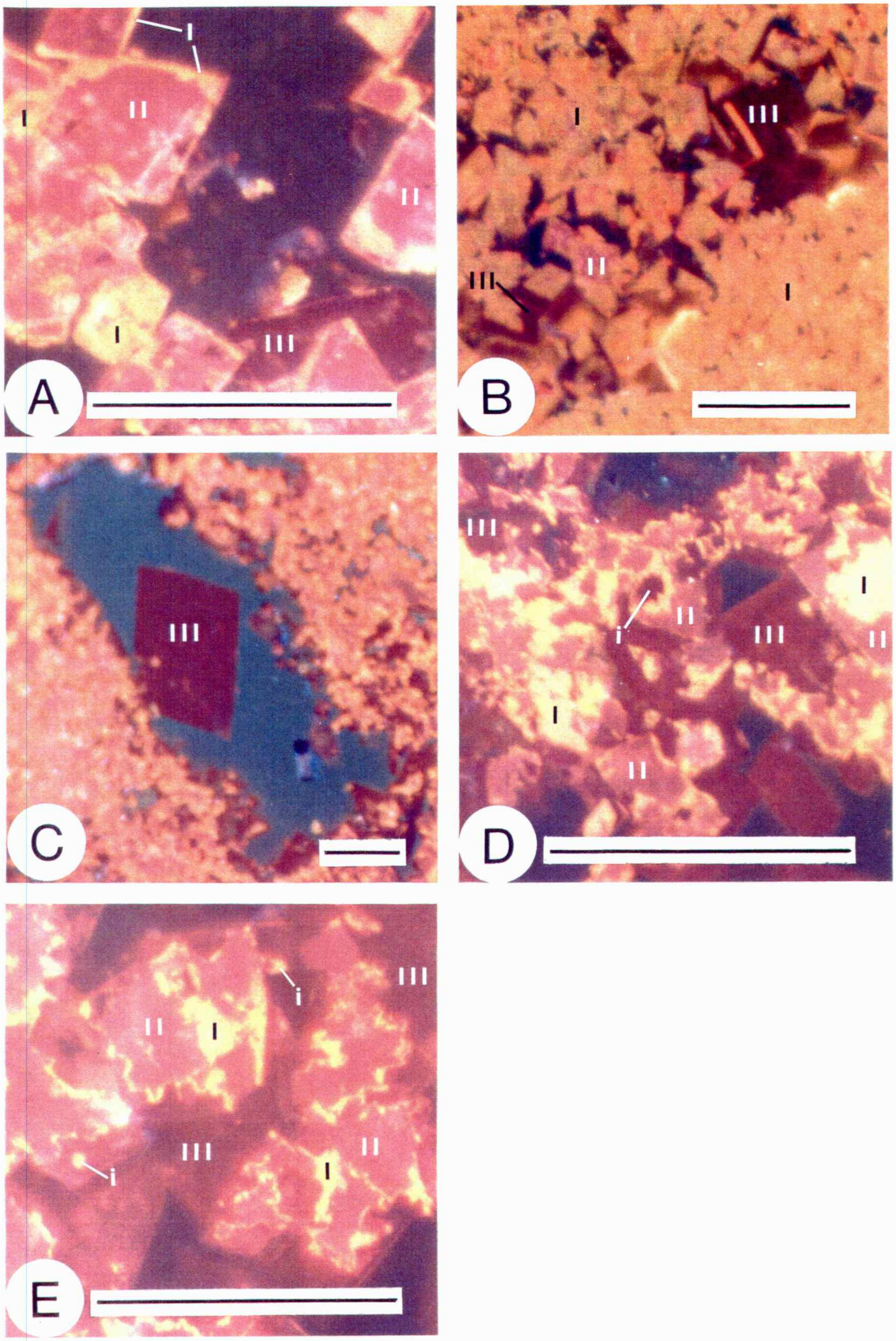
A
I
II
III
B
I
II
III
C
III
D
I
II
III
i
E
I
II
III
i

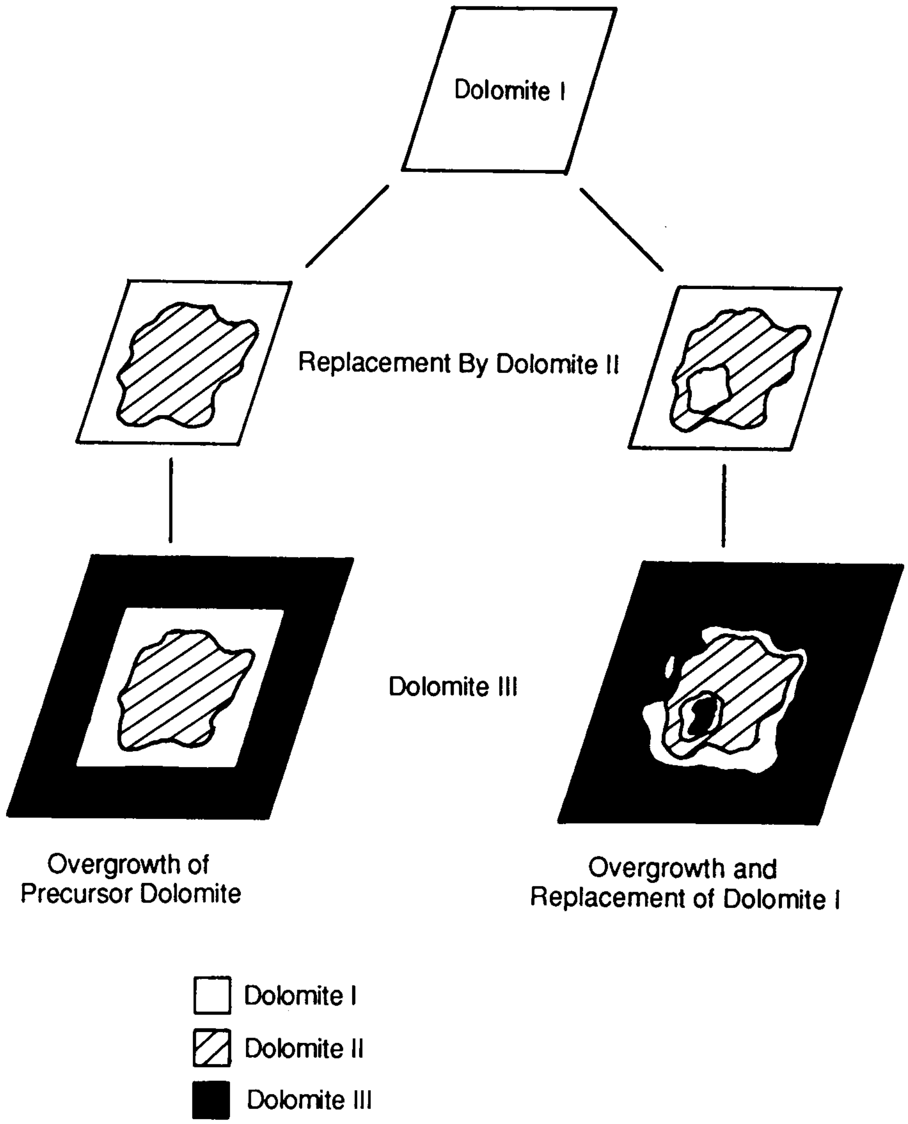

FIGURE 30- Schematic illustration of petrographic associations between dolomites I, II, and III.

chronological relationship between the two; however, the observed distribution of the two phases suggests that Dolomite II is a replacement of the interior portions of Dolomite I. Dolomite I is prevalent in areas of anhedral fabric and Dolomite II occurs primarily in areas with subhedral to euhedral fabrics (Figure 29B) which represent porous zones associated with molds of partially dolomitized skeletal grains. This implies that Dolomite II did not replace Dolomite I until after the dissolution of undolomitized calcite which created the moldic porosity associated with the occurrence of Dolomite II (refer to discussion of dissolution below). The pervasive replacement of the interior portions of precursor dolomite rhombs by a subsequent phase of dolomite, leaving rims of the precursor dolomite in irregular contact with the replacing dolomite, has been described by Harris and Meyers (1987) and Cander et al. (1988) in rocks of Osagian age from Iowa, Missouri, and Illinois.

Dolomite III is non-luminescent and occurs as euhedral overgrowths of precursor Dolomites I and II (Figures 29A and 29B), as a replacement of precursor Dolomite I, and as large, isolated, euhedral rhombs within skeletal molds (Figure 29C). Staining indicates that the dolomite is non-ferroan. Dolomite III represents the final phase of dolomitization and is interpreted as a void-filling phase and a replacement of skeletal calcite and of precursor Dolomite I. Where Dolomite III has overgrown precursor dolomite, the precursor phase may exhibit a sharp, very irregular, contact with Dolomite III (Figure 29D). In such cases, Dolomite I rims the edge of the precursor dolomite and Dolomite II generally comprises the interior. In addition, Dolomite III is observed in the interior of precursor rhombs where the border of the precursor dolomite with Dolomite III is rimmed by Dolomite I (Figure 29D). Dolomite II may also occur in contact with Dolomite III and, in many such cases, Dolomite III then contains inclusions of Dolomite I (Figure 29E). These varied observations imply that Dolomite III simultaneously overgrew precursor rhombs and replaced relict Dolomite I in the same precursor rhombs. As such, the occurrence of Dolomite I bordering the irregular edges represents relict edges of Dolomite I which were not replaced by Dolomite II. The occurrence of patches of Dolomite III which are bordered by relict Dolomite I within the interior of Dolomite I/II rhombs (Figure 29D) also attests to the preferential replacement of Dolomite I by Dolomite III. In other cases, Dolomite III has overgrown euhedral rhombs of precursor Dolomites I and II with no evidence of replacement of the precursor Dolomite I. The relationships between Dolomite III and precursor dolomites I and II are similar to those described by Cander et al. (1988) and Harris and Meyers (1987) in Osagian rocks from Iowa, Missouri, and Illinois.

Dolomite III is preferentially distributed in skeletal molds as large, euhedral rhombs and as overgrowths and replacements of precursor dolomites surrounding moldic areas. This association implies that Dolomite III was a void-filling phase. However, some Dolomite III replaced skeletal calcite (Figure 29F). It thus probable that Dolomite III represents both void-filling and replacement of undissolved skeletal calcite to the extent that Dolomite III simultaneously grew in dissolution voids and replaced skeletal calcite which had not been dissolved.

Because Dolomites I and II exhibit a replacive association, the later of the two phases does not alter the volume of sediment which was initially dolomitized by the earlier phase. Dolomite in mud-supported non-reservoir rocks consists primarily of Dolomite I and Dolomite II. Dolomite in grain-supported rocks consists of Dolomites I, II, and III. Due to the possible void-filling nature of Dolomite III, its emplacement may have led to some degree of porosity reduction, but did not significantly occlude porosity in the samples studied.

The timing of dolomitization relative to burial history is not well constrained. Dolomite I, as the initial replacive dolomite phase, likely occurred during late initial burial or during late Mississippian-early Pennsylvanian uplift (Figure 26, phases 1 and 2, respectively). The timing of Dolomite II is uncertain other than its chronological position between Dolomites I and III. Due to the void-filling nature of Dolomite III, its occurrence post-dated dissolution of undolomitized calcite. It is probable that Dolomite III occurred subsequent to late Mississippian-early Pennsylvanian subaerial exposure (Figure 26, end of phase 2).

Dissolution of Undolomitized Calcite

In rocks which were substantially dolomitized (i.e. Lithotypes 4A-4C), undolomitized calcite (both skeletal and cement) was leached at some point in their diagenetic history. Little or no dissolution took place in undolomitized rocks (i.e. Lithotype 4D), and the degree of dissolution is related to the degree of dolomitization (Figures 31A, 31B, 31C). Dissolution of skeletal calcite resulted in the formation of open molds and, in the case of partially dolomitized skeletal grains, dolomitic pseudomorphs of grains (Figure 31D). Dissolution of interparticle cement resulted in voids which define the edges of dolomitized grains.

FIGURE 31- Thin-Section Photomicrographs

A) Thin-section photomicrograph of Lithotype 4D which has experienced minimal dolomitization (D) and no dissolution. The rock is composed of echinoderm (E) and bryozoan (B) bioclasts and interparticle, syntaxial calcite (C). Dolomite is principally associated with bryozoan bioclasts. Scale bar is 100 microns. Oasis #7 Deutsch (SE/4SW/4, 34-21S-24W), 4,650.1'.

B) Thin-section photomicrograph of partially dolomitized Lithotype 4D and porosity (blue) associated with dolomitized areas. Scale bar is 100 microns. Oasis #7 Deutsch (SE/4SW/4, 34-21S-24W), 4,650.1'.

C) Thin-section photomicrograph of pervasively dolomitized Lithotype 4C containing undissolved skeletal calcite (E). Dolomite contains abundant inclusions of calcite. A pseudomorph of a partially dolomitized and dissolved echinoderm grain is situated at the center of the upper portion of the photo. Porosity (P) is abundant in intraparticle (moldic) and interparticle areas. Scale bar is 100 microns. Oasis #1 Deutsch (NE/4 SE/4, 33-21S-24W), 4,629.9'.

D) Thin-section photomicrograph of pervasively dolomitized, probable former grainstone in which all undolomitized calcite has been dissolved. Dolomitized pseudomorphs of skeletal grains (G), probable partially dolomitized interparticle cements (C), and open skeletal molds (M) are evident. Scale bar is 100 microns. Oasis #6 Deutsch (SW/4 SW/4, 34-21S-24W), 4,655.5'.

E) Thin-section photomicrograph of purple to pink-stained, zoned ferroan and non-ferroan calcite (Z). Fully cemented voids are outlined by a film of residual oil (O). Scale bar is 100 microns. Oasis #1 Smith (SW/4 NW/4, 34-21S-24W), 4,659.1'.

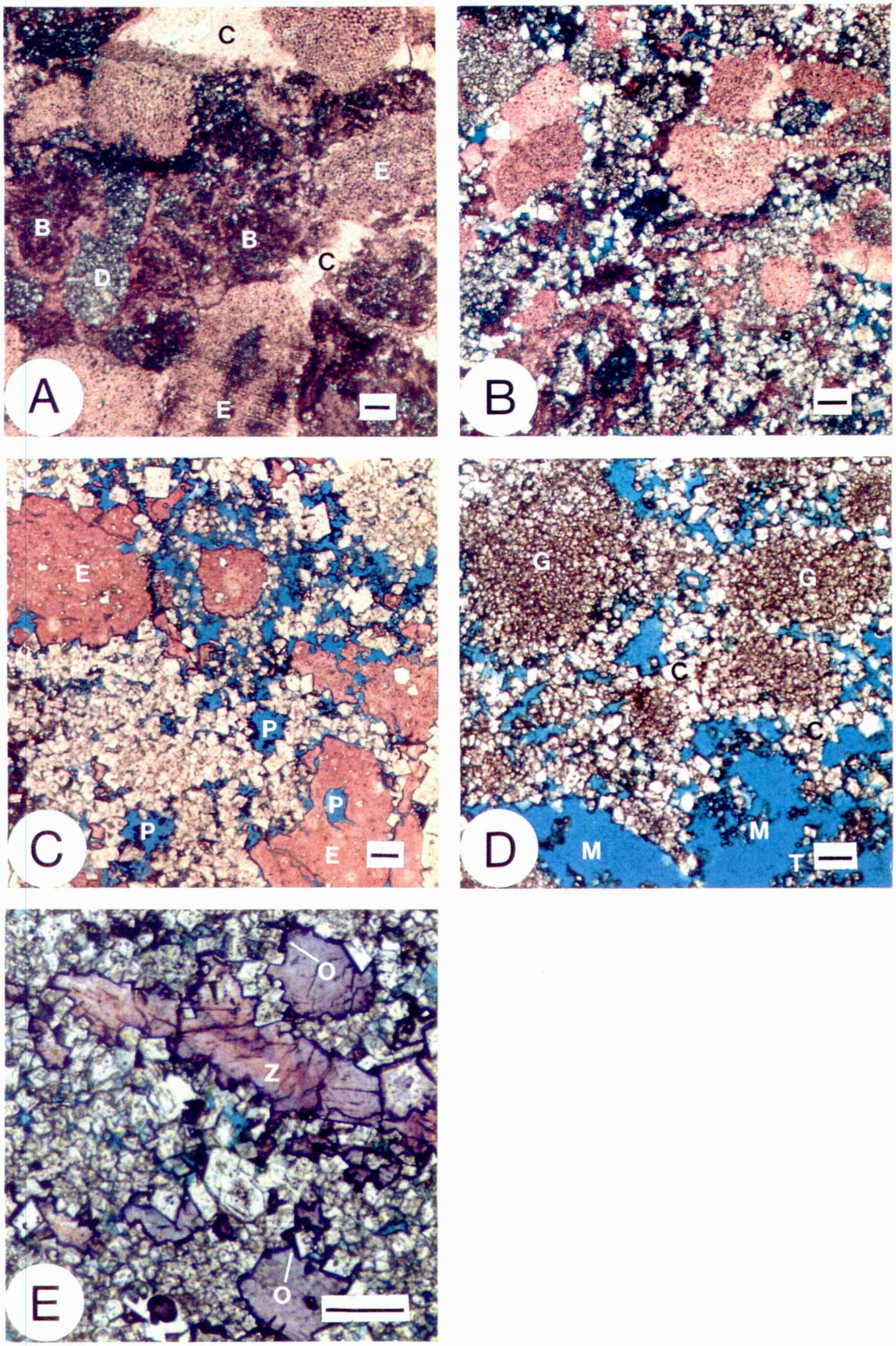
C
E
B
B
C
D
A
E
B
E
P
P
P
E
C
G
G
C
C
M
M
T
D
O
Z
O
E

The timing of dissolution is uncertain, although a relation to meteoric water influx associated with the pre-Pennsylvanian unconformity (Figure 26, late phase 2) is a reasonable hypothesis. The assumption is made that all dissolution is related to the same mechanism, although the possibility of dissolution of some portion of the calcitic host in association with early dolomitization cannot be dismissed. Where Dolomite III grew in voids, dissolution predated Dolomite III as evidenced by the occurrence of single, euhedral Dolomite III rhombs within skeletal molds (Figure 29C). The relationship between the timing of dissolution and the formation of Dolomites I and II is less clear. It was suggested above that Dolomite II replaced the interior of Dolomite I after dissolution based on the association of Dolomite II with subhedral/euhedral dolomite fabrics indicative of porosity and permeability created by dissolution of skeletal calcite. If this interpretation is correct, then some dissolution preceded the replacement of Dolomite I by Dolomite II.

Brecciation

Brecciation in Bindley Field is related to meteoric water influx during the time of the basal Pennsylvanian unconformity (Figure 26, late phase 2). Brecciation was not observed to have significantly affected reservoir development or preservation in the

Meramec 2 interval in Bindley Field cores, but its effects may be anticipated under the proper circumstances. Infiltration/eluviation of clays into solution-widened fractures which penetrate the Meramec 2 reservoir subintervals would be expected to plug pores adjacent to the fractures and probably disrupt horizontal continuity in preexisting reservoir. Erosional truncation of the upper portion of the Meramec 2 interval, which presumably evolved through a brecciation stage, is evident in the northwestern portion of the field (Figures 9 and 10). Although no cores are available from this part of the field, and it is uncertain whether the truncated intervals actually contained any reservoir, brecciation may be regarded as having led to reservoir destruction in the sense that those subintervals which contain reservoir elsewhere in the field were truncated.

Late Cementation by Zoned Ferroan and Non-Ferroan Calcite

In localized areas, zoned ferroan and non-ferroan calcite cement fills larger pores that resulted from dissolution of undolomitized calcite (Figure 31E). Cementation of individual pores is complete but cementation of the rock is incomplete in that the majority of smaller pores contain no cement. The occurrence of zoned calcite cements is limited to areas below the zone of oil saturation which are typically within the Meramec 2A and 2B subintervals. A residual film of oil is observed lining fully cemented pores (Figure 31E) but is absent bordering undissolved skeletal calcite. The confinement of zoned calcite cements to areas below oil saturated horizons and the presence of residual oil which outlines fully cemented pores indicates that this zoned cement was emplaced within pores which contained residual oil at the time of cementation and therefore postdated oil migration. When oil migration occurred relative to burial history (Figure 26) is unknown; however, it is likely that it occurred between Pennsylvanian burial and post-Cretaceous uplift.

Summary

The critical diagenetic events leading to the creation of porous reservoir rock are 1) pervasive, but incomplete, dolomitization of grain-supported depositional fabrics, and 2) dissolution of undolomitized calcite (skeletal and cement), whether in association with or postdating early dolomitization. Dolomite III, a late addition, occluded some porosity but is not observed to be volumetrically significant in the Meramec 2 interval. However, it is conceivable that the precipitation of small volumes of Dolomite III caused significant reductions in pore-throat sizes.

Late cementation by zoned ferroan and non-ferroan calcite reduced porosity but occurred subsequent to oil migration and therefore did not affect reservoir quality within the oil-saturated portions of the reservoir. Other diagenetic features (isopachous intraparticle cement, compaction, and brecciation) had no discernable effect on reservoir development and/or preservation.

CHAPTER VI

RESERVOIR DESCRIPTION

The petrophysical characterization of reservoir quality and its distribution are critical to understanding the factors leading to creation of reservoir, the causes of its distribution, and reservoir production performance. The relationship between porosity and permeability, the permeability distribution in the field, the relationship of reservoir quality to lithotypes (depositional and diagenetic factors), and capillary pressure characteristics of reservoir samples were examined. A model for the formation of reservoir quality rock and its distribution is then presented, followed by comparison of the model to actual well production histories.

Petrophysical Characteristics

Porosity and Permeability

Ebanks (1987) noted the wide range of permeability corresponding to a narrow range of porosity within the "bryozoan dolomite facies" (reservoir facies) of Ebanks et al. (1977). This facies exhibits permeability values ranging from less than 0.5

millidarcys to over 100 millidarcys (Figure 14 of Ebanks, 1987). It is evident that the reservoir properties of this facies are quite variable and that all rocks included in the "bryozoan dolomite facies" are not of equal reservoir quality. The "bryozoan dolomite facies" of Ebanks et al. (1977) is equivalent to Lithotypes 4A-C of this study.

The factors which define reservoir quality in Bindley Field are of importance. In a fundamental sense, reservoir rock must possess the dual attributes of fluid storage capacity (porosity) and capability to transmit fluid (permeability). Rock with only one of the two properties, or a low magnitude of either, generally will not function as reservoir rock within the context of economic production of oil or gas. Relatively high average porosity (i.e. 10 to 25%) is present in the bulk of the rocks sampled by cores in Bindley Field (Lithotypes 1, 2A, 2B, 3, 4 A-C), yet permeability is distributed in discrete intervals (Figure 32). The non-linear relationship between porosity and permeability is evident in a crossplot representing all lithotypes cored in a single well from the center of the field (Figure 33). Because most of the rock in Bindley Field contains relatively high porosity (except Lithotype 4D), permeability is the determining factor in reservoir quality. Reservoir

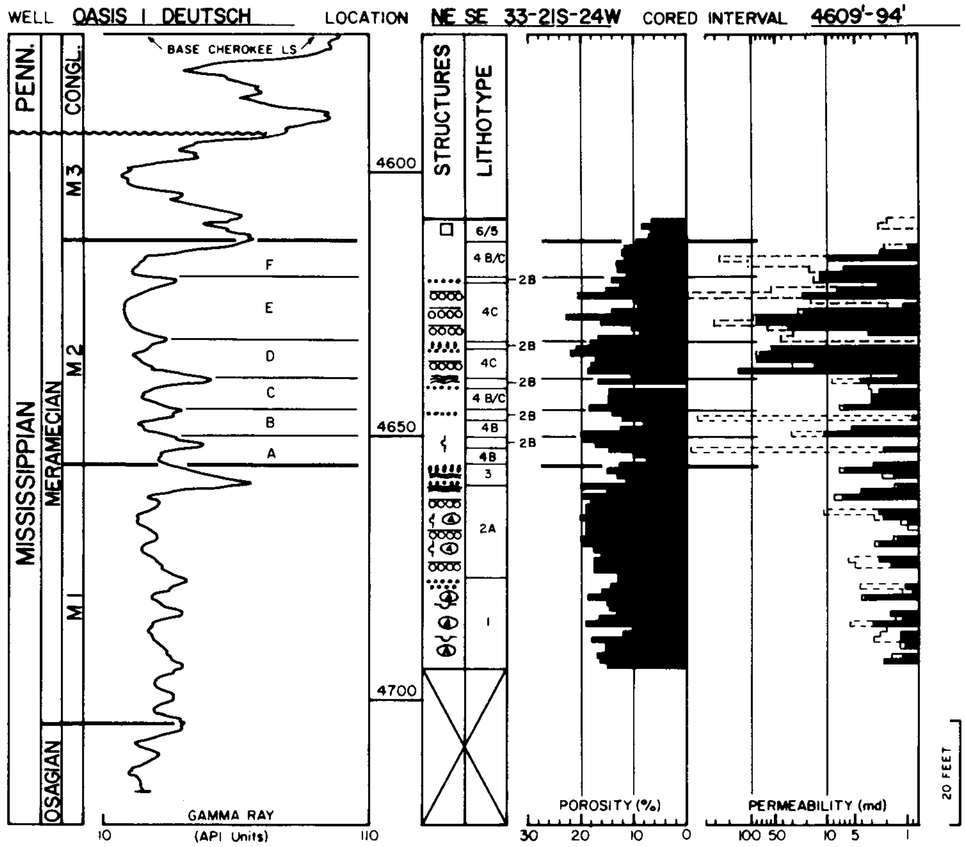

FIGURE 32- Correlation of porosity and permeability in a representative Bindley Field well (same well as illustrated in Figure 20). Permeability values indicated by a dashed line indicate the maximum, directional, horizontal permeability of the sample (k_{max}). The permeability values indicated by solid black represent horizontal permeability at right angles to the direction of maximum permeability (k_{90}). If the two values differ significantly, fracturing is generally indicated. In a sample with homogeneous matrix permeability, the two values will be in close agreement. Most of the Meramec 1 and Meramec 2 intervals contain porosity exceeding 10%. Permeability is not correlated to porosity as exemplified by the Meramec 1 interval where porosity approaches 20% but permeability is generally less than 5 millidarcys. Note that permeability is distributed in discrete intervals separated by thin zones of very low matrix permeability. In the Meramec 2 interval, these low permeability zones correlate to the Lithotype 2B caps on top of each subinterval. Refer to Appendix A for key to structures.

quality in Bindley Field cannot be calculated directly from logs due to the fact that permeability does not exhibit a linear relationship to porosity, and because permeability is not directly measurable from wireline logs. Gamma-ray/neutron porosity/ resistivity (single depth of investigation) logs were typically run in Bindley Field wells, and these log suites do not allow qualitative estimation of permeability as may be done with other suites such as invasion profiles in dual induction logs.

Relationship of permeability to lithotype. Core permeability is strongly dependent on lithotype in Bindley Field. Using the Oasis #1 Deutsch (NE/4 SE/4, 33-T21S-R24W) as an example (Figure 32), Lithotypes 1, 2A, 2B, 3, 4A, 4B, and 6 typically exhibit maximum core permeability to air of less than 10 millidarcys (Figure 34). Lithotypes 4D and 5 are not present in this well but exhibit very low permeability in adjacent wells (Appendix B). Only one lithotype, Lithotype 4C, exhibits permeability that consistently exceeds 10 millidarcys and reaches a maximum of 159 millidarcys (higher in other wells). This correlation of high permeability to Lithotype 4C is consistent throughout the field.

Variability in permeability within Lithotype 4C is partially explained by the gradational nature of

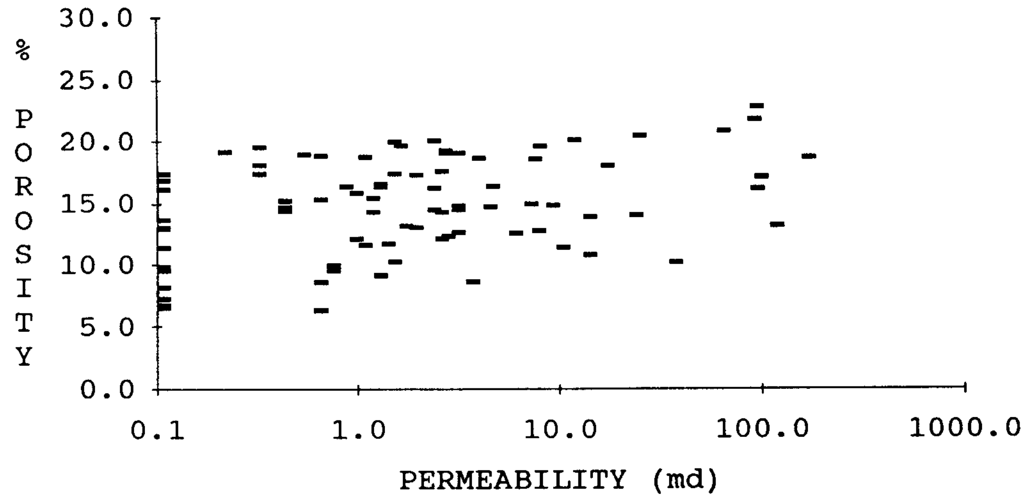

FIGURE 33- Crossplot of porosity and permeability in a representative Bindley Field well (same well as illustrated in Figure 32) derived from whole-core analysis. All lithotypes described in Bindley Field are represented except Lithotypes 4D and 5. Without segregating lithotypes, no relationship between porosity and permeability is evident. For this reason, porosity expressed on open-hole logs does not necessarily relate to permeability and reservoir quality.

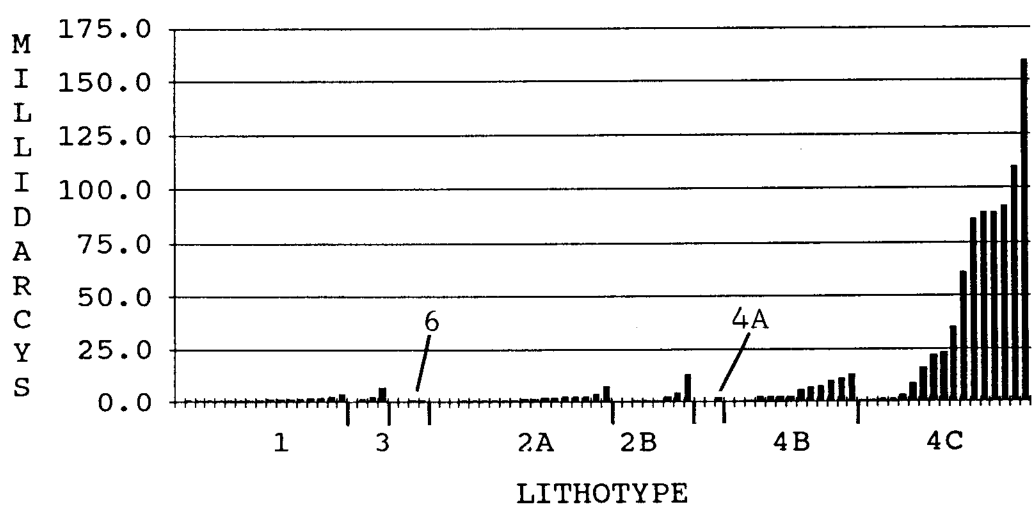

FIGURE 34- Distribution of permeability (k_{90}) sorted by lithotype from data illustrated in Figure 33. High permeability is confined to Lithotype 4C.

sedimentary fabrics. The fact that rocks with mud-supported fabrics (i.e., Lithotypes 1, 2A, 2B, 3, 4A, 4B, 5) have the lowest permeability, and certain rocks with grain-supported fabrics (i.e., Lithotype 4C) have the highest permeability indicates that permeability is partially related to dolomitized mud content. The range of fabrics in Lithotype 4C includes pure grain-supported intervals as well as grain-supported intervals with substantial mud-supported interlayers, thus some variability in permeability is to be expected. In addition to mud content, variability in permeability within Lithotype 4C is also related to diagenetic factors as discussed below.

Due to the correlation of permeability to lithotype, the distribution of permeability throughout the field should mimic the distribution of Lithotype 4C. Because Lithotype 4C comprises the majority of all grain-supported rocks, the overall distribution of permeability in the Meramec 2 interval (Figure 35) parallels the distribution of grain-supported subtypes (Figure 24A). The areas of thickest grain-supported lithotypes correspond to areas of greatest permeability development.

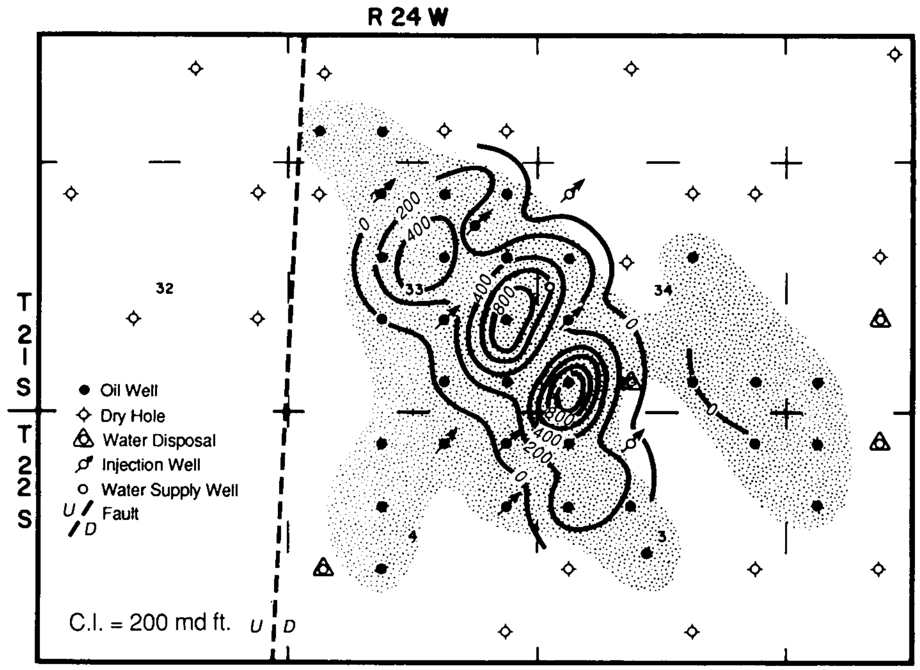

FIGURE 35- Distribution of Meramec 2 permeability equal to or exceeding 10 millidarcys. Values are expressed in millidarcy-feet, calculated by multiplying the thickness (in feet) of permeable intervals by the average permeability (in millidarcys) of the intervals. Permeability development is coincident with the central axis of the field, and correlates to the areas of thickest grain-supported lithotypes (Figure 23A) and to areas of positive structural relief (Figure 11A). The field area is indicated by the stipled background.

Capillary Pressure Results

Principles of mercury porosimetry. Reservoir quality is further characterized by mercury intrusion/extrusion capillary pressure analysis, also known as mercury porosimetry. Principles of mercury porosimetry are described by Purcell (1949), Berg (1975), Wardlaw and Taylor (1976), Jennings (1987), and Wardlaw et al. (1988). Wardlaw (1976) and Amthor et al. (1988) provide examples of the application of capillary pressure analysis to carbonate rocks. The following discussion of basic principles is derived largely from these sources.

In mercury intrusion/extrusion analysis, porosity and permeability of each sample is first determined. Then, mercury is injected into an evacuated rock sample at increments of increasing pressure (referred to as "drainage" or "injection"). At each pressure increment, the volume of mercury injected, expressed as a percentage of total rock pore volume, is recorded. Once the maximum pressure and mercury saturation are reached, pressure is incrementally decreased while recording the volume of mercury extruded after each increment of pressure reduction (referred to as "imbibition" or "withdrawal"). The injection process is designed to simulate the displacement of the wetting phase in a porous rock (commonly assumed to be water) by a non-wetting phase (e.g. oil). Conversely, the withdrawal process simulates the displacement of the non-wetting phase (e.g. oil) due to pressure reduction. In standard mercury intrusion analysis, air is considered the wetting phase and mercury is considered to be the non-wetting phase.

Fluid movement between pores in a rock is controlled by the constrictions between pores referred to as pore throats (or pore apertures), which are, by definition, of smaller areal dimension than the cross-sectional area of the associated pores (Wardlaw, 1976). A single pore may be connected to other pores by more than one pore throat. The ability of a rock to transmit fluid between pores is largely dependent on the size of pore throats (pore aperture radius), the shape of pore throats, and the number of throats accessing each pore. During mercury injection, as pressure is increased, pores accessed by successively smaller throats are intruded. During withdrawal, the amount of non-wetting fluid in a pore which can be expelled during pressure reduction is partially dependent on the ratio of pore-throat size to pore volume. The ratio of the volume of mercury extruded during pressure reduction to the volume injected is referred to as the withdrawal efficiency (or recovery efficiency).

The increment of rock pore volume intruded by mercury at each pressure increment is a measure of the volume of pores which are controlled by pore throats of a certain size. Access to pore space intruded at higher pressure is controlled by smaller pore throats than pore space intruded at lower pressure. Pore-throat size may be estimated from injection pressure. Pore-throat shapes in dolostones are likely to be different from those in other rock types and are typically defined by the planar surfaces of dolomite crystals. The appropriate equation for the estimation of pore-throat dimensions from capillary pressures in dolostones is given in Wardlaw (1976) and Amthor et al. (1988). By plotting the cumulative pore volume intruded (mercury saturation) versus pressure, a general characterization of the pore and pore-throat network is achieved. Intrusion of mercury at relatively low pressure indicates large pore throats. Intrusion of a large portion of the pore volume of a rock over a narrow range of pressure indicates a well sorted pore-throat distribution (displayed as a flattened horizontal portion of the pore volume vs. mercury saturation graph). A histogram of the fraction of total pore volume governed by each pore-throat size increment (calculated from injection pressure) graphically displays the distribution of pore-throat sizes and the fraction of total pore volume controlled by each pore-throat size increment.

Bindley Field analysis. Twelve core plugs were analyzed from Bindley Field, eight with injection only, and four with injection and withdrawal. The plugs were selected to represent the major lithotypes associated with reservoir intervals. Data for all samples are compiled in Appendix C. Pore-throat sizes were estimated from injection pressure according to the equation given in Appendix C.

Pore-throat sizes in Bindley Field samples repeatedly cluster into one or more of four groups. The pressure range and calculated pore-throat size range for each group are as follow:

	Pressure Range (psi)	Pore-throat Range (microns)
Group A	1000 - 2000	0.11 - 0.05
Group B	100 - 1000	1.1 - 0.11
Group C	27 - 100	3.9 - 1.1
Group D	0 - 27	35 - 3.9

Pore space not saturated at the maximum pressure of 2,000 psi is governed by pore throats with calculated radii of less than 0.05 microns. Each sample analyzed exhibits a characteristic signature ranging from a unimodal distribution which is confined to Group A (smallest pore throats), to polymodal distributions dominated by one or more pore-throat size groups. Figures 36-42 illustrate the range of capillary pressure response in seven selected samples.

Permeability is positively correlated to the median size of all pore throats injected (i.e. adjusted for pore throats not injected). A plot of permeability vs. the injection pressure at the point of saturation of 50% of the invaded pore volume (second quartile pressure; Jennings, 1987) demonstrates a linear log-log relation (Figure 43). Permeability is also related to the dominant pore-throat size group (i.e. Groups A-D) represented in the pore-throat size distribution (Figure 44). Samples with pore-throat distributions confined to Group A (smallest pore throats) display permeability on the order of 0.01 millidarcy (Figures 36, 37). Samples with pore-throat distributions which include, but do not exceed, those of Group B or Group C exhibit permeability on the order of 0.1 and 1 to 5 millidarcys, respectively (Figures 38, 39, 42). Samples with pore-throat distributions dominated by Group D (largest pore throats) have measured permeabilities of 4 to 461 millidarcys (Figures 40, 41). Higher permeability samples exhibit a larger percentage of total pore volume controlled by the larger throats (Figure 45). It is clear that the highest quality reservoir, as measured by permeability, corresponds to samples with a high

FIGURE 36- Mercury intrusion charts and photomicrograph of Lithotype 2B (spiculitic dolomudstone). The dolomudstone sample is characterized by very low permeability, moderate porosity, very high entry pressure, high uninvaded pore volume, and Group A pore throats. Thin section is impregnated with blue epoxy and stained with Alizarin Red S and potassium ferricyanide. Note the unimpregnated spicule molds (M). Disseminated black specks are pyrite. Scale bar is 250 microns.

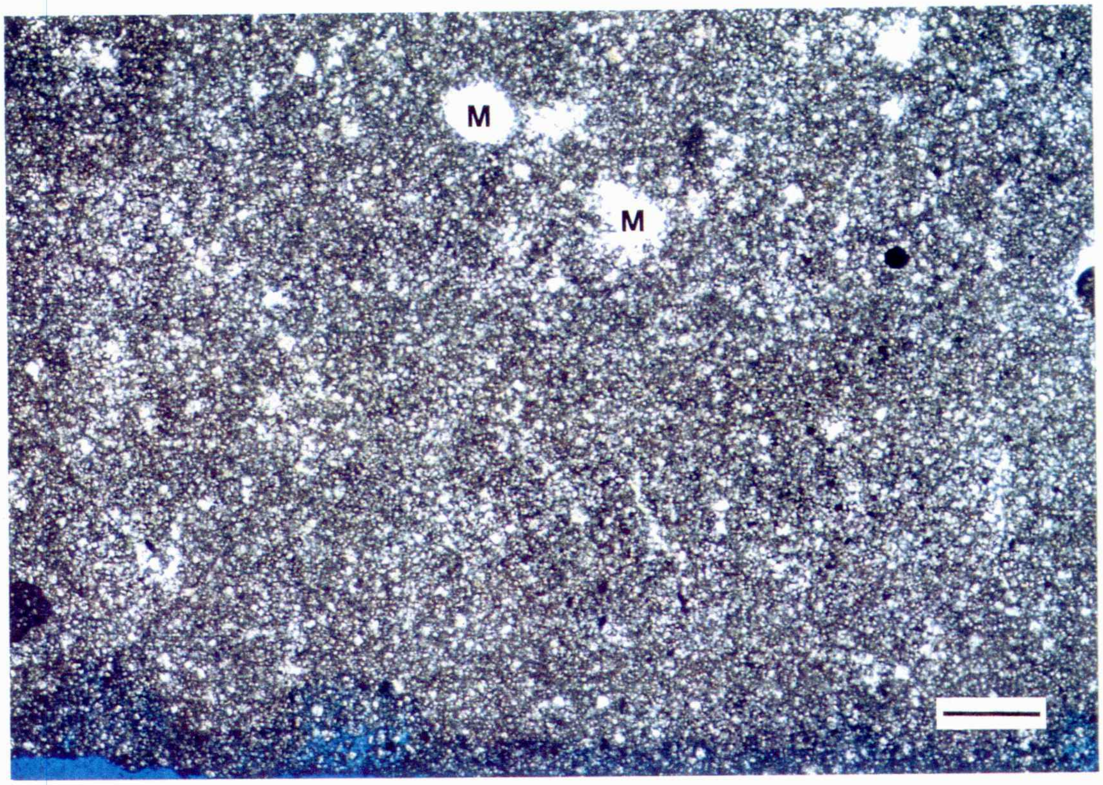
M
M

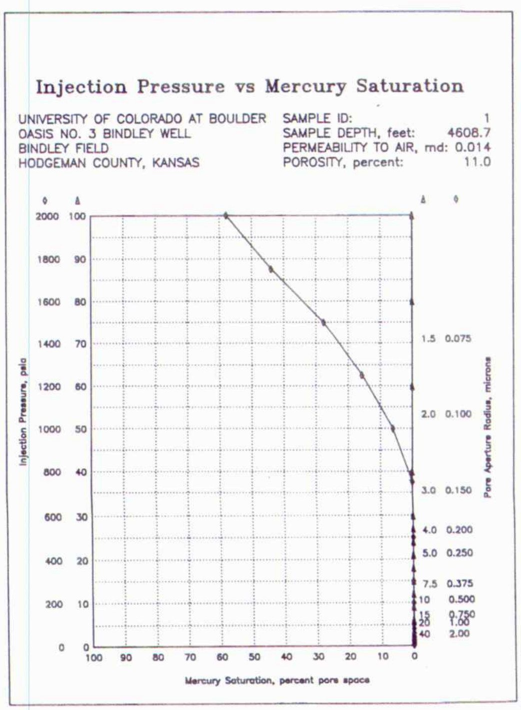
Injection Pressure vs Mercury Saturation
UNIVERSITY OF COLORADO AT BOULDER
OASIS NO. 3 BINDLEY WELL
BINDLEY FIELD
HODGEMAN COUNTY, KANSAS
SAMPLE ID: 1
SAMPLE DEPTH, feet: 4608.7
PERMEABILITY TO AIR, md: 0.014
POROSITY, percent: 11.0
Injection Pressure, psia
Pore Aperture Radius, microns
Mercury Saturation, percent pore space

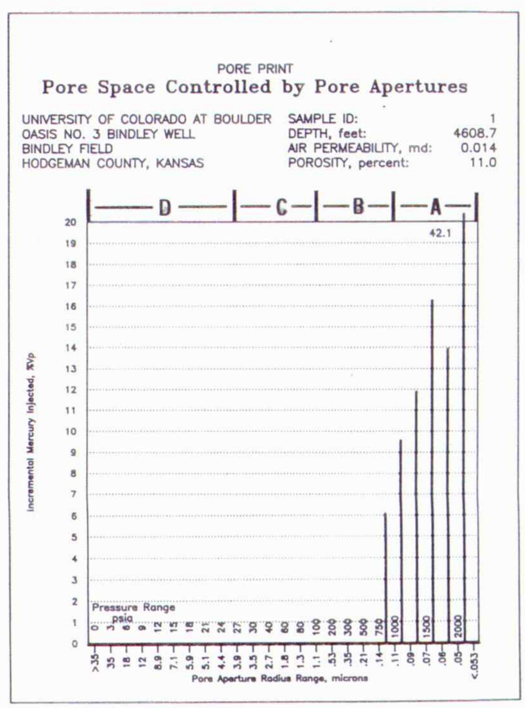
PORE PRINT
Pore Space Controlled by Pore Apertures
UNIVERSITY OF COLORADO AT BOULDER
OASIS NO. 3 BINDLEY WELL
BINDLEY FIELD
HODGEMAN COUNTY, KANSAS
SAMPLE ID: 1
DEPTH, feet: 4608.7
AIR PERMEABILITY, md: 0.014
POROSITY, percent: 11.0
D
C
B
A
42.1
Incremental Mercury Injected, %Vp
Pressure Range psia
Pore Aperture Radius Range, microns

FIGURE 37- Mercury intrusion charts and photomicrograph of Lithotype 4B (echinoderm/bryozoan dolowackestone) containing partially dolomitized and dissolved skeletal grains (M). The dolowackestone sample is characterized by very low permeability, relatively low porosity, high entry pressure, high uninvaded pore volume, and Group A pore throats. A small volume of pore space is accessed by Group B pore throats. The Group B pore system is considered to represent skeletal-moldic pores which are in communication with the exterior surface of the sample. To the extent that some portion of the skeletal molds are in communication, this small portion of pore volume is intruded first. The remaining pore volume is mud-controlled. Thin section is impregnated with blue epoxy and stained with Alizarin Red S and potassium ferricyanide. Note that some skeletal molds are impregnated and some are not. Black circles in unimpregnated molds are air bubbles. Black cubic minerals to left of photo are pyrite. Scale bar is 250 microns.

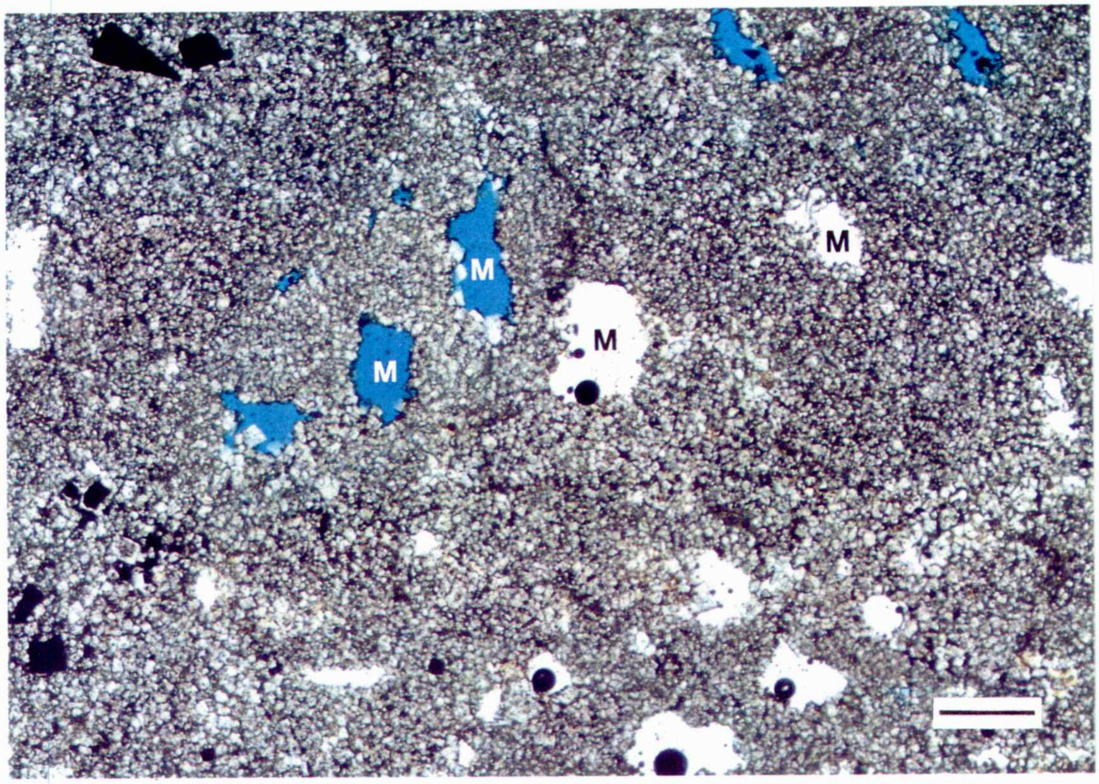
M
M
M
M

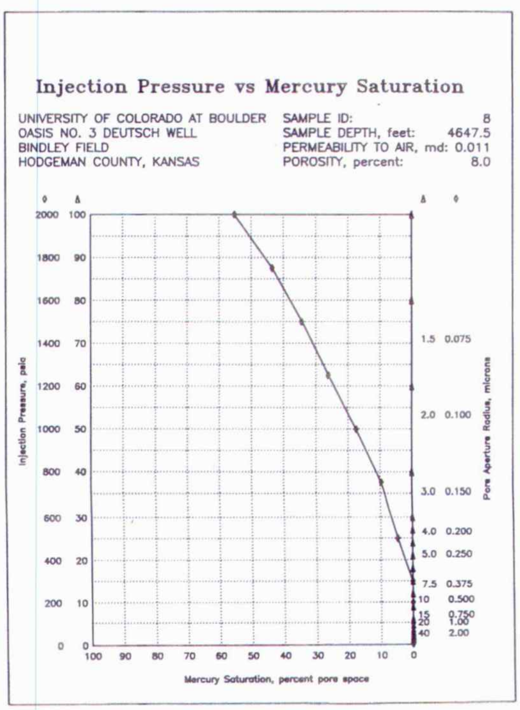
Injection Pressure vs Mercury Saturation
UNIVERSITY OF COLORADO AT BOULDER
OASIS NO. 3 DEUTSCH WELL
BINDLEY FIELD
HODGEMAN COUNTY, KANSAS
SAMPLE ID: 8
SAMPLE DEPTH, feet: 4647.5
PERMEABILITY TO AIR, md: 0.011
POROSITY, percent: 8.0
Injection Pressure, psia
2000 1800 1600 1400 1200 1000 800 600 400 200 0
100 90 80 70 60 50 40 30 20 10 0
Pore Aperture Radius, microns
1.5 0.075
2.0 0.100
3.0 0.150
4.0 0.200
5.0 0.250
7.5 0.375
10 0.500
15 0.750
20 1.00
40 2.00
100 90 80 70 60 50 40 30 20 10 0
Mercury Saturation, percent pore space

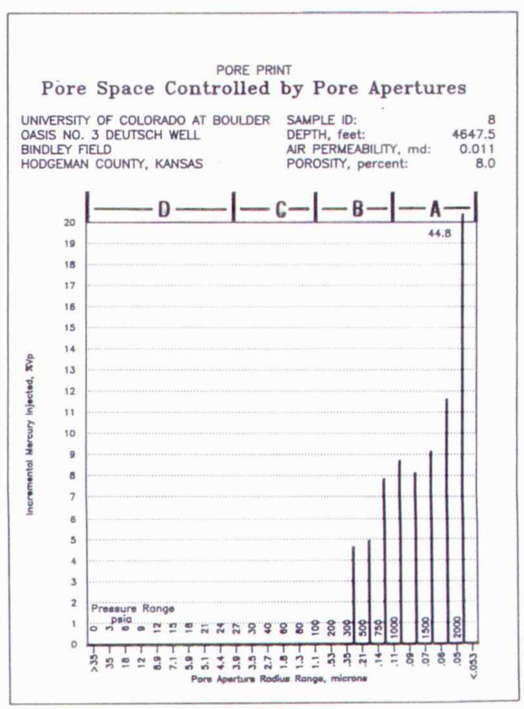
PORE PRINT
Pore Space Controlled by Pore Apertures
UNIVERSITY OF COLORADO AT BOULDER
OASIS NO. 3 DEUTSCH WELL
BINDLEY FIELD
HODGEMAN COUNTY, KANSAS
SAMPLE ID: 8
DEPTH, feet: 4647.5
AIR PERMEABILITY, md: 0.011
POROSITY, percent: 8.0
D C B A
44.8
Incremental Mercury Injected, %Vp
20 19 18 17 16 15 14 13 12 11 10 9 8 7 6 5 4 3 2 1 0
Pressure Range psia
0 3 6 9 12 15 18 21 24 27 30 40 60 80 100 200 300 500 750 1000 1500 2000
>35 35 18 12 8.9 7.1 5.9 5.1 4.4 3.9 3.5 2.7 1.8 1.3 1.1 .53 .35 .21 .14 .11 .09 .07 .06 .05 <.053
Pore Aperture Radius Range, microns

FIGURE 38- Mercury intrusion charts and photomicrograph of Lithotype 4C cemented by late, ferroan calcite (purple in photomicrograph). This sample is characterized by very low permeability, moderate porosity (blue in photomicrograph), relatively high entry pressure, moderate uninvaded pore volume, and Group B pore throats. The calcite cement occludes larger pore throats and available porosity is accessed by small, interboundary sheet throats. Undissolved skeletal calcite is stained pink. Thin section is impregnated with blue epoxy and stained with Alizarin Red S and potassium ferricyanide. Scale bar is 250 microns.

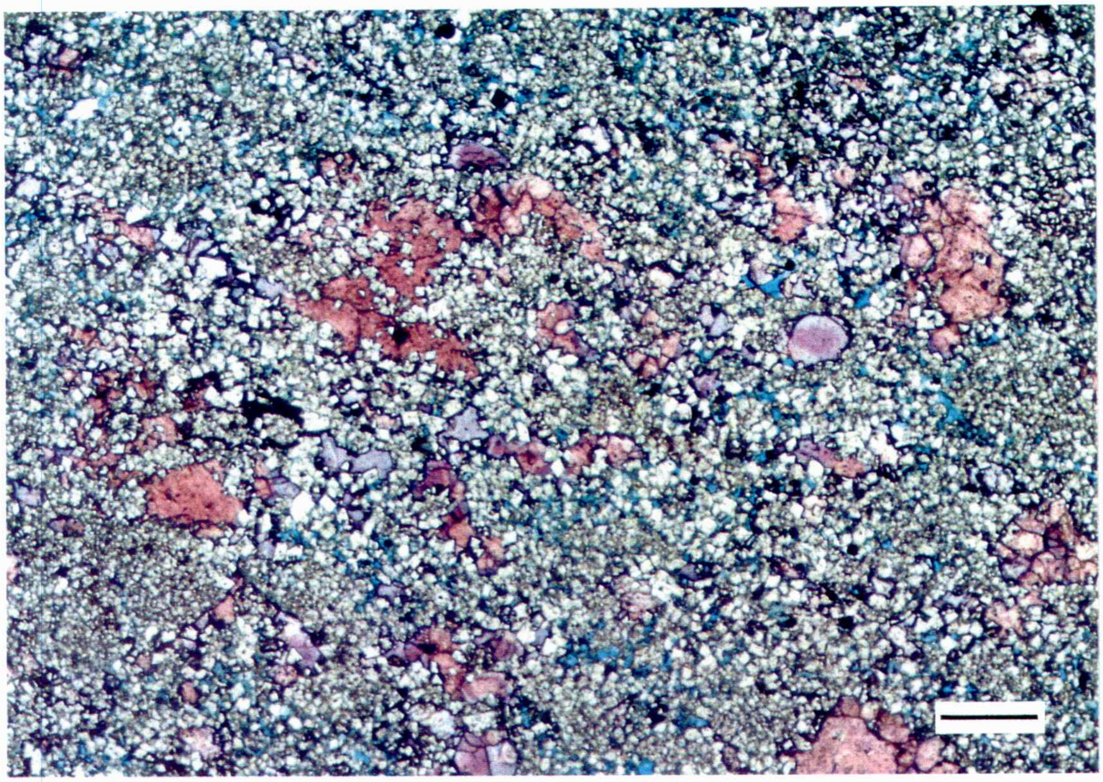

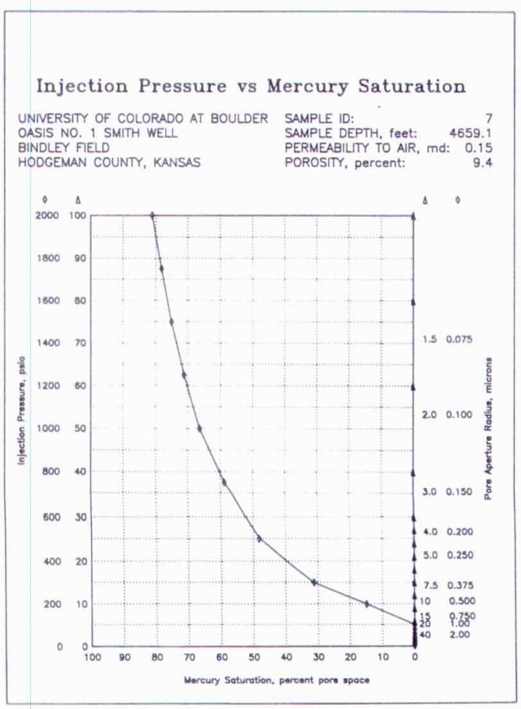
Injection Pressure vs Mercury Saturation
UNIVERSITY OF COLORADO AT BOULDER
OASIS NO. 1 SMITH WELL
BINDLEY FIELD
HODGEMAN COUNTY, KANSAS
SAMPLE ID: 7
SAMPLE DEPTH, feet: 4659.1
PERMEABILITY TO AIR, md: 0.15
POROSITY, percent: 9.4
Injection Pressure, psia
Pore Aperture Radius, microns
Mercury Saturation, percent pore space

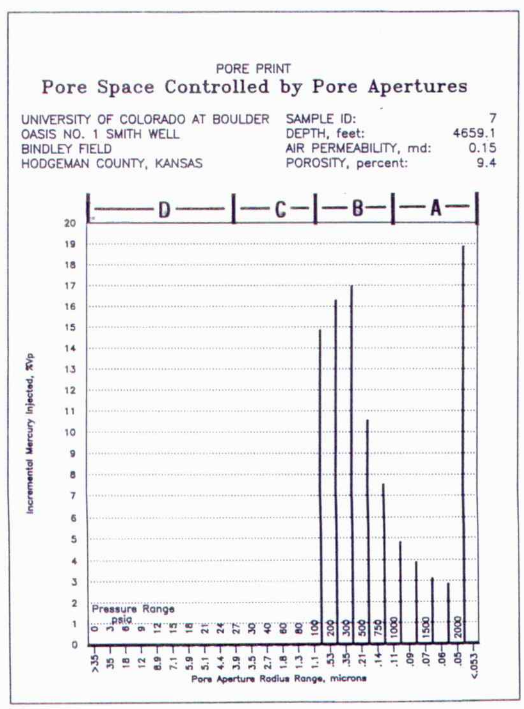
PORE PRINT
Pore Space Controlled by Pore Apertures
UNIVERSITY OF COLORADO AT BOULDER
OASIS NO. 1 SMITH WELL
BINDLEY FIELD
HODGEMAN COUNTY, KANSAS
SAMPLE ID: 7
DEPTH, feet: 4659.1
AIR PERMEABILITY, md: 0.15
POROSITY, percent: 9.4
D
C
B
A
Incremental Mercury Injected, %Vp
Pressure Range psia
Pore Aperture Radius Range, microns

FIGURE 39- Mercury intrusion charts and photomicrograph of partially dolomitized Lithotype 4D. This sample is characterized by low permeability, moderate porosity (blue in photomicrograph), low entry pressure, relatively low uninvaded pore volume, and Group C and B pore throats. Pore space is contained largely within dolomitized areas between echinoderm grains (E). Partially dolomitized areas have undergone dissolution leaving an intercrystalline dolomite pore system controlled by interboundary sheet throats and small tetrahedral throats. Thin section is impregnated with blue epoxy and stained with Alizarin Red S and potassium ferricyanide. Scale bar is 250 microns.

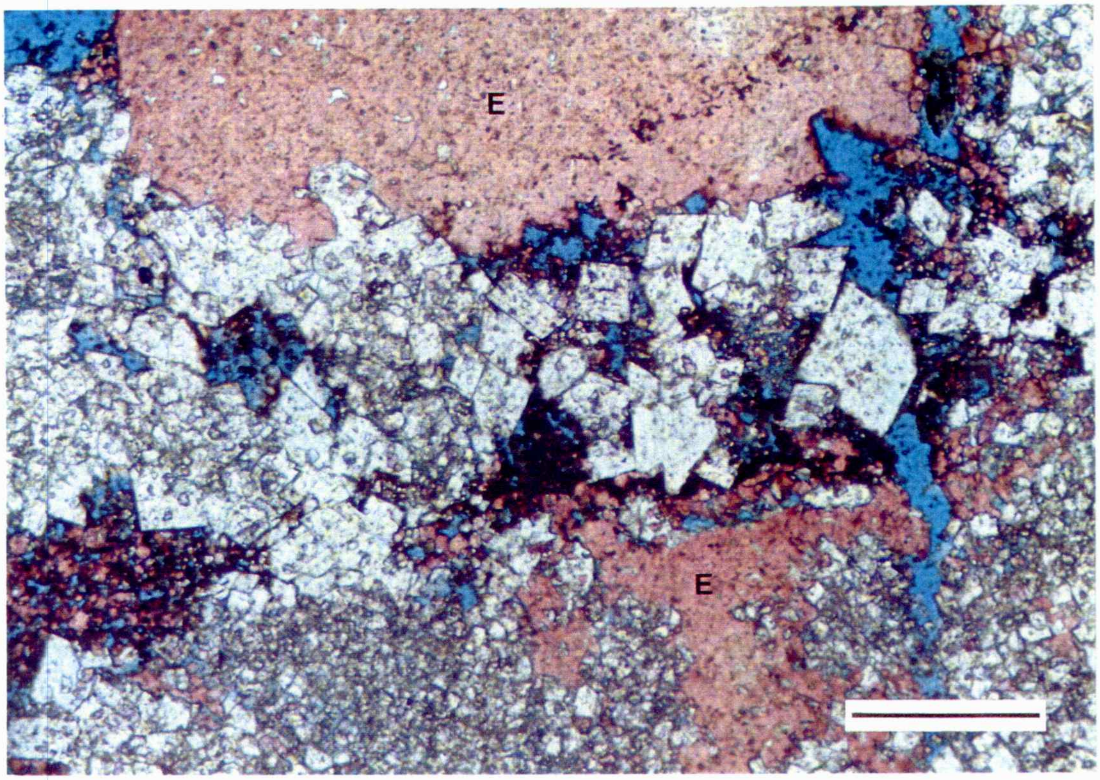
E
E

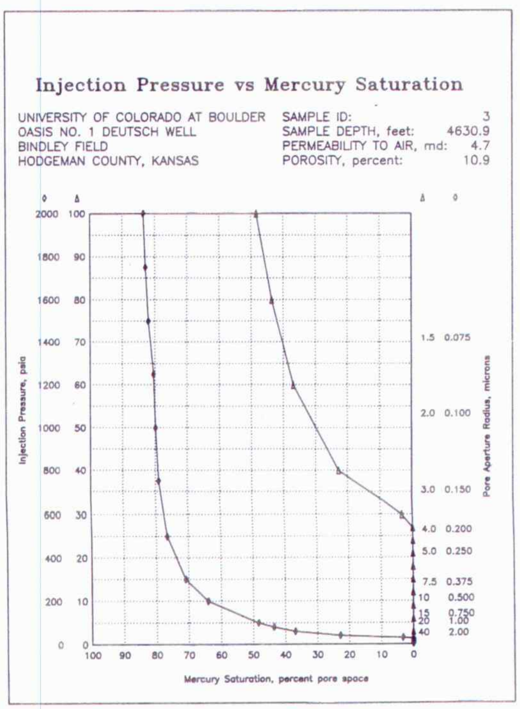
Injection Pressure vs Mercury Saturation
UNIVERSITY OF COLORADO AT BOULDER
OASIS NO. 1 DEUTSCH WELL
BINDLEY FIELD
HODGEMAN COUNTY, KANSAS
SAMPLE ID: 3
SAMPLE DEPTH, feet: 4630.9
PERMEABILITY TO AIR, md: 4.7
POROSITY, percent: 10.9
Injection Pressure, psia
Pore Aperture Radius, microns
Mercury Saturation, percent pore space

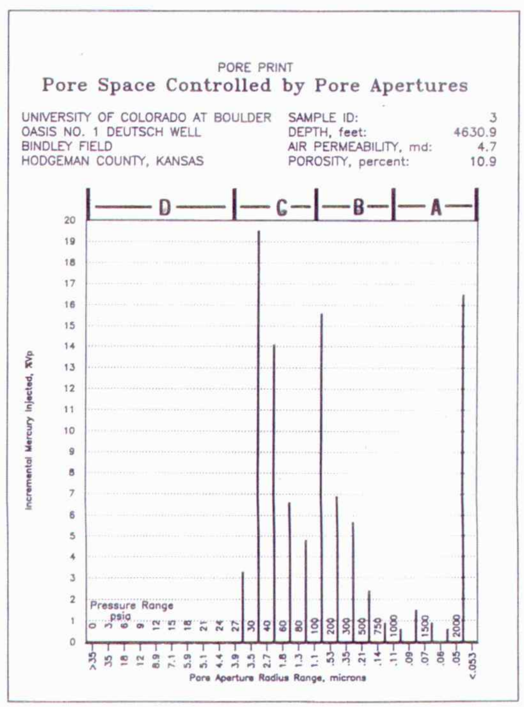
PORE PRINT
Pore Space Controlled by Pore Apertures
UNIVERSITY OF COLORADO AT BOULDER
OASIS NO. 1 DEUTSCH WELL
BINDLEY FIELD
HODGEMAN COUNTY, KANSAS
SAMPLE ID: 3
DEPTH, feet: 4630.9
AIR PERMEABILITY, md: 4.7
POROSITY, percent: 10.9
D
C
B
A
Incremental Mercury Injected, %Vp
Pressure Range psia
Pore Aperture Radius Range, microns

FIGURE 40- Mercury intrusion charts and photomicrograph of Lithotype 4C. This sample is characterized by high porosity (blue in photomicrograph), very high permeability, very low entry pressure, very low uninvaded pore volume, and large Group D pore throats. The pore system consists of molds and partial molds of skeletal grains (S) and former cement which are interconnected by large, open throats and large, polyhedral dolomite throats. Thin section is impregnated with blue epoxy and stained with Alizarin Red S and potassium ferricyanide. Scale bar is 250 microns.

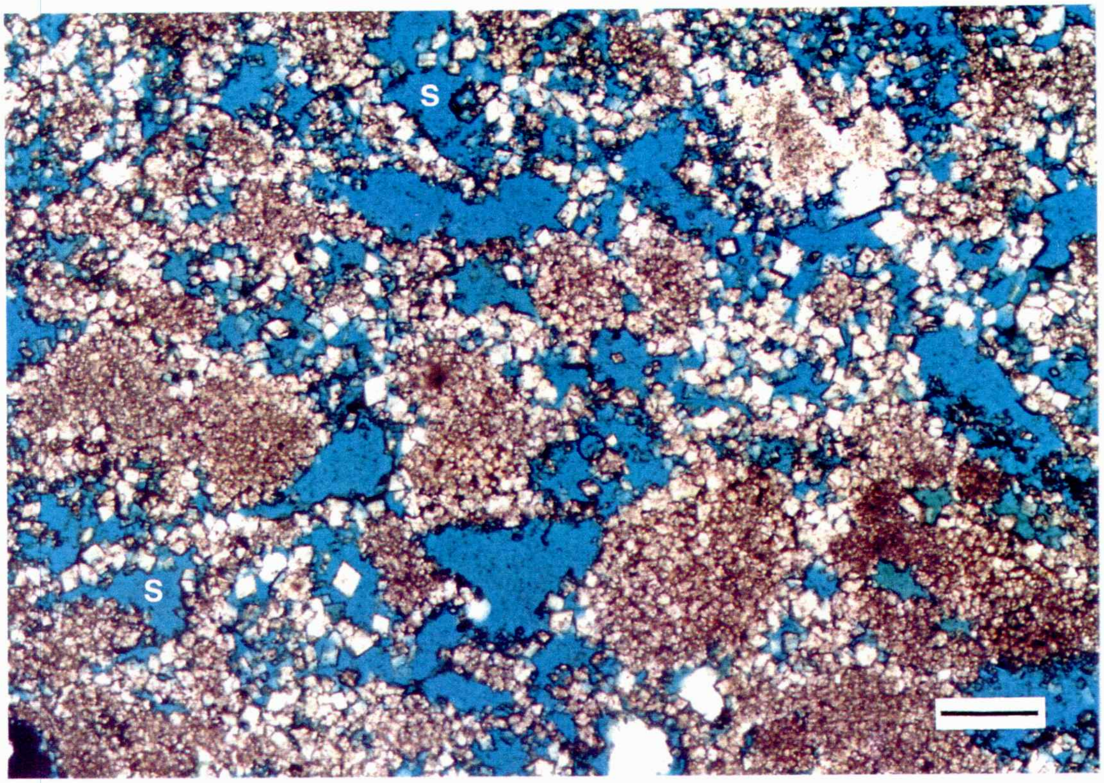
S
S

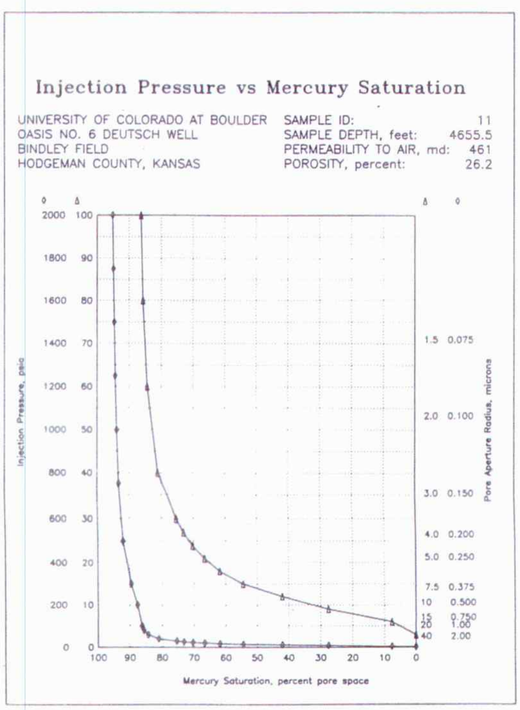
Injection Pressure vs Mercury Saturation
UNIVERSITY OF COLORADO AT BOULDER
OASIS NO. 6 DEUTSCH WELL
BINDLEY FIELD
HODGEMAN COUNTY, KANSAS
SAMPLE ID: 11
SAMPLE DEPTH, feet: 4655.5
PERMEABILITY TO AIR, md: 461
POROSITY, percent: 26.2
Injection Pressure, psia
Pore Aperture Radius, microns
Mercury Saturation, percent pore space

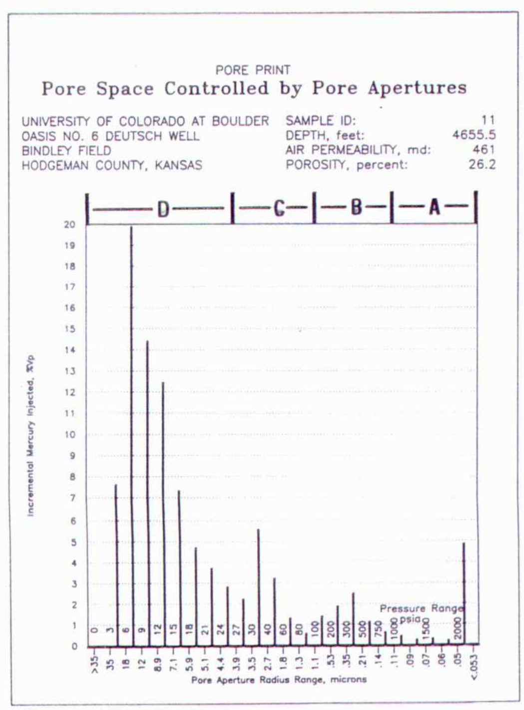
PORE PRINT
Pore Space Controlled by Pore Apertures
UNIVERSITY OF COLORADO AT BOULDER
OASIS NO. 6 DEUTSCH WELL
BINDLEY FIELD
HODGEMAN COUNTY, KANSAS
SAMPLE ID: 11
DEPTH, feet: 4655.5
AIR PERMEABILITY, md: 461
POROSITY, percent: 26.2
D
C
B
A
Incremental Mercury Injected, %Vp
Pressure Range psia
Pore Aperture Radius Range, microns

FIGURE 41- Mercury intrusion charts and photomicrograph of Lithotype 4C. This sample is characterized by high porosity (blue in photomicrograph), moderate permeability, low entry pressure, low uninvaded pore volume, and Group C and smaller Group D pore throats. The pore system consists of molds and partial molds of skeletal grains (S) and probable former cement which is interconnected by tetrahedral and small polyhedral pore throats. A greater degree of dolomitization than that of the sample illustrated in Figure 40 resulted in the smaller pore-throat geometries accessing the abundant moldic pores. Thin section is impregnated with blue epoxy and stained with Alizarin Red S and potassium ferricyanide. Dark circular areas are air bubbles in thin section. Scale bar is 250 microns.

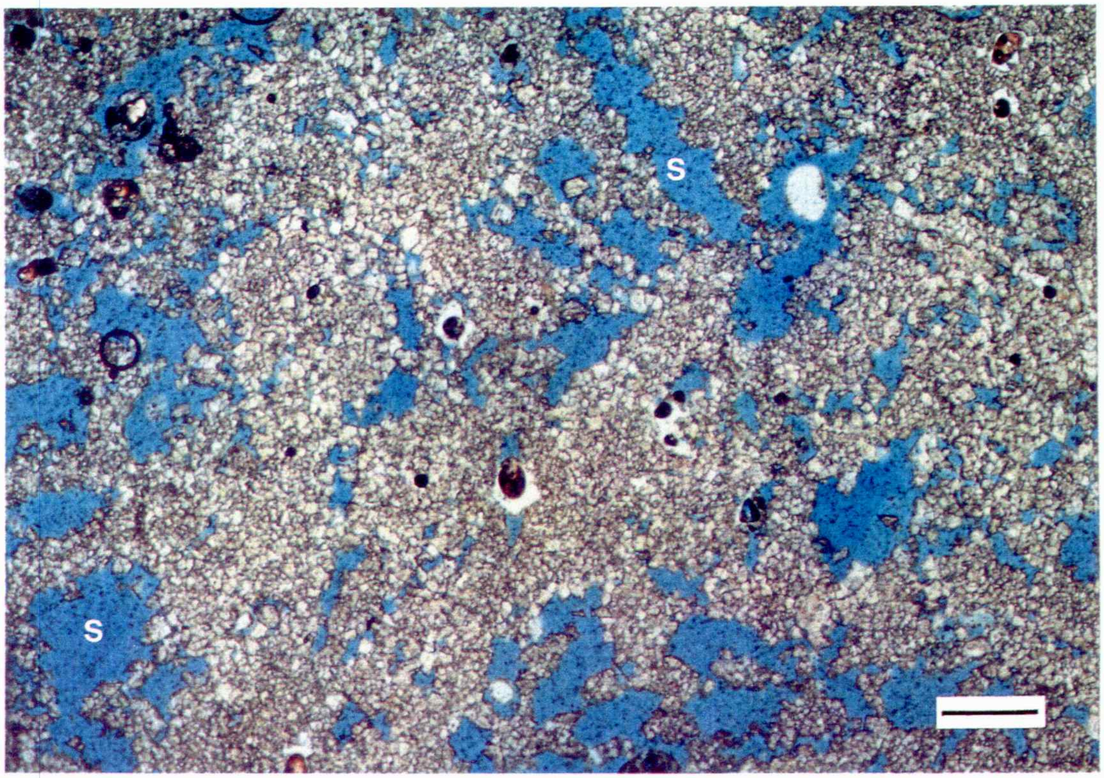
S
S

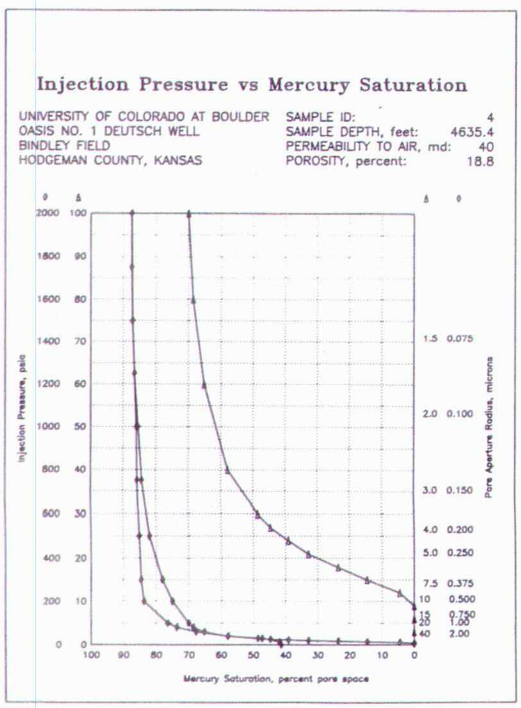
Injection Pressure vs Mercury Saturation
UNIVERSITY OF COLORADO AT BOULDER
OASIS NO. 1 DEUTSCH WELL
BINDLEY FIELD
HODGEMAN COUNTY, KANSAS
SAMPLE ID: 4
SAMPLE DEPTH, feet: 4635.4
PERMEABILITY TO AIR, md: 40
POROSITY, percent: 18.8
Injection Pressure, psia
Pore Aperture Radius, microns
Mercury Saturation, percent pore space

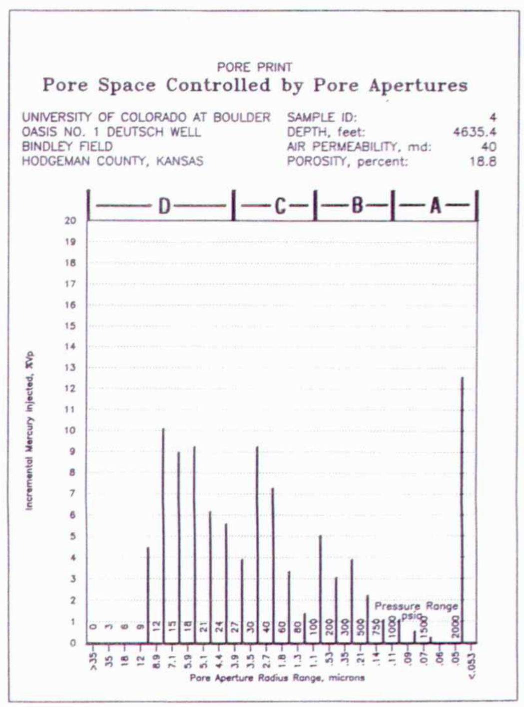
PORE PRINT
Pore Space Controlled by Pore Apertures
UNIVERSITY OF COLORADO AT BOULDER
OASIS NO. 1 DEUTSCH WELL
BINDLEY FIELD
HODGEMAN COUNTY, KANSAS
SAMPLE ID: 4
DEPTH, feet: 4635.4
AIR PERMEABILITY, md: 40
POROSITY, percent: 18.8
D
C
B
A
Incremental Mercury Injected, %Vp
Pressure Range psia
Pore Aperture Radius Range, microns

FIGURE 42- Mercury intrusion charts and photomicrograph of Lithotype 4C. This sample is characterized by moderately high porosity (blue in photomicrograph), low permeability, moderate entry pressure, moderate uninvaded pore volume, and Group C and B pore throats. The pore system consists of small, partial molds of skeletal grains and voids outlining fully dolomitized grains which are interconnected by dolomite networks with small tetrahedral and interboundary sheet throats. This rock was a probable grainstone which was extensively dolomitized. Dolomite fabrics separating moldic pores are anhedral to subhedral. Thin section is impregnated with blue epoxy and stained with Alizarin Red S and potassium ferricyanide. Dark circular areas are air bubbles in thin section. Scale bar is 250 microns.

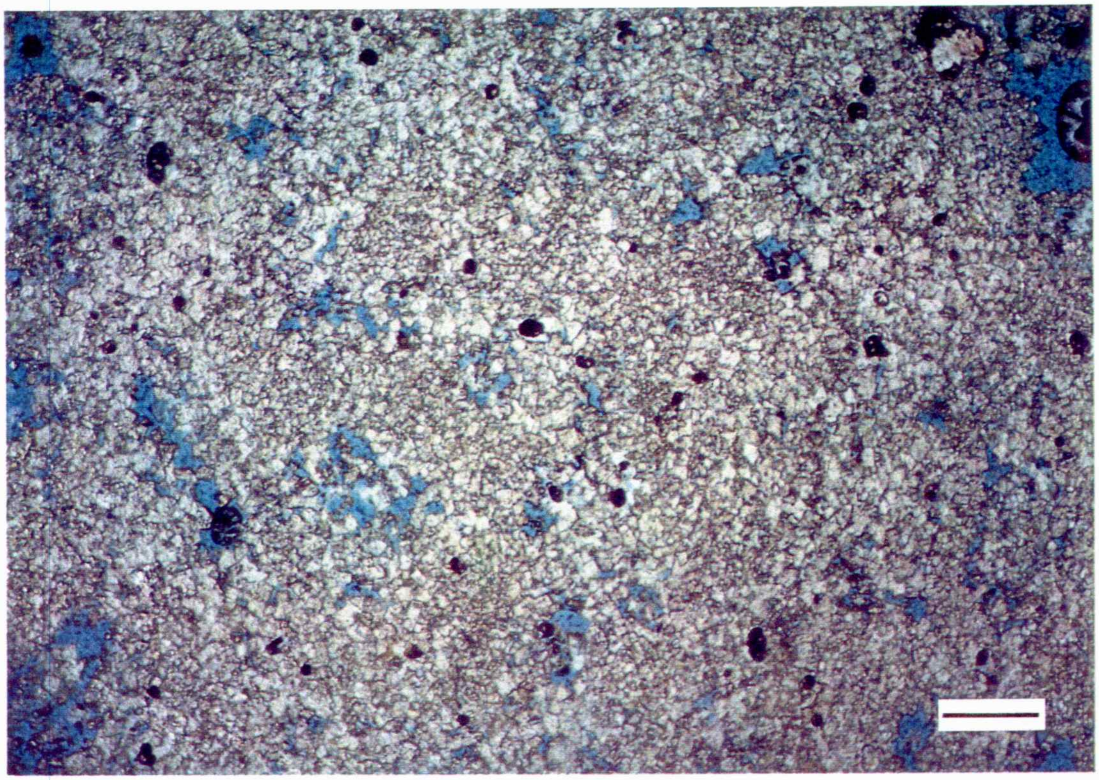

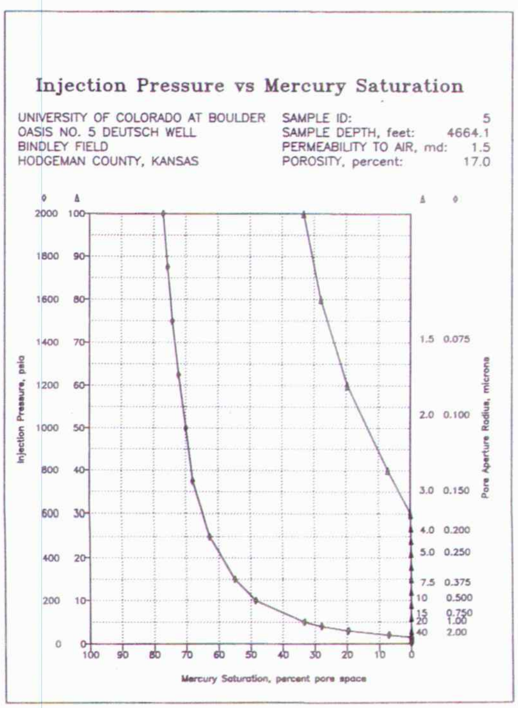
Injection Pressure vs Mercury Saturation
UNIVERSITY OF COLORADO AT BOULDER
OASIS NO. 5 DEUTSCH WELL
BINDLEY FIELD
HODGEMAN COUNTY, KANSAS
SAMPLE ID: 5
SAMPLE DEPTH, feet: 4664.1
PERMEABILITY TO AIR, md: 1.5
POROSITY, percent: 17.0
Injection Pressure, psia
Pore Aperture Radius, microns
Mercury Saturation, percent pore space

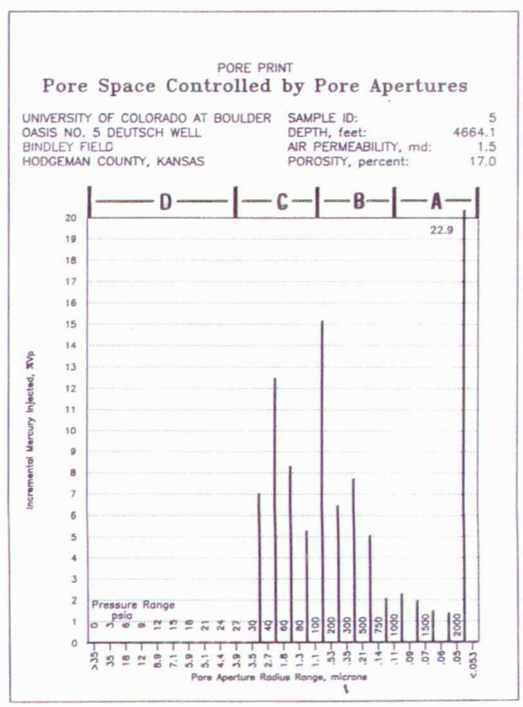
PORE PRINT
Pore Space Controlled by Pore Apertures
UNIVERSITY OF COLORADO AT BOULDER
OASIS NO. 5 DEUTSCH WELL
BINDLEY FIELD
HODGEMAN COUNTY, KANSAS
SAMPLE ID: 5
DEPTH, feet: 4664.1
AIR PERMEABILITY, md: 1.5
POROSITY, percent: 17.0
D
C
B
A
22.9
Incremental Mercury Injected, %Vp
Pressure Range psia
Pore Aperture Radius Range, microns

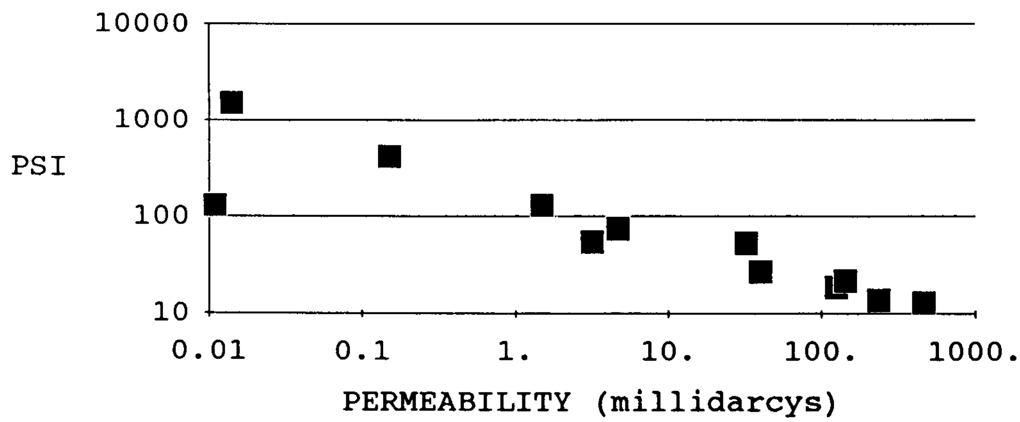

FIGURE 43- Crossplot of permeability versus second quartile pressure of all mercury intrusion samples. Second quartile pressure is the injection pressure at the point of 50% saturation of invaded pore volume (adjusted for uninvaded pore volume). For most samples, permeability is linearly correlated to second quartile pressure.

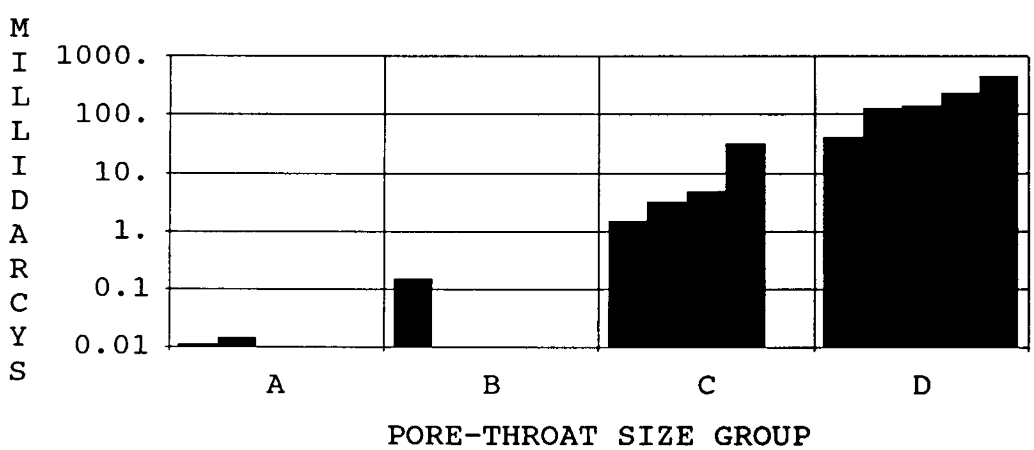

FIGURE 44- Permeability of mercury intrusion samples sorted by the dominant pore-throat size group. Group A represents the smallest pore throats and Group D represents the largest. As demonstrated in Figure 43, permeability is higher in larger pore-throat groups. Sample 10 is dominated by Group C pore throats (i.e. the largest volume of pores is accessed by Group C throats) but exhibits permeability similar to some samples dominated by Group D throats. This is due to the fact that sample 10 contains Group D pore throats but they access less pore volume than Group C throats.

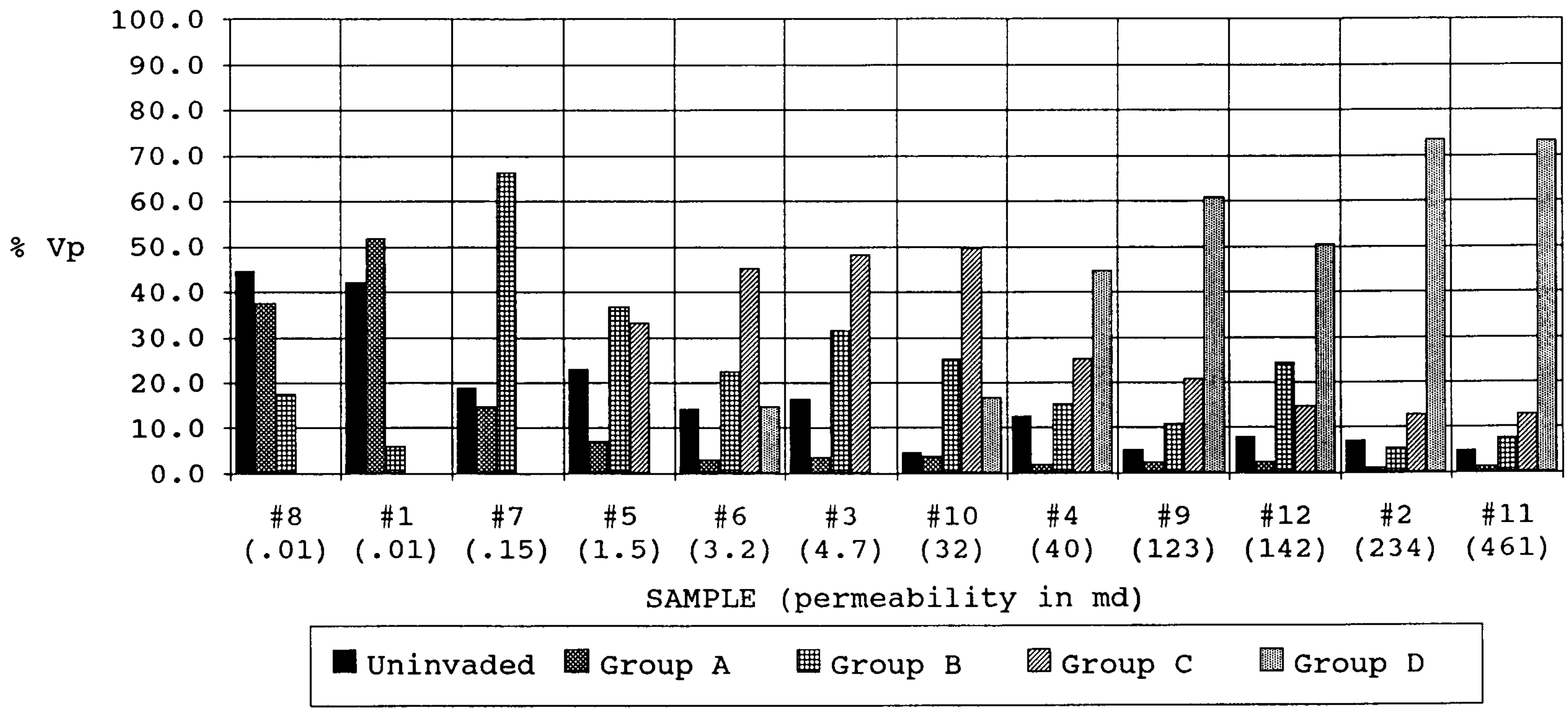

FIGURE 45- Distribution of pore-throat sizes by group in mercury intrusion samples. Samples are sorted in order of increasing permeability. Increasing permeability is accompanied by a shift in pore-throat distributions to larger pore-throat groups.

percentage of pore volume which is accessed by Group D pore throats.

Relationship to dolomite fabric. The clustering of pore-throat sizes into specific size ranges strongly implies a fabric and/or textural influence on pore-throat size and, therefore, permeability. Petrographic examination of analyzed samples lends clues to the causes of segregation of pore-throat sizes. Distributions dominated by Group A and Group D are most easily resolved.

Samples which are characterized by Group A pore-throat distributions are mud-supported rocks. Dolomudstone (Lithotype 2B; Figure 37) and skeletal-moldic dolowackestone (Lithotype 4B; Figure 36) have similar permeability (approximately 0.01 millidarcy) and pore-throat size distributions, and exhibit over 40% uninvaded pore volume (Figure 45). Even though the dolowackestone sample contains open skeletal molds, fluid movement between molds is mediated by dolomudstone fabric due to the fact that the molds are not generally interconnected. Rocks dominated by Group A pore-throat distributions are thus considered to have mud-controlled properties. The proportion of total pore volume of a sample which is accessed by Group A pore throats, however, can not be unequivocally viewed as representative of the apparent mud fraction of the rock because it has not been proven that no other rock constituents exhibit similar characteristics.

Samples dominated by Group D pore-throat distributions are generally characterized by a very low apparent mud fraction (i.e. a very small percentage Group A pore throats), a low percentage of uninvaded pore volume (Figure 45), and interconnected networks of open skeletal molds and interparticle voids (Figures 40, 41). The pore throats connecting large pores in high permeability samples are commonly observed in thin section (Figure 40A) to be relatively large openings which are not occluded by interlocking dolomite crystals. Areas separating large pores in lower permeability Group D samples (Figure 41A) are generally characterized by networks of euhedral to subhedral dolomite crystals, and these samples exhibit higher proportions of Group C pore throats and a slightly larger apparent mud fraction (i.e. Group A pore throats). The size of Group D pore throats observed in thin section falls within the range calculated from mercury intrusion pressure (4 to 35 microns).

In order to address the relation of rock texture and fabric to Group B and Group C pore-throat size distributions, the modes of crystal growth and pore geometry in dolostones must be considered. Wardlaw (1976) has described the general properties of dolomite crystal growth as they affect pore throat shapes and the resulting capillary pressure response. Correlation of capillary pressure characteristics to actual three-dimensional pore and throat geometry was accomplished by the use of epoxy pore casts. As described by Wardlaw (1976), dolostones comprised of an open mosaic of rhombohedral crystals (euhedral fabric) are characterized by pores which are bordered by randomly oriented, planar crystal faces, described as polyhedral pores. Pore throats between polyhedral pores are numerous and exhibit relatively large (in comparison to pore size) and multifaceted shapes (Figure 46). Pore-throat size is positively correlated to dolomite crystal size in euhedral fabrics. In rocks which were further dolomitized, continued growth of individual dolomite crystals resulted in crystal interference and the formation of compromise boundaries between adjacent crystals, resulting in a subhedral fabric. Pore geometry evolved from large polyhedral shapes to smaller tetrahedral shapes as crystal faces bordering individual pores grew outward. In an advanced stage of dolomite growth in which most pores are tetrahedral, pores are connected by thin sheet-like spaces between the compromise boundaries, referred to as interboundary sheet throats. With continued dolomite crystallization, tetrahedral pores are reduced to intercrystal triple

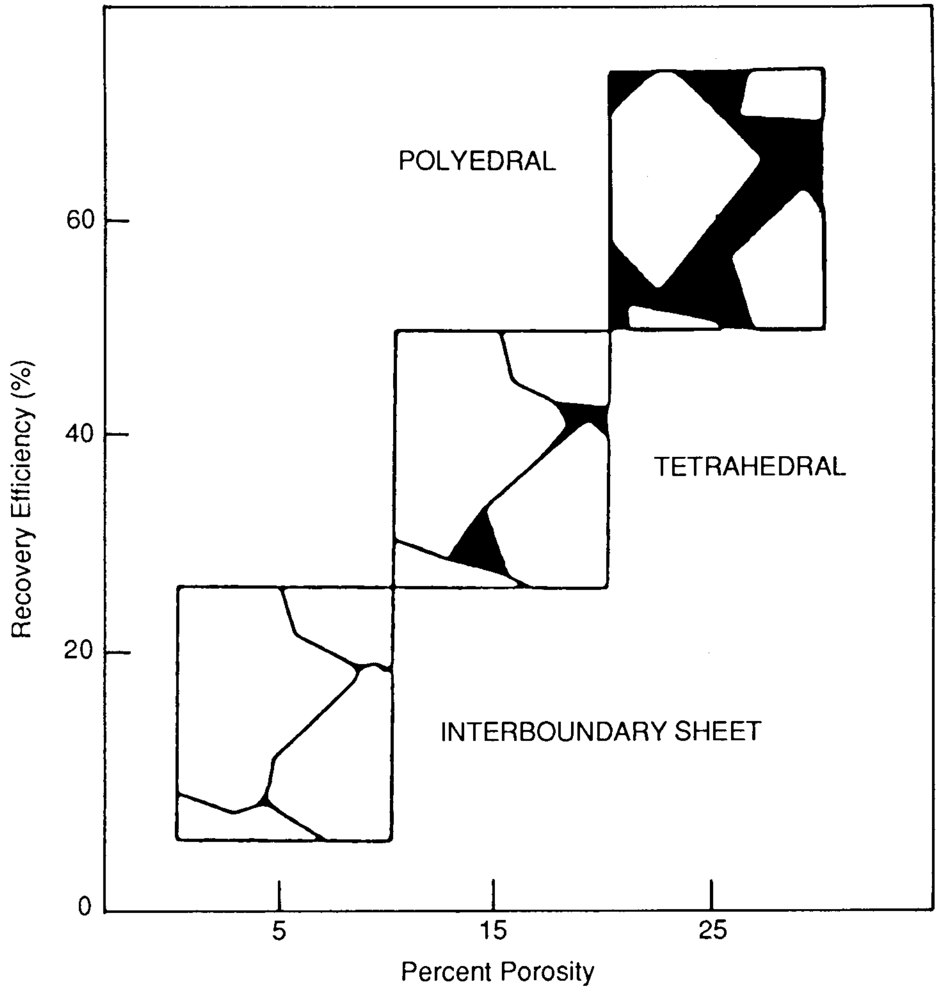

FIGURE 46- Schematic representation of dolomite pore and throat geometries in the progression from polyhedral to tetrahedral to interboundary sheet pore systems. Porosity of dolomite matrix decreases with increased crystal interference. Ejection efficiency (recovery efficiency) decreases also in conjunction with increased pore/throat ratio. (modified from Wardlaw, 1976).

junctions and the entire pore system is comprised of interboundary sheet pores (anhedral fabric). Wardlaw (1976) determined that interboundary sheet pores and throats do have measureable dimensions and are demonstrably open at depth. The range of interboundary sheet widths measured from epoxy pore casts was 0.1 to 4 microns, with an average of 2 microns. Widths less than 0.1 micron were not observed due to the limits of epoxy impregnation, but were assumed to be present.

Although two-dimensional petrographic analysis is deficient in the consideration of three-dimensional arrays, a generalized relationship is observed between pore-throat size distribution and dolomite fabric. Petrographic examination of samples which are dominated by Group B and/or Group C pore-throat size distributions suggests that Group B pore throats are dominated by interboundary sheets, and that Group C pore throats are dominated by smaller polyhedral throats (in comparison to Group D pore throats). Figure 42 illustrates an example of a pore-throat size distribution which includes both Group B and Group C. Pores are represented by open skeletal molds and partially dolomitized interparticle areas. Areas between pores are characterized by anhedral dolomite mosaics as well as subhedral dolomite mosaics. Pore throats in the anhedral mosaics are principally interboundary sheets

(Group B) whereas the more open, subhedral mosaics likely contain a higher percentage of polyhedral pore throats (Group C). The degree of crystal interference in subhedral fabrics will affect the size of polyhedral pore throats. For a given crystal size, less growth interference will result in larger throats whereas greater degrees of growth interference will result in progressively smaller throats.

An example of a pore-throat size distribution dominated by Group B throats is illustrated in Figure 38. This dolostone sample contains late, zoned, ferroan calcite cement and undissolved skeletal calcite. Dolomitization of grains was pervasive such that dissolution resulted in a pore system comprised of intercrystalline dolomite pores distributed within former intraparticle and interparticle areas. Few open molds are evident and cementation has occluded many of the larger pores. While much subhedral to euhedral dolomite is evident, it is patchily distributed. Areas between porous patches are dominated by anhedral dolomite fabrics indicating that interboundary sheet pore throats control fluid movement between porous areas. The fact that calcite cement fully occludes larger pores and that the abundant pores which remain open contain no cement indicates that cementation was controlled by pre-cementation permeability which, in turn, was controlled by dolomite fabric. Because no Group C or D pore throats are recorded in this sample, the calcite cement probably selectively filled pores controlled by pre-existing Group C and D pore throats. The presence of undissolved skeletal calcite may further explain the absence of porosity controlled by Group C and Group D pore throats.

The continuum of pore-throat sizes (i.e. Group A-D) reflects mud content and the degree of dolomitization of the non-mud components (grains and cement). Pore systems dominated by Group A pore throats are characteristic of mud-supported dolostones. Pore systems controlled by Group B, C, and D pore throats are indicative of grain-supported fabrics. The difference between the grain-supported groups is related to the degree of dolomitization and the resultant dolomite fabrics controlling access to pores, the degree of dissolution of undolomitized calcite, and the degree of later calcite cementation. The majority of pores in grain-supported samples is comprised of large molds and partial molds of skeletal grains and former cement. In rocks with no residual calcite, Group D pore throats are large polyhedral pore throats contained within euhedral to subhedral dolomite fabrics. Group C pore throats are smaller polyhedral pore throats contained within subhedral and smaller euhedral dolomite fabrics. Group

B pore throats are interboundary sheet throats contained within subhedral to anhedral dolomite fabrics. Undissolved calcite, whether skeletal or cement, has the effect of occluding the larger pore-throat groups, Groups C and D. The greater the degree of overall dolomitization of a grain-supported rock, the more the pore-throat distribution will be shifted toward smaller pore-throat sizes. The degree of dolomitization is influenced by a host of factors including the dolomitized substrate (i.e. mud, skeletal grain, type of skeletal grain, cement), accessibility to dolomitizing fluids, and time. The relationship of specific dolomite phases (i.e. Dolomites I, II, and III) to pore-throat geometry has not been addressed. It is important to remember, the description of dolomite fabrics which relate to each pore-throat size group refers only to the areas between larger pores (e.g. molds) and not to the pores themselves. Different pore-throat groups can control access to similar networks of moldic porosity. This can account for varying permeability between rocks of similarly high porosity (Appendix B, Samples 2 and 10).

<u>Recovery efficiency</u>. Imbibition analysis (withdrawal) was conducted on four samples representative of high-quality (high permeability) reservoir. The purpose was to characterize the recovery efficiency (RE) of the

rock, or the percentage of initial mercury saturation which is ejected upon pressure reduction. Recovery efficiency in an air-mercury system is considered to be indicative of the relative proportion of a non-wetting phase (e.g. oil) which can be recovered from a reservoir due to simple pressure reduction. The absolute value calculated from the air-mercury system is not applicable to a water-oil system, but the relative difference between rock samples is applicable. Of the four samples, three yielded satisfactory results. In the fourth sample (Appendix B, Sample 4), the measured volume of mercury ejected and that calculated by gravimetric analysis varied significantly. Therefore, the imbibition results of this sample are disregarded. The results of the remaining three analyses are as follow:

Sample	Porosity (%)	Permeability (md)	RE (%)	% Pore Volume D	C	B	A	Uninvaded
2	25.3	234	41.9	74	13	5	1	7
9	23.4	123	36.0	61	21	11	2	5
10	25.3	32	33.0	17	50	25	4	5

The recovery efficiency decreases with permeability and the shift to smaller pore-throat distributions (smaller percentage of pores accessed by Group D pore throats). Wardlaw (1976) has demonstrated a relation between decreasing recovery efficiency and increasing pore diameter/pore throat diameter ratio (pore/throat ratio). As pore throats become smaller in comparison to the associated pores, expulsion of the non-wetting phase becomes less efficient (i.e. a smaller percentage is expelled). In Bindley Field samples, pore throats of different groups connect large moldic pores, therefore a decrease in pore-throat size can be accompanied by an increase in the pore/throat ratio.

Reservoir Model

The integration of subsurface geology, core description, petrography, and petrophysical data results in a model which describes the origin of porous and permeable reservoir rock, its three-dimensional distribution, and the segregation of reservoir layers into discrete, horizontal flow units. The purpose of the model is to 1) explain production history, 2) assist in more efficient recovery of remaining reserves, 3) serve as a reference for other, similar reservoirs, and 4) lead to improved exploration models for possible undiscovered fields of a similar nature.

Origin of Reservoir Rock

A definition of reservoir quality which is constrained by economic factors is both subjective and ephemeral. Therefore, for the purposes of the model, an absolute definition is adopted which is consistent with empirical observations of well performance. In Bindley Field, the descriptive term "reservoir-quality" refers to rock containing porosity of 10 percent or greater, and exhibiting matrix permeability of 10 millidarcys or greater. Matrix permeability refers to permeability controlled by the matrix of the rock as opposed to that related to fracturing.

Three factors are critical in the creation of reservoir-quality rock in Bindley Field; 1) grain-supported depositional fabric, 2) pervasive, but incomplete dolomitization, and 3) dissolution of undolomitized calcite (Figure 47). Later occlusion of pore space by calcite cement is observed, but is not considered critical in the destruction of porosity and permeability prior to oil migration. For the purposes of the model, all dolomite phases (Dolomites I, II, III) are considered in aggregate, even though the relative timing of each phase in relation to cementation and dissolution may be different.

Of primary importance is depositional fabric. Mud-supported rocks possess relatively high porosity (10 to 20%), but regardless of diagenetic history, exhibit very low permeability (less than 10 millidarcys). Where skeletal molds are abundant, permeability is low due to the very small pore-throat sizes associated with the dolomudstone fabric which separates the isolated molds.

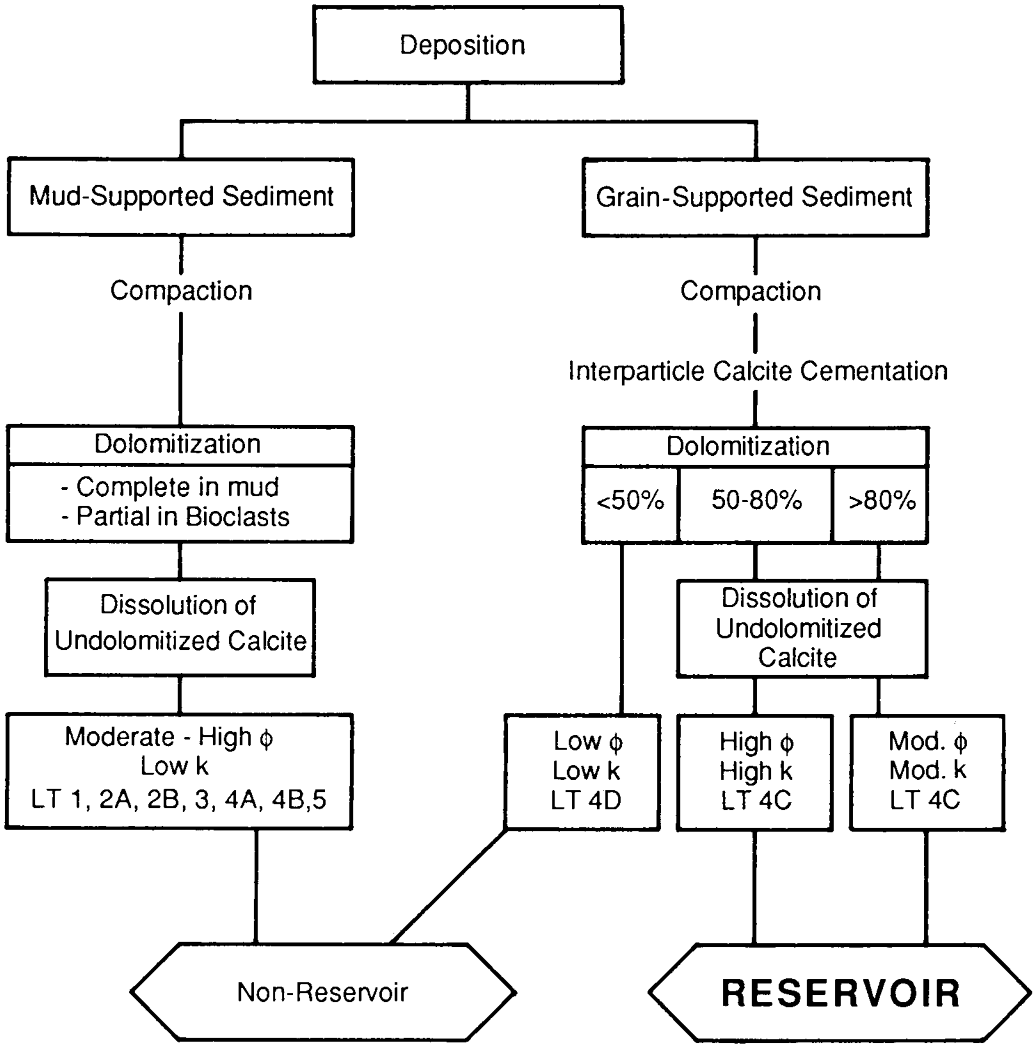

FIGURE 47- Generalized flow diagram illustrating the critical factors in the evolution of Bindley Field reservoir rock. The three critical factors in creation of reservoir rock are 1) depositional fabric, 2) degree of dolomitization, and 3) extent of dissolution of undolomitized calcite. The diagram is simplified in that all interparticle cementation and all dolomitization are each represented as single events. The division of degrees of dolomitization (i.e. 50-80%) are not absolute and are intended to indicate general ranges. Mechanisms of porosity destruction after creation of reservoir are not included.

Virtually all reservoir-quality intervals display grain-supported fabrics.

Within the categories of grain-supported depositional fabrics, some portion was diagenetically altered into reservoir rock (Lithotype 4C) and the remainder was transformed into non-reservoir rock (Lithotype 4D). Lithotype 4D is comprised of skeletal grainstone fabrics which were pervasively cemented by interparticle calcite, experienced little or no dolomitization, and underwent minimal dissolution (Figures 27E, 28C, 31A). Lithotype 4C is comprised of skeletal packstones and grainstones which also were cemented by interparticle calcite, were dolomitized to varying degrees (Figures 28A, 28D, 31B, 31C), and were subjected to dissolution of undolomitized calcite (Figures 27B, 31D). Based on petrographic criteria, it is interpreted that the highest permeability reservoir rock is derived from calcite-cemented, skeletal grainstones. The causes of pervasive dolomitization of certain grainstones while others remain undolomitized are related to the thickness of grainstone accumulations, proximity to muddy intervals, and time. Access of dolomitizing fluids to cemented grainstones is likely to occur via associated muddy sediments. Dolomitization of cemented grainstone accumulations is envisioned to progress from the outer margins toward the interior portions which, in the case of relatively thick accumulations, can leave the interior portions undolomitized. Skeletal composition does not appear to exert a significant influence on whether a grainstone is dolomitized. Once dolomitization in a grainstone begins, mud-filled bryozoa and other non-echinoderm grains are preferentially dolomitized. Large echinoderm grains and calcite cement exhibit the least dolomitization.

Permeability within the reservoir rocks of Lithotype 4C is related to the percentage of dolomitized mud, the degree of dolomitization of bioclasts and calcite cement, the extent of dissolution of undolomitized calcite, and the volume and distribution of late calcite cements. Greater degrees of dolomitization result in dolomite fabrics with smaller pore throats (less permeability potential) and less undolomitized calcite (less porosity potential). Dissolution of undolomitized grains and cement results in the creation of moldic, interparticle, and intercrystalline pore space. Failure of this calcite to dissolve, or later cementation of the larger pores and throats, will result in low permeability.

The ideal reservoir rock (highest permeability) consisted of cemented echinoderm/bryozoan grainstone, was approximately 75% dolomitized, and all undolomitized calcite was subsequently dissolved (Figures 28B, 31D, 40). The end result is a rock composed of dolomitized pseudomorphs of skeletal grains, numerous large skeletal molds, and molds of former, partially dolomitized, interparticle cement. The pores are interconnected primarily by large, open throats (undolomitized grain boundaries) and large polyhedral dolomite throats (dolomitized grains or cement with euhedral to subhedral fabric). Porosity exceeds 25% and permeability may exceed 200 millidarcys. This ideal reservoir rock is observed in the Meramec 2D and 2E subintervals in wells along the crest of the field.

In summary, reservoir quality is quantified by matrix permeability. Matrix permeability is determined, in order, by 1) depositional fabric, 2) degree of dolomitization, and 3) extent of dissolution of undolomitized calcite.

Reservoir Architecture

The reservoir architecture in the Meramec 2 interval (Figure 48) is primarily controlled by depositional morphology. The general configuration is represented by stacked, horizontal layers of relatively high permeability rocks (Lithotype 4C) which are separated by thin layers of very low permeability rock (Lithotypes 2B, 4A, 4B, 5). The layers correspond to the stacking of parasequences. The three-dimensional

FIGURE 48- Distribution of permeability (k_{90}) perpendicular to the long axis of the field (cross-section Kd-Kd') equal to or greater than 10 millidarcys. Trend of cross-section is the same as that of cross-section Fd-Fd' illustrated in Figure 23A. The distribution of permeability mimics the distribution of Lithotype 4C and depositional architecture (compare to Figure 21). Permeability is highly stratified and permeable layers are segregated by relatively impermeable horizons. The majority of permeable rock is located in the Meramec 2D and 2E subintervals (flow units). The datum of the cross-section is the base of the Meramec 1 interval.

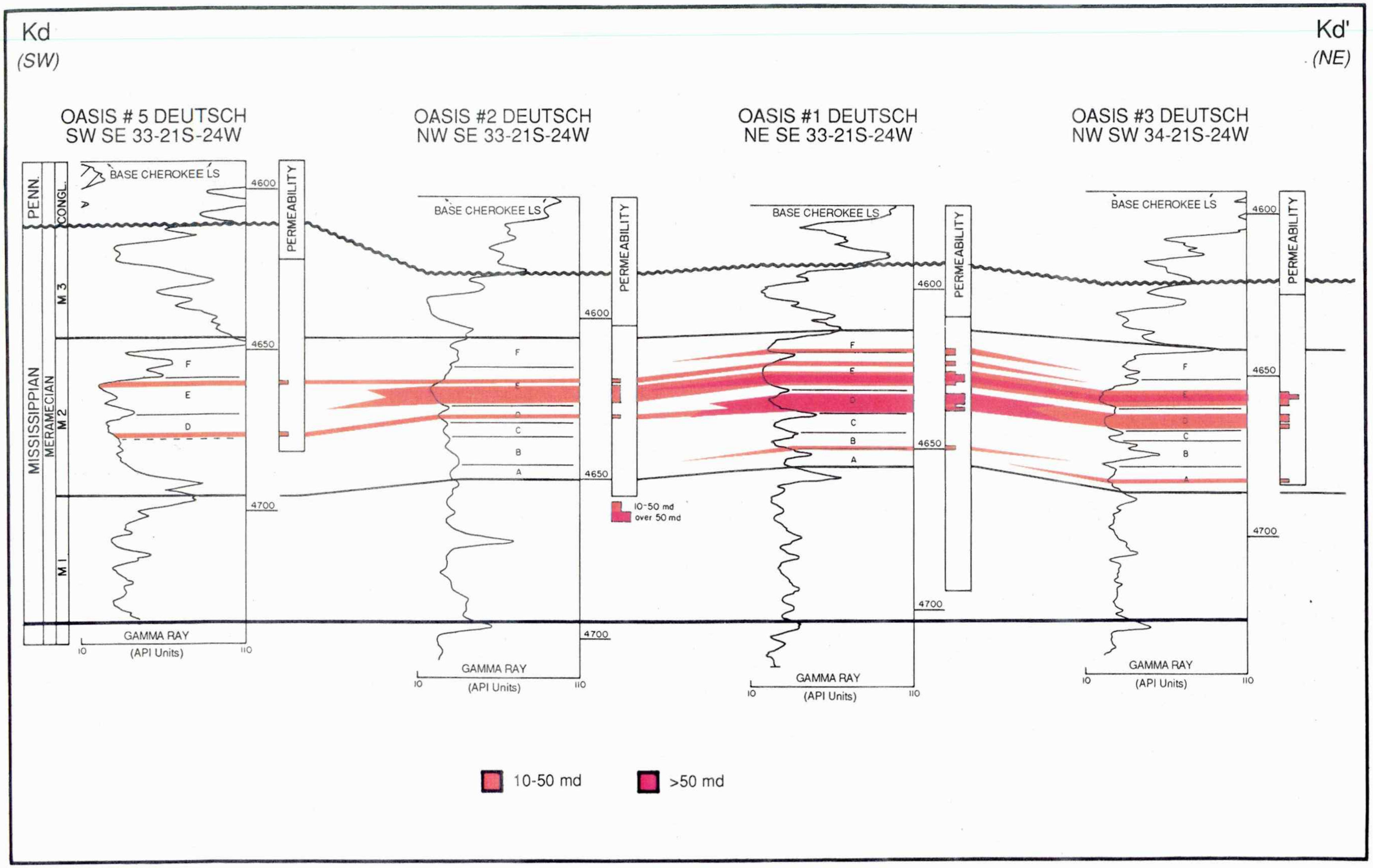

Kd
(SW)
Kd'
(NE)
OASIS # 5 DEUTSCH
SW SE 33-21S-24W
OASIS #2 DEUTSCH
NW SE 33-21S-24W
OASIS #1 DEUTSCH
NE SE 33-21S-24W
OASIS #3 DEUTSCH
NW SW 34-21S-24W
PENN.
CONGL.
MISSISSIPPIAN
MERAMECIAN
M 3
M 2
M I
BASE CHEROKEE LS
PERMEABILITY
GAMMA RAY
(API Units)
10-50 md
over 50 md
10-50 md
>50 md

distribution of reservoir-quality rock mimics the distribution of Lithotype 4C in conjunction with the correlation of Lithotype 4C to permeability values of 10 millidarcys or greater (compare Figures 21 and 48). A small fraction of Lithotype 4B exceeds 10 millidarcys due to the presence of grain-supported interlayers which can occur within Lithotype 4B. Permeability decreases laterally in areas of muddier rock fabrics and thinner grain-supported layers, probably due to a greater degree of dolomitization in thin layers.

The thin, relatively impermeable layers which separate the higher permeability layers are likely to serve as confining layers which inhibit vertical movement of reservoir fluids between permeable layers. These confining layers generally exhibit permeability of .01 to 1 millidarcy. The lack of oil staining in these layers where they separate oil-saturated zones indicates that the matrix is impermeable to oil under extant reservoir conditions. The very low measured permeability and very high capillary pressure characteristics of these rocks suggest that matrix permeability to water is similarly negligible. Vertical fractures are observed in these layers and are commonly cemented by calcite. Measured directional permeability in fractured samples ranges from a few millidarcys to a few hundreds of millidarcys, but the degree to which fractures were enhanced by coring and handling is unknown. Vertical communication between permeable layers via fractures is probable; however, it is likely to result in "leakage" in discontinuous areas of the reservoir rather than uniformly distributed communication.

Each permeable Meramec 2 subinterval can thus be viewed as a separate flow unit insofar as fluid recovery is concerned. The highly layered nature of the stacked reservoir intervals and the intervening, laterally continuous barriers to vertical fluid flow are likely to cause each permeable layer to act as a separate reservoir. Pressure isolation between layers may not occur due to some degree of fracture communication, but containment of the bulk of reservoir fluids is likely. The three-dimensional distribution of permeability may be viewed in a series of layer (flow unit) maps (Figures 49 A-D). The distribution of permeability within each flow unit is greatest along the axis of the field and diminishes on the flanks. The Meramec 2D and 2E flow units contain the maximum permeability development in terms of thickness and areal extent, and are the primary producing intervals in the field.

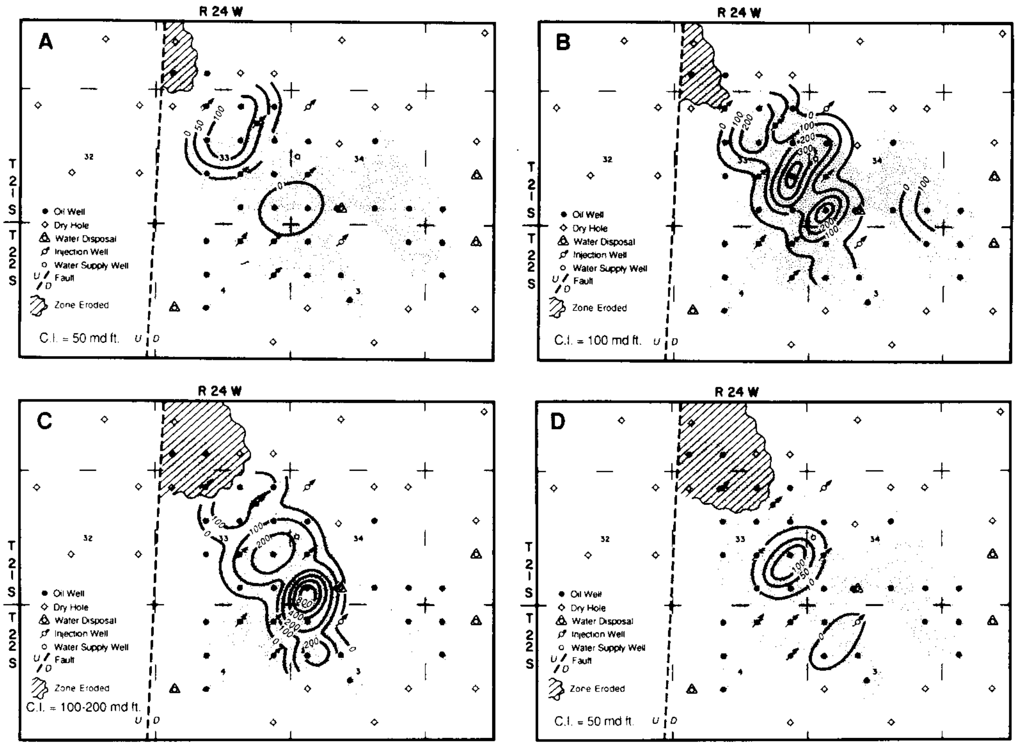

FIGURE 49- Distribution of permeability by Meramec 2 subinterval. Values are in millidarcy-feet. A. Meramec 2C. B. Meramec 2D. C. Meramec 2E. D. Meramec 2F. Permeability development increases in magnitude and areal extent in each successive subinterval culminating in Meramec 2E. Permeability development is considerably diminished in Meramec 2F. The field area is indicated by the stipled background.

Reservoir Performance

The reservoir model predicts that matrix permeability is the primary factor governing fluid productivity. If so, the cumulative volume of fluids produced from each well should parallel the magnitude of permeability development. Because all permeable flow units have not been perforated in each well, if significant communication between flow units does not occur, then fluid productivity should relate only to the permeability development in the flow units which are open to the wellbore (Figure 50A). The measure of permeability development used for comparison is derived by multiplying the thickness of permeable rock (in feet) by the average permeability (in millidarcys). Intervals with permeability values of less than 10 millidarcys were excluded. In order to eliminate the effect of fracture permeability, permeability values in samples with large variance between maximum directional permeability and permeability at right angles to the maximum (indicative of fracturing) were adjusted to reflect the average matrix permeability of adjacent samples.

Individual well production data is available only for wells within the Conoco waterflood unit (Conoco, Inc. data). Individual well production was estimated by allocating a percentage of each month's

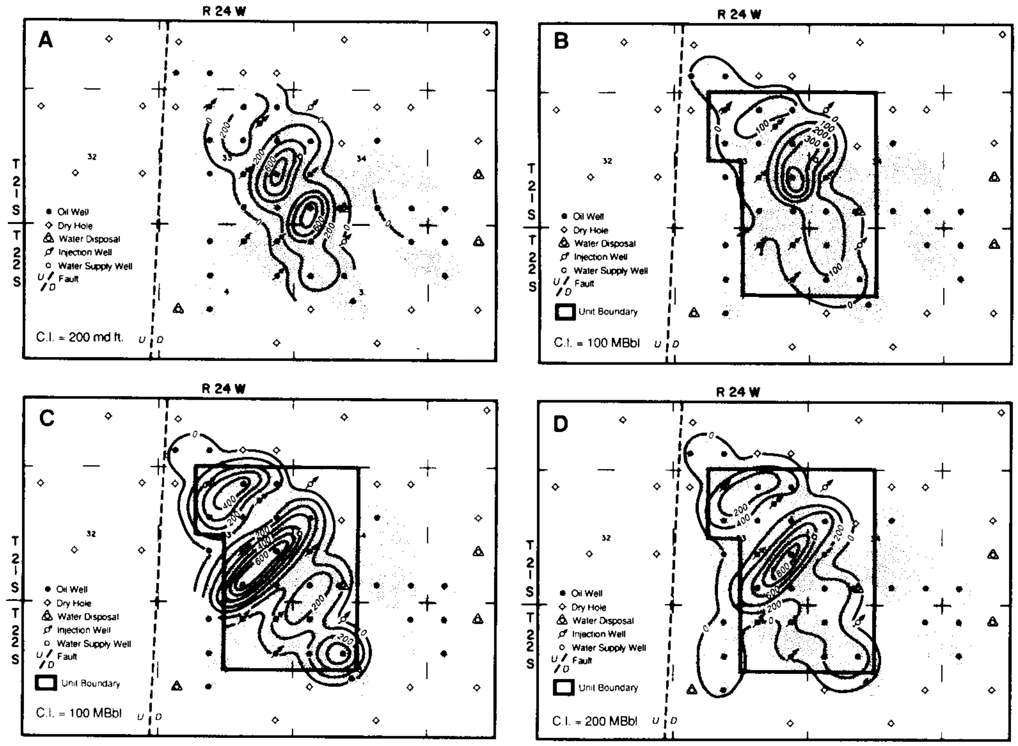

FIGURE 50A- Distribution of permeability equal to or greater than 10 millidarcys in perforated flow units. Values are in millidarcy-feet. Assuming that flow units are not vertically communicated, production should correspond to the permeability development in the perforated flow units. The field area is indicated by the stipled background.

FIGURE 50B- Cumulative oil production (thousands of barrels) from September, 1973 through June, 1990 for wells in the Conoco, Inc. waterflood unit. Oil production generally mimics the distribution of permeability in perforated flow units (Figure 50A).

FIGURE 50C- Cumulative water production (thousands of barrels) from September, 1973 through June, 1990 for wells in the Conoco, Inc. waterflood unit. Water production coincides with the distribution of permeability in perforated flow units with the exception of a prominent high water area trending northeast-southwest through the center of the field.

FIGURE 50D- Cumulative total fluid production (thousands of barrels) from September, 1973 through June, 1990 for wells in the Conoco, Inc. waterflood unit.

lease production to each well based on monthly well tests. Production from wells outside the waterflood unit is reported by lease, which may include production from multiple wells and cannot be accurately allocated to individual wells. The data for wells within the waterflood unit reflect cumulative production from September, 1973 (16 months after field discovery) through June, 1990. Even though the data do not include the first 16 months of production from the unit wells, the omitted data represents a minor fraction of the cumulative production (approximately 13% of cumulative oil from the unit wells), and relative production between wells is considered to be accurate.

The distribution of oil production exhibits a close correlation to permeability development in perforated intervals (Figures 50A, 50B). Water production and total fluid production (oil and water) are similarly distributed (Figures 50C, 50D), with the exception that a prominent northeast-southwest trending, high-fluid area is evident which extends into the low permeability southwestern flank of the field (SW/4 SE/4, 33-21S-24W). Cumulative oil production per well ranges from 1,000 barrels to 448,000 barrels (Figure 50B). Cumulative water production per well ranges from 2,000 barrels to 791,000 barrels (Figure 50C).

Crossplots of permeability in perforated intervals versus cumulative total fluid production quantify the relationship between permeability development and productivity (Figure 51A). In the majority of wells, total fluid production increases linearly with increasing permeability development in perforated intervals. This linear trend is considered representative of matrix permeability and is referred to as the permeability/productivity baseline. However, two additional trends are evident. One trend consists of two wells characterized by anomalously high fluid production in low permeability wells. These wells exhibit oil production which falls on the permeability/productivity baseline (Figure 51B). The other trend consists of three wells characterized by anomalously high fluid production in relatively high permeability wells. These wells exhibit oil production which is also in excess of that of the permeability/productivity baseline. Comparison of the cumulative water/oil ratio to permeability demonstrates a baseline water/oil ratio for most wells ranging between a value of 1:1 and 2:1 (Figure 51C). The ratio reaches 4:1 in a few structurally low wells. The water/oil ratio in the anomalous, low permeability wells of Figure 51A far exceeds the baseline, reaching a value of 20:1, indicating that water production is disproportionately

FIGURE 51A- Crossplot of permeability-feet in perforated flow units (>10 md) versus cumulative fluid production (September,1973 - June, 1990). Most wells follow a linear relationship between permeability-feet and production (permeability/productivity baseline). Two anomalous trends are observed; 1) higher total fluid than predicted by the baseline in high permeability wells, and 2) higher total fluid than predicted by the baseline in low permeability wells.

FIGURE 51B- Crossplot of permeability-feet in perforated flow units (>10 md) versus cumulative oil production (September,1973 - June, 1990). Most wells follow a linear relationship between permeability-feet and production (permeability/productivity baseline). Anomalously high volumes of oil were produced in three wells as compared to wells on the baseline trend. The magnitude of the anomalous oil production is proportional to permeability development.

FIGURE 51C- Crossplot of permeability-feet in perforated flow units (>10 md) versus cumulative water/oil ratio (September,1973 - June, 1990). Wells which fall on the permeability/productivity baseline (Figures 52A, 52B) display a uniform water/oil ratio. A small cluster of wells with a slightly elevated water/oil ratio represents wells in structurally low positions. Two wells have a very high water/oil ratio and correspond to the anomalous, low permeability wells in Figure 52A.

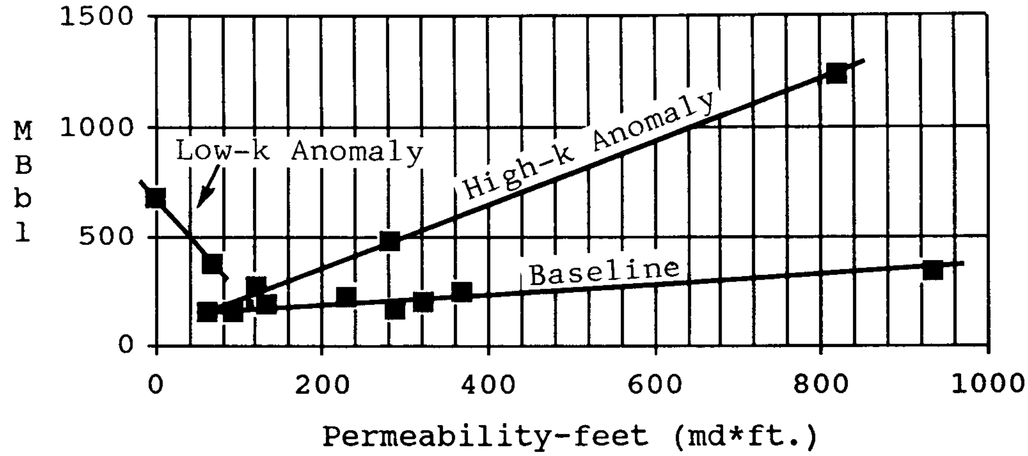
1500
1000
500
0
M
B
b
l
Low-k Anomaly
High-k Anomaly
Baseline
0
200
400
600
800
1000
Permeability-feet (md*ft.)

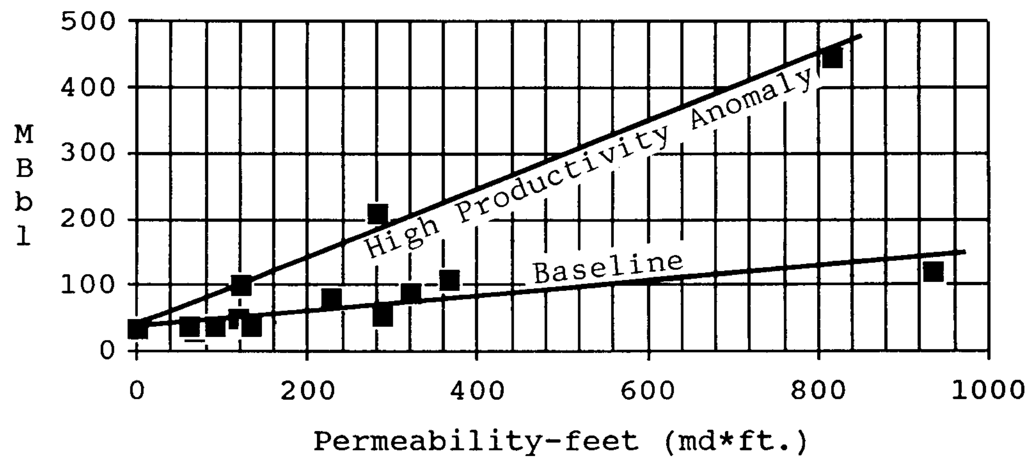
500
400
300
200
100
0
M
B
b
l
High Productivity Anomaly
Baseline
0
200
400
600
800
1000
Permeability-feet (md*ft.)

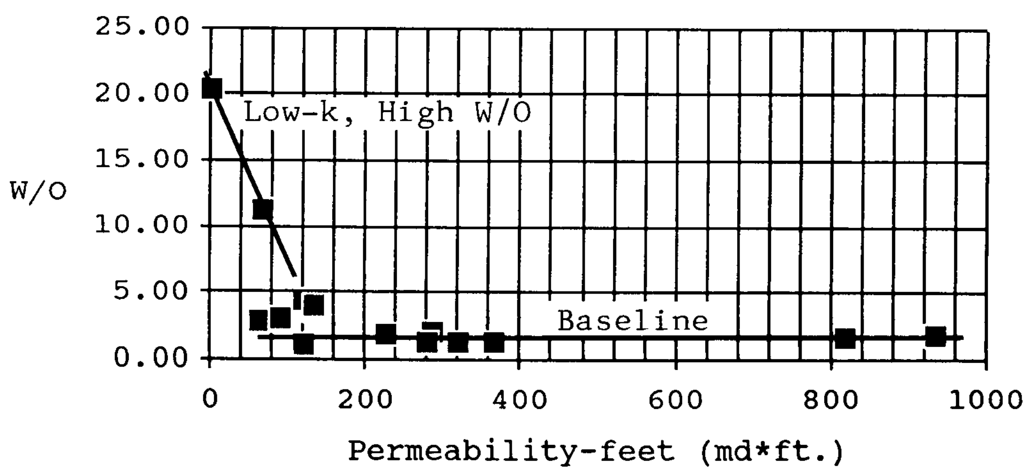
25.00
20.00
15.00
10.00
5.00
0.00
W/O
Low-k, High W/O
Baseline
0
200
400
600
800
1000
Permeability-feet (md*ft.)

high. The water/oil ratio in the anomalous, high permeability wells of Figure 51A falls within the baseline water/oil ratio range, indicating that oil and water production were both proportionally high.

Excessive water production in the anomalous, low permeability wells is most easily explained by communication to permeable, water-bearing zones via natural fractures, possibly enhanced by acid stimulation. Excessive volumes of acid or excessive treatment pressure may open and etch pre-existing zones of weakness. The anomalous well with the highest water/oil ratio (SW/4 SE/4, 33-21S-24W) indicated low permeability in a drillstem test of the perforated interval (very low fluid recovery) and contained no permeability in excess of 10 millidarcys in the producing interval. The anomalous volume of water produced from such a low permeability zone indicates that matrix permeability is not the controlling factor. Brecciated zones in this well were observed to occur farther below the basal Pennsylvanian unconformity than in any other well. Both wells with anomalously high water cuts are situated along the southwestern flank of the Bindley Field structure (Figure 11A).

The cause of the anomalously high oil and water production from the three high permeability wells is more problematic. Examination of factors such as structural position, thickness of permeable zone, and storage volume were inconclusive in explaining the phenomenon relative to other high permeability wells. All three wells were perforated in all major, permeable, oil-bearing zones, therefore, contribution from unperforated intervals is not a factor. The two most anomalous wells are direct offsets to the pilot water injection well. However, cumulative production data prior to implementation of the pilot waterflood exhibits the same anomalous patterns, indicating that the anomalies are not a result of response to the pilot waterflood. The production of oil and water volumes significantly in excess of the matrix permeability baseline, and in a normal water/oil ratio, suggests higher recovery efficiency of oil in place, a more widely communicated drainage area than in other high permeability wells, and/or a more efficient recharge of the reservoir.

The two most anomalous, high permeability wells and the most anomalous, high water-cut well are all aligned along the axis of the northeast-southwest trending, high-fluid trend illustrated in Figure 51B. The linear alignment of these three wells is suggestive of a linear fracture trend. If fracturing is a factor, the effect of fracturing on high permeability wells does not appear to cause direct communication of water to the wellbore as in low permeability wells. This may be due to the fact that high permeability zones typically accept acid treatments at very low pressure or on vacuum and, therefore, acid treatments do not induce the opening and etching of fractures near the wellbore which are outside of the permeable zones. The existence of unetched natural fractures distal from the wellbore may allow leakage of external fluids into the producing flow units along the fracture trend, resulting in recharge of the flow units and, possibly, a natural waterflood effect.

In summary, quantitative comparison of cumulative production data to permeability development confirms that the fundamental control on reservoir quality and performance is the degree of matrix permeability development. Correlation of cumulative fluid production and permeability reveals a linear, baseline matrix-permeability/productivity relationship. Additional factors modify the baseline relationship in two ways. In the first case, probable vertical fracturing within and between low permeability zones, combined with high volume or high pressure acid treatments, causes opening and etching of pre-existing vertical fractures near the wellbore which are in communication with permeable, water-bearing strata. The result is anomalously high water production and an abnormally high water/oil ratio. An alternative to communication via fractures is communication behind well casing as a result of poor cement bonding; however, the presence of breccia well below the basal Pennsylvanian unconformity is consistent with fracturing. In the second case, water and oil production substantially in excess of that predicted by the permeability/ productivity baseline, and in a normal, cumulative water/oil ratio, may be explained by a pre-existing vertical fracture system which permits leakage of fluids into producing flow units from external sources. A high water/oil ratio is not observed because the fracture system was not effectively communicated throughout and acid treatment of permeable zones may not have opened and etched the fractures between and external to perforated flow units. Therefore, fluid flows to the wellbore via flow units rather than fractures communicated with the wellbore.

CHAPTER VII

DISCUSSION

Integration of subsurface geology, core analysis, petrography, petrophysical analysis, and production information in Bindley Field has resulted in a descriptive model of the stratigraphy, depositional geometry, reservoir origin, reservoir architecture, and reservoir performance. The practical significance of the model includes 1) the application to Bindley Field reservoir management and exploitation, and the application to reservoir management in other, similar reservoirs, 2) the development of improved exploration models, and 3) the possible contribution to a more meaningful stratigraphic subdivision of the lower Meramecian stage in western Kansas.

Application to Bindley Field

The recognition of the lower Meramecian stratigraphic framework, the highly stratified nature of the reservoir zones, and the relationship between permeability and depositional/diagenetic factors have direct application to the effective management of the Bindley Field reservoir. Reservoir quality is directly related to matrix permeability development which is, in turn, related to the distribution of grain-supported depositional fabrics. Lateral and vertical facies changes are the primary control on reservoir distribution. Diagenetic overprinting of grain-supported fabrics determines the final distribution of reservoir rock and its quality. The result is a sequence of vertically stacked flow units separated by thin layers of very low matrix permeability. Each couplet of permeable layer and its associated impermeable cap correspond to a depositional parasequence. The impermeable layers are likely to provide semi-effective barriers to vertical fluid movement in most areas of the field, and fluid flow will be largely confined within each flow unit. The Meramec 2 interval is comprised of six stacked flow units with the highest quality reservoir developed in the Meramec 2D and 2E flow units. In certain areas of the field, vertical fracturing may modify reservoir performance. The degree to which communication between flow units occurs in various areas of the field is best determined by production behavior and production testing.

The most fundamental application of this model to Bindley Field reservoir management is in the recognition of flow units as segregated reservoirs, and the proper correlation of flow units throughout the field. Completion of only one of two or more adjacent flow units may not efficiently drain the unperforated flow units, resulting in non-optimal primary recovery. Assuming that unperforated, oil-saturated flow units will yield oil reserves in accordance with the permeability/productivity baseline, unperforated flow units in cored wells containing in excess of 50 millidarcy-feet of permeability can contribute up to 175,000 barrels of incremental, primary oil. Allowing for possible reduced reservoir pressure, this estimate is considered an upper limit; however, it includes cored wells only. Permeability measurements in uncored wells are not available for estimation of potential, untapped reserves, but Meramec 2D and Meramec 2E zones which exhibit porosity and which were not perforated during initial completion have the potential to contribute additional primary oil reserves in five additional wells.

In the implementation of pressure maintenance or secondary recovery, proper correlation of flow units between wells is critical to successful performance. Failure of adjacent injection and producing wells to be open in the same flow units will result in the absence of a production response. Failure to recognize that certain flow units have been eroded beneath the basal

Pennsylvanian unconformity may also lead to lack of communication between injection and producing wells.

Recovery efficiency in mercury intrusion samples was observed to be reduced in lower permeability, grain-supported samples in conjunction with more complete dolomitization and reduction in the size of pore throats. If this relationship holds true under reservoir conditions, recovery efficiency will be lower in low permeability areas of the field (flanks) than in the higher permeability areas (central axis). In addition, if oil and water production which significantly exceeds that predicted by the permeability/productivity baseline in higher permeability wells is due to fracture-mediated reservoir recharge and natural waterflooding, wells which lie on the permeability/productivity baseline may produce incremental reserves if waterflooded.

Trapping in Bindley Field is a function of lateral facies change and true structural closure. "True" structure refers to relief mapped on a stratigraphic horizon (e.g. the top of the Meramec 2 interval) rather than relief mapped on the unconformity surface. True structure reflects the structural configuration of the reservoir layers. Permeability in flow units decreases laterally away from the central axis of the field as a function of increasing mud content and more complete dolomitization. The distribution of permeable flow units correlates to present structure due to probable recurrent structural amplification of earlier, structurally induced bathymetry. Individual impermeable layers between flow units provide at least a partial seal of each flow unit. Where intact, the argillaceous dolomudstone and dolomitic shale (Lithotype 5) capping the Meramec 2 interval provides a seal of the overall interval. Where Lithotype 5 or individual flow unit barriers are disrupted at the basal Pennsylvanian unconformity, clays and shales of the basal Pennsylvanian conglomerate form the seal.

Bindley Field is likely to be representative of other lower Meramecian fields in the western Kansas subcrop belt and, to that extent, the Bindley Field reservoir model and the applications cited above are likely to be applicable to the management and exploitation of such fields.

Application to Exploration

Several aspects of the Bindley Field model and the proposed stratigraphic framework have relevance to the search for similar, undiscovered fields. The recognition that discrete reservoir developments (i.e. fields) occur within individual Meramecian intervals (e.g. Meramec 2, Meramec 3, etc.) indicates that the ability to recognize, correlate, and individually map each interval is critical to understanding the distribution of known fields and exploring for undiscovered fields. Many of the factors relevant in localization of lower Meramecian fields are discernable only beneath the basal Pennsylvanian unconformity. Delineation of true structure, recognition of subcrop trends, and definition of reservoir trends are all predicated on the proper correlation of lower Meramecian intervals.

The correlation of Bindley Field reservoir distribution to depositional fabric, and the relation of depositional fabric to probable structurally induced bathymetry may provide useful clues in delineation of exploration areas. Reservoir layering and lateral heterogeneity are important considerations in the interpretation of well test data. Knowledge of the variability in rock types, their vertical and lateral distribution, and the relation to reservoir development are applicable to the evaluation of cores and sample cuttings and the construction of facies concepts in exploration. The relation of lithotypes to specific depositional environments is useful in consideration of other viable exploration areas in the search for similar types of reservoir development. The geologic model can serve as a reference in the development of a seismic model for use in exploration for similar reservoirs.

Lower Meramecian Stratigraphy

An informal stratigraphic framework for lower Meramecian rocks has been proposed which has been demonstrated to have time-stratigraphic significance. Lower Meramecian intervals can be correlated with open-hole logs within an area at least as extensive as Hodgeman and Ness Counties. The log markers which separate the intervals reflect distinctive lithotypes which cap Meramecian parasequence sets. The log signature may change character on a more regional scale due to changes in the facies tracts which are represented above and below the parasequence set boundaries.

If this stratigraphic subdivision proves to be more widely applicable, it will provide a useful tool in the correlation of time-bounded sequences, in the interpretation of the depositional dynamics of the lower Meramecian strata, and in the reconstruction of lower Meramecian paleogeography in western Kansas.

Areas for Further Study

The Bindley Field model is envisioned as a descriptive working model. It is intended to provide a basic, practically based understanding of the stratigraphic framework, depositional geometry, diagenetic history of reservoir intervals, reservoir architecture, and petrophysics of reservoir-related rocks. Many areas remain to be explored further, particularly in a quantitative sense.

Cathodoluminescence petrography has demonstrated the presence of three distinct dolomite phases (Dolomites I, II, and III). This study did not examine the petrographic and chronological relationships of these phases in detail. Of particular interest is the specific relationship of the three dolomite phases to one another, the timing of each dolomitization phase relative to calcite cementation and dissolution, and the distribution of Dolomite III and its effect on pore-throat distributions. Study of the relationships between interparticle cementation by calcite and the individual dolomite phases may contribute additional evidence related to the interpretation of this study that the highest quality reservoir rocks originated from dolomitization of calcite-cemented grainstones. Detailed petrography (transmitted light and cathodoluminescence) of the dolomites, combined with geochemical analyses, may also lead to an interpretation of their origin.

The comparisons of pore-throat distributions to dolomite fabrics and pore-throat geometry were based on two-dimensional petrographic analysis. Preparation of three-dimensional pore casts of rocks samples and the direct observation and measurement of pore and throat systems would provide a more meaningful analysis of the relationship of dolomite fabric to pore-throat size distribution. Further study of the relationship between each dolomite phase and pore-throat size distribution is necessary in the evaluation of the relative impact of each dolomite phase on pore-throat size and reservoir quality.

Several cores of lower Meramecian rocks from various areas of the western Kansas subcrop belt are available for study at the Kansas Geological Survey. Examination of these cores would be pertinent in evaluating the applicability of the Bindley Field model to other areas of the subcrop belt. Correlation of the lower Meramecian stratigraphic intervals in a more regional context would assist in the expansion of the model.

CHAPTER VIII

CONCLUSIONS

The following conclusions are drawn from examination and integration of the Bindley Field data and subsurface data in the Bindley Field area.

1) Time-stratigraphic intervals of lower Meramecian strata in the study area are correlative throughout Hodgeman and Ness Counties, Kansas based on the recognition of bounding markers in open-hole logs. Beginning at a widely correlated gamma-ray marker which occurs near the top of Osagian strata, the lower Meramecian intervals are named, in ascending order, Meramec 1, Meramec 2, Meramec 3, and Meramec 4. The log markers at the top of the Meramec 1 and Meramec 2 intervals record the tops of shallowing or restricting upward sequences which are terminated by an abrupt shift to more normal marine facies. As such, the log markers are associated with a time-correlative shift in facies patterns and the intervening strata are time bounded.

2) Reservoirs in northwestern Hodgeman County are developed within individual Meramecian stratigraphic intervals, and production from each major field is associated with one dominant Meramecian interval.

Bindley Field produces primarily from the Meramec 2 interval.

3) The Meramec 2 interval consists of six stacked parasequences, each of which aggrades upward from more normal marine, skeletal sediments to restricted, subtidal sediments. The boundary between parasequences is generally sharp and denotes a rapid shift from restricted sediments to overlying, more normal marine sediments. Meramec 2 parasequences are named, in ascending order, Meramec 2A, 2B, 2C, 2D, 2E, and 2F. The cause of parasequence evolution and stacking is likely to be related to relative changes in sea level and/or changes in the degree of restriction of sea-water circulation.

4) The Meramec 2 interval comprises a parasequence set in that it consists of parasequences stacked in a distinctive fashion and is bounded above and below by a major marine flooding event. The Meramec 2 interval displays a sharp, sometimes scoured, transgressive contact with the underlying Meramec 1 interval, and a gradational, but relatively rapid, transition to the overlying Meramec 3 interval. The Meramec 1, Meramec 3, and Meramec 4 intervals are likely to represent parasequence sets as well.

5) Bindley Field is associated with a low relief skeletal buildup within the Meramec 2 interval. The

distribution of depositional fabrics is related to structurally-induced, positive bathymetry on the seafloor. The magnitude of depositional relief across the buildup was likely less than 10 feet. Meramec 2 depositional fabrics are progressively grainier in upper parasequences in the center of the field. Sediments grade laterally to muddier fabrics on the flanks of the field. Storm processes were important in the winnowing of mud constituents and the generation of grain-supported fabrics in the positive areas of the buildup.

6) Reservoir quality is dependent on matrix permeability. High porosity occurs in many lithotypes but high matrix permeability is confined to Lithotype 4C (echinoderm/bryozoan dolopackstone/grainstone). Three factors are critical in the development of permeable reservoir rock: 1) grain-supported depositional fabric, 2) pervasive but incomplete dolomitization, and 3) dissolution of undolomitized calcite. In dolomitized rocks with no residual calcite, permeability is correlated to the pore-throat size distribution. Pore-throat size is related to the degree of dolomitization and the resulting geometry of the pore-throat network. Dolomitization in grain-supported rocks which progresses beyond the point of crystal interference results in the reduction of pore-throat sizes and permeability. Presence of undissolved calcite, as skeletal grains or

cement, or substantial dolomitized mud is associated with low permeability. The highest permeability reservoir resulted from dolomitization of cemented grainstones and the dissolution of undolomitized calcite.

7) The reservoir is segregated into stacked, horizontal flow units within which fluid flow is largely confined. The distribution of permeable rock mimics the distribution of Lithotype 4C, and therefore mimics the parasequence architecture. High permeability is confined to the grain-supported portions of each parasequence. The permeable layers are separated by thin, restricted dolomudstone caps at the top of each parasequence which provide barriers to vertical fluid movement. Vertical fractures in the confining layers may allow some degree of fluid and pressure communication between flow units.

8) Fluid production correlates quantitatively with matrix permeability development. The majority of cored wells have produced a volume of reservoir fluids in proportion to the quantitative development of permeability within perforated flow units. In wells with low permeability in perforated flow units, open vertical fractures in close proximity to the wellbore which are in communication with permeable, water-bearing strata are likely to cause anomalously high water

production. In wells with relatively high permeability in perforated flow units, anomalously high oil and water production may be caused by leakage of externally derived fluids into producing flow units along fracture trends, leading to more efficient recharge and sweep of the affected flow units.

9) Significant primary recoverable reserves are likely to remain in unperforated flow units. In cored wells alone, up to 175,000 incremental barrels of oil may be available. Additional primary recoverable oil is likely to remain in unperforated flow units in as many as five wells which were not cored, but quantitative estimates are not possible to make based on available data.

REFERENCES

Aigner, T., 1984, Dynamic stratigraphy of epicontinental carbonates, Upper Muschelkalk (Middle Triassic), South-German Basin: N. Jb. Geol. u. Pal. Abh., V. 169, p. 127-159.

Amthor, J.E., D.C. Kopaska-Merkel, and G.M. Freidman, 1988, Reservoir characterization, porosity and recovery efficiency of deeply-buried Paleozoic carbonates: examples from Oklahoma, Texas, and New Mexico: Carbonates and Evaporites, V. 3, p. 33-52.

Beauchamp, D.W., 1985, Don Field, in P.M. Gerlach and T. Hansen, eds., Kansas Oil and Gas Fields, V. 5: Wichita, Kansas Geological Society, p. 61-68.

Bebout, D.G. and Loucks, R.G., 1984, Handbook for logging carbonate rocks: Handbook 5, Bureau of Economic Geology, University of Texas at Austin, 43 p.

Beene, D.L., 1965, Hallet Field, in Kansas Oil and Gas Fields, V. 4: Wichita, Kansas Geological Society, p. 100-105.

Berg, R.R., 1975, Capillary pressures in stratigraphic traps: AAPG Bulletin, v. 59, p. 939-956.

Cander, H.S., J. Kaufman, L.D. Daniels, and W.J. Meyers, 1988, Regional dolomitization of shelf carbonates in the Burlington-Keokuk Formation (Mississippian), Illinois and Missouri: constraints from cathodoluminescence zonal stratigraphy, in V. Shukla and P.A. Baker, eds., Sedimentology and geochemistry of dolostones: SEPM Special Publication 43, p. 129-144.

Carozzi, A.V., 1989, Carbonate rock depositional models: Englewood Cliffs, Prentice Hall, 604 p.

Chowns, T.M. and J.E. Elkins, 1974, The origin of quartz geodes and cauliflower cherts through the silicification of anhydrite nodules: Journal of Sedimentary Petrology, v. 44, p. 885-903.

Dickson, J.A.D., 1966, Carbonate identification and genesis as revealed by staining: Journal of Sedimentary Petrology, v. 36, p. 491-505.

Dunham, R.J., 1962, Classification of carbonate rocks according to depositional texture, in W.E. Ham, ed., Classification of carbonate rocks: a symposium: AAPG Memoir 1, p. 108-121.

Ebanks, W.J., Jr., 1987, Geology in enhanced oil recovery, in R.W. Tillman and K.J. Weber, eds., Reservoir sedimentology: SEPM Special Publication 40. p. 1-14.

____________ R.M. Euwer, and D.E. Nodine-Zeller, 1977, Mississippian combination trap, Bindley Field, Hodgeman County, Kansas: AAPG Bulletin, v. 61, p. 309-330.

Flugel, E., 1982, Microfacies analysis of limestones: Berlin, Springer-Verlag, 633 p.

Folk, R. L. and J.S. Pittman, 1971, Length-slow chalcedony: a new testament for vanished evaporites: Journal of Sedimentary Petrology, v. 41, p. 1045-1058.

Goebel, E. D., 1966, Stratigraphy of Mississippian rocks in western Kansas: PhD thesis, University of Kansas, Lawrence, Kansas, 187 p.

____________ 1968, Mississippian rocks of western Kansas: AAPG Bulletin, v. 52, p. 1732-1778.

Goodwin, P.W. and E.J. Anderson, 1985, Punctuated aggradational cycles: a general hypothesis of episodic stratigraphic accumulation: Journal of Geology, v. 93, p. 515-533.

Handford, C.R., 1986, Facies and bedding sequences in shelf-storm-deposited carbonates- Fayetteville Shale and Pitkin Limestone (Mississippian), Arkansas: Journal of Sedimentary Petrology, v. 56, p. 123-137.

Hardie, L.A., 1977, Sedimentation on the modern carbonate tidal flats of northeast Andros Island, Bahamas: Johns Hopkins University Studies in Geology 22, Baltimore, Johns Hopkins University Press, 202 p.

Harris, D.C. and W.J. Meyers, 1987, Regional dolomitization of shelf carbonates: Burlington and Keokuk Formations (Mississippian), Iowa and Illinois, in J.D. Marshall, ed., Diagenesis of sedimentary sequences: Geological Society Special Publication 36, p. 237-258.

Heckel, P.H., 1972, Recognition of ancient shallow marine environments, in J.K. Rigby and W.K. Hamblin, eds., Recognition of ancient sedimentary environments: SEPM Special Publication 16, p. 226-286.

____________ 1974, Carbonate buildups in the geologic record: a review, in L. Laporte, ed., Reefs in time and space: SEPM Special Publication 18, p. 90-154.

Irwin, M.L., 1965, General theory of epeiric clear water sedimentation: AAPG Bulletin, v. 49, p. 445-459.

James, N.P. and P.W. Choquette, 1983, Diagenesis 6. Limestones- the sea floor diagenetic environment: Geoscience Canada, v. 10, p. 162-179.

James, A. III, 1985, Fralick West Field, in P.M. Gerlach and T. Hansen, eds., Kansas Oil and Gas Fields, V. 5: Wichita, Kansas Geological Society, p. 69-76.

Jennings, J.B., 1987, Capillary pressure techniques: application to exploration and development geology: AAPG Bulletin, v. 71, p. 1196-1209.

Kreisa, R.D., 1981, Storm-generated sedimentary structures in subtidal marine facies with examples from the Middle and Upper Ordovician of southwestern Virginia, Journal of Sedimentary Petrology, v. 51, p. 823-848.

Lane, H.R. and T.L. DeKeyser, 1980, Paleogeography of the late early Mississippian (Tournasian 3) in the central and southwestern United States, in T.D. Fouch and E.R. Magathan, eds., Paleozoic paleogeography of the west-central United States, Rocky Mountain Paleogeography Symposium 1, Denver, Rocky Mountain Section, SEPM, p. 149-162.

Lee, W., 1940, Subsurface Mississippian rocks of Kansas: Kansas Geological Survey Bulletin 33, 114 p.

Linehan, R.M., 1965, Stairett Field, in Kansas Oil and Gas Fields, V. 4: Wichita, Kansas Geological Society, p. 229-236.

Longman, M. W., 1980, Carbonate diagenetic textures from nearsurface diagenetic environments: AAPG Bulletin, v. 64, p. 461-487.

Maliva, R.G., 1987, Quartz geodes: early diagenetic silicified anhydrite nodules related to dolomitization: Journal of Sedimentary Petrology, v. 57, p. 1054-1059.

Merriam, D.F., 1963, The geologic history of Kansas: Kansas Geological Survey Bulletin 162, 317 p.

Milliken, K.L., 1979, The silicified evaporite syndrome-two aspects of silicification history of former evaporite nodules from southern Kentucky and northern Tennessee: Journal of Sedimentary Petrology, v. 49, p. 245-256.

Morton, R.A., 1981, Formation of storm deposits by wind-forced currents in the Gulf of Mexico and the North Sea, in S.D. Nio, R.T.E. Schüttenhelm, and Tj.C.E. Van Weering, eds., Holocene marine sedimentation in the North Sea Basin: International Association of Sedimentologists Special Publication 5, p. 385-396.

____________ 1988, Nearshore responses to great storms, in H. Clifton, ed., Sedimentological consequences of convulsive geologic events: GSA Special Paper 229, p. 7-22.

Newell, K.D., W.L. Watney, S.W.L. Cheng, and R.L. Brownrigg, 1987, Stratigraphic and spatial distribution of oil and gas production in Kansas: Kansas Geological Survey Subsurface Geology Series 9, 86 p.

Purcell, W.R., 1949, Capillary pressures- their measurement using mercury and the calculation of permeability therefrom: Journal of Petroleum Technology, v. 1. p. 39-48.

Read, J.F., 1985, Carbonate platform facies models: AAPG Bulletin, v. 69, p. 1-21.

Shinn, E.A., 1983, Tidal flat, in P.A. Scholle, D.G. Bebout, and C.H. Moore, eds., Carbonate depositional environments: AAPG Memoir 33, p. 171-210.

Stewart, G.F., 1965, Lippoldt Field, in Kansas Oil and Gas Fields, V. 4: Wichita, Kansas Geological Society, p. 124-131.

Thompson, T.L. and E.D. Goebel, 1963, Preliminary report on conodonts of the Meramecian Stage (Upper Mississippian) from the subsurface of western Kansas: Kansas Geological Survey Bulletin 165, pt. 1, 16 p.

____________ 1968, Meramecian conodonts and stratigraphy of Kansas, Kansas Geological Survey Bulletin 192, 56 p.

Van Wagoner, J.C., H.W. Posamentier, R.M. Mitchum, Jr., P.R. Vail, J.F. Sarg, T.S. Loutit, and J. Hardenbol, 1988, An overview of the fundamentals of sequence stratigraphy and key definitions, in C.K. Wilgus, B.S. Hastings, C.G.St.C. Kendall, H.W. Posamentier, C.A. Ross, and J.C. Van Wagoner, eds., Sea-level changes: an integrated approach: SEPM Special Publication 42, p. 39-46.

Wardlaw, N.C. and R.P. Taylor, 1976, Mercury capillary pressure curves and the interpretation of pore structure and capillary behavior in reservoir rocks: Bulletin of Canadian Petroleum Geology, v. 24, p. 225-262.

Wardlaw, N.C., M. McKellar, and Y. Li, 1988, Pore and throat size distributions determined by mercury porosimetry and by direct observation: Carbonates and Evaporites, v. 3, p. 1-15.

Wardlaw, N.C., 1976, Pore geometry of carbonate rocks as revealed by pore casts and capillary pressure: AAPG Bulletin, v. 60, p. 245-257.

Warren, J.K., 1989, Evaporite sedimentology: Englewood Cliffs, Prentice Hall, 285 p.

___________ and C.G.St.C. Kendall, 1985, Comparison of sequences formed in marine sabkha (subaerial) and salina (subaqueous) settings- modern and ancient: AAPG Bulletin, v. 69, p. 1013-1023.

Wilson, M.E., 1988, Petrology and petroleum geology of the Meramecian (Upper Mississippian) Warsaw Formation, Kiowa and Comanche Counties, Kansas: Master's thesis, University of Kansas, Lawrence, Kansas.

Zeller, D.E., 1968, The stratigraphic succession in Kansas: Kansas Geological Survey Bulletin 189, 81 p.

APPENDIX A

CORE DESCRIPTIONS

Cores from eighteen Bindley Field wells were examined. Twelve cores were loaned by the Kansas Geological Survey and six cores were provided by Conoco, Inc. All cores were examined with binocular microscope, and the majority of core pieces were etched in 10% HCl to accentuate dolomite and grain textures. Thin sections were prepared from selected samples to further characterize rock types.

All core descriptions were logged on a form modified from that of Bebout and Loucks (1984). The principal modifications include 1) the addition of new structure symbols, 2) the replacement of the "crystal shape" column with an "oil stain" column, and 3) modification of the "fossil" symbology to reflect moldic and non-moldic skeletal preservation. A key to the symbols used in logging Bindley Field cores is provided on the following page. Refer to Appendix B for correlation of core properties to gamma-ray log signatures.

WELL Beardmore #1 Shelton LOCATION SE SE 28-21S-24W COUNTY/STATE Hodgeman, KS

STRATIGRAPHIC INTERVAL 4615'-4643' LOGGED BY R.A. Johnson DATE

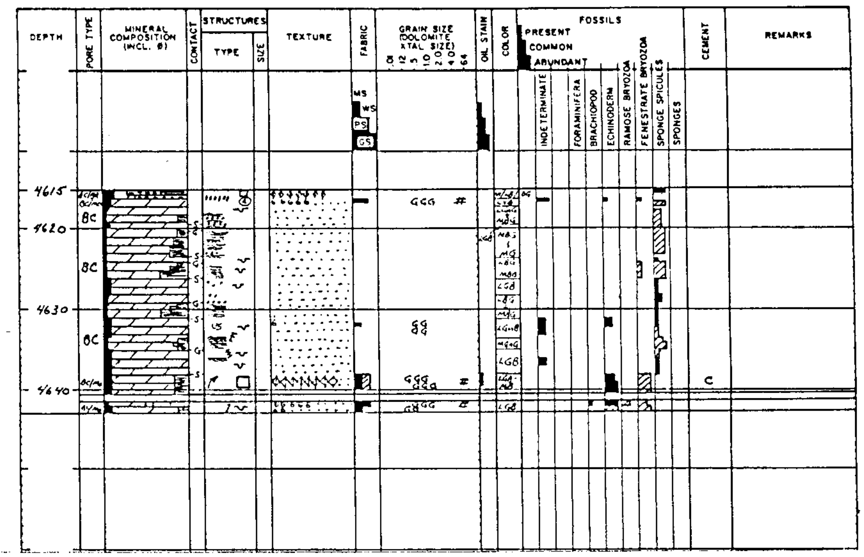

CORE LOG SYMBOL KEY

As Used in Bindley Field Core Logs

Pore Type

BC Intercrystalline
BP Interparticle
MO Moldic
BR Breccia

Texture

Skeletal Grains
Lithoclasts
Indeterminate Grains
Micrite

Grain Size

G Skeletal Grains
Lithoclasts

Fossils

Moldic
Partially Moldic
Non-Moldic

Mineral Composition

Calcite
Dolomite
Shale
Anhydrite
Replacement Silica

Color

B Brown
G Gray
Gn Green
Bl Black
C Cream
Y Yellow
L Light
M Medium
D Dark
Mot Mottled

Cement

C Calcite
D Dolomite
A Anhydrite

Structures

Quartz Nodule Layer (Vertically Elongate)
Quartz Nodule Layer (Subround)
Chert Nodule
Graded Beds (Fining Up)
Scoured Surface
Wavy Laminated
Horizontally Laminated
Burrows- Vertical
Burrows- Horizontal
Bored Surface
Fracture
Breccia
Stylolite
Rotated Bedding

Contacts

G Gradational
S Sharp
SD Sharp Disconformable
ST Stylolitic
VS Visibly Scoured
? Contact Missing

WELL Oasis #3 Bindley LOCATION NE NE 33-21S-24W COUNTY/STATE Hodgeman, KS

STRATIGRAPHIC INTERVAL 4594'-4643' LOGGED BY R.A. Johnson DATE

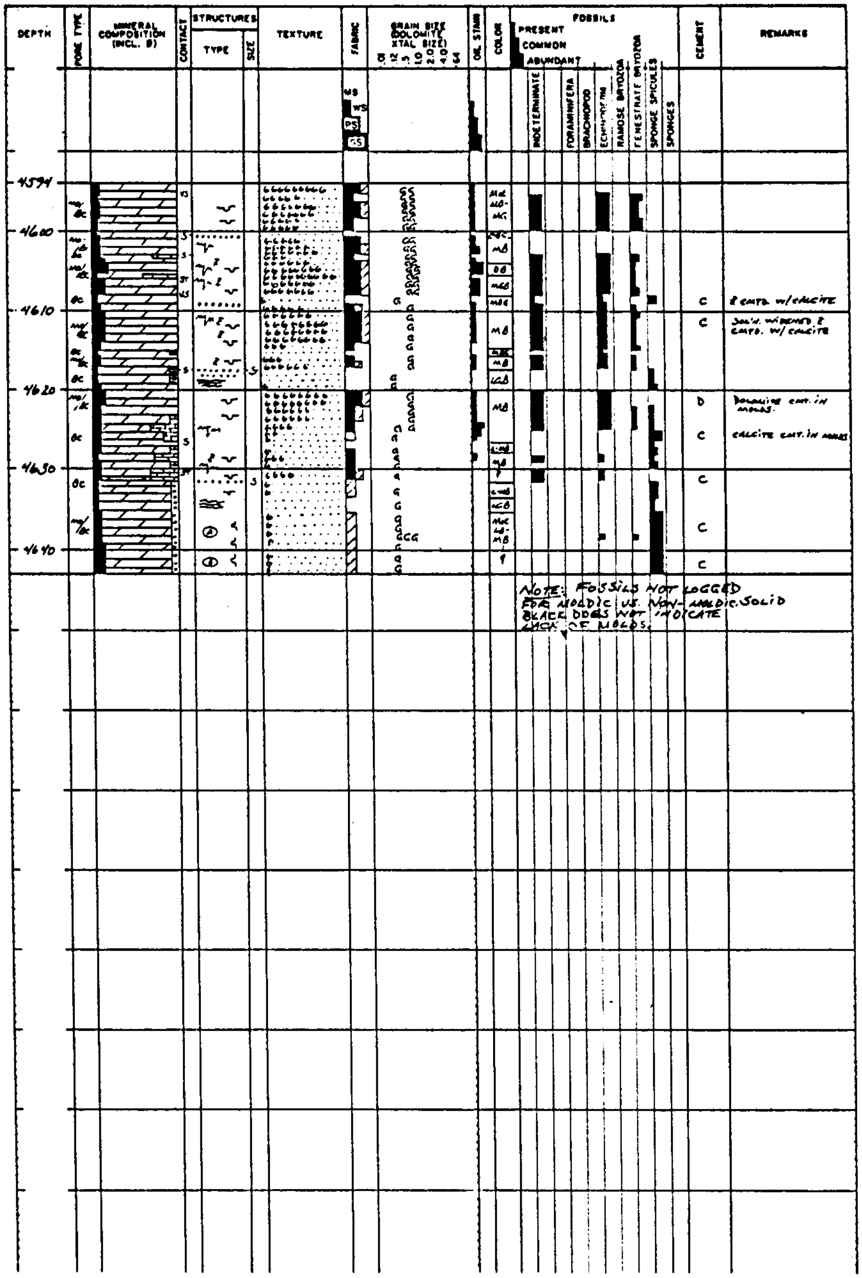

WELL OASIS #1 SCHAUVLIEGE LOCATION SE NW 33-21S-24W COUNTY/STATE HODGEMAN, KS

STRATIGRAPHIC INTERVAL 4654'-4711' LOGGED BY R.A. JOHNSON DATE

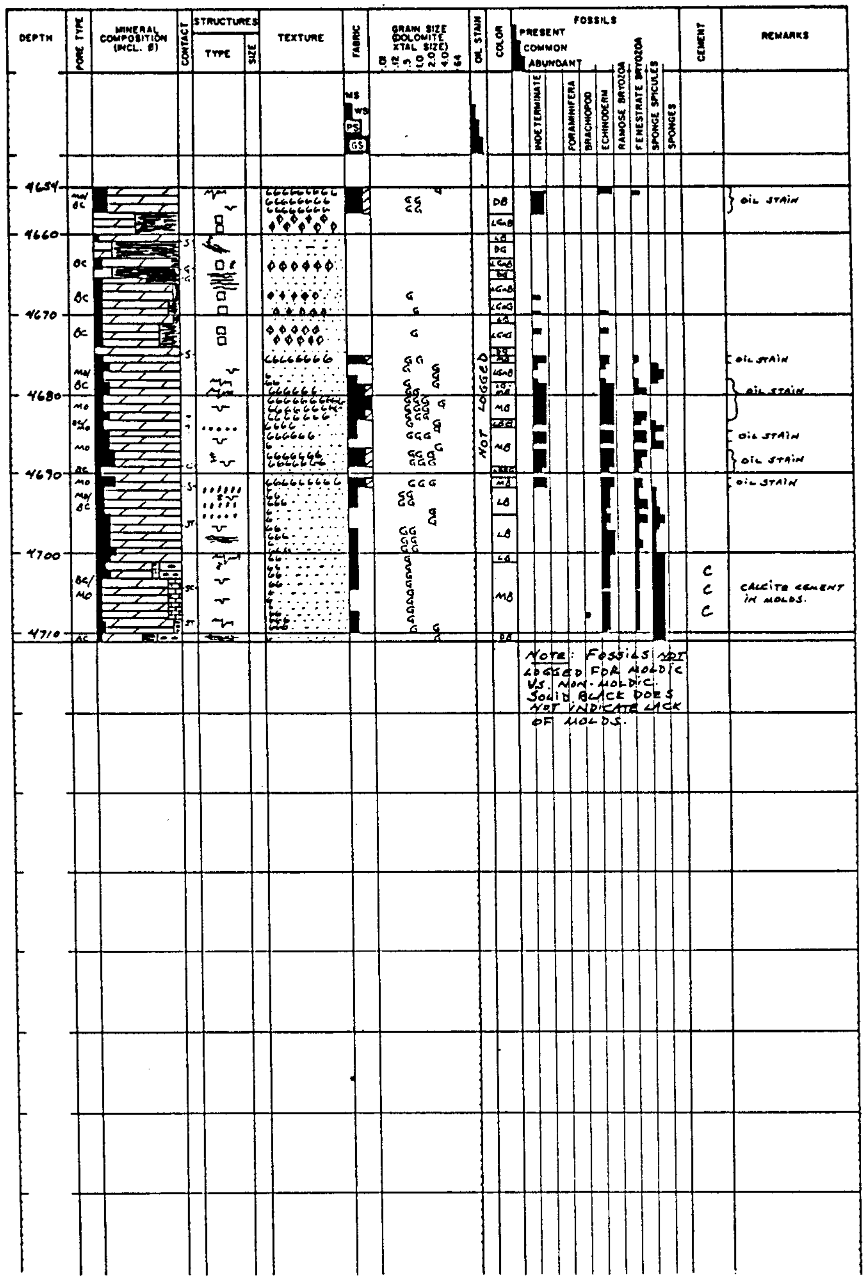

WELL OASIS #2 BINDLEY LOCATION SW NE 33-21S-24W COUNTY/STATE HODGEMAN, KS

STRATIGRAPHIC INTERVAL 4637'-4669' LOGGED BY R. A. JOHNSON DATE

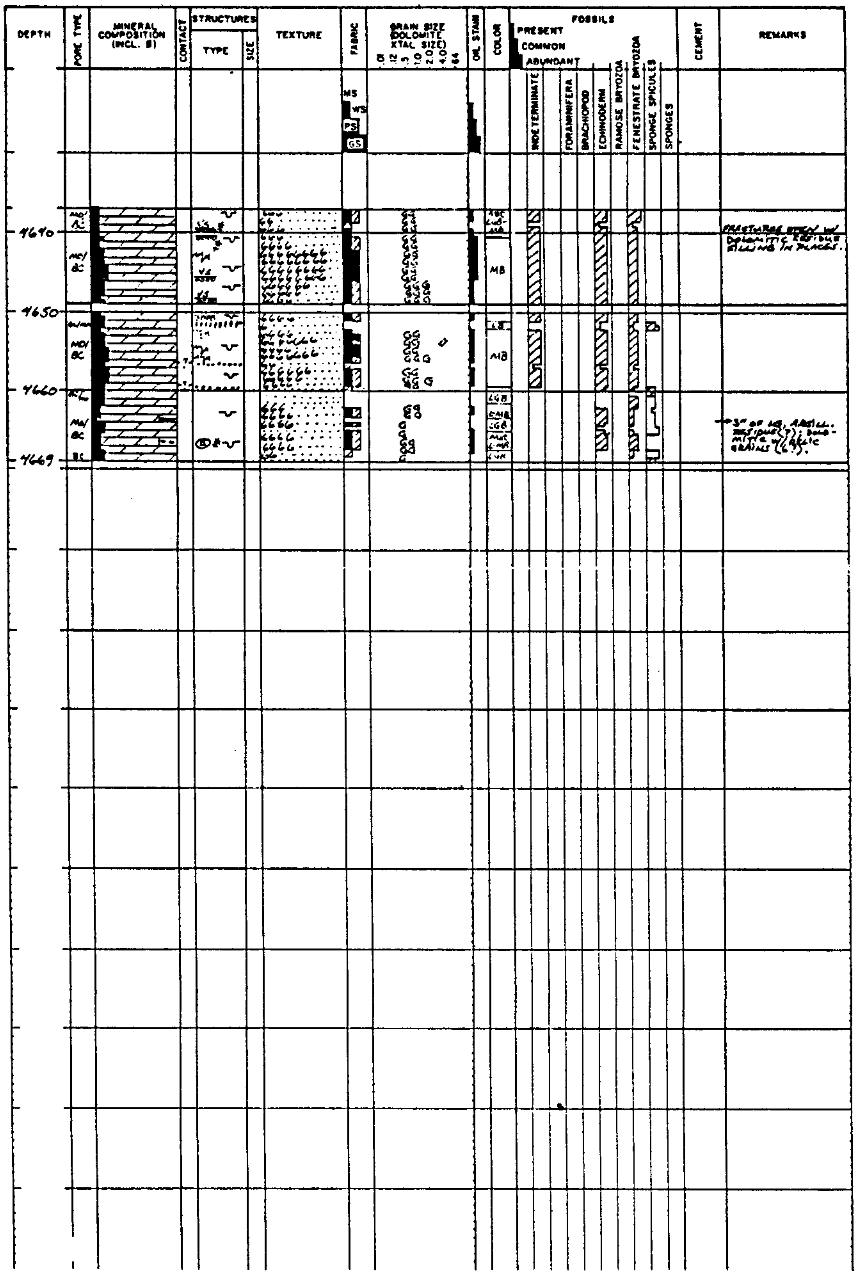

WELL OASIS #1 DEUTSCH LOCATION NE SE 33-21S-24W COUNTY/STATE HODGEMAN, KS

STRATIGRAPHIC INTERVAL 4609'-4694' LOGGED BY R.A. JOHNSON DATE

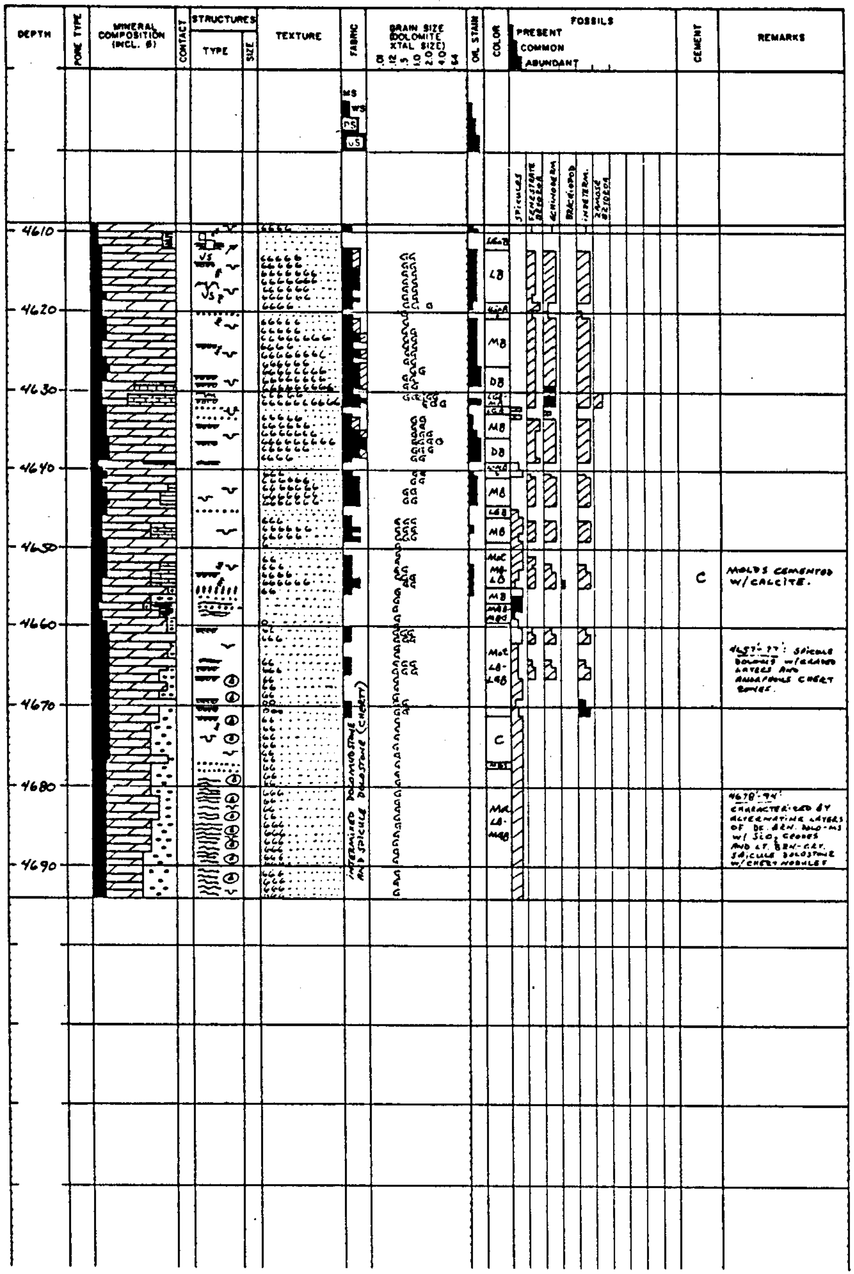

WELL OASIS #2 DEUTSCH LOCATION NW SE 33-21S-24W COUNTY/STATE HODGEMAN, KS

STRATIGRAPHIC INTERVAL 4602'-4653' LOGGED BY R.A. JOHNSON DATE

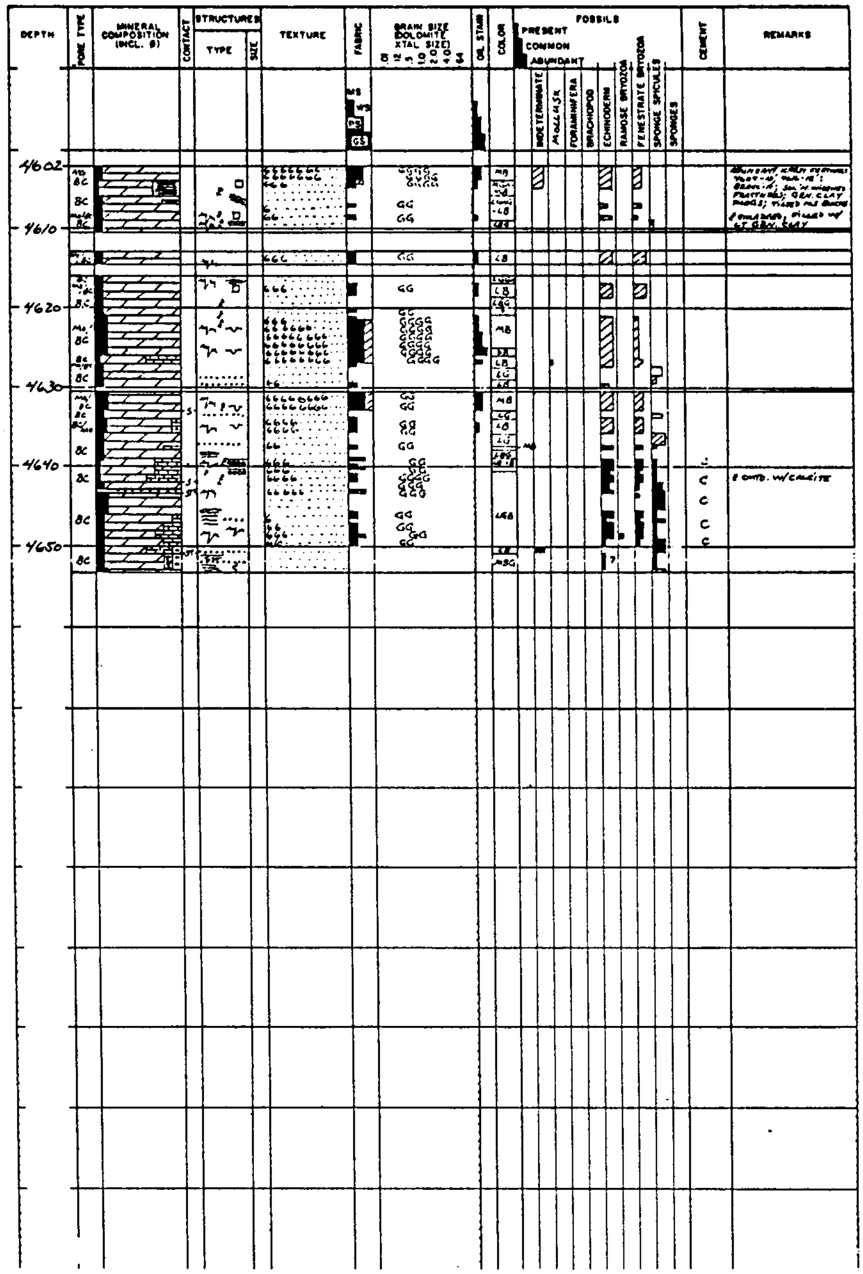

WELL *OASIS #1 ADAMS* LOCATION *NE SW 33-21S-24W* COUNTY/STATE *HODGEMAN, KS*

STRATIGRAPHIC INTERVAL *4665-4673.5'* LOGGED BY *R. A. JOHNSON* DATE ______

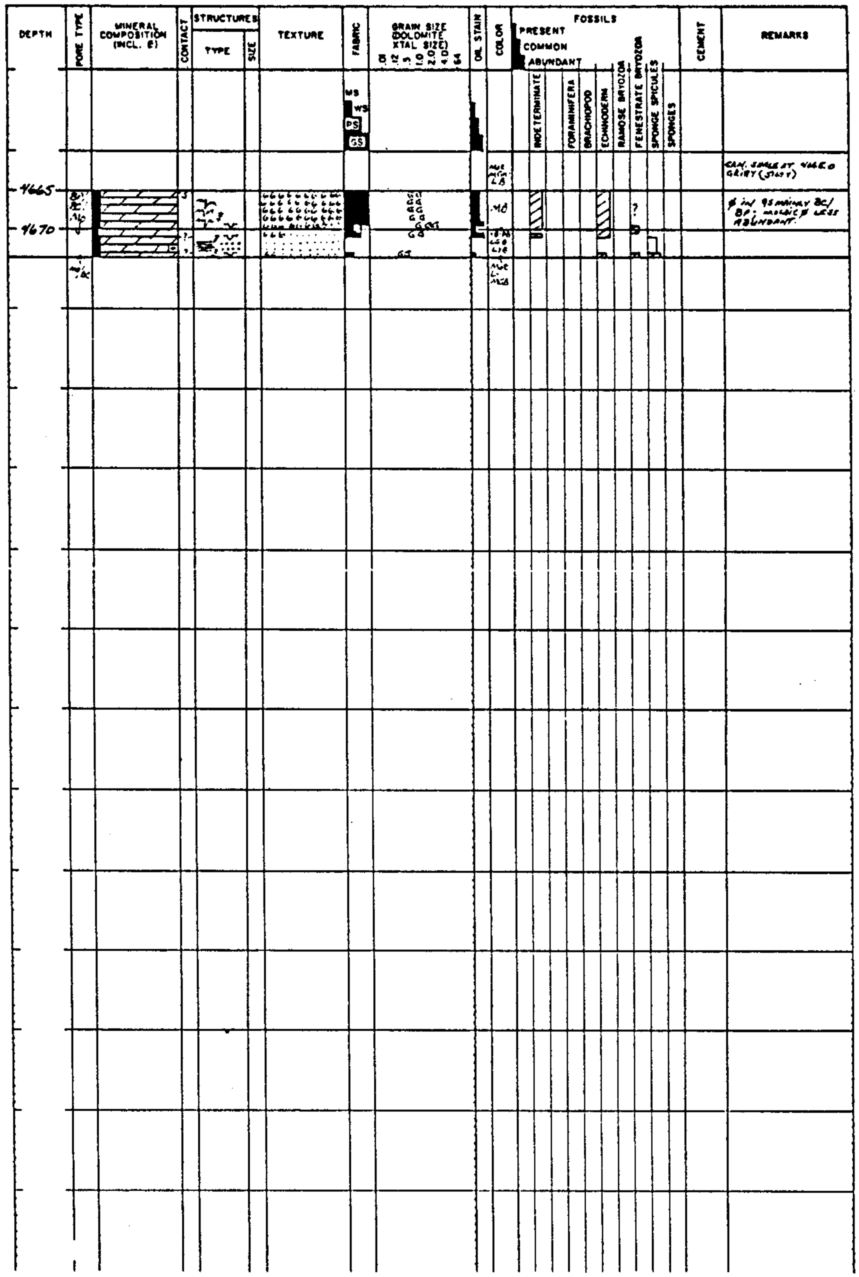

WELL Oasis #5 Deutsch LOCATION SW SE 33-21S-24W COUNTY/STATE Hodgeman, KS

STRATIGRAPHIC INTERVAL 4622'-4681' LOGGED BY R. A. Johnson DATE

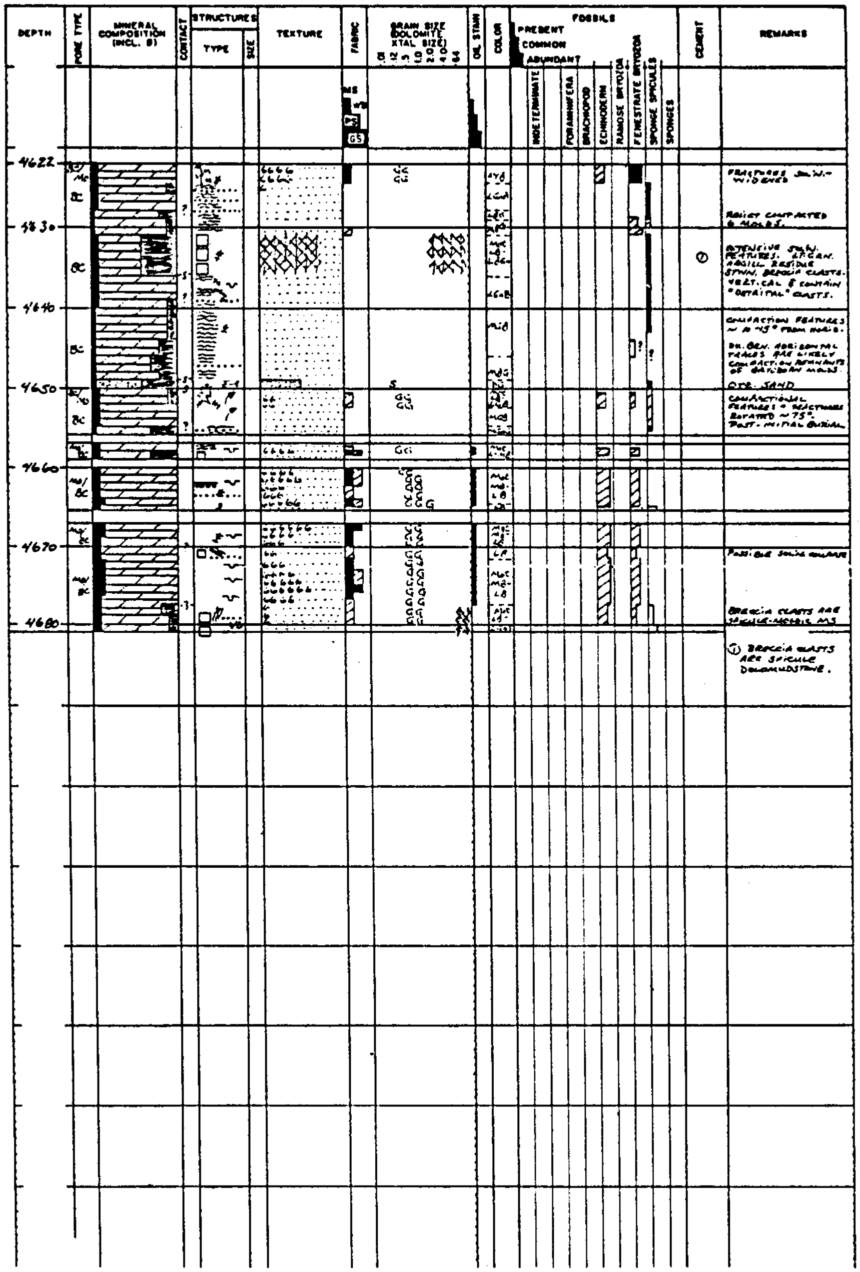

WELL OASIS #4 DEUTSCH LOCATION SE SE 33-21S-24W COUNTY/STATE HODGEMAN, KS

STRATIGRAPHIC INTERVAL 4636'-4688' LOGGED BY R. A. JOHNSON DATE

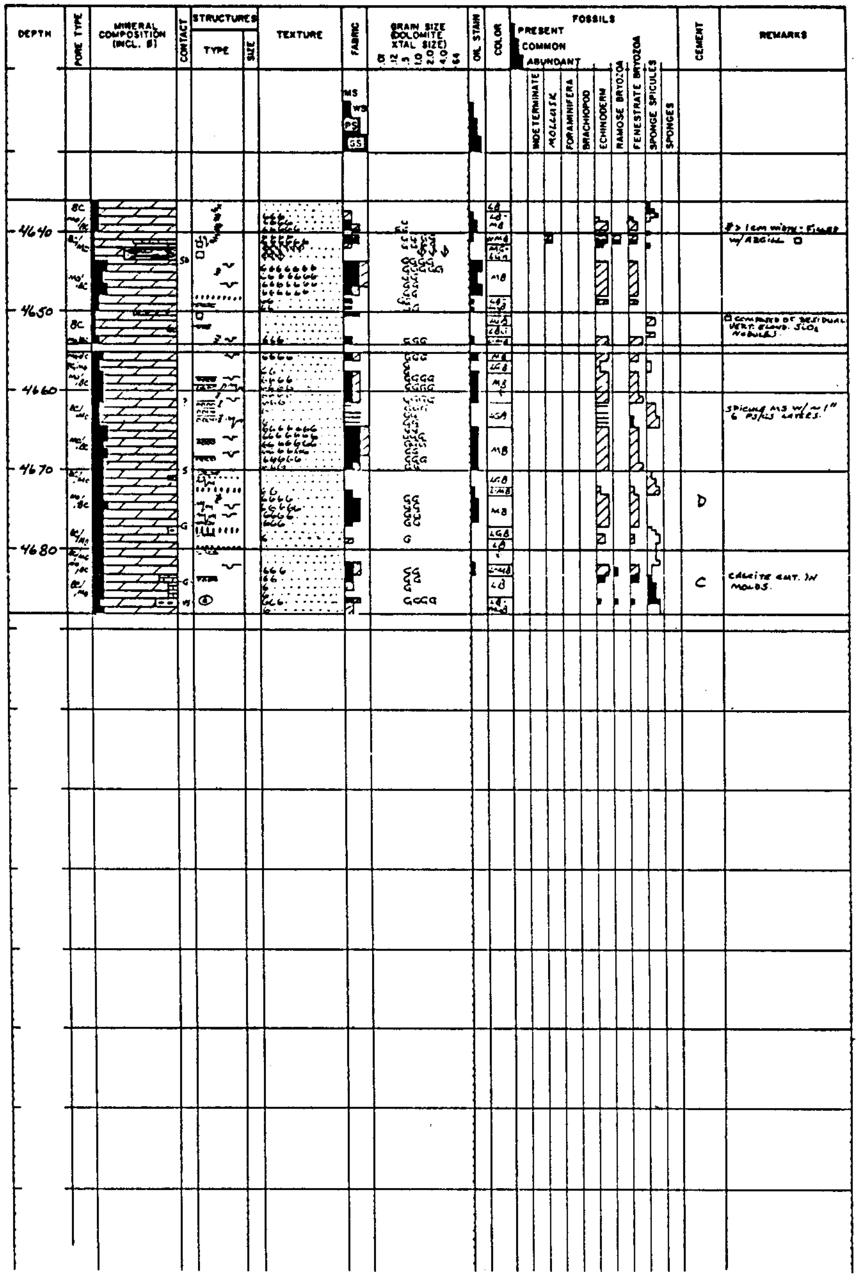

WELL Oasis #1 Smith LOCATION SW NW 34-21S-24W COUNTY/STATE Hodgeman, KS

STRATIGRAPHIC INTERVAL 4621.5'-4674' LOGGED BY R.A. Johnson DATE

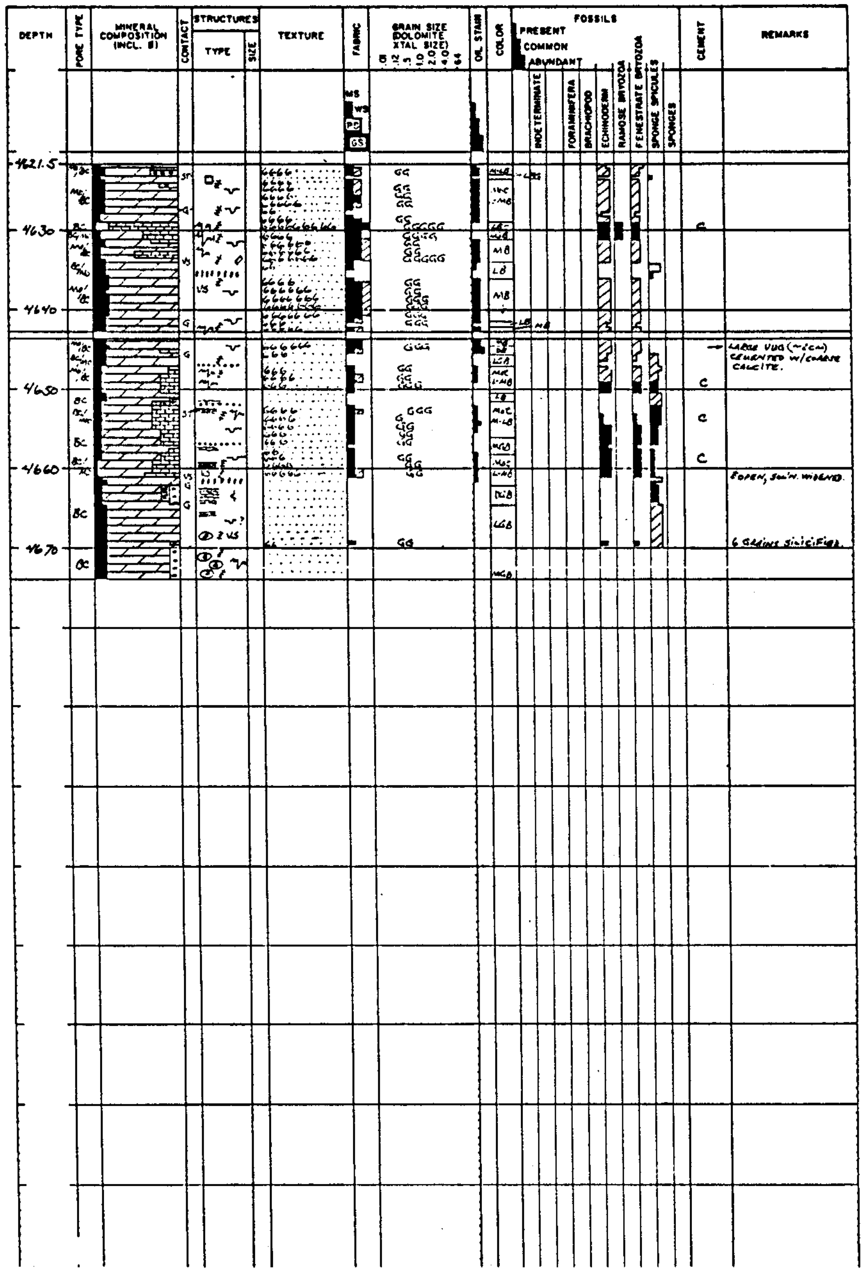

WELL OASIS #3 DEUTSCH LOCATION NW SW 34-21S-24W COUNTY/STATE HODGEMAN, KS

STRATIGRAPHIC INTERVAL 4625'-4683.5' LOGGED BY R.A. JOHNSON DATE

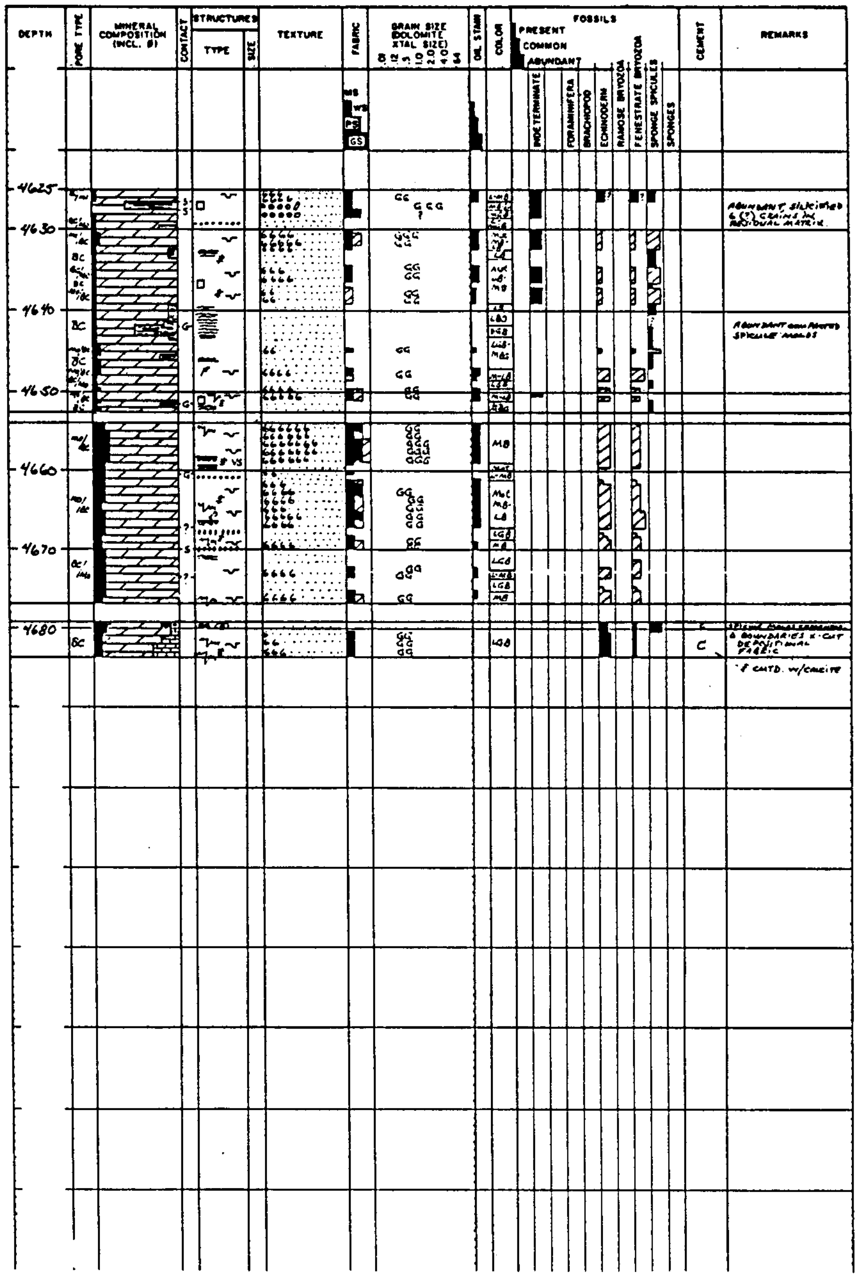

WELL OASIS #6 DEUTSCH LOCATION SWSW 34-21S-24W COUNTY/STATE HODGEMAN, KS

STRATIGRAPHIC INTERVAL 4639'-4697' LOGGED BY R.A. JOHNSON DATE

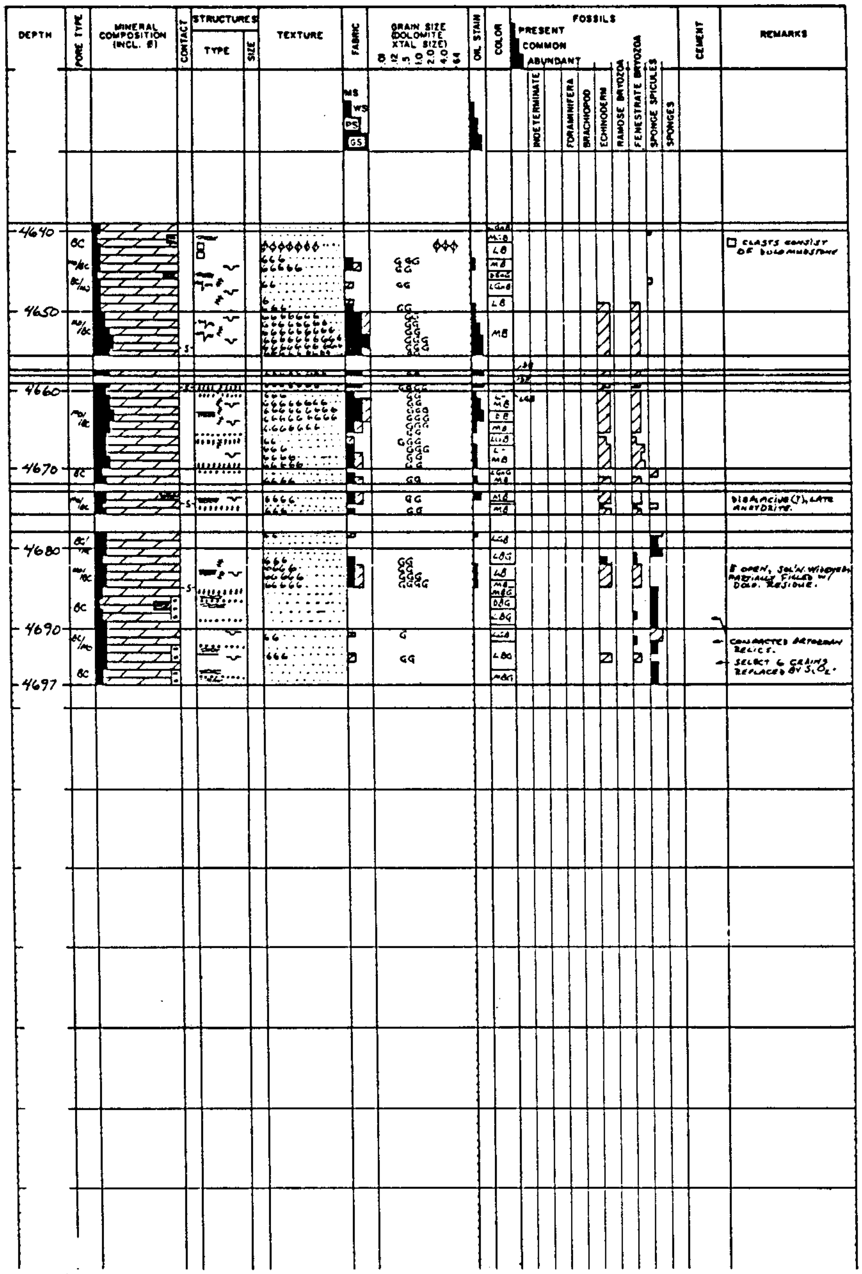

WELL OASIS #7 DEUTSCH LOCATION SE SW 34-21S-24W COUNTY/STATE HODGEMAN KS

STRATIGRAPHIC INTERVAL 4637'-4696' LOGGED BY R. A. JOHNSON DATE

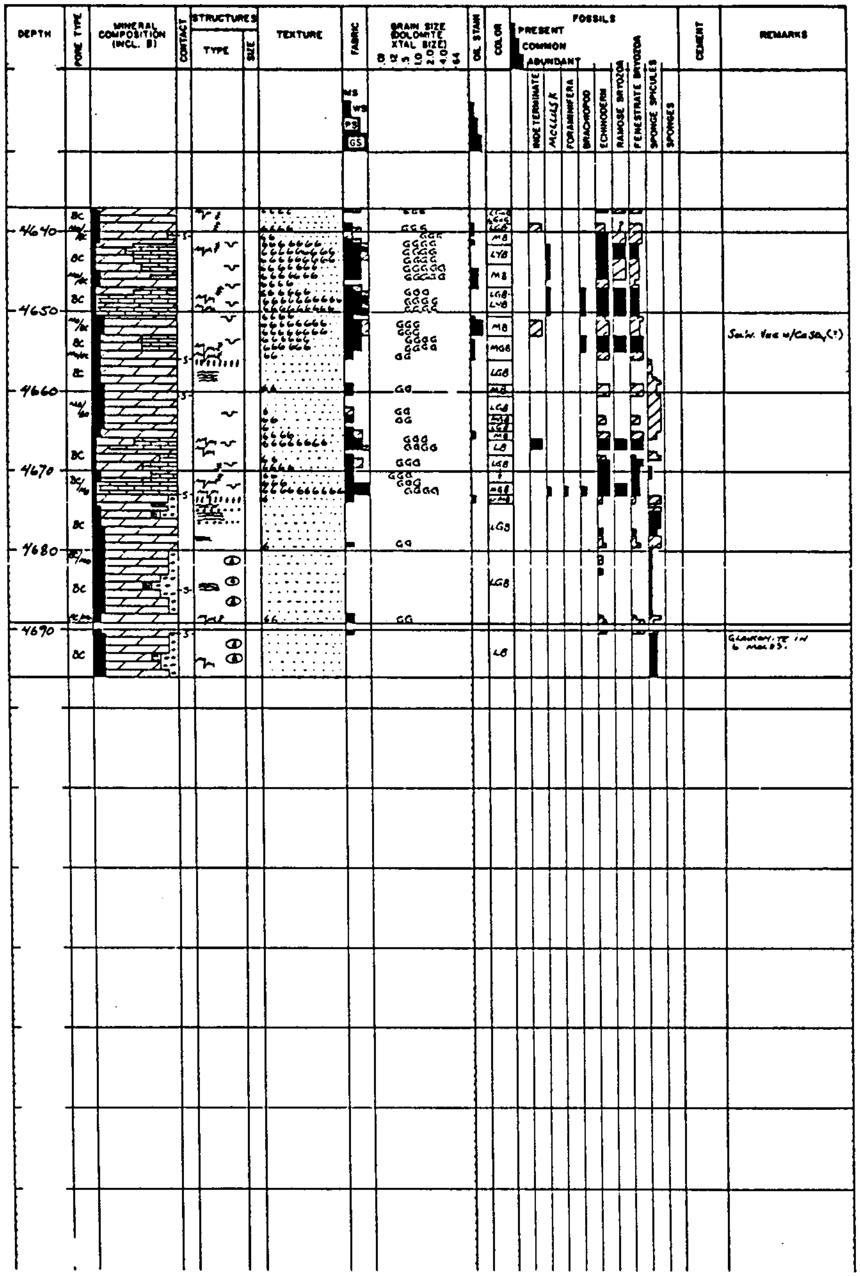

WELL *OASIS #1 EVERTON* LOCATION *SW SE 34-21S-24W* COUNTY/STATE *HODGEMAN, KS*

STRATIGRAPHIC INTERVAL *4663'-4709'* LOGGED BY *R.A. JOHNSON* DATE ______

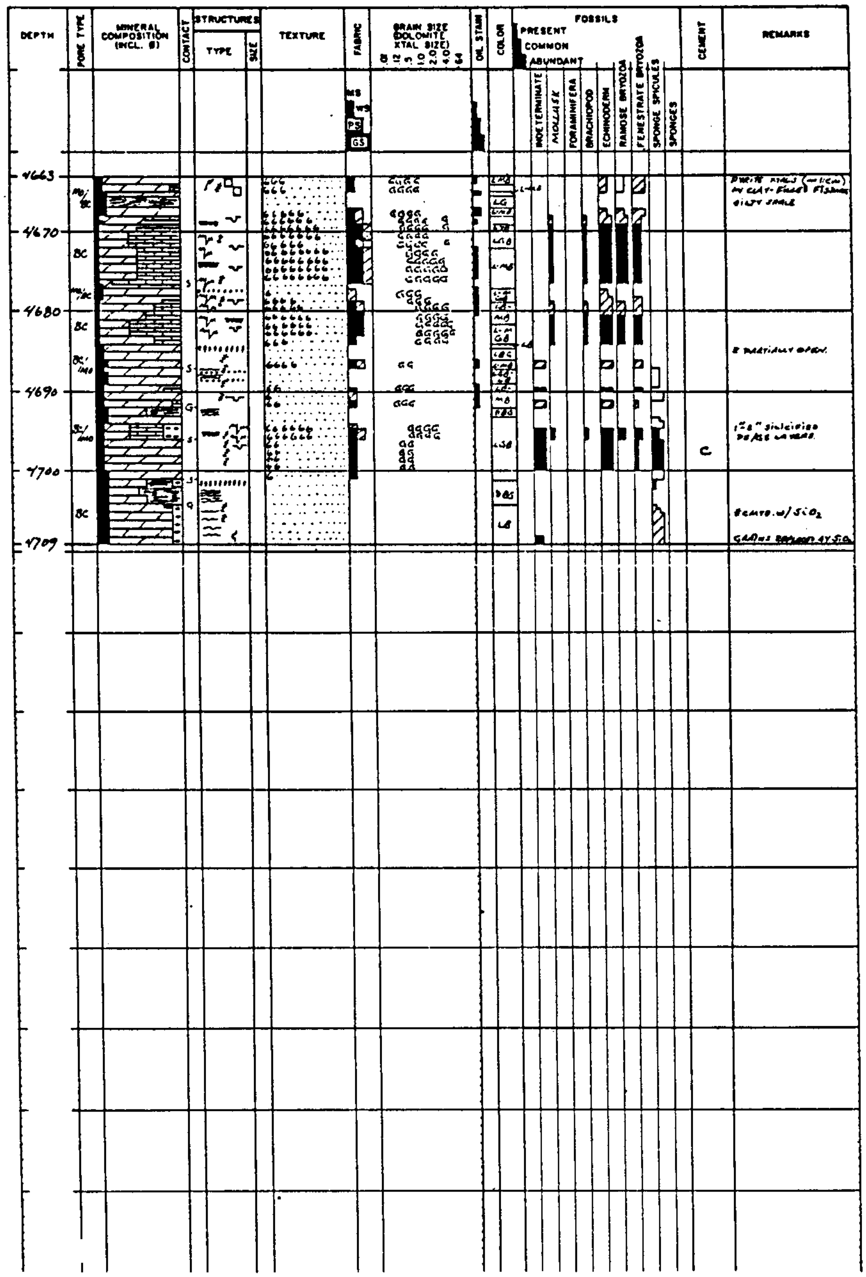

WELL OASIS #2 EVERTON LOCATION SESE 34-21S-24W COUNTY/STATE HODGEMAN, KS

STRATIGRAPHIC INTERVAL 4642'-4701' LOGGED BY R.A. JOHNSON DATE

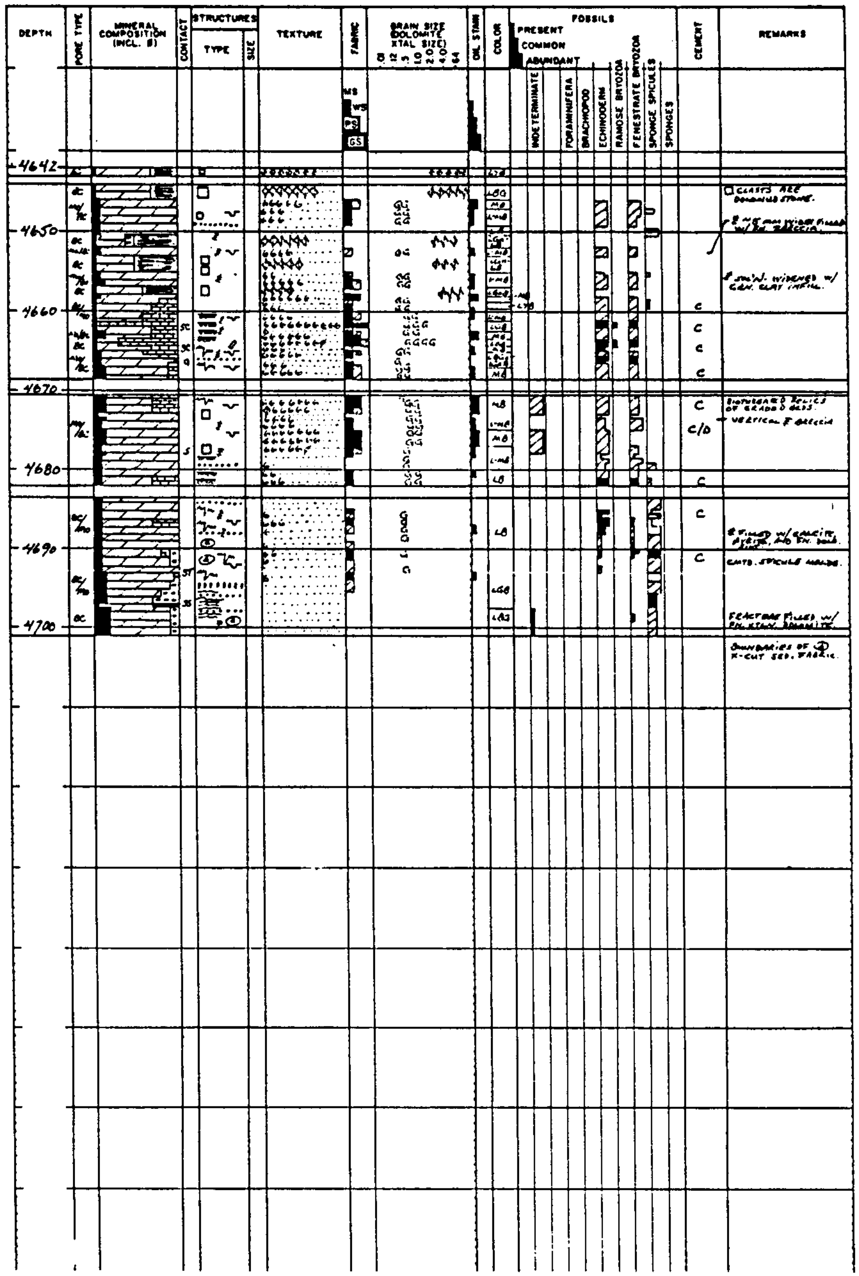

WELL OASIS #2 WALTER LOCATION NE NW 3-22S-24W COUNTY/STATE HODGEMAN, KS

STRATIGRAPHIC INTERVAL 4652'-4686' LOGGED BY R. A. JOHNSON DATE

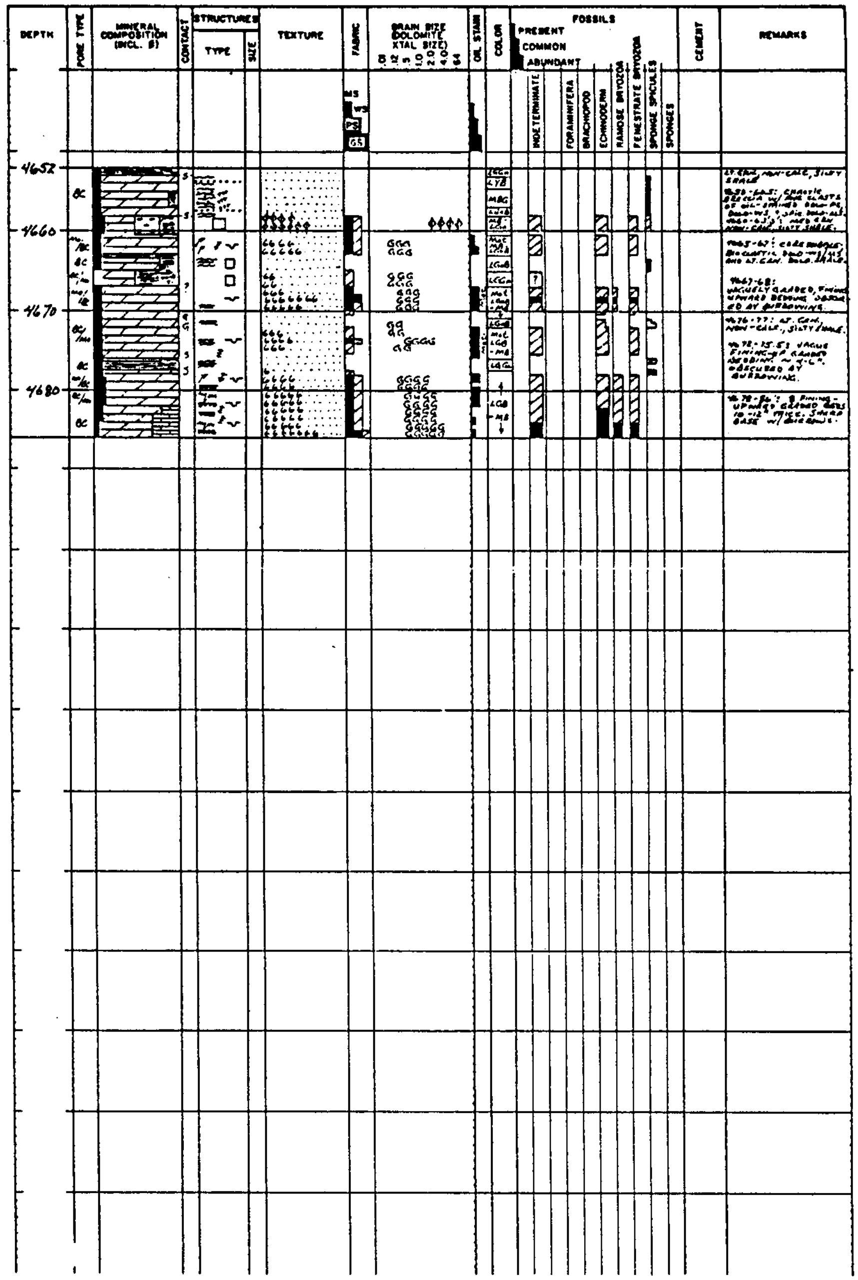

WELL Oasis #1 Walter LOCATION NW NW 3-22S-24W COUNTY/STATE Hodgeman, KS

STRATIGRAPHIC INTERVAL 4642'–4718' LOGGED BY R. A. Johnson DATE

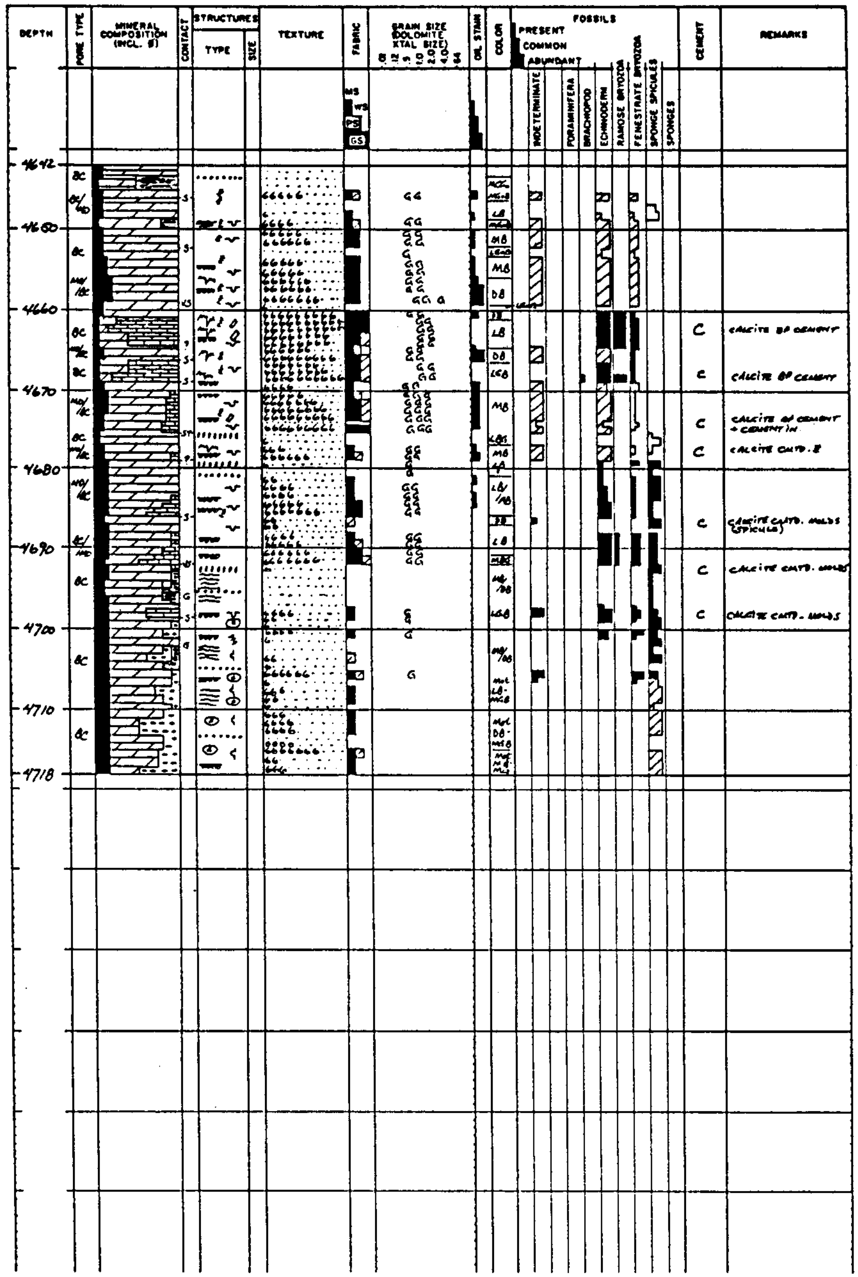

WELL OASIS #1 DIXON LOCATION NE NE 4-22S-24W COUNTY/STATE HODGEMAN, KS

STRATIGRAPHIC INTERVAL 4642'-4700' LOGGED BY R.A. JOHNSON DATE

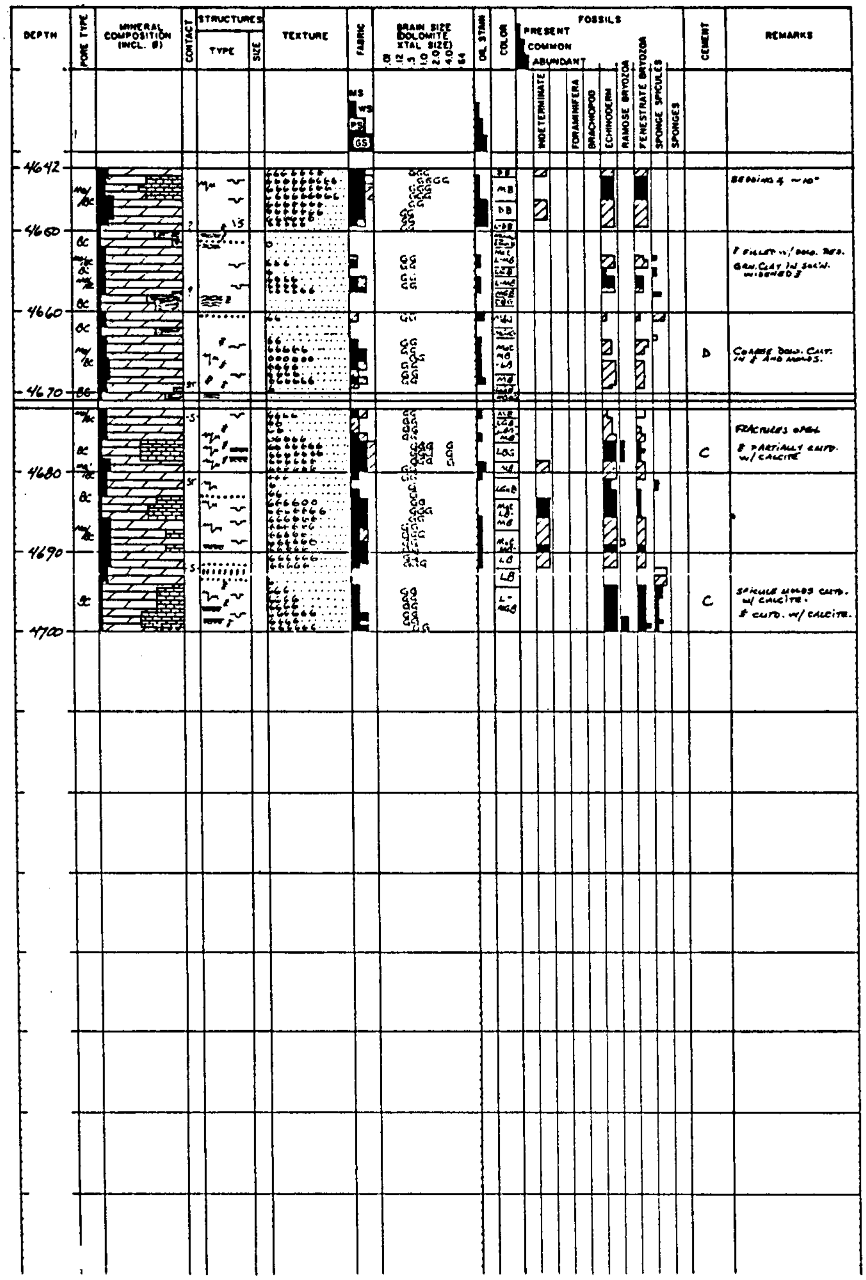

APPENDIX B

CORE PROPERTIES/LOG CORRELATIONS

Core properties are correlated to gamma-ray log character for each core for which a gamma-ray log and porosity and permeability data are available. Each figure contains, from left to right, gamma-ray curve, depth, sedimentary structures, lithotype, core porosity, and core permeability. The gamma-ray curves are from open-hole logs unless otherwise stipulated. Gamma-ray log depths have been adjusted to conform to core depth.

Sedimentary structures and lithotypes are derived from the core descriptions (Appendix A). Only those structures which are useful in distinguishing lithotypes and stratigraphic boundaries are included. Refer to Appendix A for the key to structure symbols.

Porosity and permeability data are from whole-core analyses collected immediately after each core was cut. The maximum directional, horizontal permeability (k_{max}) is indicated by the dashed lines. The horizontal permeability at right angles to the direction of maximum permeability (k_{90}) is represented by solid black. Wide variation between the two measurements is indicative of fractures.

No figure is included for the Beardmore Oil #1 Shelton (SE/4 SE/4, 28-T21S-R24W) due to the fact that no log was run in the well and no porosity and permeability analyses were collected.

WELL OASIS 3 BINDLEY LOCATION NE NE 33-21S-24W CORED INTERVAL 4594'-4643'

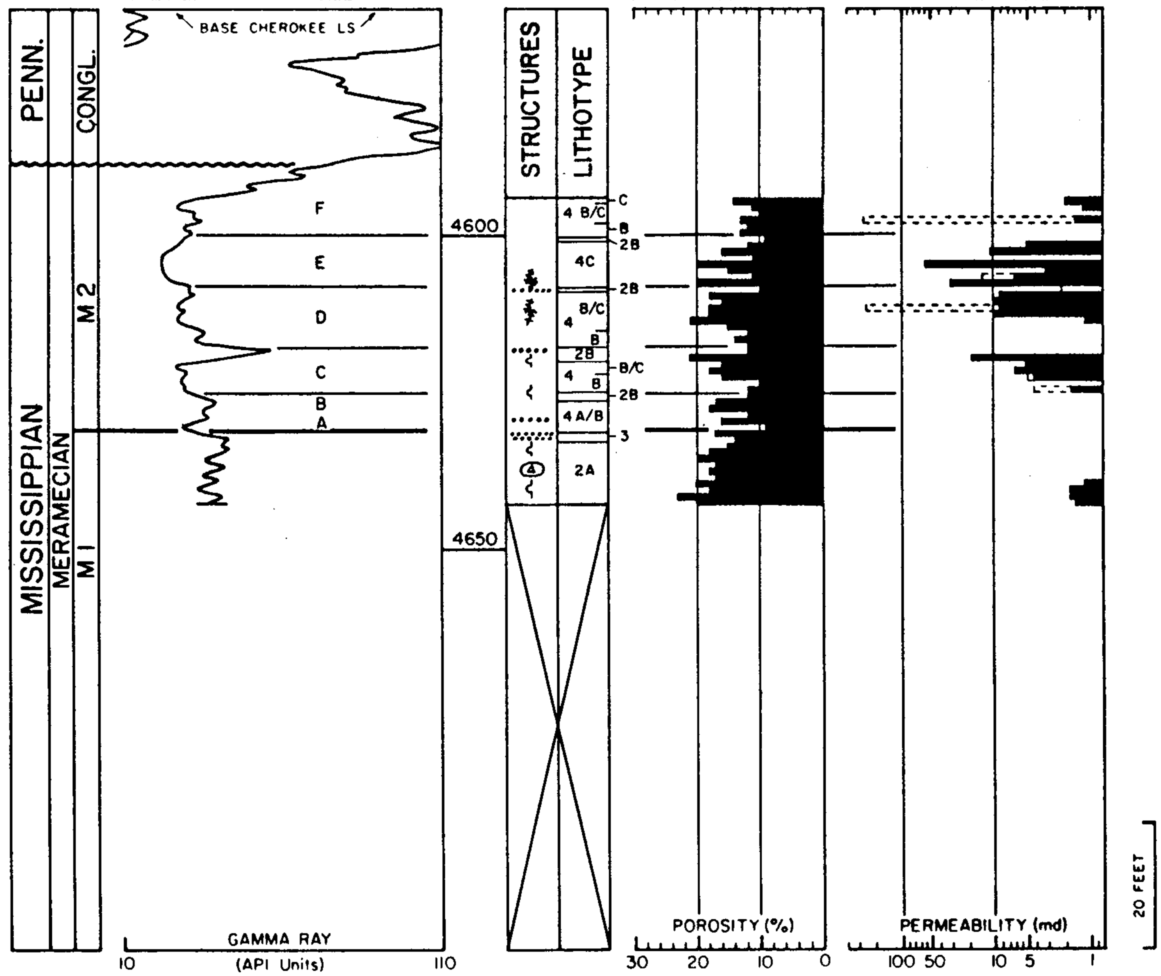

WELL OASIS I SCHAUVLIEGE LOCATION SE NW 33-21S-24W CORED INTERVAL 4654'-4712'

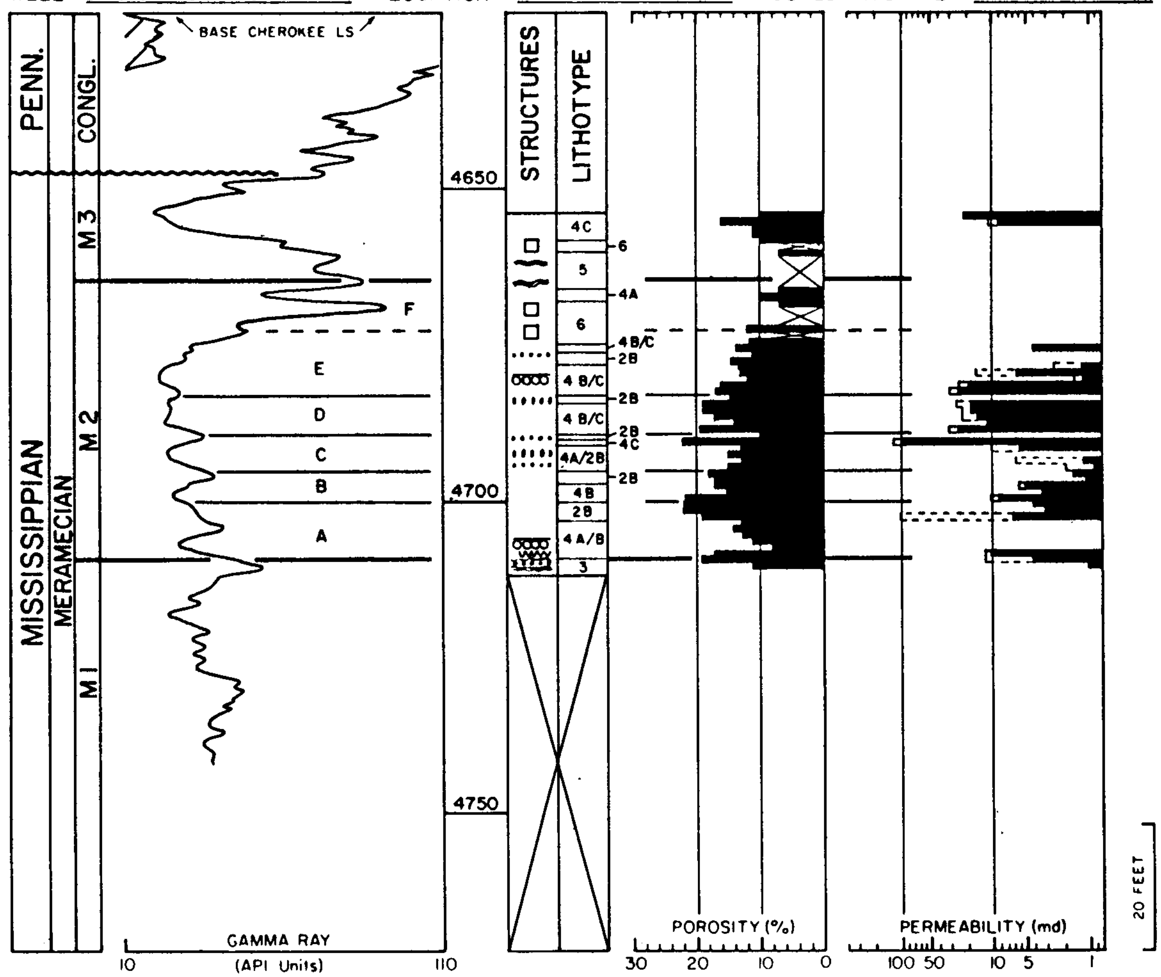

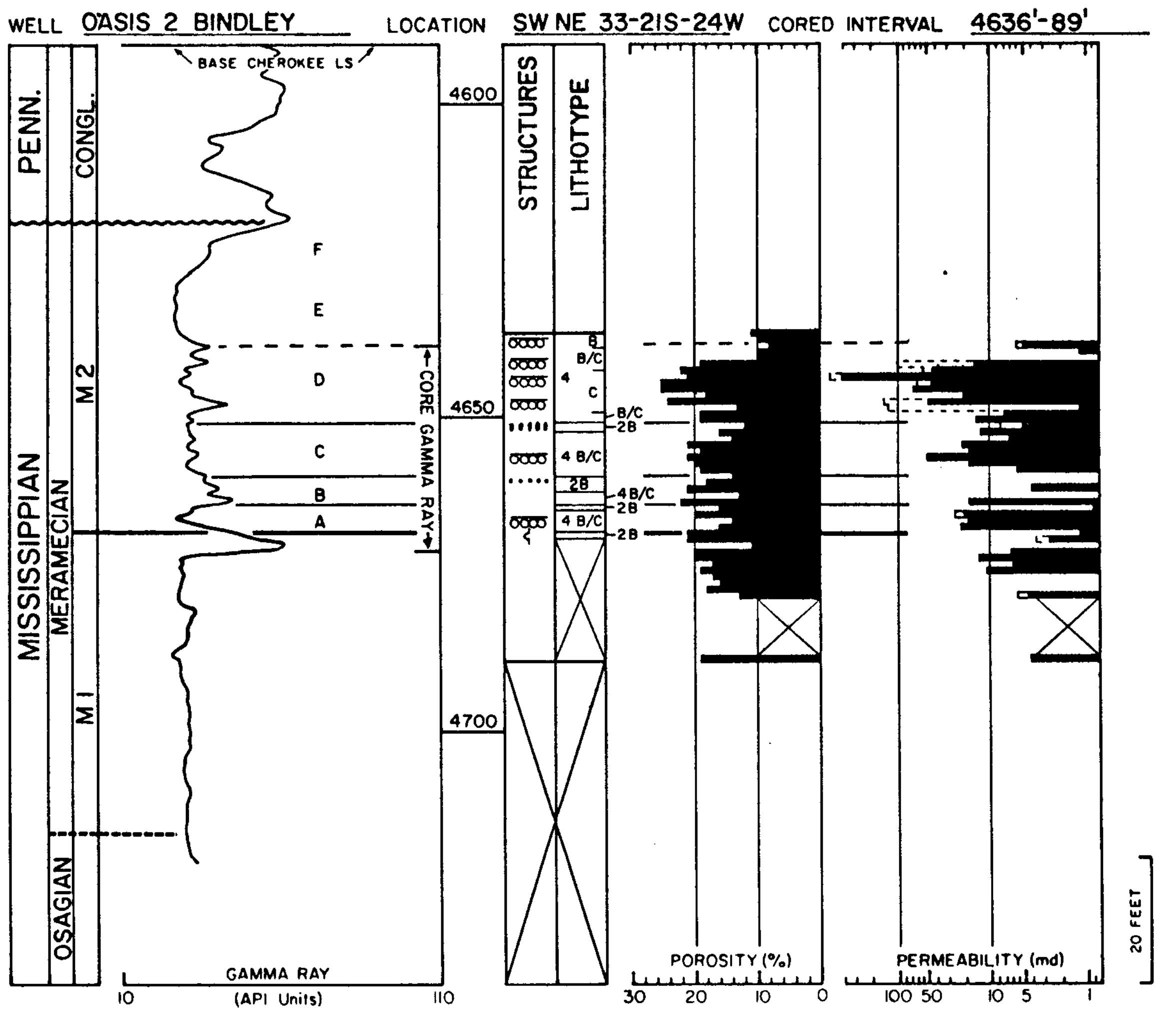
WELL OASIS 2 BINDLEY
LOCATION SW NE 33-21S-24W
CORED INTERVAL 4636'-89'
BASE CHEROKEE LS
PENN.
CONGL.
MISSISSIPPIAN
MERAMECIAN
OSAGIAN
M 2
M 1
F
E
D
C
B
A
CORE GAMMA RAY
4600
4650
4700
STRUCTURES
LITHOTYPE
B/C
4
C
2B
4 B/C
4B/C
GAMMA RAY
(API Units)
10
110
POROSITY (%)
30
20
10
0
PERMEABILITY (md)
100
50
10
5
1
20 FEET

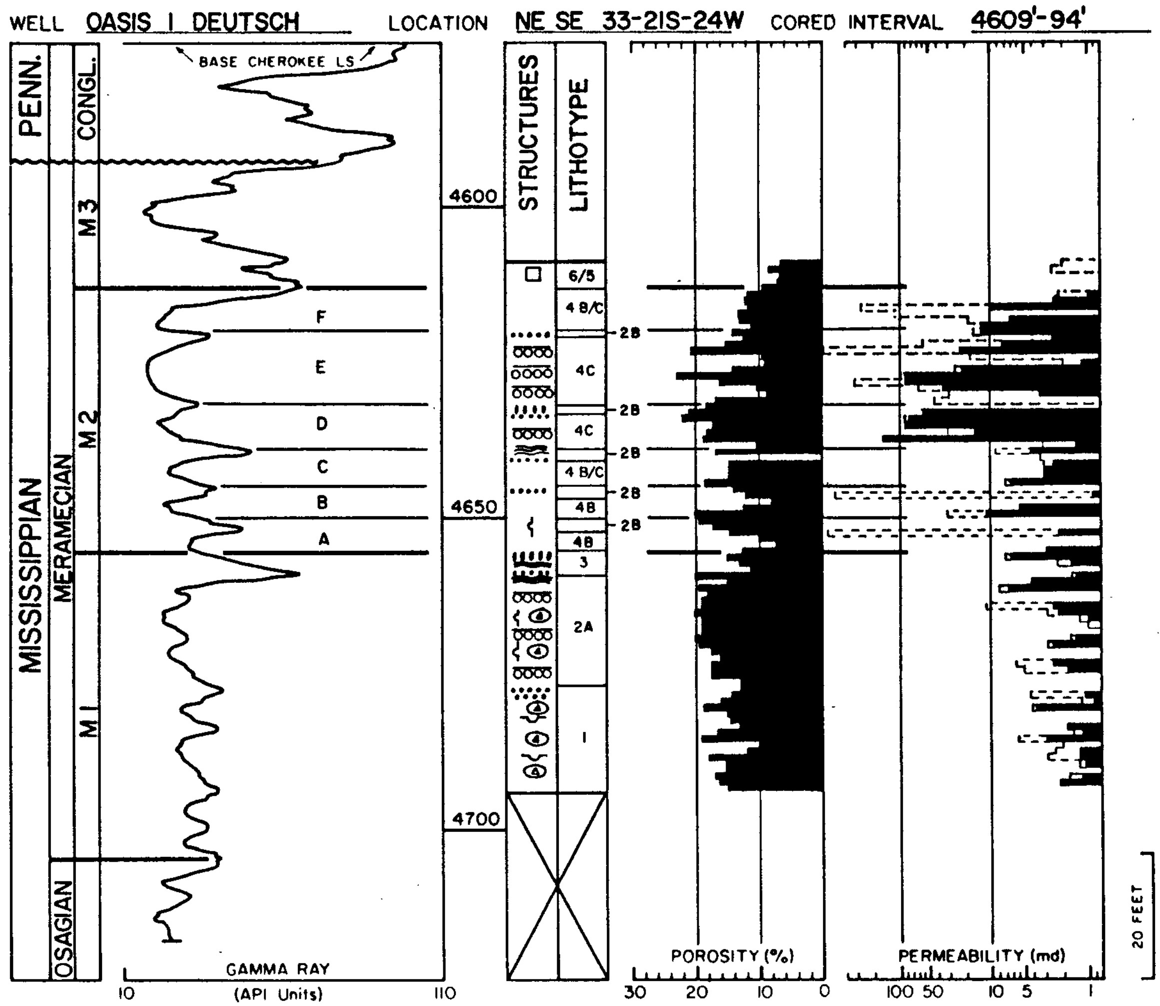
WELL OASIS I DEUTSCH
LOCATION NE SE 33-21S-24W
CORED INTERVAL 4609'-94'
PENN.
CONGL.
MISSISSIPPIAN
MERAMECIAN
OSAGIAN
M3
M2
M1
BASE CHEROKEE LS
F
E
D
C
B
A
4600
4650
4700
GAMMA RAY
(API Units)
10
110
STRUCTURES
LITHOTYPE
6/5
4 B/C
4C
4C
4 B/C
4B
4B
3
2A
1
2B
2B
2B
2B
2B
POROSITY (%)
30
20
10
0
PERMEABILITY (md)
100
50
10
5
1
20 FEET

WELL OASIS 2 DEUTSCH LOCATION NW SE 33-21S-24W CORED INTERVAL 4602'-55'

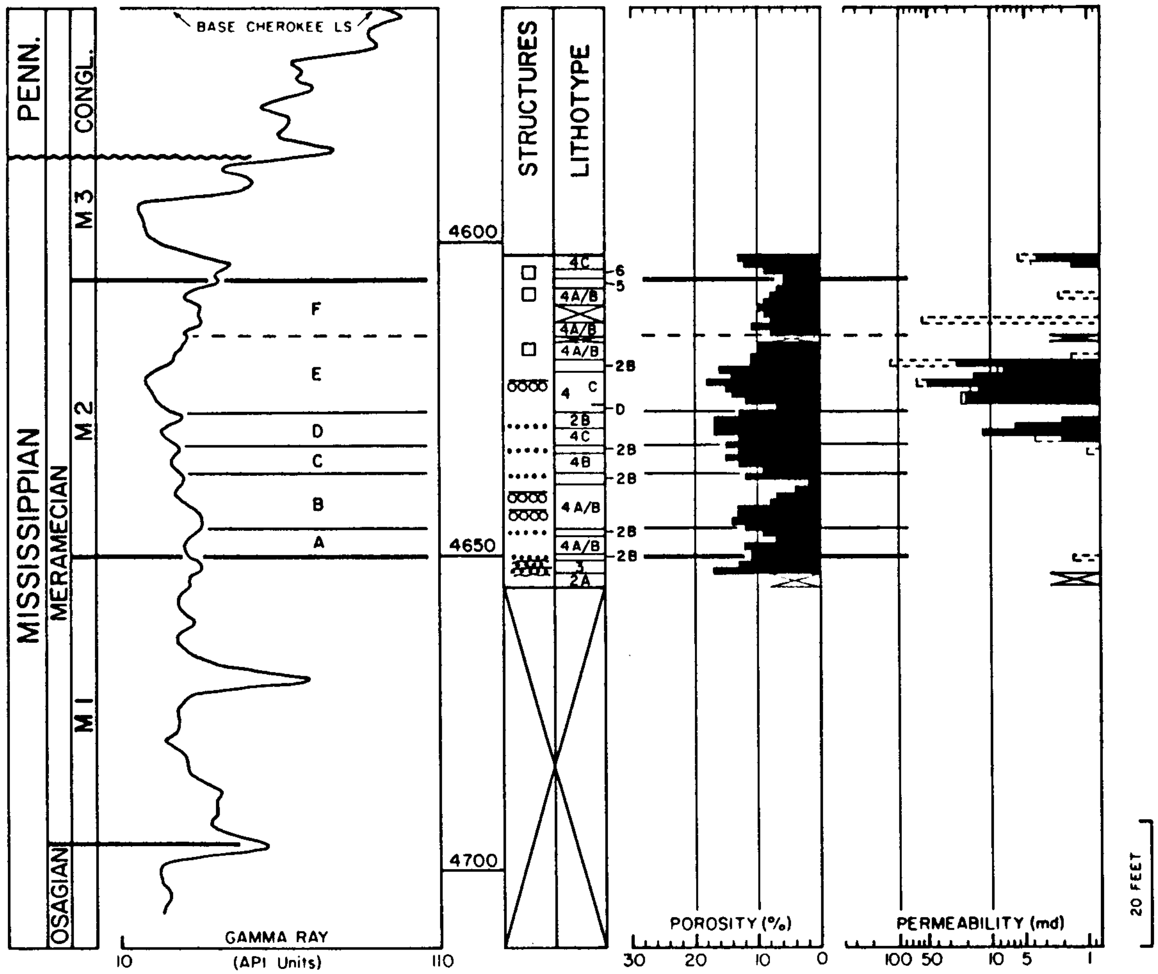

WELL OASIS I ADAMS LOCATION NE SW 33-21S-24W CORED INTERVAL 4653'-87'

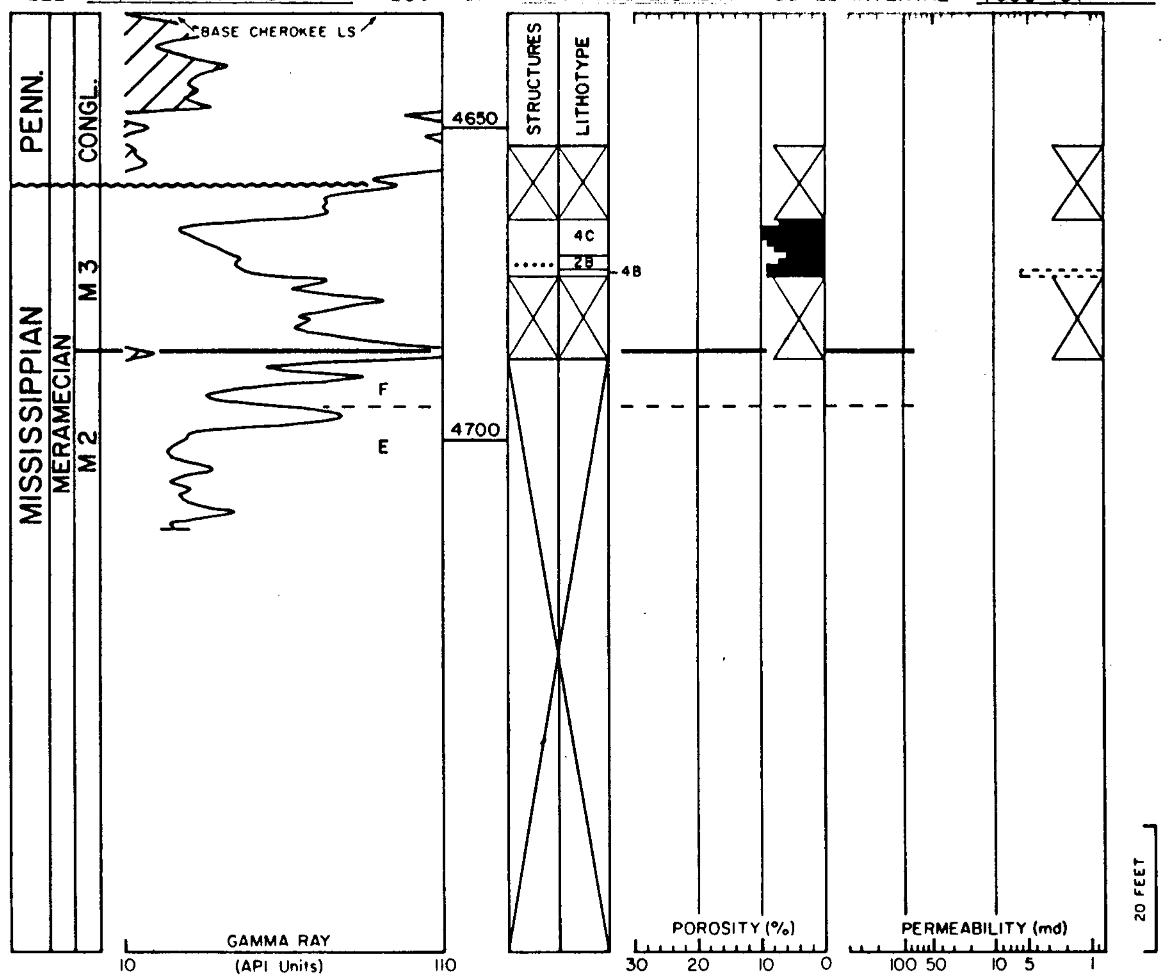

227

WELL OASIS 5 DEUTSCH LOCATION SW SE 33-21S-24W CORED INTERVAL 4622'-82'

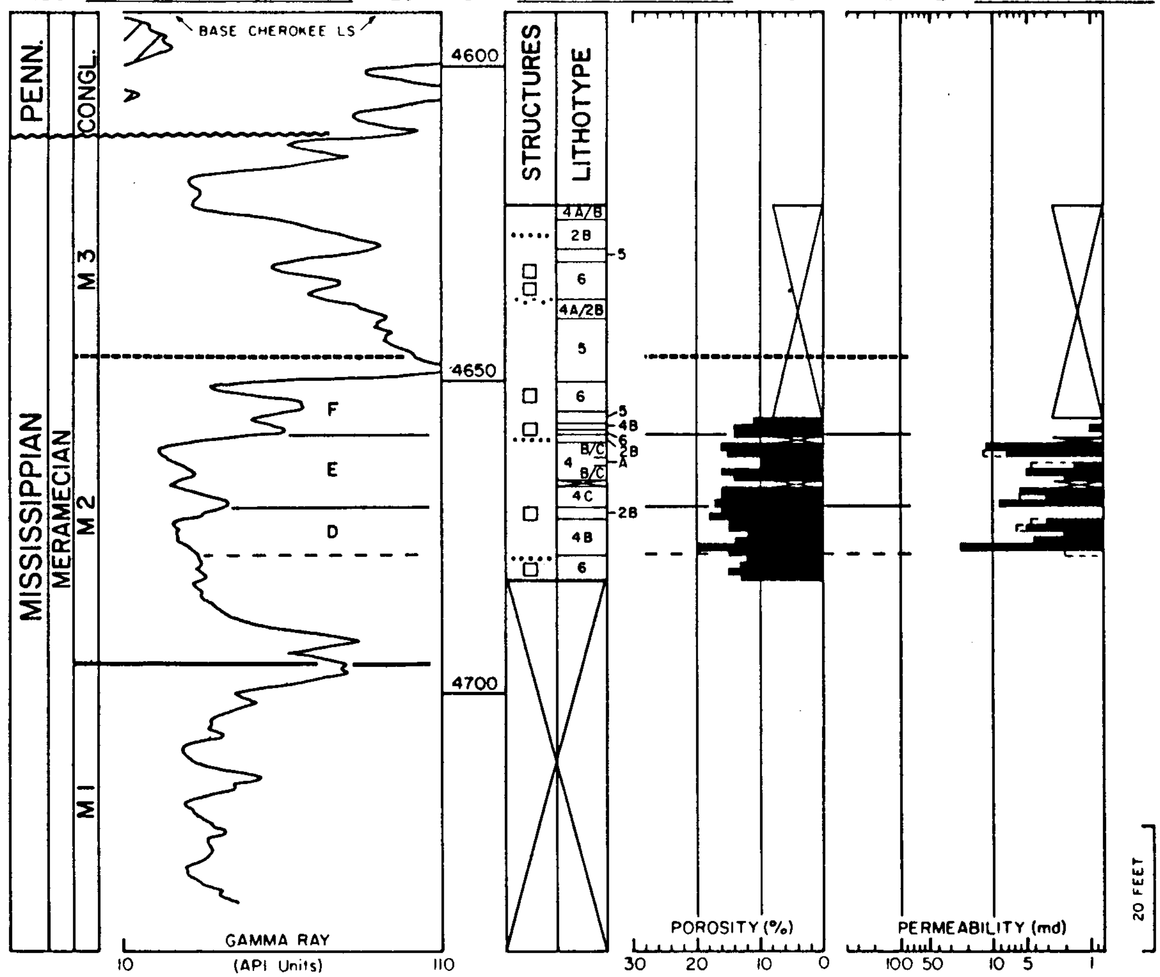

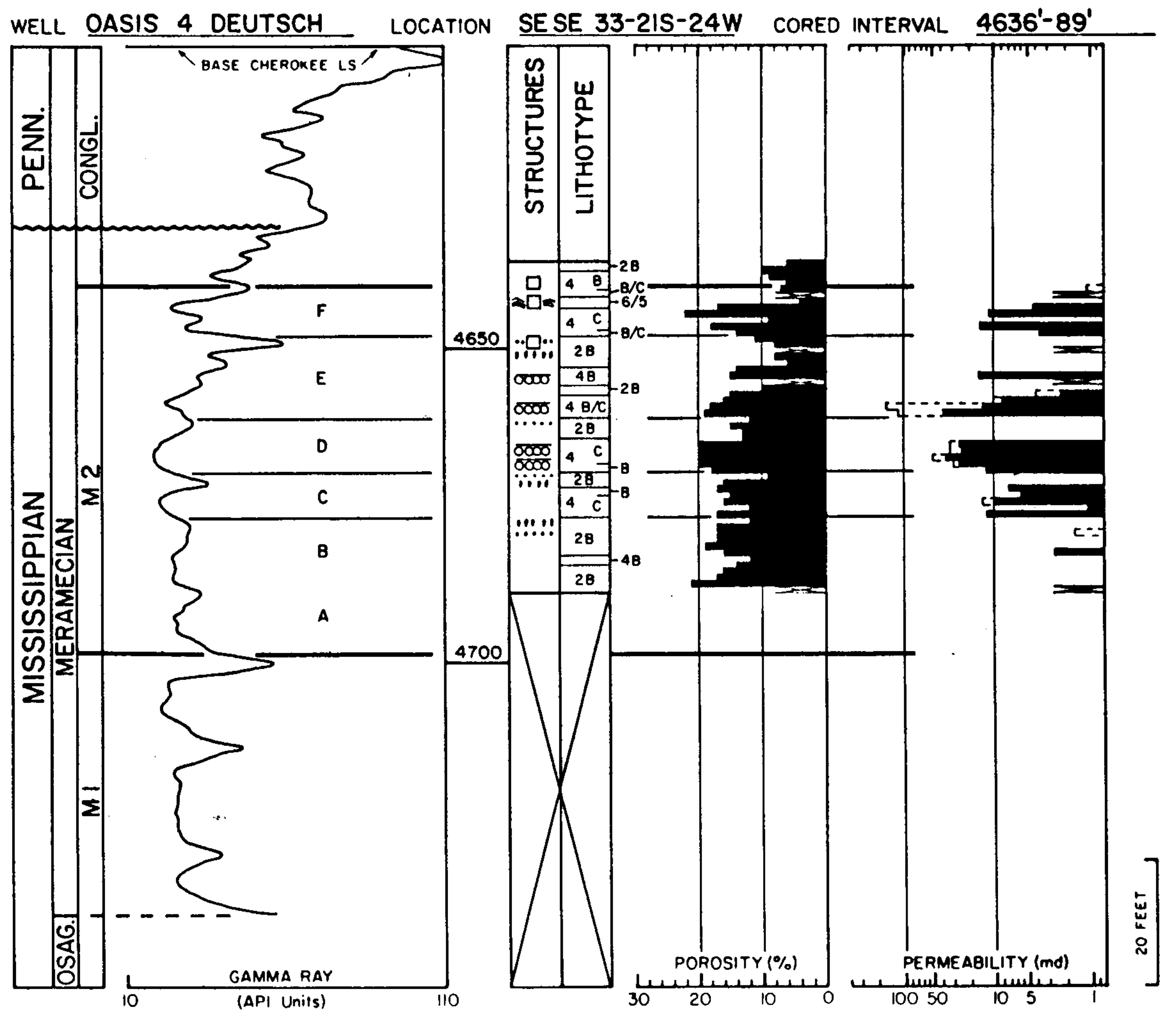
WELL OASIS 4 DEUTSCH
LOCATION SESE 33-21S-24W
CORED INTERVAL 4636'-89'
BASE CHEROKEE LS
PENN.
CONGL.
MISSISSIPPIAN
MERAMECIAN
M 2
M 1
OSAG.
F
E
D
C
B
A
4650
4700
GAMMA RAY
(API Units)
10
110
STRUCTURES
LITHOTYPE
2B
B/C
6/5
4B
B
POROSITY (%)
30
20
10
0
PERMEABILITY (md)
100
50
5
1
20 FEET

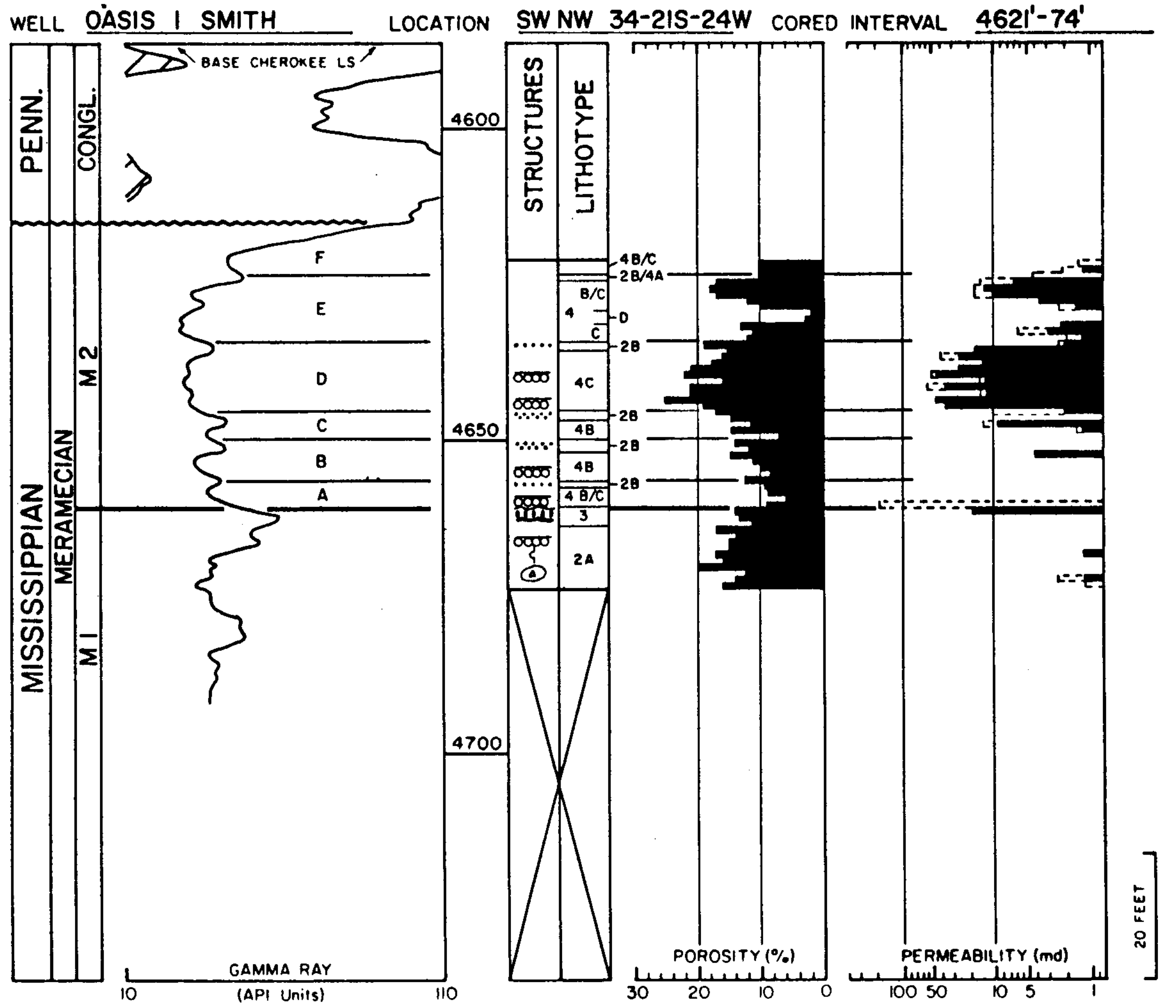
WELL OASIS I SMITH
LOCATION SW NW 34-21S-24W
CORED INTERVAL 4621'-74'
BASE CHEROKEE LS
PENN.
CONGL.
MISSISSIPPIAN
MERAMECIAN
M 2
M 1
F
E
D
C
B
A
4600
4650
4700
STRUCTURES
LITHOTYPE
4B/C
2B/4A
B/C
4
D
C
2B
4C
2B
4B
2B
4B
2B
4 B/C
3
2A
GAMMA RAY
(API Units)
10
110
POROSITY (%)
30
20
10
0
PERMEABILITY (md)
100
50
10
5
1
20 FEET

WELL OASIS 3 DEUTSCH LOCATION NW SW 34-21S-24W CORED INTERVAL 4625'-84'

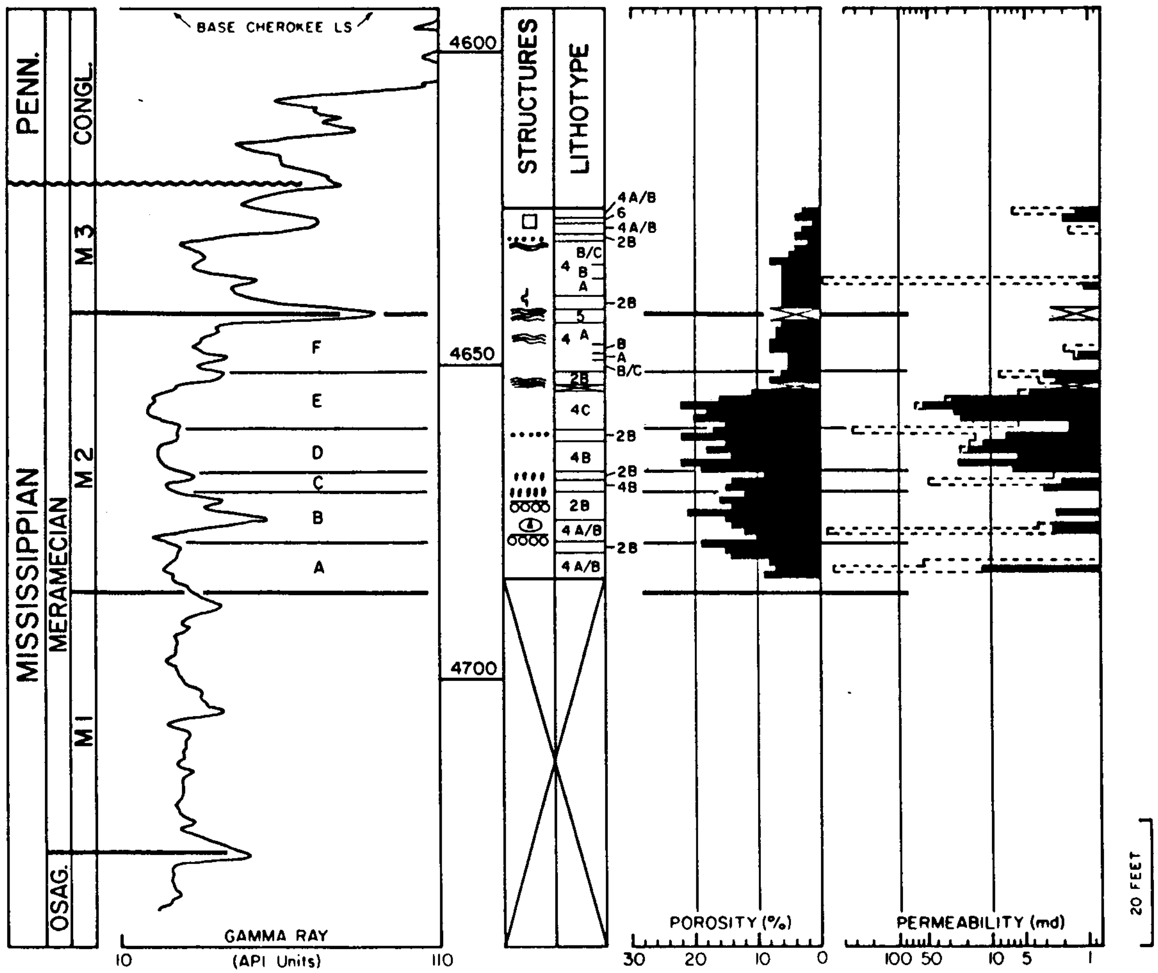

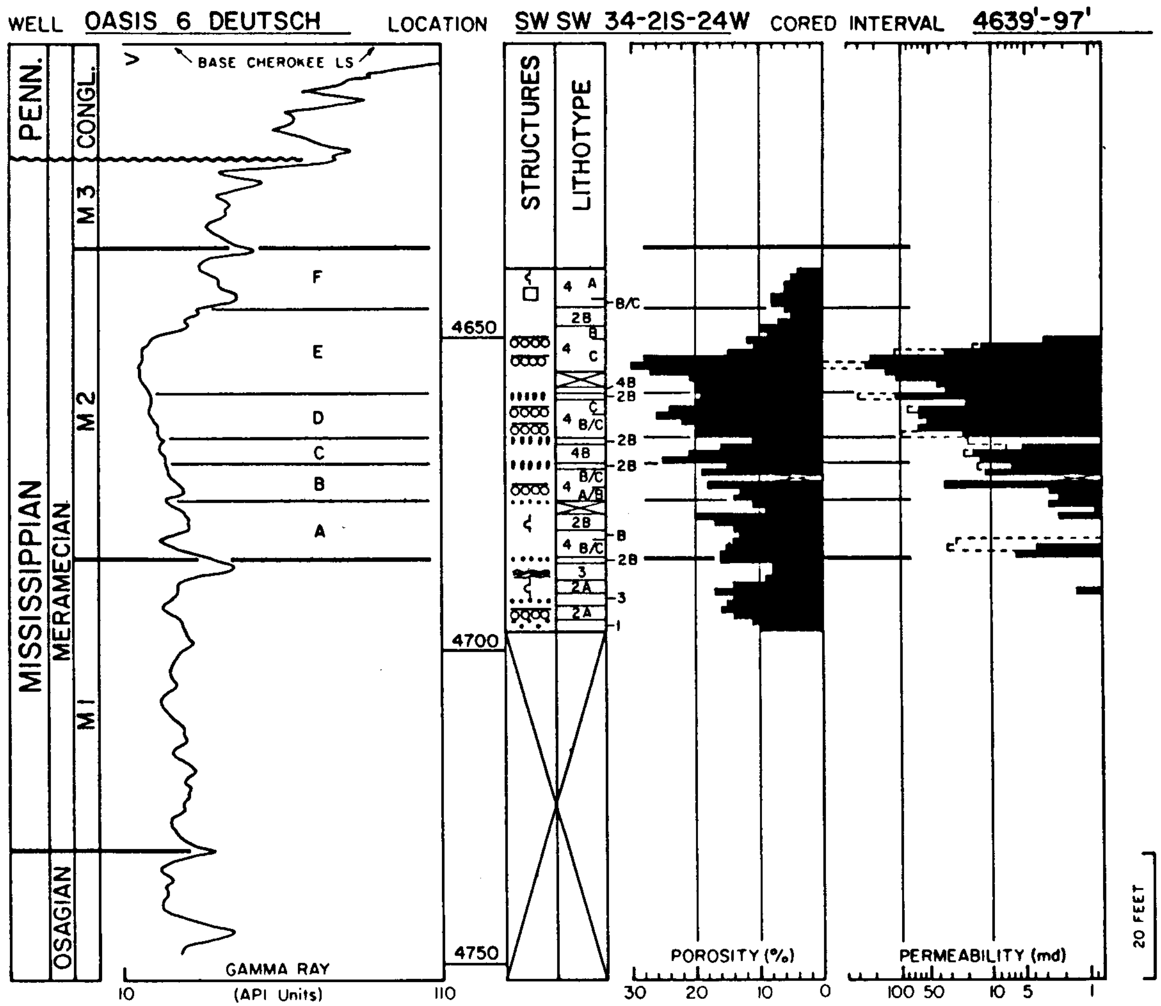
WELL OASIS 6 DEUTSCH
LOCATION SW SW 34-21S-24W
CORED INTERVAL 4639'-97'
PENN.
CONGL.
BASE CHEROKEE LS
MISSISSIPPIAN
MERAMECIAN
M 3
M 2
M 1
OSAGIAN
F
E
D
C
B
A
4650
4700
4750
GAMMA RAY
(API Units)
10
110
STRUCTURES
LITHOTYPE
POROSITY (%)
30
20
10
0
PERMEABILITY (md)
100 50
10 5
1
20 FEET

WELL OASIS 7 DEUTSCH LOCATION SE SW 34-21S-24W CORED INTERVAL 4637'-96'

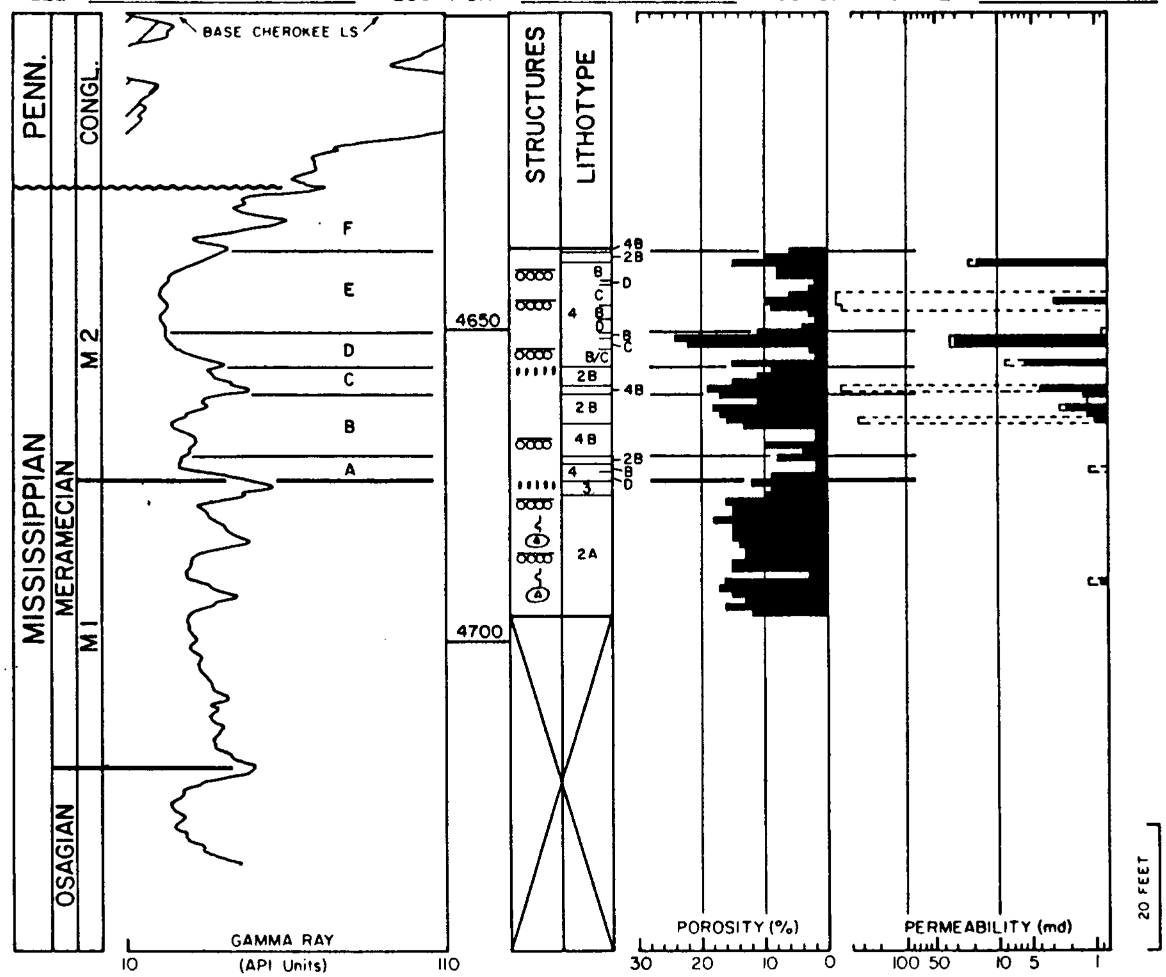

WELL OASIS I EVERTON LOCATION SW SE 34-21S-24W CORED INTERVAL 4663'-4709'

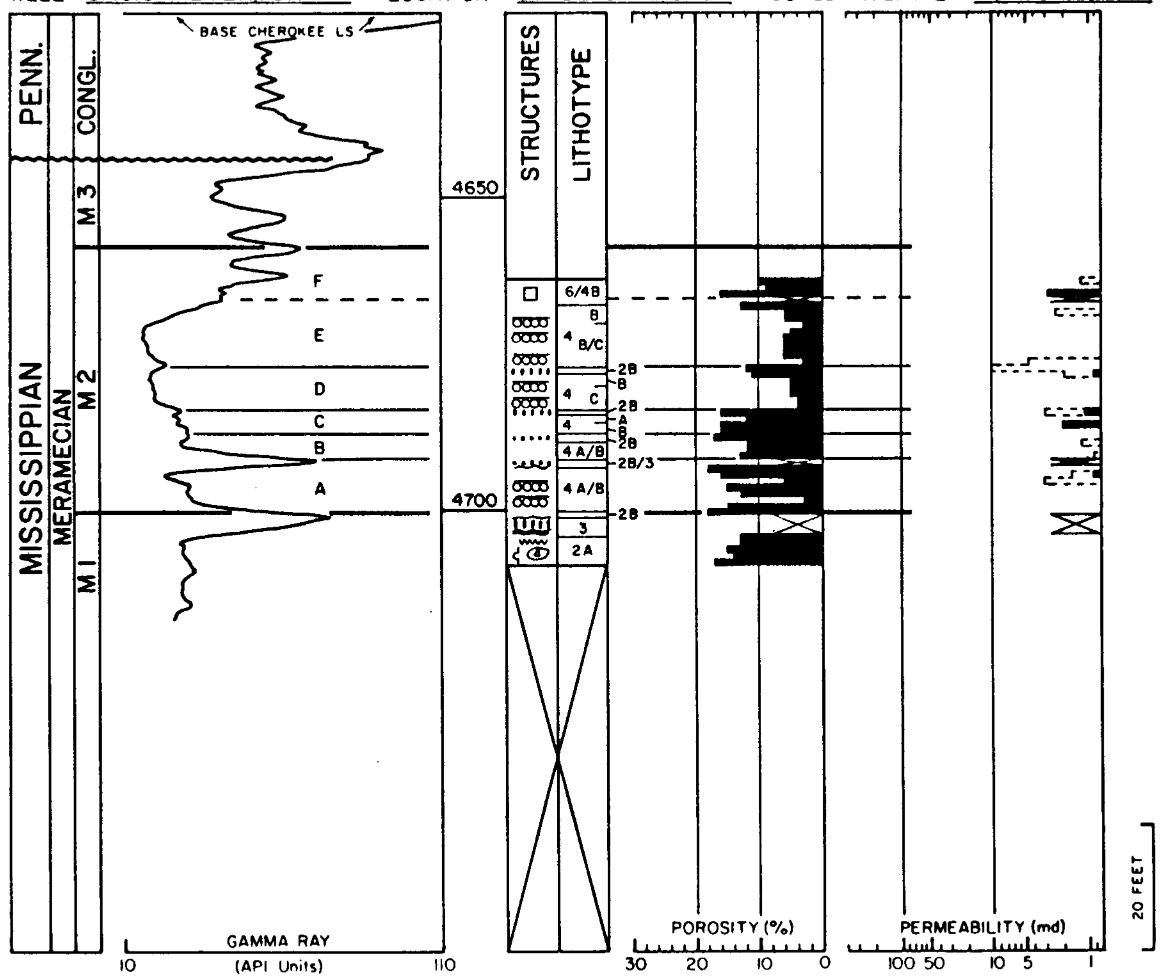

WELL OASIS 2 EVERTON LOCATION SE SE 34-21S-24W CORED INTERVAL 4642'-4701'

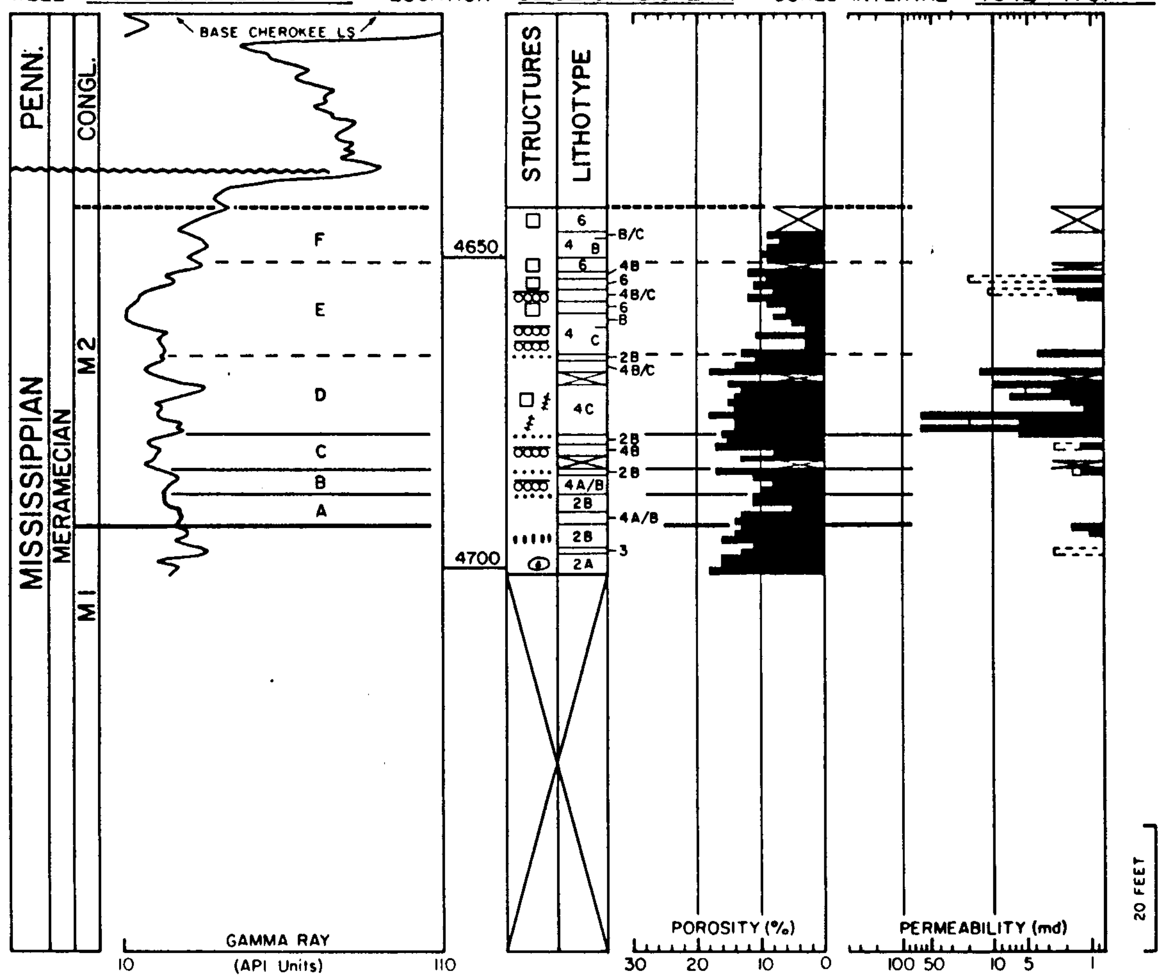

WELL OASIS 2 WALTER LOCATION NE NW 3-22S-24W CORED INTERVAL 4651'-85'

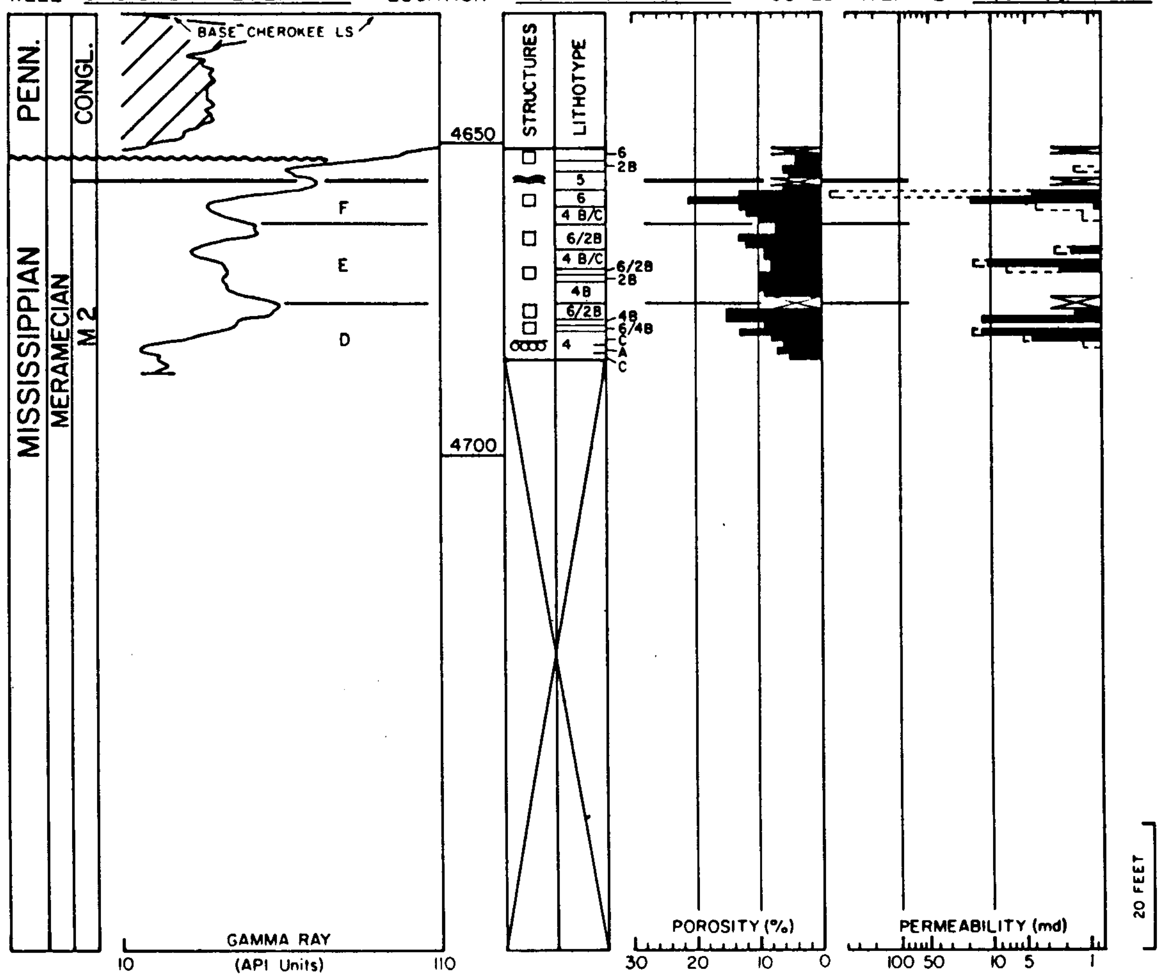

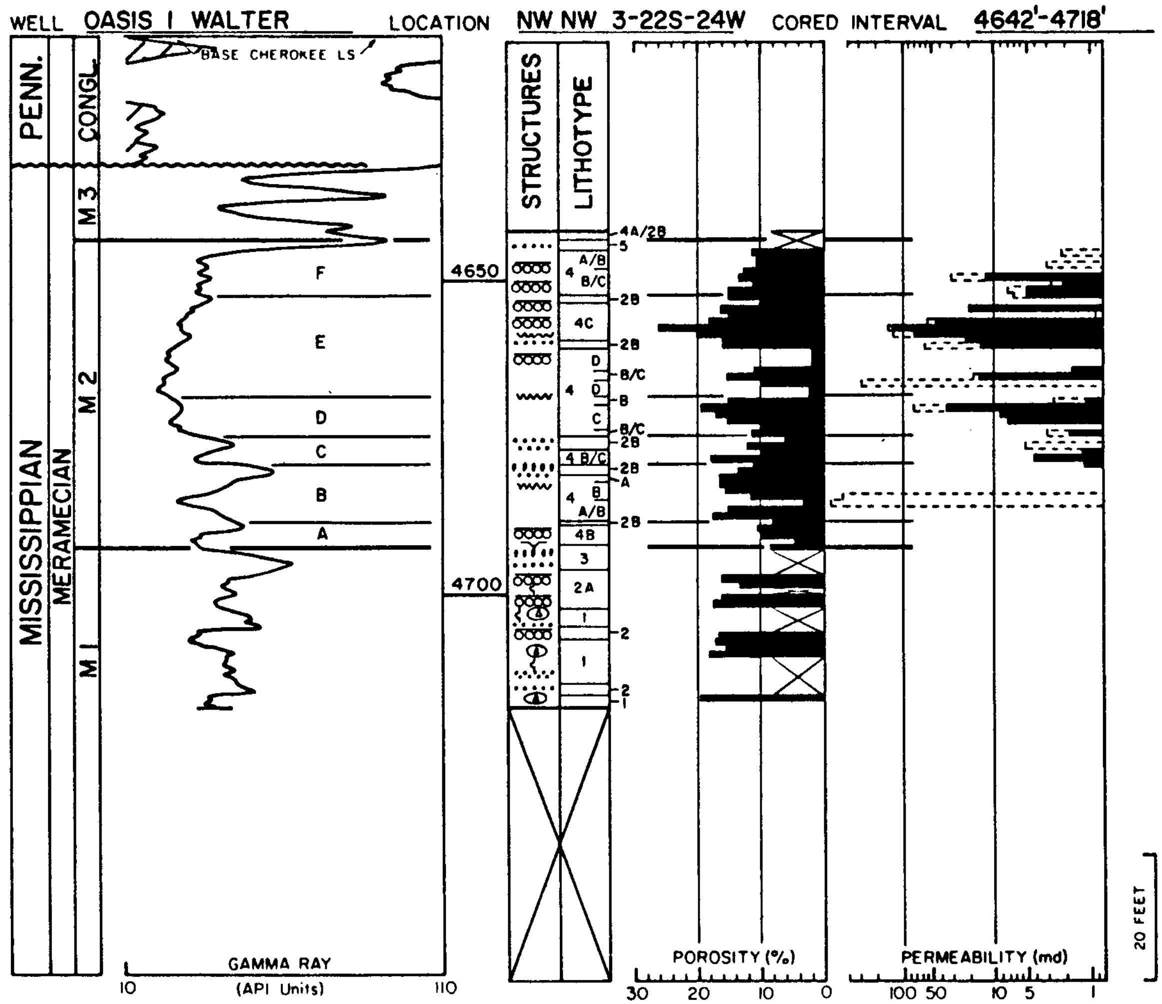
WELL OASIS I WALTER
LOCATION NW NW 3-22S-24W
CORED INTERVAL 4642'-4718'
PENN.
CONGL.
BASE CHEROKEE LS
MISSISSIPPIAN
MERAMECIAN
M 3
M 2
M I
F
E
D
C
B
A
4650
4700
GAMMA RAY
(API Units)
10
110
STRUCTURES
LITHOTYPE
4A/2B
5
A/B
B/C
2B
4C
D
B/C
B
C
4B/C
A
A/B
4B
3
2A
1
2
POROSITY (%)
30 20 10 0
PERMEABILITY (md)
100 50 10 5 1
20 FEET

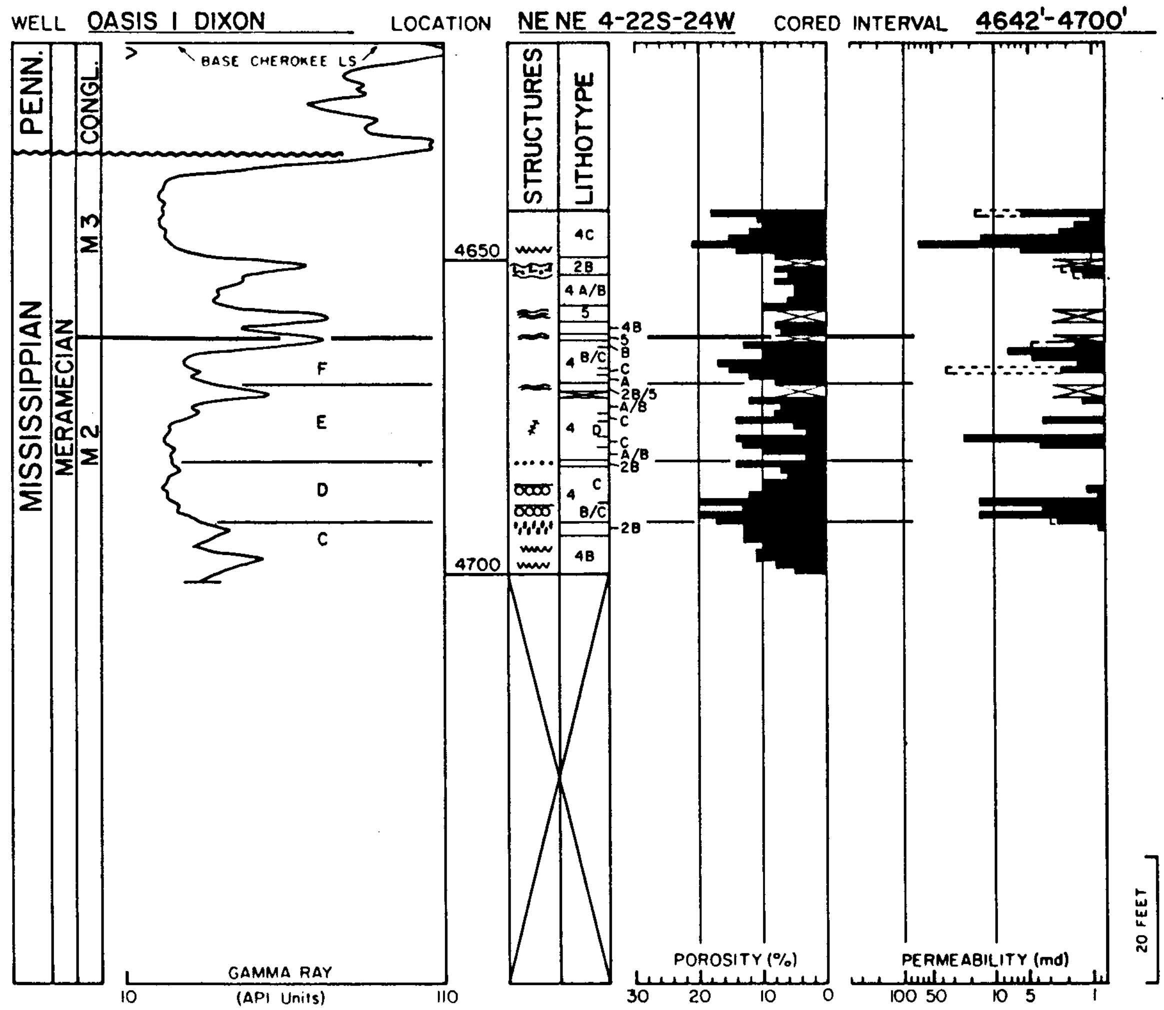
WELL OASIS I DIXON
LOCATION NE NE 4-22S-24W
CORED INTERVAL 4642'-4700'
PENN.
CONGL.
MISSISSIPPIAN
MERAMECIAN
M 3
M 2
BASE CHEROKEE LS
F
E
D
C
4650
4700
STRUCTURES
LITHOTYPE
4C
2B
4 A/B
5
4B
4 B/C
4 D
4 C
B/C
2B/5
A/B
GAMMA RAY
(API Units)
10
110
POROSITY (%)
30 20 10 0
PERMEABILITY (md)
100 50 10 5 1
20 FEET

APPENDIX C

CAPILLARY PRESSURE DATA

Twelve cylindrical plugs were taken from Bindley Field cores for mercury intrusion/extrusion analysis. Samples were selected to represent Lithotypes 2B, 4B, and 4C, and to represent Meramec 2D and 2E reservoir zones in a transect perpendicular to the long axis of the field. Eight samples underwent intrusion (drainage) analysis only (Samples 1,3,5,6,7,8,11,12). The remaining four samples (Samples 2,4,9,10) underwent intrusion (drainage) and extrusion (imbibition) analysis. The origin and lithotype of each sample are given on the following page.

Sample plugs ranged in size from 1-1.25 inches in diameter and were trimmed to form right cylinders of approximately 2 inches in length. Samples were cleaned by cycle flushing with chloroform-methanol azeotrope and toluene. One sample (Sample #8) retained some hydrocarbon after cleaning. All samples were oven-dried at 240 degrees Fahrenheit.

Porosity was determined by Boyle's Law. Permeability to helium was measured, mathematically corrected to air as the fluid medium, and reported as permeability to air.

CAPILLARY PRESSURE SAMPLE IDENTIFICATION

Well/Sample #	Depth	Interval	Lithotype	Comments
#3 Bindley				
NE NE, 33-21S-24W				
1	4608.7'	M2-D	2B	Mudstone
#1 Deutsch				
NE SE, 33-21S-24W				
2	4627.7'	M2-E	4C	
3	4630.9'	M2-E	4C	Skel. calcite
4	4635.4'	M2-D	4C	
#5 Deutsch				
SW SE, 33-21S-24W				
5	4664.1'	M2-E	4C	
6	4673.0'	M2-D	4C	Packstone
#1 Smith				
SW NW, 34-21S-24W				
7	4659.1'	M2-A	4C	Calcite cement
#3 Deutsch				
NW SW, 34-21S-24W				
8	4647.5'	M2-F	4B	Wackestone
9	4657.1'	M2-E	4C	
10	4665.9'	M2-D	4C	
#6 Deutsch				
SW SW, 34-21S-24W				
11	4655.5'	M2-E	4C	Max. k
12	4663.1'	M2-D	4C	

Following air evacuation, mercury was intruded and extruded in 23 pressure increments ranging from 0 psia to 2,000 psia. Results for each sample are reported in the following pages in tabular and three graphic forms; 1) injection pressure vs. mercury saturation, 2) pore aperture radius vs. mercury saturation, and 3) pore print (pore aperture histogram).

For samples which underwent mercury intrusion and extrusion, the recovery efficiency was calculated and is stated in the tabular data which follows.

Western Atlas International

CORE LABORATORIES

October 17, 1990

Attention: Reed A. Johnson

Subject: Special Core Analysis Study
Oasis Wells
Bindley Field
Hodgeman County, Kansas
File: 57183-90110

Gentlemen:

In a letter dated August 31, 1990 Reed A. Johnson requested the Special Core Analysis Laboratory of Core Laboratories to perform Mercury Injection Capillary Pressure tests on core material from several wells in the Bindley field. These analyses represent thesis research at the University of Colorado. The final results are reported herein.

Twelve plug samples were submitted to the Core Laboratories facility in Tulsa for analyses. Upon arrival, the samples were trimmed to create right cylinders suitable for testing. The samples were cleaned by cycle flushing a chloroform-methanol azeotrope and toluene through each sample. Drying was accomplished in an oven at 240 degrees Fahrenheit. One sample (No. 8) was not of sufficient permeability to solvent clean using conventional techniques. More expensive cleaning protocol was not authorized due to budgetary limitations. Sample No. 8 was dried at 240°F after limited solvent cleaning. Therefore, non volatile contaminants may still exist in the sample. Permeability to air and Boyle's Law porosity were then determined. Permeability and porosity values are presented in tabular form on Page 1 and graphically on Page 2.

Following permeability and porosity determinations, each sample was placed in a mercury injection cell and evacuated. The core sample was injected with mercury at pressures ranging from 0 psia to 2000 psia (drainage cycle). Four samples were selected to continue with injection (imbibition cycle) from 2000 psia to 0 psia. The volumes of mercury injected were recorded as a function of pressure. Mercury injection and pore size

Attn: Reed A. Johnson
File: 57183-90110
Page Two

distribution data are presented in tabular form and in graphic form, with Pore Print included, on Pages 3 through 46.

Pore aperture radius is calculated using the following equation:

$$Ri = \frac{2 \times \sigma \times \cos\theta}{Pc}$$

where, Ri = average pore entry radius, microns
Pc = capillary pressure, psi
σ = interfacial tension = 480 dynes/cm
θ = contact angle = 140 degrees

Rearranging the terms in the above equation and multiplying by a series of unit conversion factors results in an expression for pore entry radius:

$$Ri,\ \text{microns} = \frac{106.43}{Pc}$$

Data for the 2000-0 psia (imbibition) cycle of Sample No. 4 should be used with caution. Comparing gravimetric versus volumetric saturations at the conclusion of the test yield anomalous results. There were no observations as to the cause of this variation.

It has been a pleasure working with the University of Colorado in performing this study. If there are any questions concerning the test procedures or the results reported, please contact me at (918) 664-9071.

Sincerely,

Core Laboratories, a Division of
WESTERN ATLAS INTERNATIONAL

Mercer L. Brugler
Manager
Special Services

MLB:MR:reh

Western Atlas International

CORE LABORATORIES

File 57183-90110

PERMEABILITY TO AIR, POROSITY, AND GRAIN DENSITY

Company: University of Colorado at Boulder
Formation: Dolomite
County, State: Hodgeman, Kansas

Well: As Specified
Field: Bindley

Sample Identification	Depth, feet	Permeability to Air, millidarcys	Porosity, percent	Grain Density, g/cc
Oasis No. 3 Bindley Well				
1	4608.7	0.014	11.0	2.81
Oasis No. 1 Deutsch Well				
2	4627.7	234	25.3	2.84
3	4630.9	4.7	10.9	2.72
4	4635.4	40	18.8	2.83
Oasis No. 5 Deutsch Well				
5	4664.1	1.5	17.0	2.86
6	4673.0	3.2	17.4	2.85
Oasis No. 1 Smith Well				
7	4659.1	0.15	9.4	2.82
Oasis No. 3 Deutsch Well				
8*	4647.5	0.011	8.0	2.87
9	4657.1	123	23.4	2.86
10	4665.9	32	25.3	2.81
Oasis No. 6 Deutsch Well				
11	4655.5	461	26.2	2.83
12	4663.1	142	21.1	2.78

*Sample may possibly still retain some residual contamination.

Permeability vs Porosity

UNIVERSITY OF COLORADO AT BOULDER
SEVERAL WELLS
BINDLEY FIELD
HODGEMAN COUNTY, KANSAS

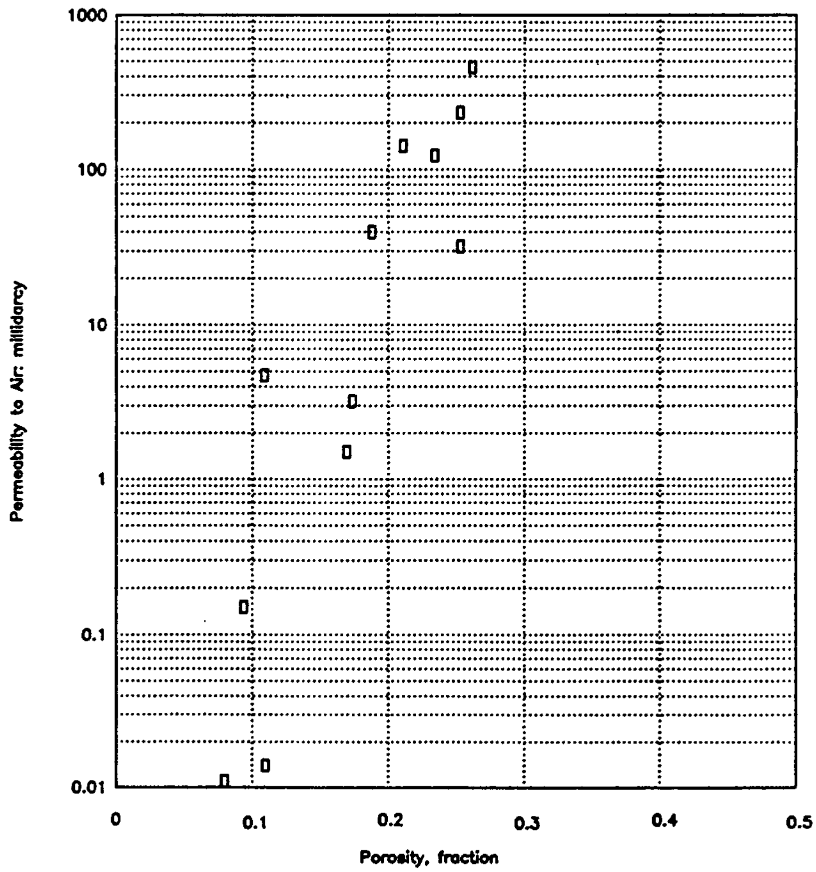

Core Laboratories

CORE LABORATORIES

File 57183-90110

SUMMARY OF MERCURY INJECTION TEST RESULTS

Company: University of Colorado at Boulder
Formation: Dolomite
County, State: Hodgeman, Kansas
Well: Oasis No. 3 Bindley
Field: Bindley

Sample Identification: 1
Depth, feet: 4608.7
Permeability to Air, md: 0.014
Porosity, percent: 11.0

Injection Pressure, psia	Pore Aperture Radius, microns	Mercury Saturation, percent pore space
3	35.5	0.0
6	17.7	0.0
9	11.8	0.0
12	8.87	0.0
15	7.09	0.0
18	5.91	0.0
21	5.07	0.0
24	4.44	0.0
27	3.94	0.0
30	3.55	0.0
40	2.66	0.0
60	1.77	0.0
80	1.33	0.0
100	1.06	0.0
200	.532	0.0
300	.355	0.0
500	.213	0.0
750	.142	0.0
1000	.106	6.1
1250	.085	15.7
1500	.071	27.6
1750	.061	43.9
2000	.053	57.9

Page 4 of 46
File 57183-90110

Injection Pressure vs Mercury Saturation

UNIVERSITY OF COLORADO AT BOULDER	SAMPLE ID:		1
OASIS NO. 3 BINDLEY WELL	SAMPLE DEPTH, feet:		4608.7
BINDLEY FIELD	PERMEABILITY TO AIR, md:		0.014
HODGEMAN COUNTY, KANSAS	POROSITY, percent:		11.0

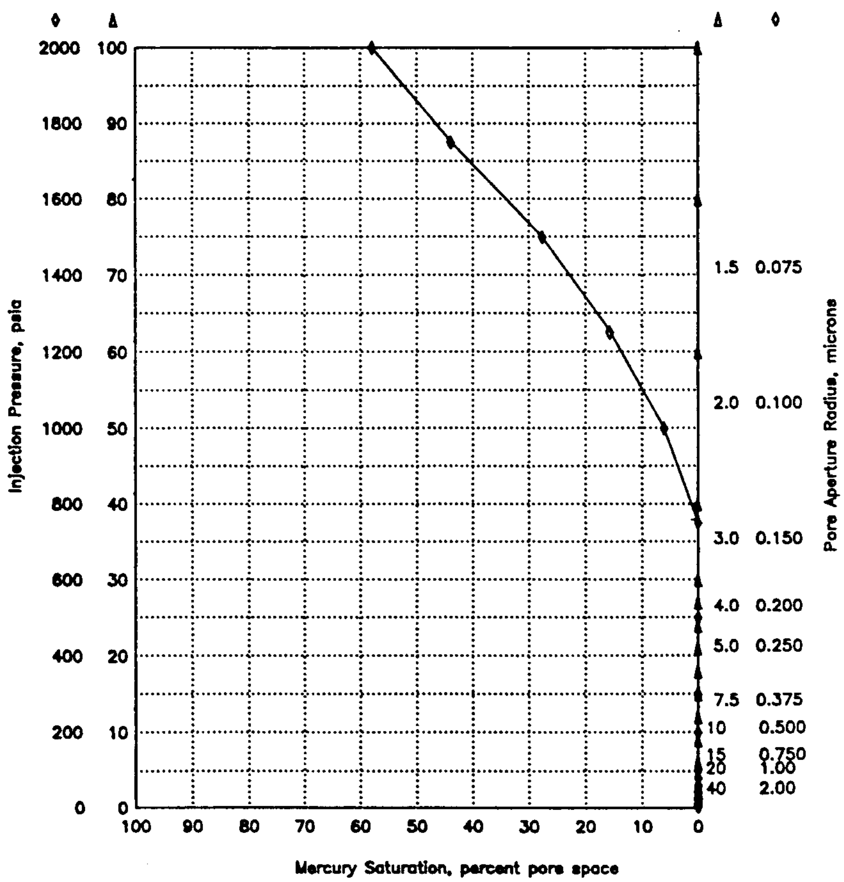

Core Laboratories

Pore Aperture Radius vs Mercury Saturation

UNIVERSITY OF COLORADO AT BOULDER
OASIS NO. 3 BINDLEY WELL
BINDLEY FIELD
HODGEMAN COUNTY, KANSAS

SAMPLE ID: 1
SAMPLE DEPTH, feet: 4608.7
PERMEABILITY TO AIR, md: 0.014
POROSITY, percent: 11.0

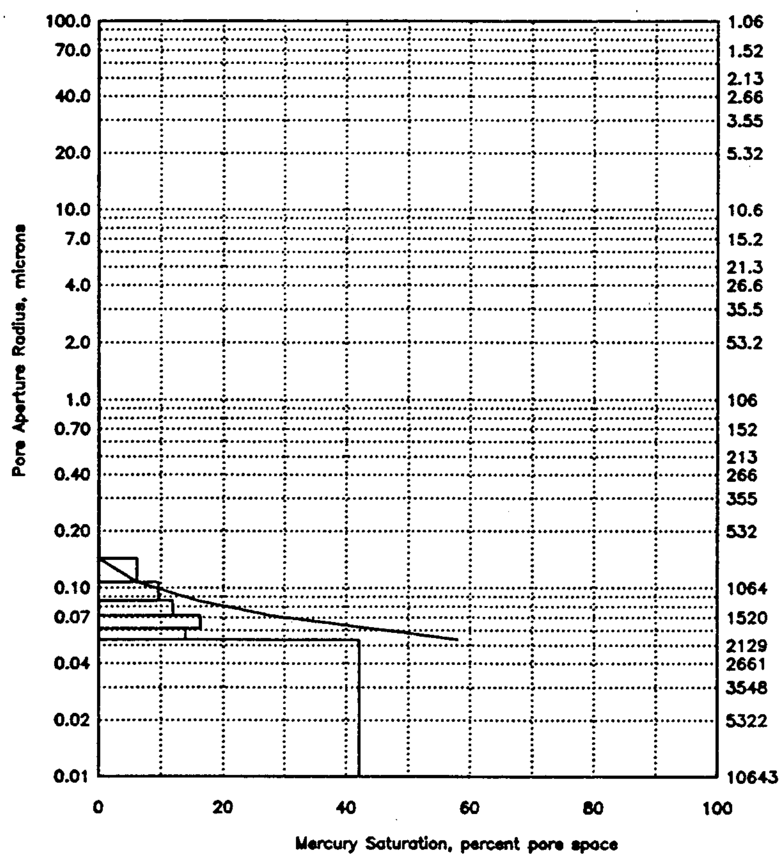

Core Laboratories

PORE PRINT

Pore Space Controlled by Pore Apertures

UNIVERSITY OF COLORADO AT BOULDER	SAMPLE ID: 1
OASIS NO. 3 BINDLEY WELL	DEPTH, feet: 4608.7
BINDLEY FIELD	AIR PERMEABILITY, md: 0.014
HODGEMAN COUNTY, KANSAS	POROSITY, percent: 11.0

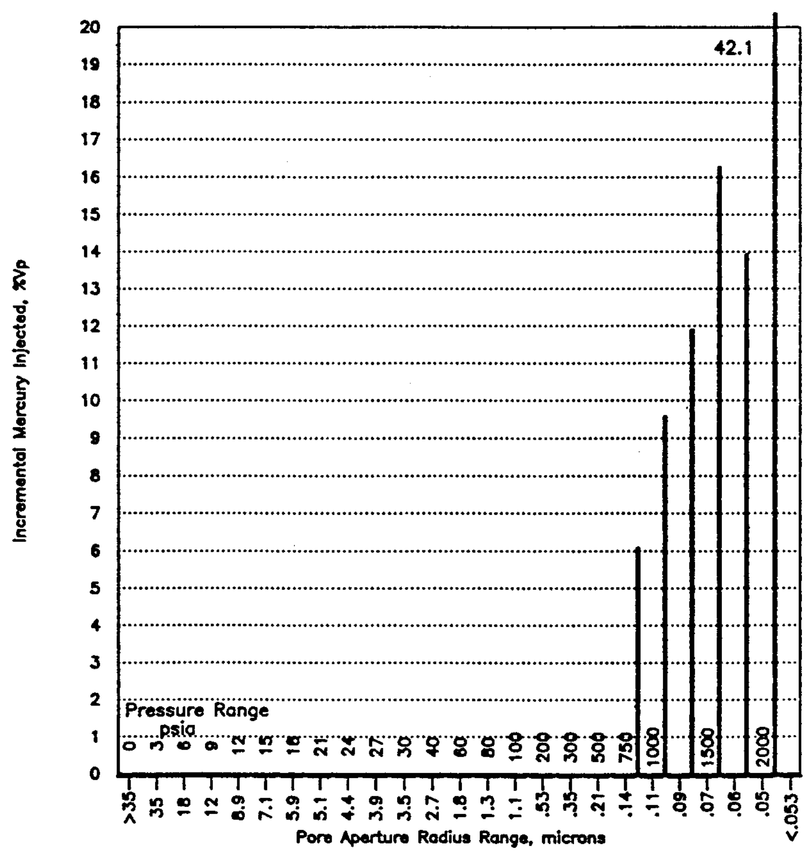

Core Laboratories

Western Atlas International

CORE LABORATORIES

Page 7 of 46

File 57183-90110

SUMMARY OF MERCURY INJECTION TEST RESULTS

Company: University of Colorado at Boulder
Formation: Dolomite
County, State: Hodgeman, Kansas

Well: Oasis No. 1 Deutsch
Field: Bindley

Sample Identification:	2	3	4
Depth, feet:	4627.7	4630.9	4635.4
Permeability to Air, md:	234	4.7	40
Porosity, percent:	25.3	10.9	18.8

Injection Pressure, psia	Pore Aperture Radius, microns	Mercury Saturation, percent pore space		
3	35.5	0.0	0.0	0.0
6	17.7	3.1	0.0	0.0
9	11.8	12.4	0.0	0.0
12	8.87	32.5	0.0	4.5
15	7.09	50.7	0.0	14.6
18	5.91	59.9	0.0	23.6
21	5.07	65.8	0.0	32.9
24	4.44	70.2	0.0	39.1
27	3.94	73.6	0.0	44.7
30	3.55	76.1	3.3	48.6
40	2.66	82.1	22.8	57.9
60	1.77	85.3	36.9	65.2
80	1.33	85.7	43.5	68.6
100	1.06	86.4	48.3	70.0
200	.532	87.2	64.0	75.0
300	.355	88.0	70.9	78.1
500	.213	90.2	76.6	82.1
750	.142	91.5	79.0	84.3
1000	.106	91.8	79.9	85.4
1250	.085	92.4	80.5	86.6
1500	.071	92.6	82.0	87.1
1750	.061	92.7	82.9	87.4
2000	.053	92.9	83.5	87.4

Western Atlas International

CORE LABORATORIES

File 57183-90110

SUMMARY OF MERCURY INJECTION TEST RESULTS

Company: University of Colorado at Boulder
Formation: Dolomite
County, State: Hodgeman, Kansas

Well: Oasis No. 1 Deutsch
Field: Bindley

Sample Identification:	2	3	4
Depth, feet:	4627.7	4630.9	4635.4
Permeability to Air, md:	234	4.7	40
Porosity, percent:	25.3	10.9	18.8

Injection Pressure, psia	Pore Aperture Radius, microns	Mercury Saturation, percent pore space		
1500		92.9		87.1
1250		92.9		86.6
1000		92.9		86.0
750		92.9		85.7
500		92.9		85.2
300		92.9		84.6
200		92.7		83.8
100		91.6		76.4
80		91.5		73.6
60		91.5		67.7
40		91.1		57.9
30		90.9		47.2
15		88.8		41.9
0		54.0		41.3

Injection Pressure vs Mercury Saturation

UNIVERSITY OF COLORADO AT BOULDER
OASIS NO. 1 DEUTSCH WELL
BINDLEY FIELD
HODGEMAN COUNTY, KANSAS

SAMPLE ID: 2
SAMPLE DEPTH, feet: 4627.7
PERMEABILITY TO AIR, md: 234
POROSITY, percent: 25.3

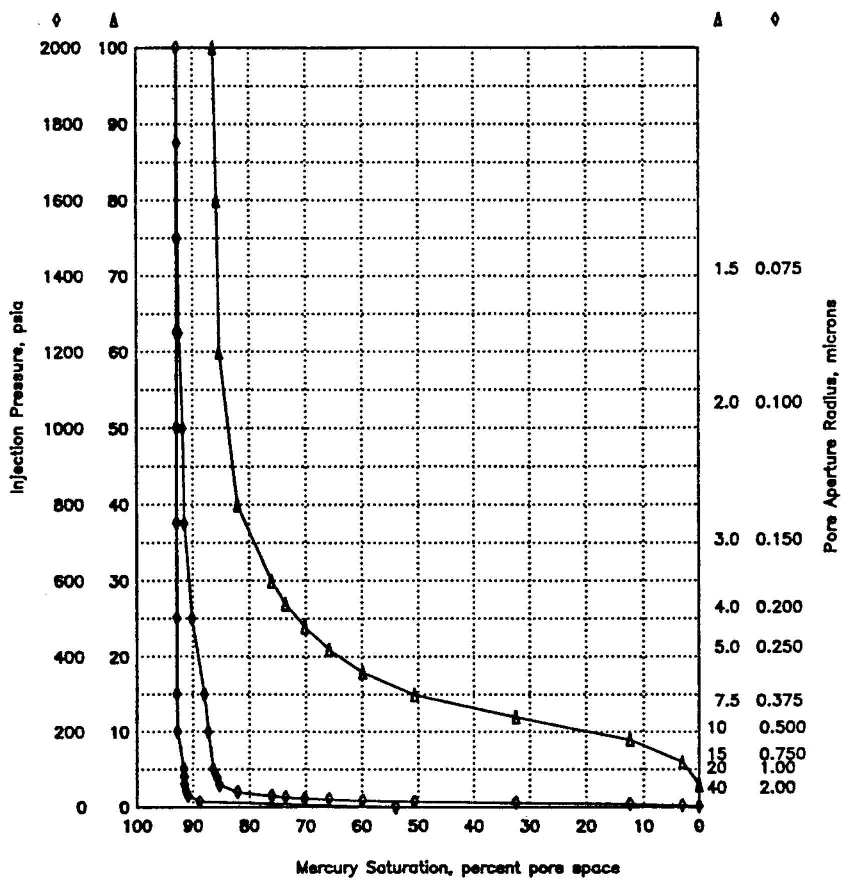

Pore Aperture Radius vs Mercury Saturation

UNIVERSITY OF COLORADO AT BOULDER
OASIS NO. 1 DEUTSCH WELL
BINDLEY FIELD
HODGEMAN COUNTY, KANSAS

SAMPLE ID: 2
SAMPLE DEPTH, feet: 4627.7
PERMEABILITY TO AIR, md: 234
POROSITY, percent: 25.3

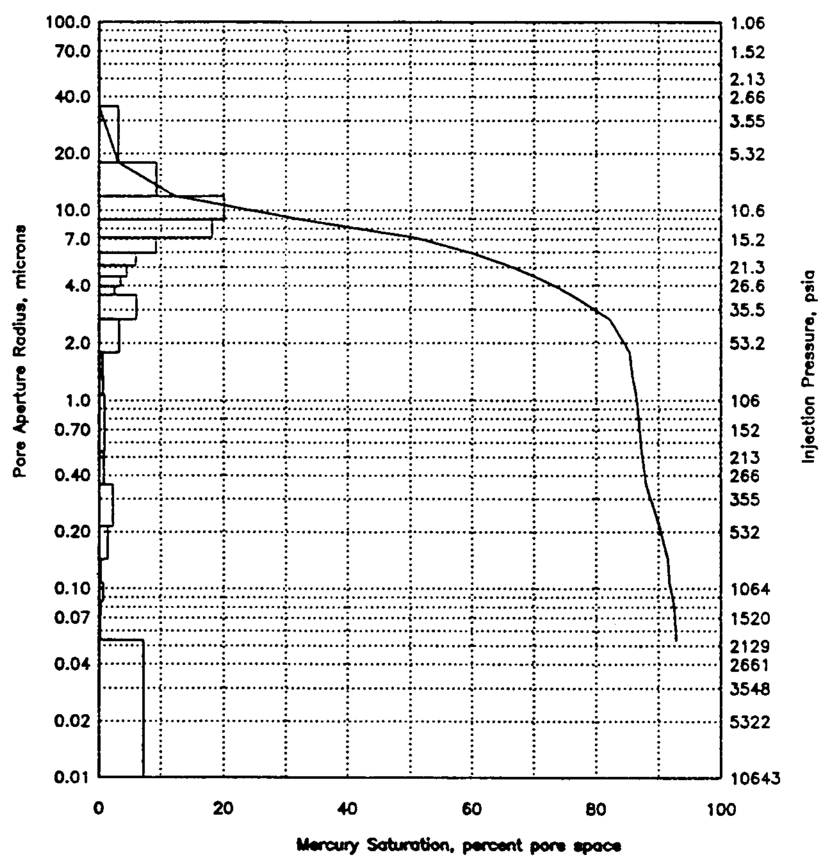

Core Laboratories

PORE PRINT

Pore Space Controlled by Pore Apertures

UNIVERSITY OF COLORADO AT BOULDER		SAMPLE ID:	2
OASIS NO. 1 DEUTSCH WELL		DEPTH, feet:	4627.7
BINDLEY FIELD		AIR PERMEABILITY, md:	234
HODGEMAN COUNTY, KANSAS		POROSITY, percent:	25.3

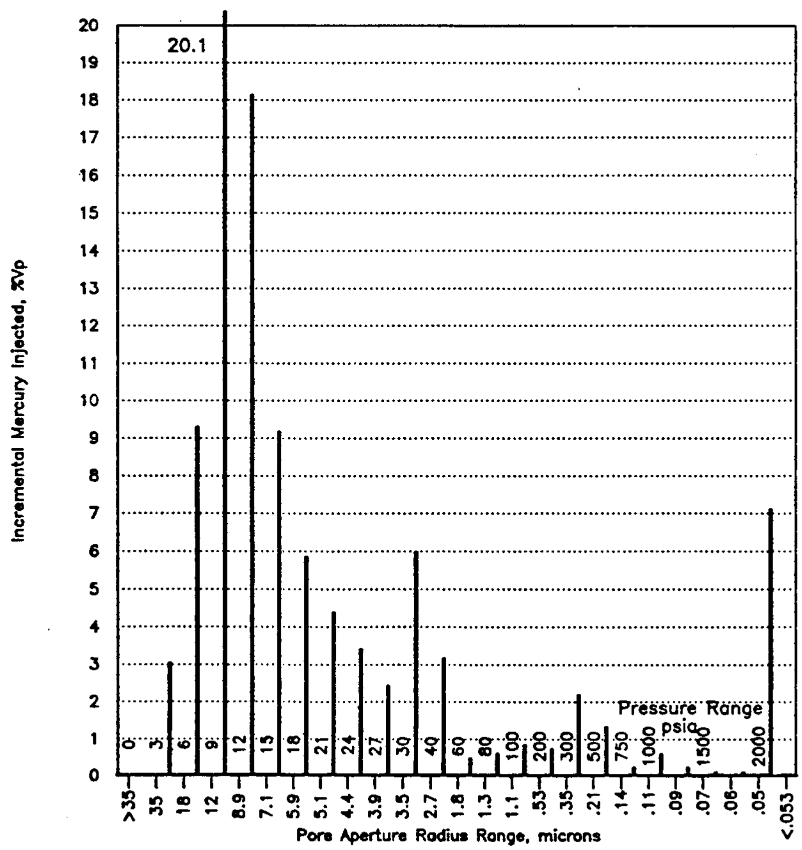

Core Laboratories

Injection Pressure vs Mercury Saturation

UNIVERSITY OF COLORADO AT BOULDER	SAMPLE ID:	3
OASIS NO. 1 DEUTSCH WELL	SAMPLE DEPTH, feet:	4630.9
BINDLEY FIELD	PERMEABILITY TO AIR, md:	4.7
HODGEMAN COUNTY, KANSAS	POROSITY, percent:	10.9

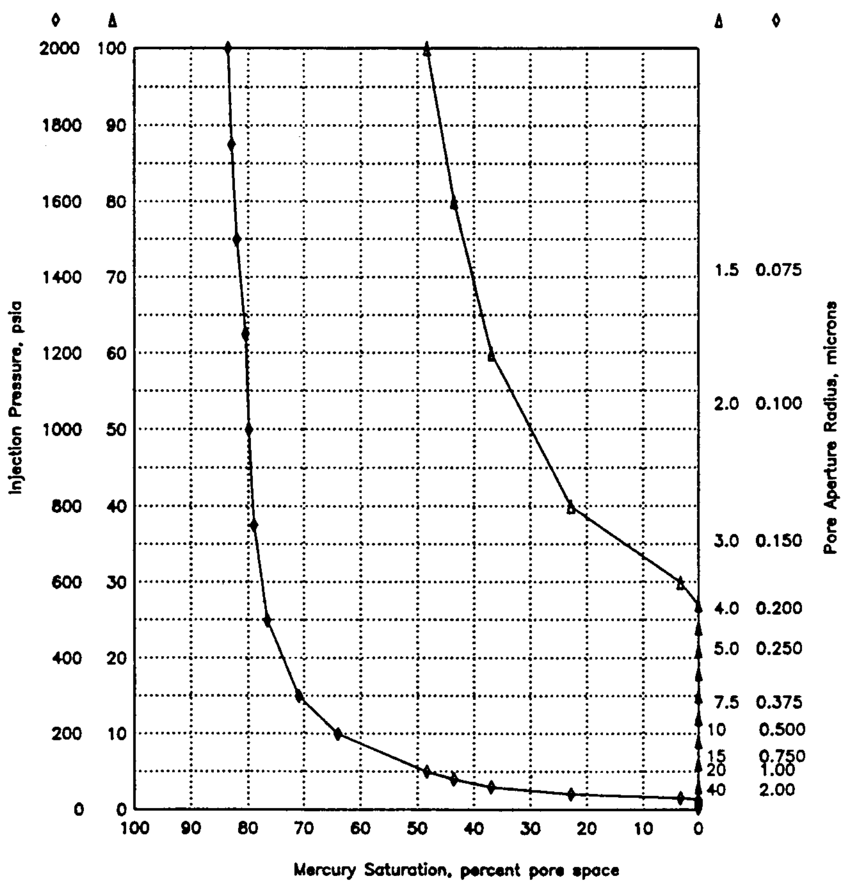

Core Laboratories

Page 13 of 46
File 57183-90110

Pore Aperture Radius vs Mercury Saturation

UNIVERSITY OF COLORADO AT BOULDER
OASIS NO. 1 DEUTSCH WELL
BINDLEY FIELD
HODGEMAN COUNTY, KANSAS

SAMPLE ID: 3
SAMPLE DEPTH, feet: 4630.9
PERMEABILITY TO AIR, md: 4.7
POROSITY, percent: 10.9

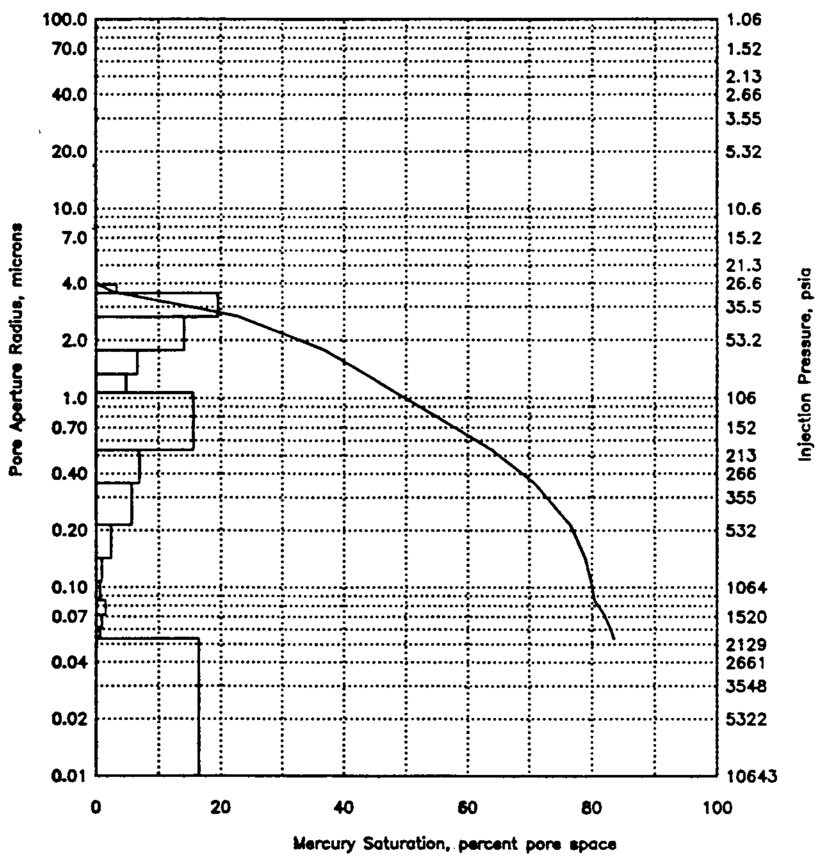

Core Laboratories

PORE PRINT

Pore Space Controlled by Pore Apertures

UNIVERSITY OF COLORADO AT BOULDER		SAMPLE ID:	3
OASIS NO. 1 DEUTSCH WELL		DEPTH, feet:	4630.9
BINDLEY FIELD		AIR PERMEABILITY, md:	4.7
HODGEMAN COUNTY, KANSAS		POROSITY, percent:	10.9

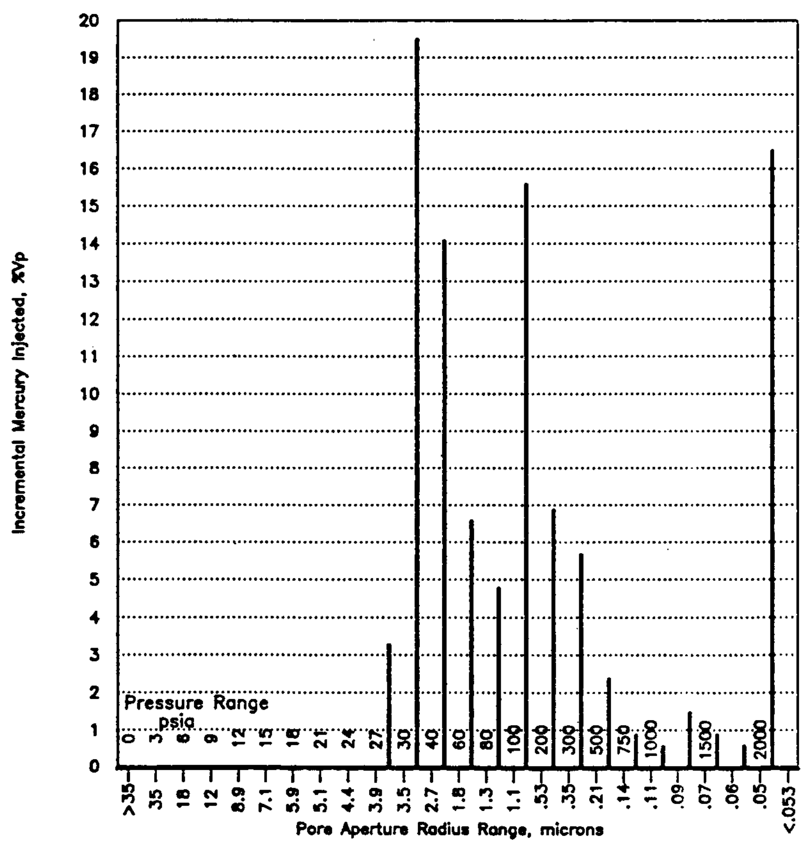

Core Laboratories

Injection Pressure vs Mercury Saturation

UNIVERSITY OF COLORADO AT BOULDER
OASIS NO. 1 DEUTSCH WELL
BINDLEY FIELD
HODGEMAN COUNTY, KANSAS

SAMPLE ID:	4
SAMPLE DEPTH, feet:	4635.4
PERMEABILITY TO AIR, md:	40
POROSITY, percent:	18.8

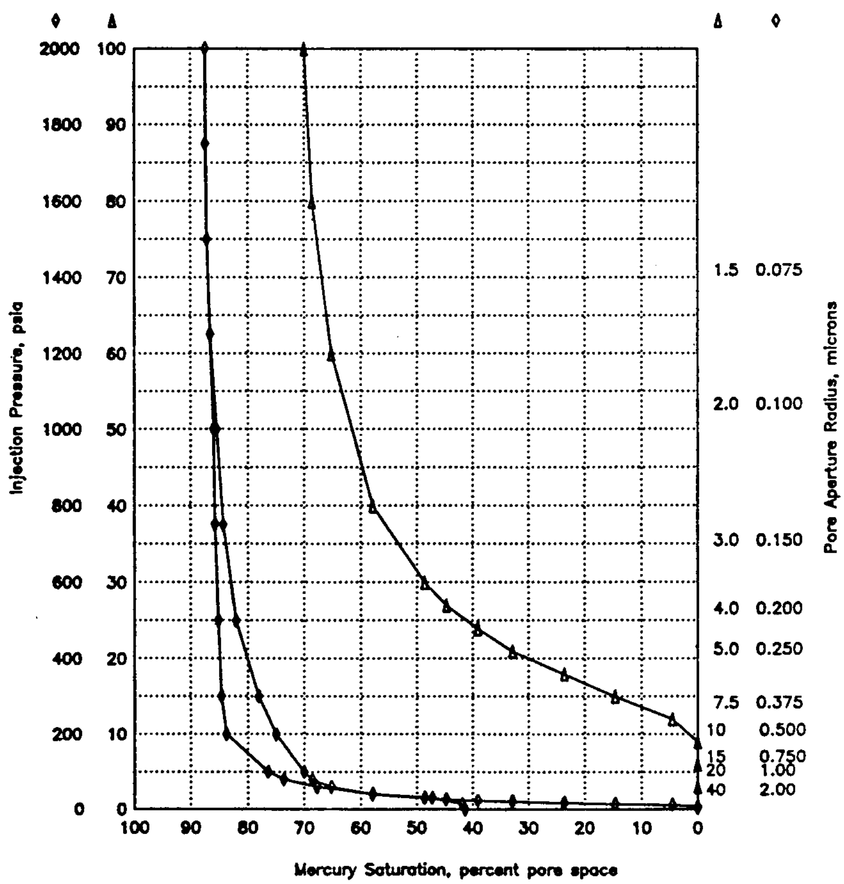

Pore Aperture Radius vs Mercury Saturation

UNIVERSITY OF COLORADO AT BOULDER	SAMPLE ID: 4
OASIS NO. 1 DEUTSCH WELL	SAMPLE DEPTH, feet: 4635.4
BINDLEY FIELD	PERMEABILITY TO AIR, md: 40
HODGEMAN COUNTY, KANSAS	POROSITY, percent: 18.8

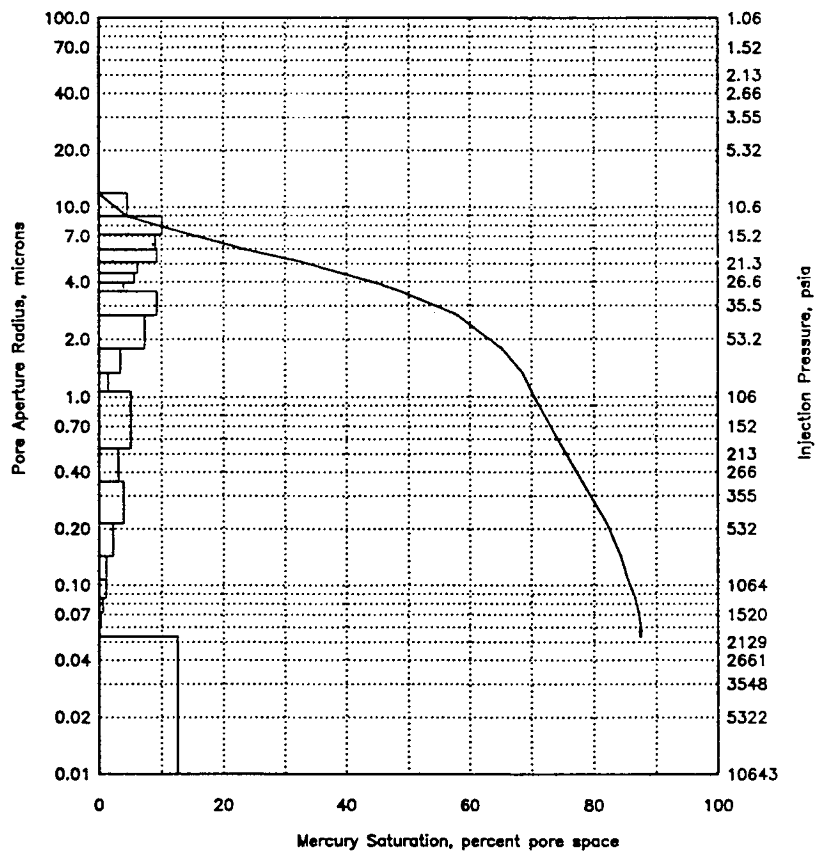

Core Laboratories

PORE PRINT

Pore Space Controlled by Pore Apertures

UNIVERSITY OF COLORADO AT BOULDER		SAMPLE ID:	4
OASIS NO. 1 DEUTSCH WELL		DEPTH, feet:	4635.4
BINDLEY FIELD		AIR PERMEABILITY, md:	40
HODGEMAN COUNTY, KANSAS		POROSITY, percent:	18.8

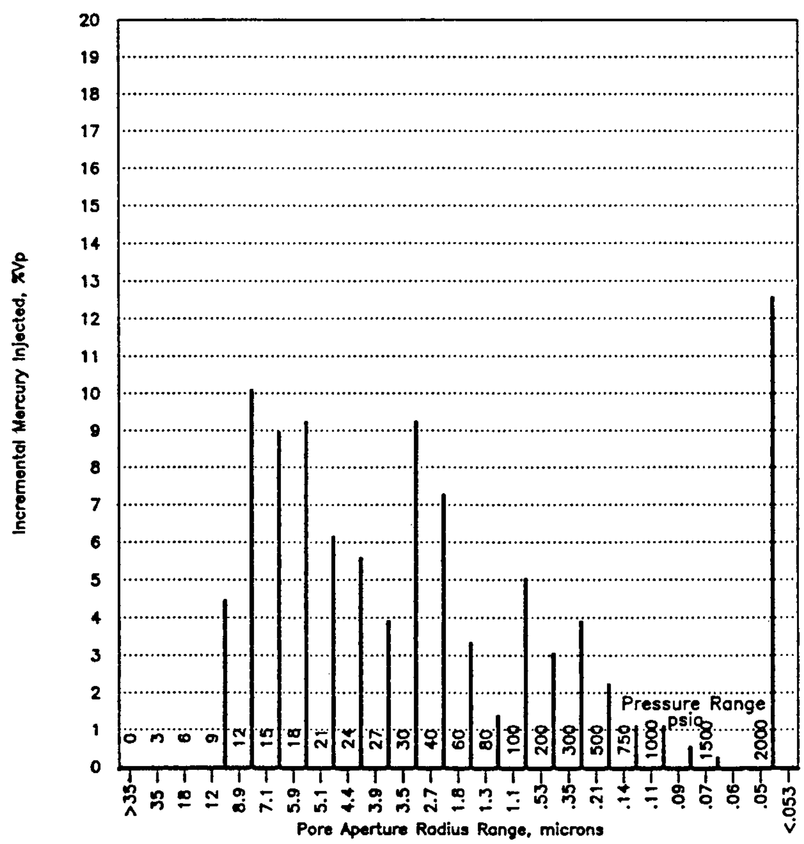

Western Atlas International

CORE LABORATORIES

File 57183-90110

SUMMARY OF MERCURY INJECTION TEST RESULTS

Company: University of Colorado at Boulder
Formation: Dolomite
County, State: Hodgeman, Kansas
Well: Oasis No. 5 Deutsch
Field: Bindley

Sample Identification:	5	6
Depth, feet:	4664.1	4673.0
Permeability to Air, md:	1.5	3.2
Porosity, percent:	17.0	17.4

Injection Pressure, psia	Pore Aperture Radius, microns	Mercury Saturation, percent pore space	
3	35.5	0.0	0.0
6	17.7	0.0	0.0
9	11.8	0.0	0.0
12	8.87	0.0	0.0
15	7.09	0.0	0.0
18	5.91	0.0	0.0
21	5.07	0.0	4.8
24	4.44	0.0	8.9
27	3.94	0.0	14.9
30	3.55	0.0	19.7
40	2.66	7.1	32.6
60	1.77	19.6	46.3
80	1.33	27.9	55.4
100	1.06	33.3	60.2
200	.532	48.5	70.2
300	.355	55.0	74.2
500	.213	62.7	78.0
750	.142	67.8	80.6
1000	.106	69.9	82.7
1250	.085	72.2	84.0
1500	.071	74.2	84.5
1750	.061	75.7	85.0
2000	.053	77.1	85.7

Injection Pressure vs Mercury Saturation

UNIVERSITY OF COLORADO AT BOULDER	SAMPLE ID: 5
OASIS NO. 5 DEUTSCH WELL	SAMPLE DEPTH, feet: 4664.1
BINDLEY FIELD	PERMEABILITY TO AIR, md: 1.5
HODGEMAN COUNTY, KANSAS	POROSITY, percent: 17.0

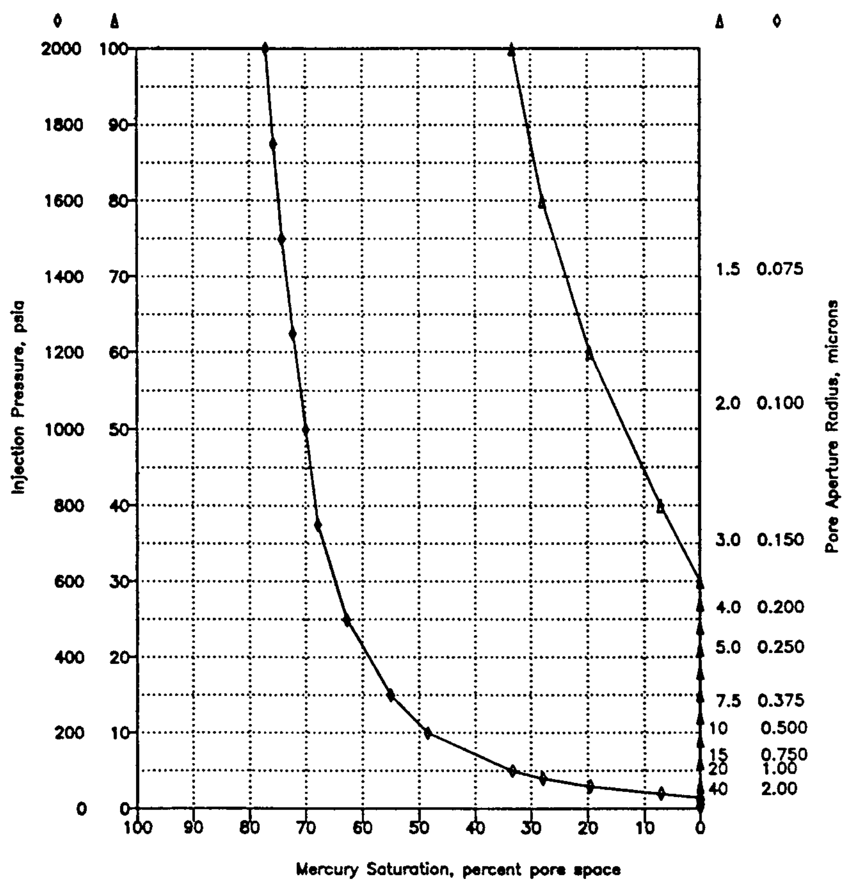

Core Laboratories

Pore Aperture Radius vs Mercury Saturation

UNIVERSITY OF COLORADO AT BOULDER		SAMPLE ID:	5
OASIS NO. 5 DEUTSCH WELL		SAMPLE DEPTH, feet:	4664.1
BINDLEY FIELD		PERMEABILITY TO AIR, md:	1.5
HODGEMAN COUNTY, KANSAS		POROSITY, percent:	17.0

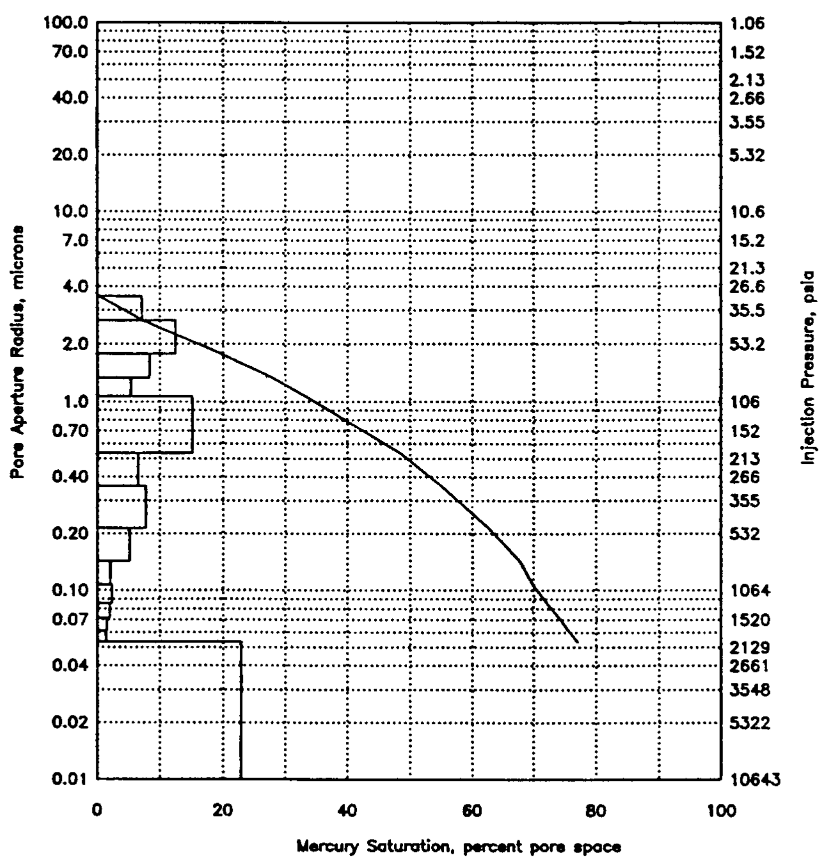

Page 21 of 46
File 57183-90110

PORE PRINT

Pore Space Controlled by Pore Apertures

UNIVERSITY OF COLORADO AT BOULDER
OASIS NO. 5 DEUTSCH WELL
BINDLEY FIELD
HODGEMAN COUNTY, KANSAS

SAMPLE ID: 5
DEPTH, feet: 4664.1
AIR PERMEABILITY, md: 1.5
POROSITY, percent: 17.0

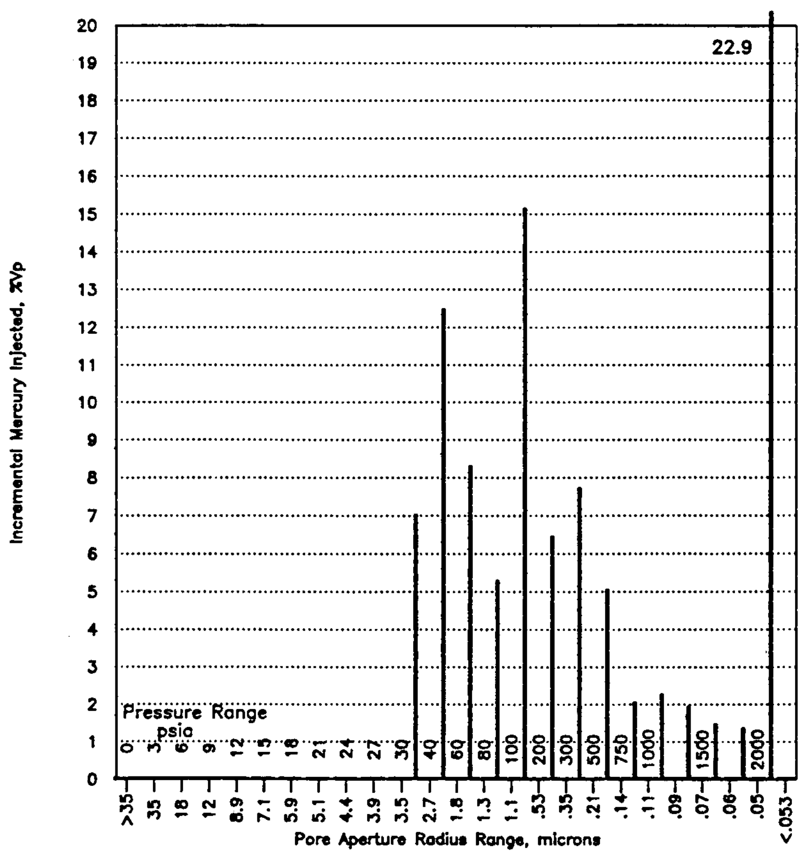

Core Laboratories

Injection Pressure vs Mercury Saturation

UNIVERSITY OF COLORADO AT BOULDER
OASIS NO. 5 DEUTSCH WELL
BINDLEY FIELD
HODGEMAN COUNTY, KANSAS

SAMPLE ID: 6
SAMPLE DEPTH, feet: 4673.0
PERMEABILITY TO AIR, md: 3.2
POROSITY, percent: 17.4

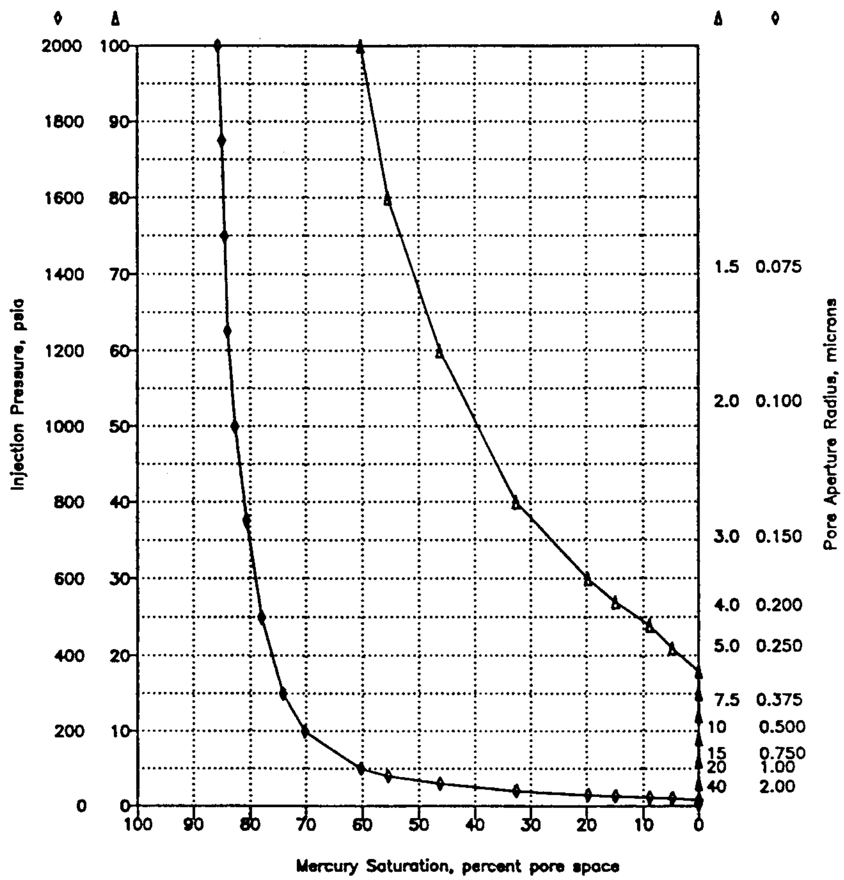

Pore Aperture Radius vs Mercury Saturation

UNIVERSITY OF COLORADO AT BOULDER
OASIS NO. 5 DEUTSCH WELL
BINDLEY FIELD
HODGEMAN COUNTY, KANSAS

SAMPLE ID:	6
SAMPLE DEPTH, feet:	4673.0
PERMEABILITY TO AIR, md:	3.2
POROSITY, percent:	17.4

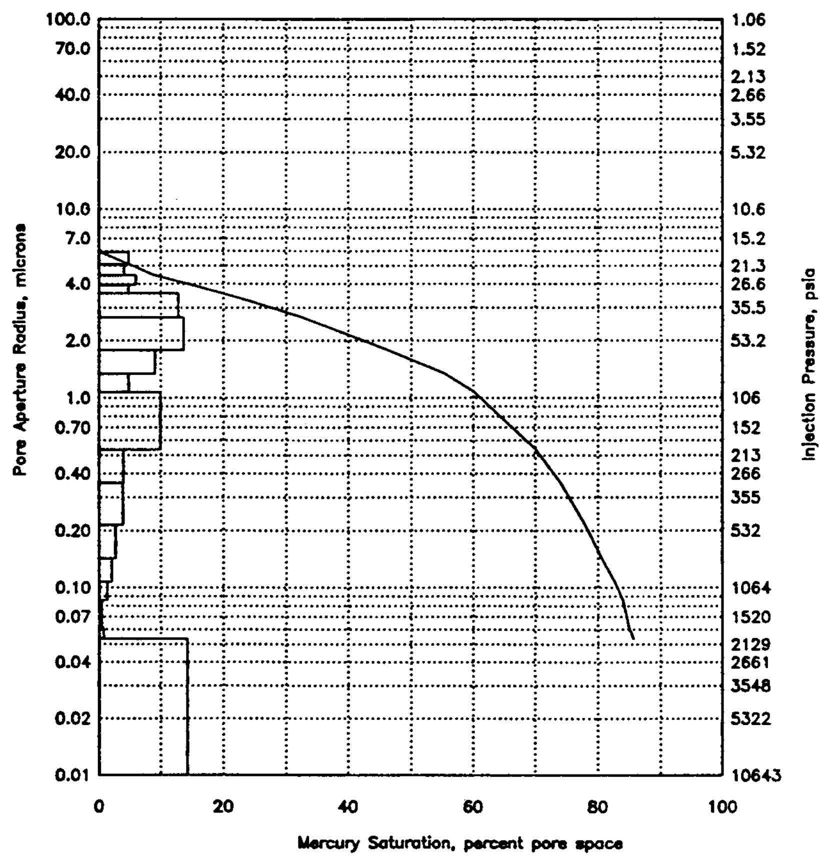

PORE PRINT

Pore Space Controlled by Pore Apertures

UNIVERSITY OF COLORADO AT BOULDER
OASIS NO. 5 DEUTSCH WELL
BINDLEY FIELD
HODGEMAN COUNTY, KANSAS

SAMPLE ID: 6
DEPTH, feet: 4673.0
AIR PERMEABILITY, md: 3.2
POROSITY, percent: 17.4

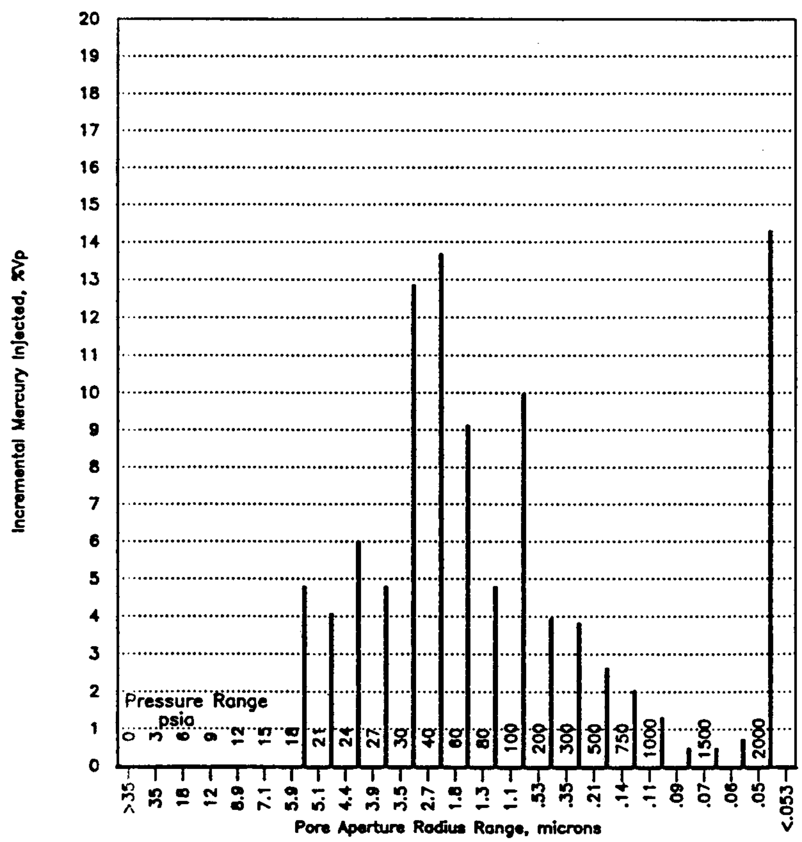

CORE LABORATORIES

Western Atlas International

File 57183-90110

SUMMARY OF MERCURY INJECTION TEST RESULTS

Company: University of Colorado at Boulder
Formation: Dolomite
County, State: Hodgeman, Kansas
Well: Oasis No. 1 Smith
Field: Not Specified

Sample Identification: 7
Depth, feet: 4659.1
Permeability to Air, md: 0.15
Porosity, percent: 9.4

Injection Pressure, psia	Pore Aperture Radius, microns	Mercury Saturation, percent pore space
3	35.5	0.0
6	17.7	0.0
9	11.8	0.0
12	8.87	0.0
15	7.09	0.0
18	5.91	0.0
21	5.07	0.0
24	4.44	0.0
27	3.94	0.0
30	3.55	0.0
40	2.66	0.0
60	1.77	0.0
80	1.33	0.0
100	1.06	0.0
200	.532	14.9
300	.355	31.2
500	.213	48.2
750	.142	58.8
1000	.106	66.4
1250	.085	71.2
1500	.071	75.1
1750	.061	78.2
2000	.053	81.1

Page 26 of 46
File 57183-90110

Injection Pressure vs Mercury Saturation

UNIVERSITY OF COLORADO AT BOULDER
OASIS NO. 1 SMITH WELL
BINDLEY FIELD
HODGEMAN COUNTY, KANSAS

SAMPLE ID: 7
SAMPLE DEPTH, feet: 4659.1
PERMEABILITY TO AIR, md: 0.15
POROSITY, percent: 9.4

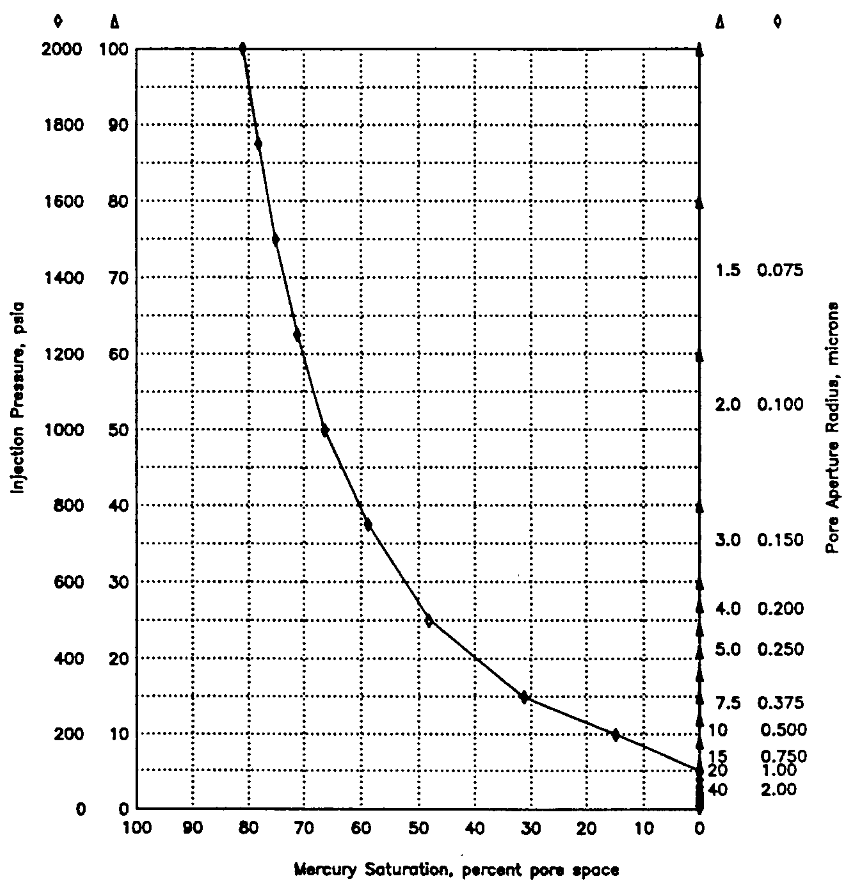

Core Laboratories

Pore Aperture Radius vs Mercury Saturation

UNIVERSITY OF COLORADO AT BOULDER
OASIS NO. 1 SMITH WELL
BINDLEY FIELD
HODGEMAN COUNTY, KANSAS

SAMPLE ID: 7
SAMPLE DEPTH, feet: 4659.1
PERMEABILITY TO AIR, md: 0.15
POROSITY, percent: 9.4

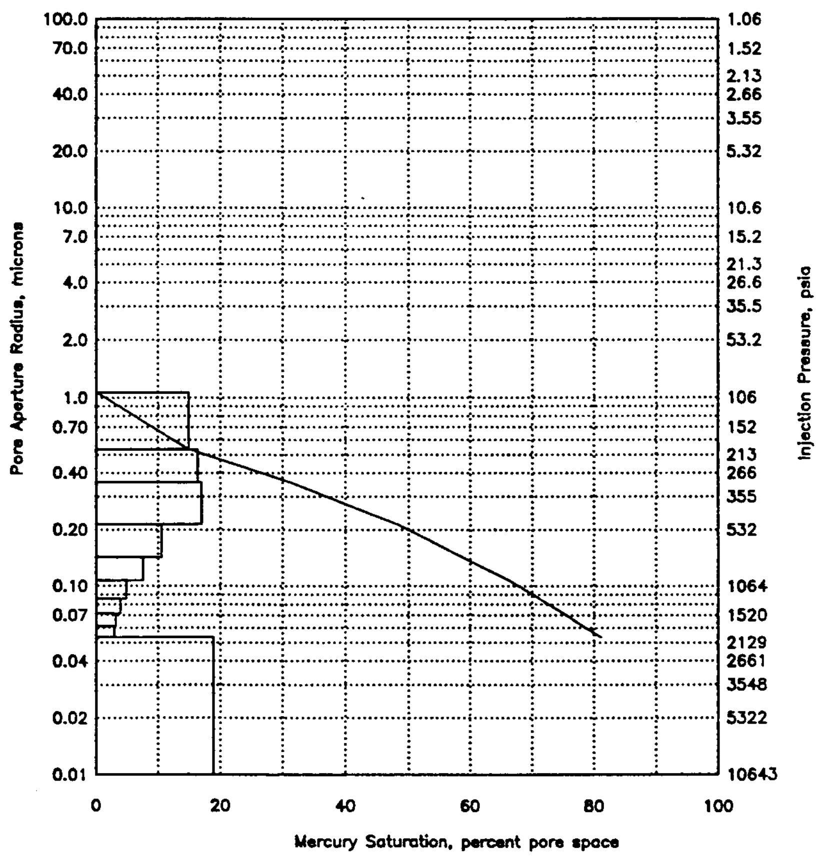

Core Laboratories

PORE PRINT

Pore Space Controlled by Pore Apertures

UNIVERSITY OF COLORADO AT BOULDER		SAMPLE ID:	7
OASIS NO. 1 SMITH WELL		DEPTH, feet:	4659.1
BINDLEY FIELD		AIR PERMEABILITY, md:	0.15
HODGEMAN COUNTY, KANSAS		POROSITY, percent:	9.4

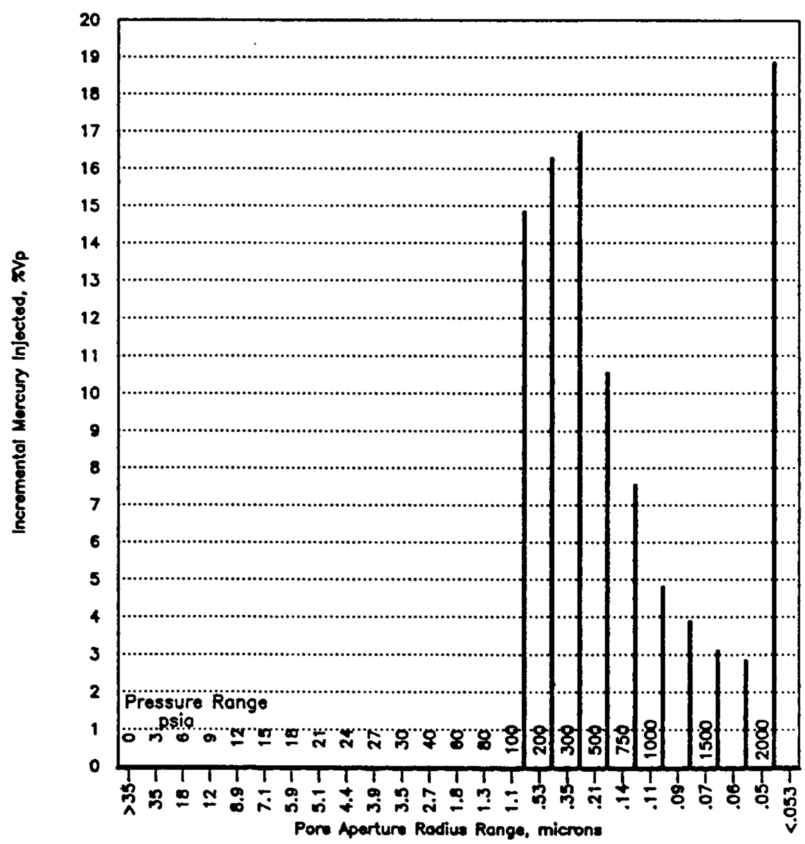

Core Laboratories

CORE LABORATORIES

Western Atlas International

File 57183-90110

SUMMARY OF MERCURY INJECTION TEST RESULTS

Company: University of Colorado at Boulder
Formation: Dolomite
County, State: Hodgeman, Kansas
Well: Oasis No. 3 Deutsch
Field: Bindley

Sample Identification:	8	9	10
Depth, feet:	4647.5	4657.1	4665.9
Permeability to Air, md:	0.011	123	32
Porosity, percent:	8.0	23.4	25.3

Injection Pressure, psia	Pore Aperture Radius, microns	Mercury Saturation, percent pore space		
3	35.5	0.0	0.0	0.4
6	17.7	0.0	3.0	1.3
9	11.8	0.0	7.5	2.4
12	8.87	0.0	18.0	4.3
15	7.09	0.0	34.4	6.1
18	5.91	0.0	44.6	8.0
21	5.07	0.0	51.8	9.7
24	4.44	0.0	57.1	13.1
27	3.94	0.0	60.8	16.7
30	3.55	0.0	64.2	19.5
40	2.66	0.0	72.1	36.0
60	1.77	0.0	77.1	53.7
80	1.33	0.0	79.8	61.5
100	1.06	0.0	81.6	66.4
200	.532	0.0	86.3	76.8
300	.355	0.0	88.2	81.0
500	.213	4.7	90.2	85.9
750	.142	9.6	91.7	89.0
1000	.106	17.5	92.5	91.6
1250	.085	26.2	93.2	93.0
1500	.071	34.4	93.7	94.2
1750	.061	43.5	94.0	94.8
2000	.053	55.2	94.9	95.3

Western Atlas International

CORE LABORATORIES

File 57183-90110

SUMMARY OF MERCURY INJECTION TEST RESULTS

Company: University of Colorado at Boulder
Formation: Dolomite
County, State: Hodgeman, Kansas
Well: Oasis No. 3 Deutsch
Field: Bindley

Sample Identification:	8	9	10
Depth, feet:	4647.5	4657.1	4665.9
Permeability to Air, md:	0.011	123	32
Porosity, percent:	8.0	23.4	25.3

Injection Pressure, psia	Pore Aperture Radius, microns	Mercury Saturation, percent pore space		
		8	9	10
1500			94.8	95.2
1250			94.8	95.1
1000			94.8	94.9
750			94.6	94.8
500			94.3	94.3
300			94.1	93.7
200			93.7	93.0
100			93.1	91.4
80			92.9	91.0
60			92.4	90.1
40			91.8	89.0
30			90.8	87.4
15			87.8	80.3
0			60.7	64.1

Page 31 of 46
File 57183-90110

Injection Pressure vs Mercury Saturation

UNIVERSITY OF COLORADO AT BOULDER	SAMPLE ID: 8
OASIS NO. 3 DEUTSCH WELL	SAMPLE DEPTH, feet: 4647.5
BINDLEY FIELD	PERMEABILITY TO AIR, md: 0.011
HODGEMAN COUNTY, KANSAS	POROSITY, percent: 8.0

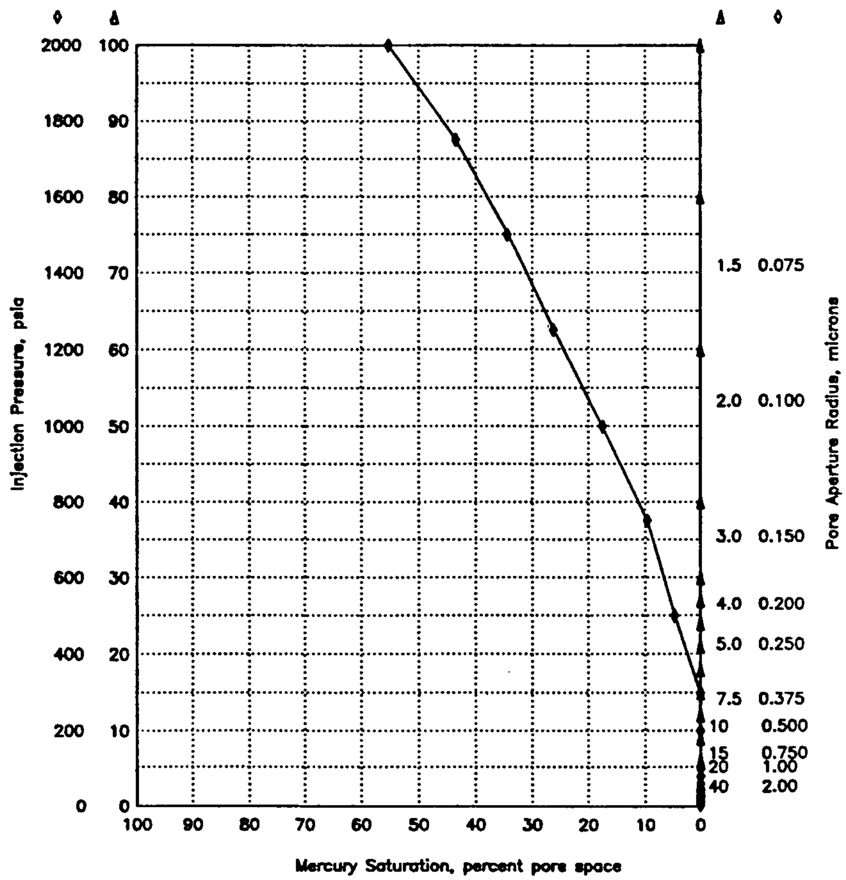

Core Laboratories

Pore Aperture Radius vs Mercury Saturation

UNIVERSITY OF COLORADO AT BOULDER
OASIS NO. 3 DEUTSCH WELL
BINDLEY FIELD
HODGEMAN COUNTY, KANSAS

SAMPLE ID: 8
SAMPLE DEPTH, feet: 4647.5
PERMEABILITY TO AIR, md: 0.011
POROSITY, percent: 8.0

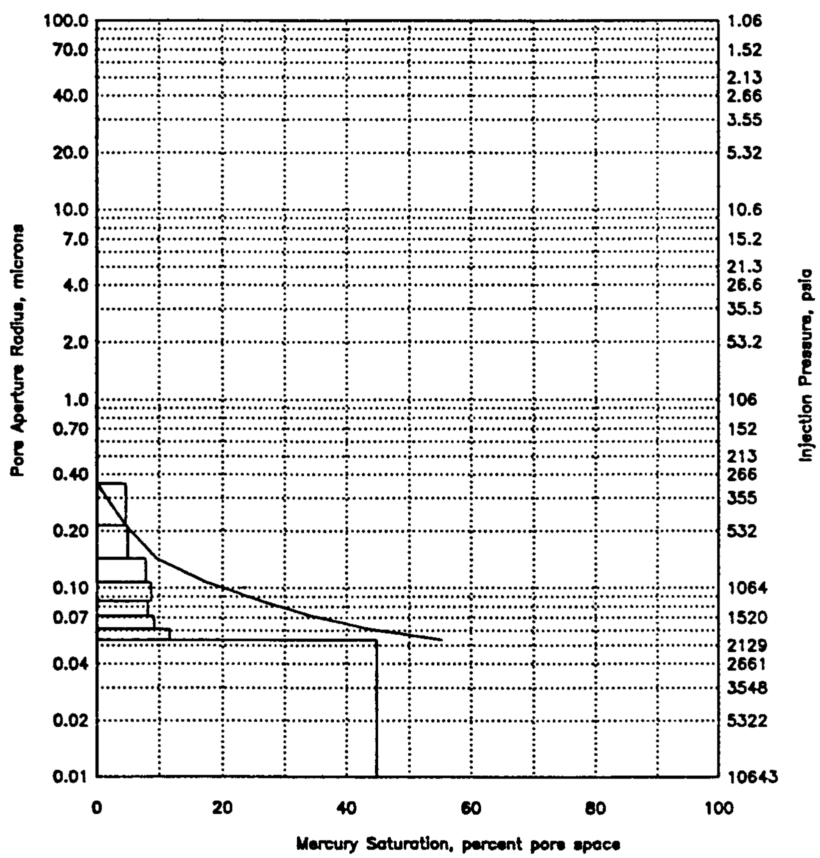

Core Laboratories

PORE PRINT

Pore Space Controlled by Pore Apertures

UNIVERSITY OF COLORADO AT BOULDER	SAMPLE ID:	8
OASIS NO. 3 DEUTSCH WELL	DEPTH, feet:	4647.5
BINDLEY FIELD	AIR PERMEABILITY, md:	0.011
HODGEMAN COUNTY, KANSAS	POROSITY, percent:	8.0

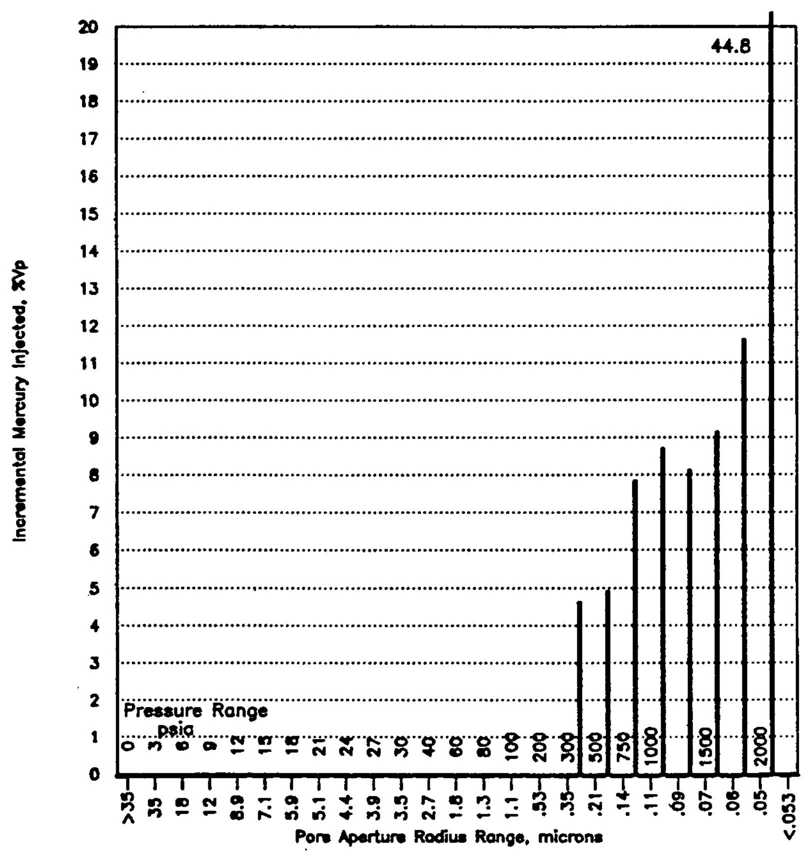

Core Laboratories

Injection Pressure vs Mercury Saturation

UNIVERSITY OF COLORADO AT BOULDER	SAMPLE ID: 9
OASIS NO. 3 DEUTSCH WELL	SAMPLE DEPTH, feet: 4657.1
BINDLEY FIELD	PERMEABILITY TO AIR, md: 123
HODGEMAN COUNTY, KANSAS	POROSITY, percent: 23.4

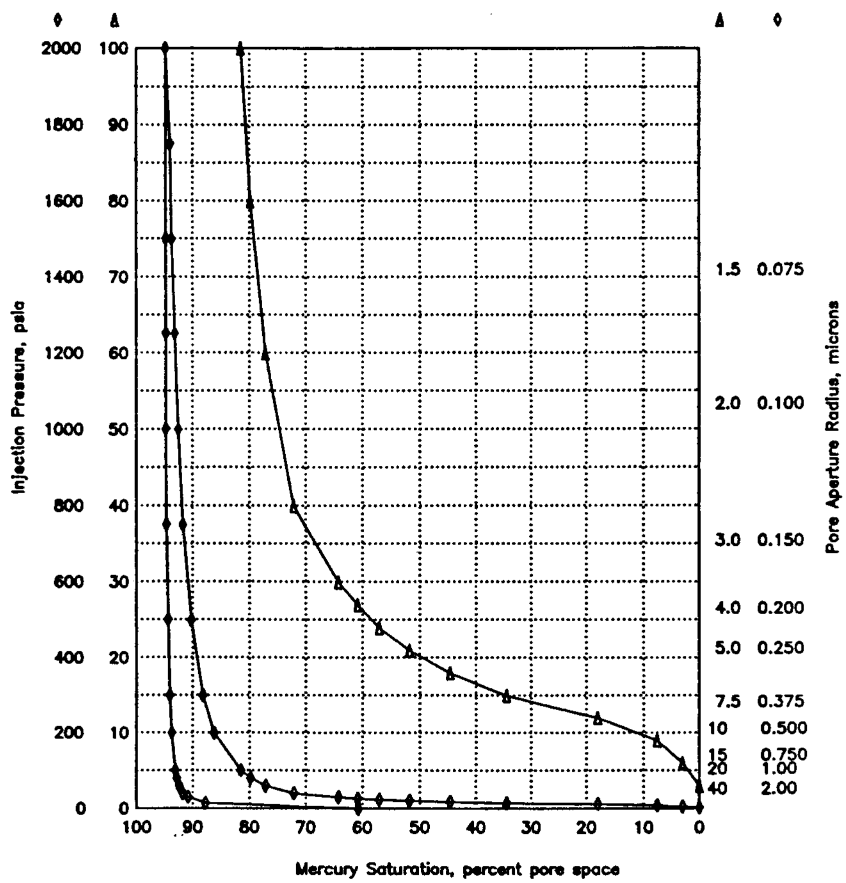

Core Laboratories

Pore Aperture Radius vs Mercury Saturation

UNIVERSITY OF COLORADO AT BOULDER
OASIS NO. 3 DEUTSCH WELL
BINDLEY FIELD
HODGEMAN COUNTY, KANSAS

SAMPLE ID:	9
SAMPLE DEPTH, feet:	4657.1
PERMEABILITY TO AIR, md:	123
POROSITY, percent:	23.4

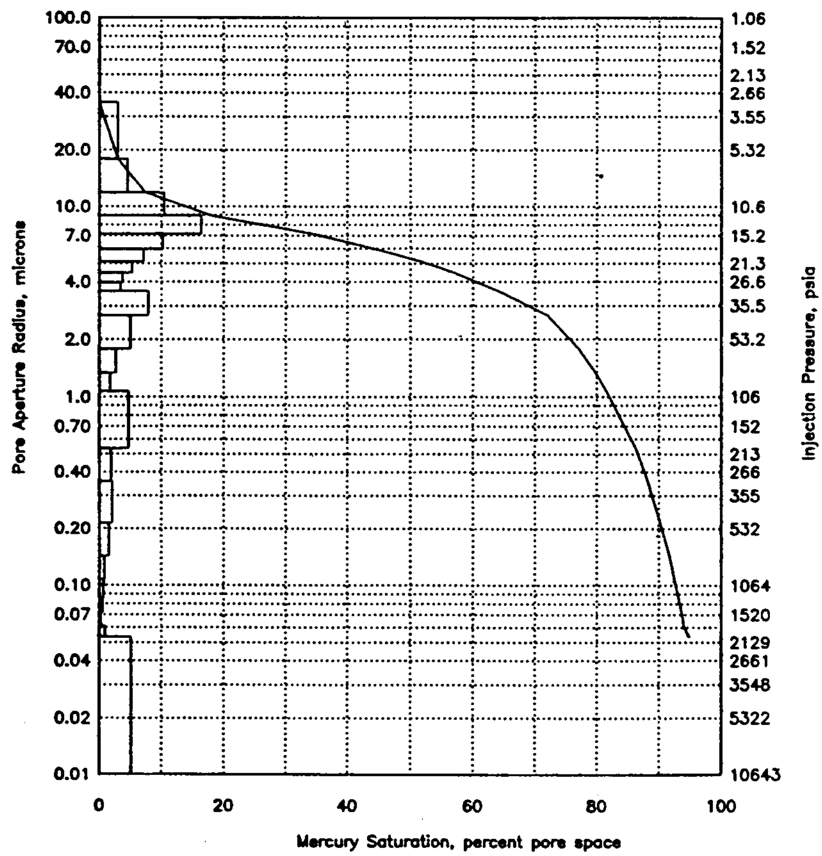

Page 36 of 46
File 57183-90110

PORE PRINT

Pore Space Controlled by Pore Apertures

UNIVERSITY OF COLORADO AT BOULDER		SAMPLE ID:	9
OASIS NO. 3 DEUTSCH WELL		DEPTH, feet:	4657.1
BINDLEY FIELD		AIR PERMEABILITY, md:	123
HODGEMAN COUNTY, KANSAS		POROSITY, percent:	23.4

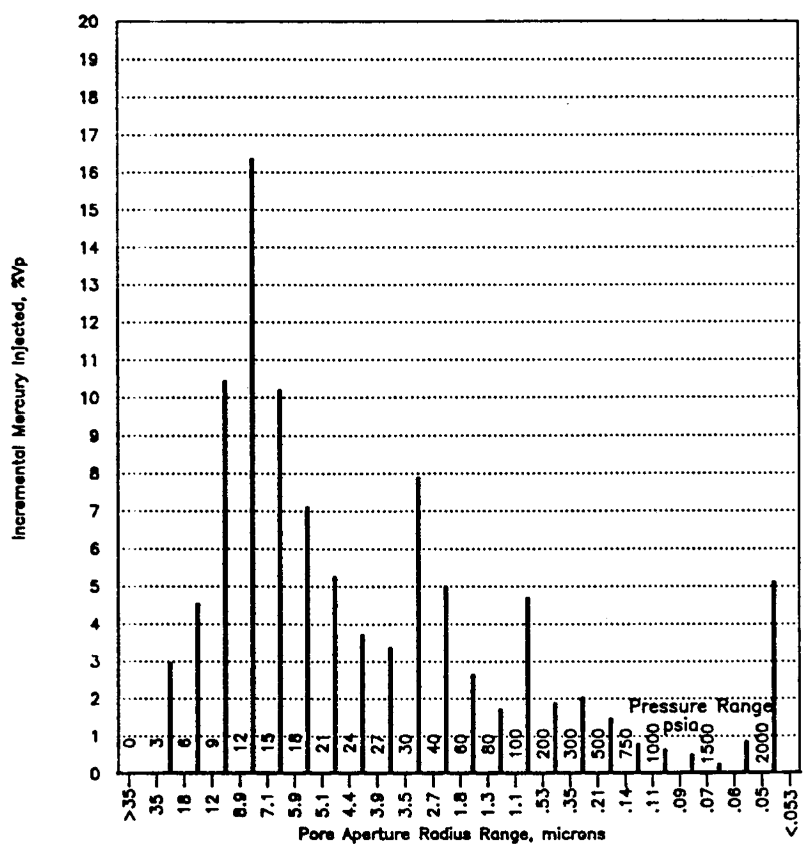

Core Laboratories

Injection Pressure vs Mercury Saturation

UNIVERSITY OF COLORADO AT BOULDER
OASIS NO. 3 DEUTSCH WELL
BINDLEY FIELD
HODGEMAN COUNTY, KANSAS

SAMPLE ID: 10
SAMPLE DEPTH, feet: 4665.9
PERMEABILITY TO AIR, md: 32
POROSITY, percent: 25.3

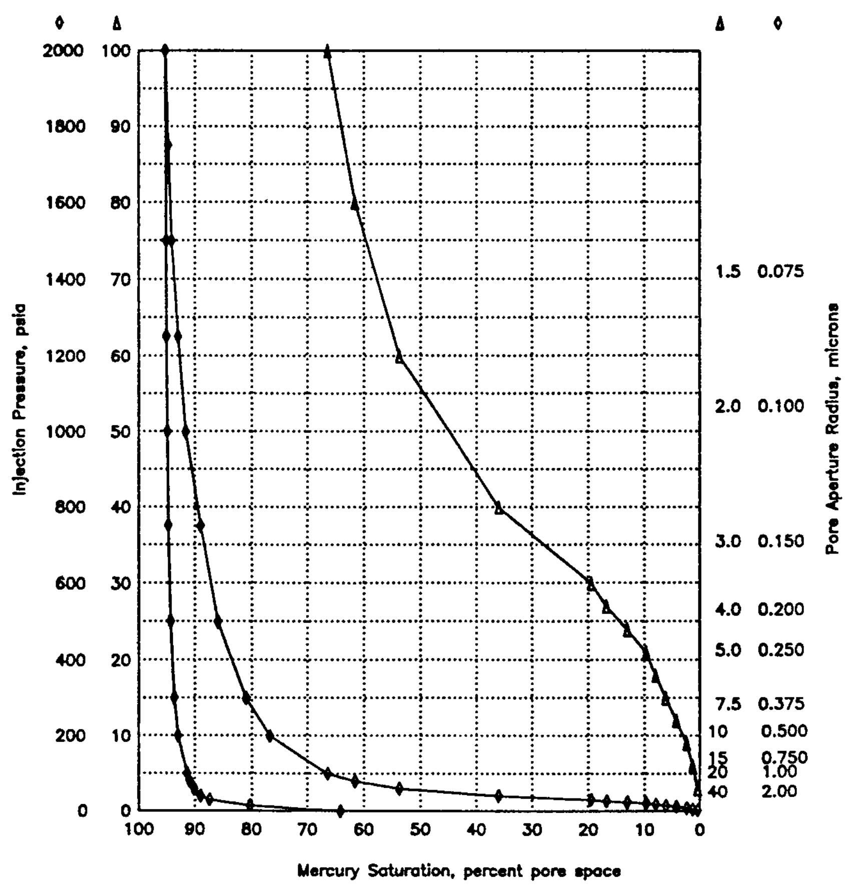

Pore Aperture Radius vs Mercury Saturation

UNIVERSITY OF COLORADO AT BOULDER
OASIS NO. 3 DEUTSCH WELL
BINDLEY FIELD
HODGEMAN COUNTY, KANSAS

SAMPLE ID: 10
SAMPLE DEPTH, feet: 4665.9
PERMEABILITY TO AIR, md: 32
POROSITY, percent: 25.3

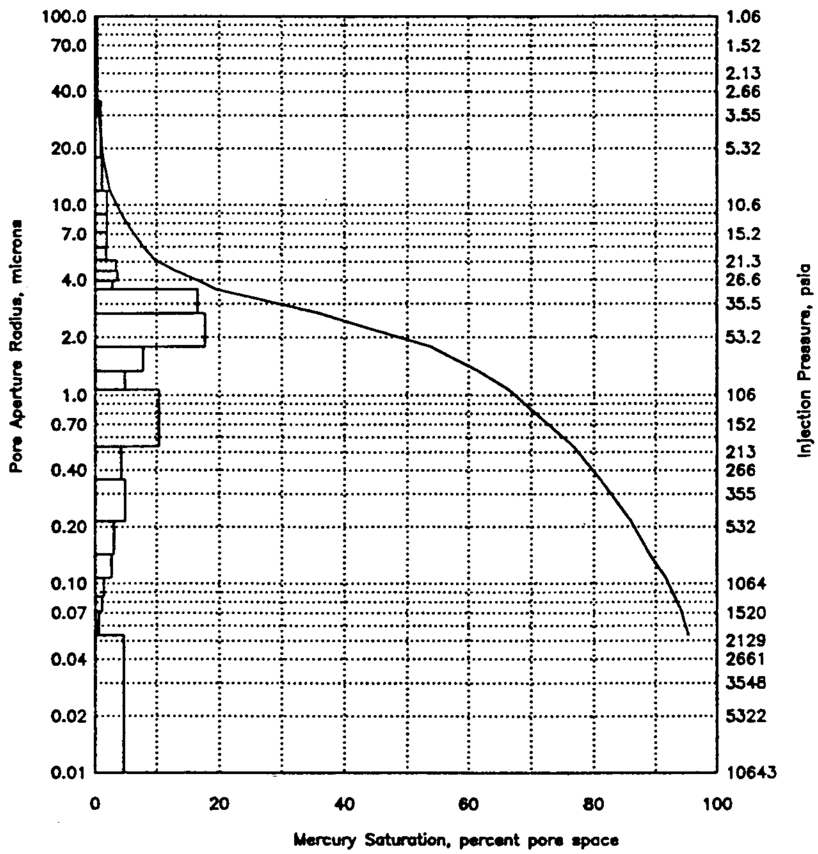

Core Laboratories

PORE PRINT

Pore Space Controlled by Pore Apertures

UNIVERSITY OF COLORADO AT BOULDER	SAMPLE ID:	10
OASIS NO. 3 DEUTSCH WELL	DEPTH, feet:	4665.9
BINDLEY FIELD	AIR PERMEABILITY, md:	32
HODGEMAN COUNTY, KANSAS	POROSITY, percent:	25.3

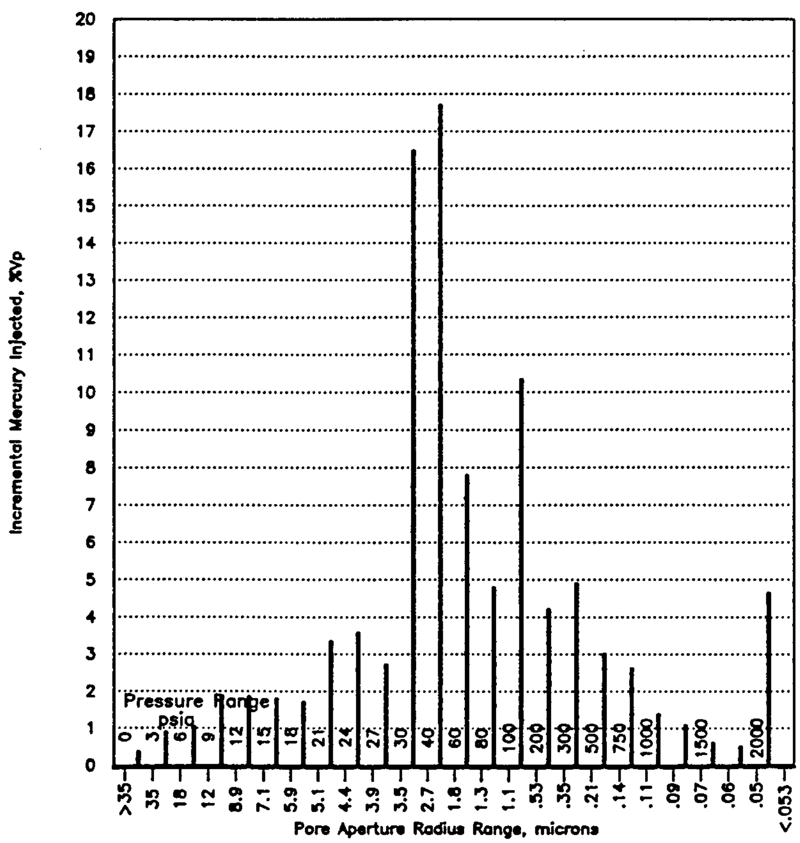

Core Laboratories

CORE LABORATORIES

Western Atlas International

File 57183-90110

SUMMARY OF MERCURY INJECTION TEST RESULTS

Company: University of Colorado at Boulder
Formation: Dolomite
County, State: Hodgeman, Kansas
Well: Oasis No. 6 Deutsch
Field: Bindley

Sample Identification:	11	12
Depth, feet:	4655.5	4663.1
Permeability to Air, md:	461	142
Porosity, percent:	26.2	21.1

Injection Pressure, psia	Pore Aperture Radius, microns	Mercury Saturation, percent pore space	
3	35.5	0.0	0.0
6	17.7	7.6	9.8
9	11.8	27.6	21.4
12	8.87	42.0	29.6
15	7.09	54.5	36.1
18	5.91	61.8	40.5
21	5.07	66.6	44.7
24	4.44	70.4	47.4
27	3.94	73.2	50.5
30	3.55	75.5	52.4
40	2.66	81.1	56.8
60	1.77	84.3	60.5
80	1.33	85.6	63.0
100	1.06	86.2	65.2
200	.532	87.6	76.5
300	.355	89.5	81.9
500	.213	92.1	86.0
750	.142	93.2	88.5
1000	.106	93.8	89.7
1250	.085	94.3	90.6
1500	.071	94.6	91.3
1750	.061	94.9	91.7
2000	.053	95.1	92.2

Injection Pressure vs Mercury Saturation

UNIVERSITY OF COLORADO AT BOULDER
OASIS NO. 6 DEUTSCH WELL
BINDLEY FIELD
HODGEMAN COUNTY, KANSAS

SAMPLE ID: 11
SAMPLE DEPTH, feet: 4655.5
PERMEABILITY TO AIR, md: 461
POROSITY, percent: 26.2

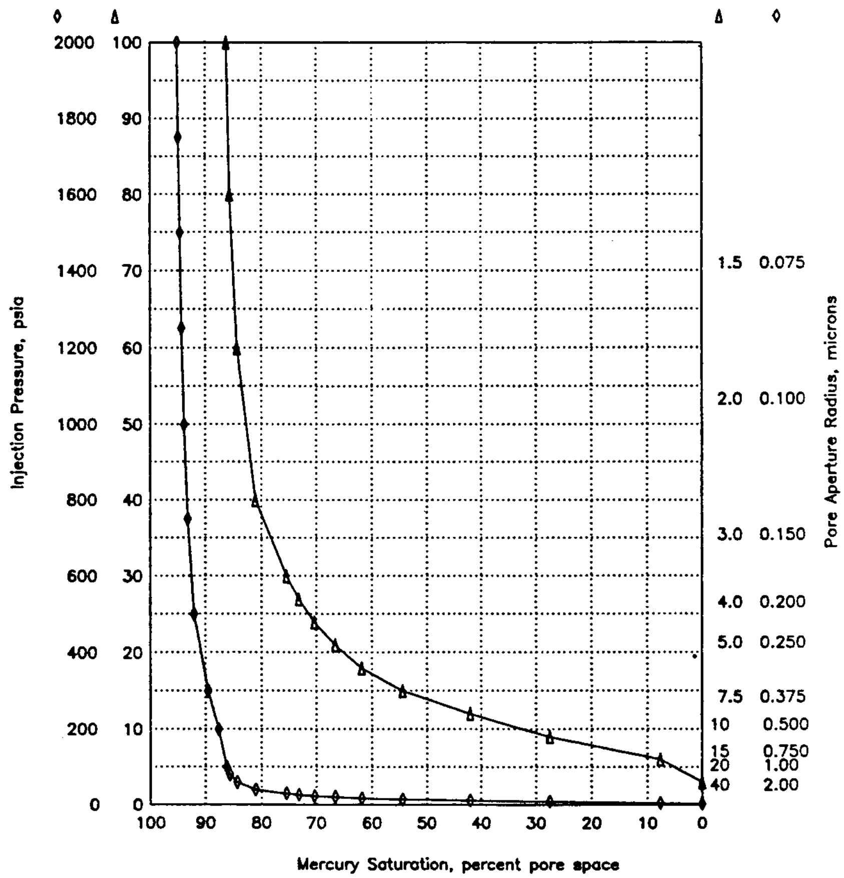

Page 42 of 46
File 57183-90110

Pore Aperture Radius vs Mercury Saturation

UNIVERSITY OF COLORADO AT BOULDER
OASIS NO. 6 DEUTSCH WELL
BINDLEY FIELD
HODGEMAN COUNTY, KANSAS

SAMPLE ID: 11
SAMPLE DEPTH, feet: 4655.5
PERMEABILITY TO AIR, md: 461
POROSITY, percent: 26.2

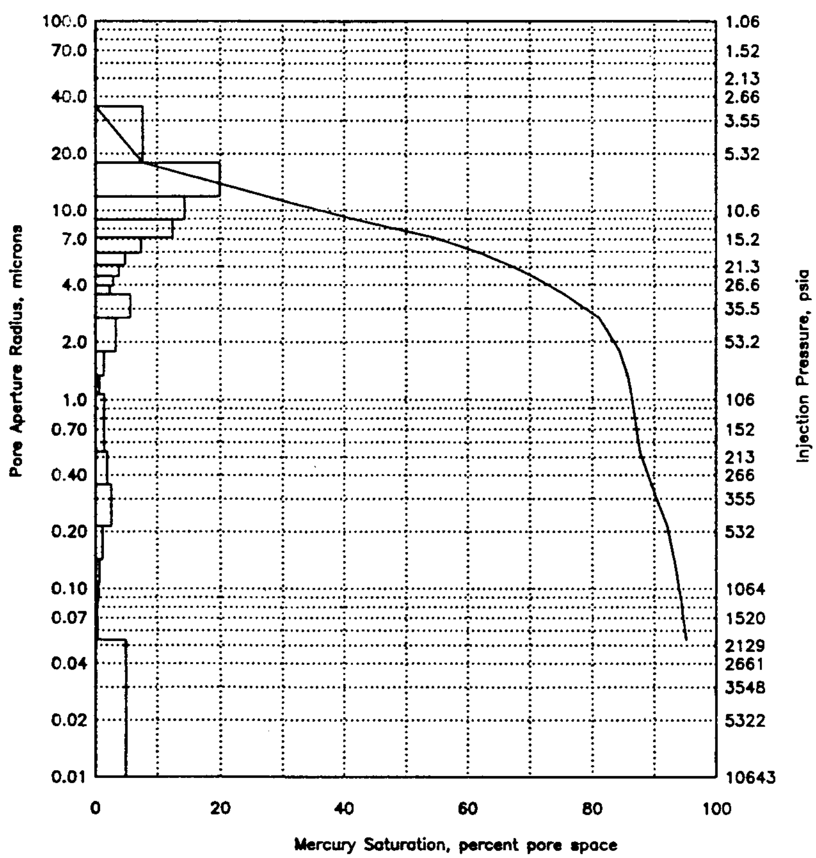

Core Laboratories

PORE PRINT

Pore Space Controlled by Pore Apertures

UNIVERSITY OF COLORADO AT BOULDER		SAMPLE ID:	11
OASIS NO. 6 DEUTSCH WELL		DEPTH, feet:	4655.5
BINDLEY FIELD		AIR PERMEABILITY, md:	461
HODGEMAN COUNTY, KANSAS		POROSITY, percent:	26.2

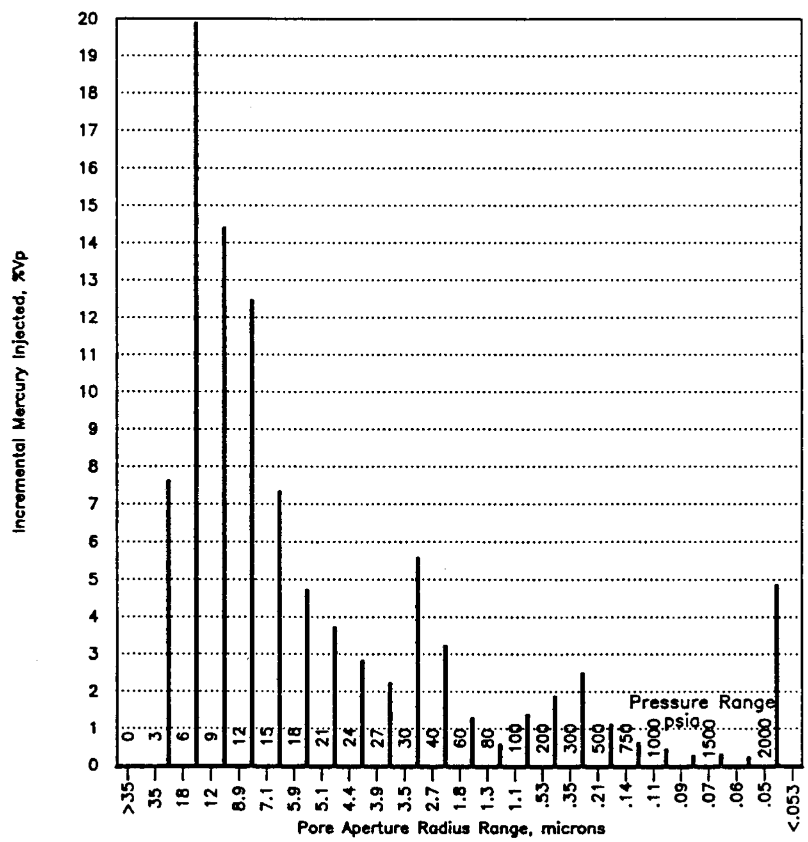

Page 44 of 46
File 57183-90110

Injection Pressure vs Mercury Saturation

UNIVERSITY OF COLORADO AT BOULDER
OASIS NO. 6 DEUTSCH WELL
BINDLEY FIELD
HODGEMAN COUNTY, KANSAS

SAMPLE ID: 12
SAMPLE DEPTH, feet: 4663.1
PERMEABILITY TO AIR, md: 142
POROSITY, percent: 21.1

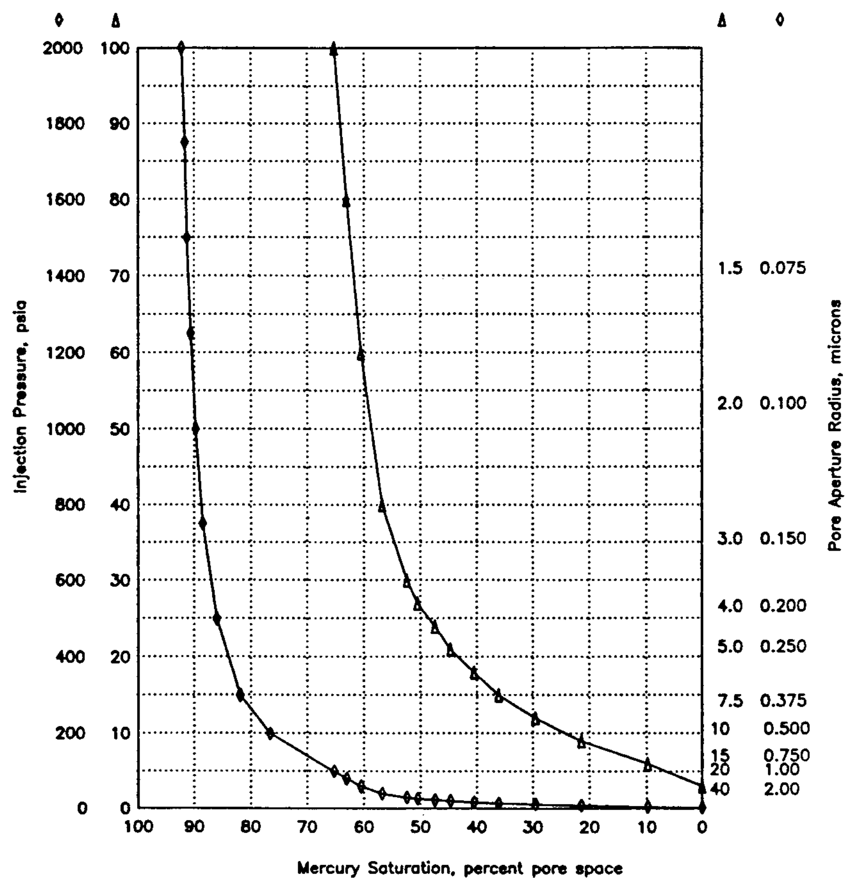

Core Laboratories

Pore Aperture Radius vs Mercury Saturation

UNIVERSITY OF COLORADO AT BOULDER
OASIS NO. 6 DEUTSCH WELL
BINDLEY FIELD
HODGEMAN COUNTY, KANSAS

SAMPLE ID: 12
SAMPLE DEPTH, feet: 4663.1
PERMEABILITY TO AIR, md: 142
POROSITY, percent: 21.1

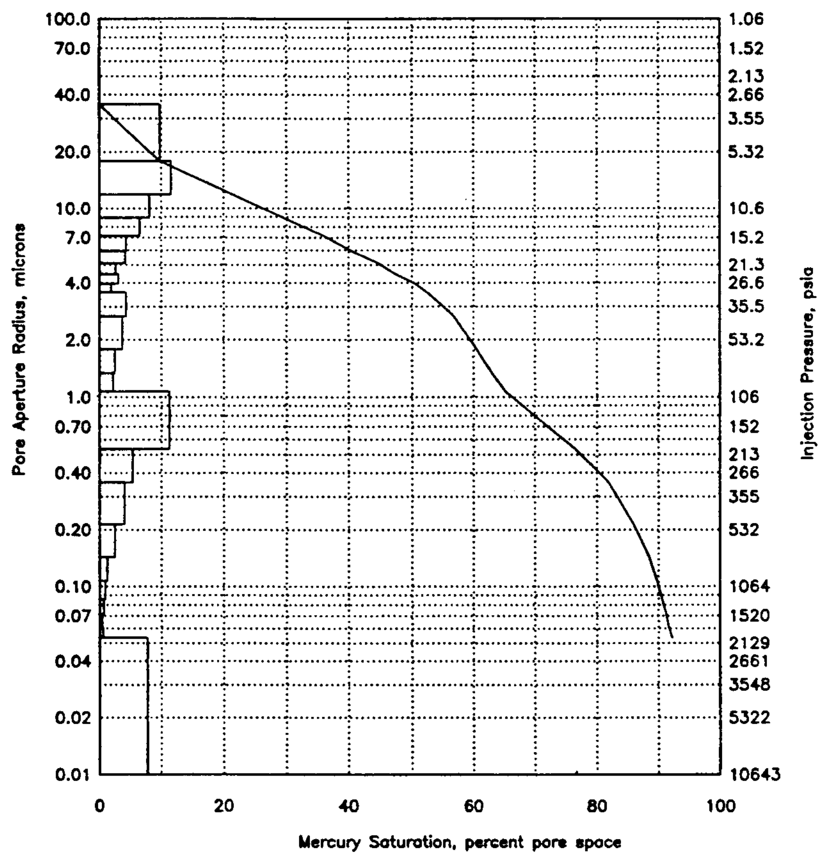

Core Laboratories

PORE PRINT

Pore Space Controlled by Pore Apertures

UNIVERSITY OF COLORADO AT BOULDER	SAMPLE ID: 12
OASIS NO. 6 DEUTSCH WELL	DEPTH, feet: 4663.1
BINDLEY FIELD	AIR PERMEABILITY, md: 142
HODGEMAN COUNTY, KANSAS	POROSITY, percent: 21.1

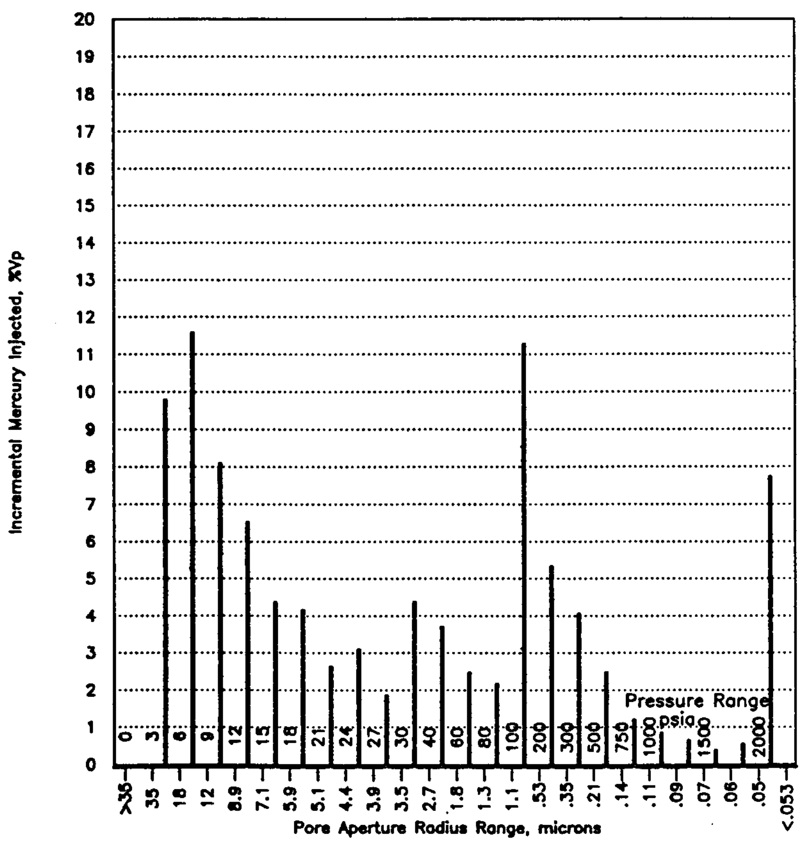

Core Laboratories